

UNCLASSIFIED

AD NUMBER

AD853122

NEW LIMITATION CHANGE

TO

Approved for public release, distribution
unlimited

FROM

Distribution authorized to DoD only;
Administrative/Operational use; 15 Nov
1968. Other requests shall be referred to
Equipment Development Branch [SMOND-2] HQ
AFSCF, AF Unit Post Office, Los Angeles
CA. 90045.

AUTHORITY

BMO ltr, 26 Sep 1980.

THIS PAGE IS UNCLASSIFIED

ORIGINAL CONTAINS COLOR PLATES: ALL DDC
PRINTED IN BLACK AND WHITE.
ORIGINAL MAY BE COPIED IN BLACK AND WHITE.

SGLS

SPACE-GROUND LINK SUBSYSTEM

GROUND STATION

SYSTEM ANALYSIS SUMMARY REPORT



WDL-TR3227-1

VOLUME I
SYSTEM DESIGN ANALYSIS

PHILCO



PHILCO-FORD CORPORATION
WDL Design
Palo Alto, California • 94301

SUBMITTED TO: USAF/SAMSO
CONTRACT F04695-67-0115

AD 853122 L

AMENDMENT NO.	
APPROVING	WHITE SECTION <input type="checkbox"/>
REQ	BUFF SECTION <input checked="" type="checkbox"/>
UNAUTHORIZED	
JUSTIFICATION.....	
BY.....	
DISTRIBUTION/AVAILABILITY CODES	
BIST.	AVAIL AND/OR SPECIAL
4	

Revised/Con Mrs. Mary
Henning (SAMSO) 10 June 69
Continue to use (SMSDT-STINFO)
TAS Controlling Office. Jde

W
N
W
C
L
I
E
R
S

ABSTRACT

PHILCO-FORD WDL-TR3227-1 UNCLASSIFIED
SPACE-GROUND LINK SUBSYSTEM
GROUND STATION
SYSTEM ANALYSIS SUMMARY REPORT 891 Pages
15 November 1968 Contract F04695-67-C-0115

This report provides a technical description of the ground station of the Space-Ground Link Subsystem (SGLS) and integrates the analyses performed by contractors who contributed to its development. The report is in three volumes:

- Volume I System Design Analysis contains the ground station description and related analyses.
Volume II Receiver Design Analysis contains a detailed analysis of the SGLS receiver.
Volume III Supplementary Analyses is a reprint of analyses originally presented in the SGLS final design report.
-

THIS UNCLASSIFIED ABSTRACT IS DESIGNED FOR RETENTION IN A STANDARD 3-BY-5 CARD-SIZE FILE, IF DESIRED. WHERE THE ABSTRACT COVERS MORE THAN ONE SIDE OF THE CARD, THE ENTIRE RECTANGLE MAY BE CUT OUT AND FOLDED AT THE DOTTED CENTER LINE. (IF THE ABSTRACT IS CLASSIFIED, HOWEVER, IT MUST NOT BE REMOVED FROM THE DOCUMENT IN WHICH IT IS INCLUDED.)

D D C
R e p o r t e d
JUN 9 1969
R e c e i v e d
C

WDL-TR3227-1
15 November 1968

SPACE-GROUND LINK SUBSYSTEM
GROUND STATION
SYSTEM ANALYSIS SUMMARY REPORT

VOLUME I SYSTEM DESIGN ANALYSIS

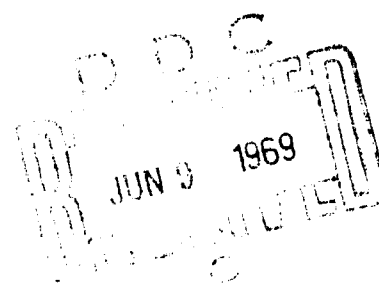
F04695-67-C-0115 *Recd*

Submitted to:
DEPARTMENT OF THE AIR FORCE
Headquarters, Space and Missile Systems Organization (AFSC)
Los Angeles, California

STATEMENT #4 UNCLASSIFIED

Each transmittal of this document outside the Department of Defense must have prior approval of Equipment Development Branch (SMOND-2) AFSCF AF 2nd Unit Post Office, Los Angeles Calif. 90045

Submitted by:
PHILCO-FORD CORPORATION
WDL Division
Palo Alto, California



FOREWORD

This System Analysis Summary Report for the ground station of the Space-Ground Link Subsystem (SGLS) has been prepared to satisfy CDRL No. B042 of Exhibit B to Air Force Contract F04695-67-C-0115. The report provides a technical description of the system and integrates the analyses performed by contractors who have contributed to its development. The latter, in turn, may be used as a point of departure for future development.

Initial development work on SGLS was accomplished under Air Force Contract No. AF04(695)-610 and included development and demonstration of both space vehicle and ground station equipments. A subsequent contract, No. F04695-67-C-0115, was awarded to Philco-Ford for the systems engineering effort required to integrate modifications developed under other Air Force contracts into the system and additionally to incorporate SGLS into the remote tracking stations of the SCF.

Current system design incorporates significant configuration modifications over that evaluated in the SGLS demonstration phase. These changes, defined by Air Force design criteria, necessitated a new high power transmitting system, signal recording facilities, PCM ground station, communications security equipment reconfiguration, and expansion of the number of operating channels to twenty. The installed system interfaces with the remote tracking station Control and Display, Data Handling, Timing, and FM/FM subsystems and is integrated with new and modified tracking station antenna subsystems.

The report is organized in three volumes:

- Volume I - "System Design Analysis" contains a technical description of ground station design and related analyses.
- Volume II - "Receiver Design Analysis" contains a detailed analysis of the SGLS receiver.
- Volume III - "Supplementary Analyses" is a reprint of the appendices to the final design report on SGLS published by TRW Systems.

PRECEDING PAGE BLANK-NOT FILMED

WDL-TR3227-1
Volume I

TABLE OF CONTENTS

<u>Section</u>		<u>Page</u>
1	SYSTEM OVERVIEW	1-1
1.1	REQUIREMENTS SUMMARY	1-1
1.2	TRACKING	1-3
1.3	UPLINK	1-5
1.3.1	Commanding	1-5
1.3.2	Analog and Ranging Data	1-5
1.4	DOWLINK	1-7
1.4.1	Carrier 1	1-7
1.4.2	Carriers 2 and 3	1-9
1.4.3	PCM Telemetry	1-10
1.4.4	Data Recording	1-10
1.4.5	Analog Data	1-11
1.4.6	Communications Security	1-11
2	TRACKING SUPPORT	2-1
2.1	Tracking Functional Description	2-1
2.1.1	Angle Tracking	2-1
2.1.2	Ranging	2-3
2.1.3	Range Rate	2-5
2.2	Tracking Performance	2-9
2.2.1	Angle Tracking Accuracy	2-10
2.2.2	Ranging Accuracy	2-12
2.2.3	Range-Rate Accuracy	2-15
3	DOWLINK SERVICES	3-1
3.1	Downlink Functional Description	3-1
3.1.1	Downlink Structure	3-1
3.1.2	Signal Detection	3-5
3.1.3	PCM Decommutation	3-12
3.1.4	Data Distribution	3-15
3.2	Signal-To-Interference Analysis	3-17
3.2.1	Intermodulation	3-18
3.2.2	Phase Nonlinearities and Amplitude Ripple	3-27
3.2.3	Spurious Interference	3-28
3.3	Downlink Performance	3-33
3.3.1	System Noise Temperature	3-33
3.3.2	Dynamic Range	3-40
3.3.3	Carrier 1 Thresholds	3-42
3.3.4	Carrier 2 Thresholds	3-49
3.3.5	Carrier 3 Thresholds	3-49
3.3.6	Typical Performance	3-51

TABLE OF CONTENTS (CONTINUED)

<u>Section</u>		<u>Page</u>
4	UPLINK SERVICES	4-1
	4.1 Uplink Functional Description	4-1
	4.1.1 Uplink Baseband Structure	4-1
	4.1.2 Uplink Transmission	4-9
	4.2 Uplink Performance	
	4.2.1 Effective Radiated Power	4-17
	4.2.2 Carrier Power Distribution	4-19
5	GROUND STATION DESCRIPTION	5-1
	5.1 Equipment Description	5-1
	5.1.1 Antenna Interface Equipment	5-1
	5.1.2 Transmitting Equipment	5-11
	5.1.3 Receiving Equipment	5-16
	5.1.4 Digital Ranging Equipment (DRE)	5-20
	5.1.5 Range-Rate Equipment	5-21
	5.1.6 Telemetry Equipment	5-22
	5.1.7 Control and Display Equipment	5-24
	5.1.8 Data Terminal Equipment	5-26
	5.1.9 Signal Switching Equipment	5-29
	5.1.10 Recording/Playback Equipment	5-31
	5.1.11 COMSEC Equipment	5-32
	5.1.12 Integration and Checkout Equipment	5-33
	5.1.13 Test Transponder and Uplink Monitor	5-35
	5.2 Equipment Arrangement	5-37
	5.2.1 Equipment in the RF Area	5-37
	5.2.2 Equipment in the Data Processing Area	5-40
	5.2.3 Equipment Peculiar to the High-Gain (TT&C) Installation	5-53
	5.2.4 Data Terminal Types 1 and 2	5-53
	5.2.5 Other Equipment	5-53
	5.3 Test Capability	5-57
	5.3.1 System Checkout	5-57
	5.3.2 System Configuration Checkout	5-73

TABLE OF CONTENTS (CONTINUED)

<u>Section</u>		<u>Page</u>
6	RELIABILITY AND MAINTAINABILITY	6-1
6.1	Reliability Analysis	6-1
6.2	Maintainability Analysis	6-7
6.2.1	Maintenance Assumptions	6-7
6.2.2	Maintainability Prediction	6-8
6.3	Point Availability	6-11
6.4	References	6-13
7	RECOMMENDATIONS	7-1
7.1	Control and Display	7-1
7.2	Signal Acquisition	7-1
7.3	Other Recommended Developments	7-2
7.3.1	Test Transponder Improvements	7-2
7.3.2	System Reliability Improvements	7-3
7.3.3	System Alignment/Adjustment Improvements	7-3
7.3.4	Test Equipment Upgrading	7-4
7.3.5	Tape Playback Improvements	7-4
7.3.6	PCM Demodulator Improvements	7-4
7.3.7	Automation of the Digital Ranging Equipment	7-5
7.3.8	Signal Switching Facility Improvements	7-5
7.3.9	Terminal Send/Receive Equipment Improvements	7-5
7.3.10	PCM Ground Station Improvements	7-6
7.3.11	Second PCM Bit-Stream Simulate Capability	7-6
7.3.12	Command Loop Improvements	7-7
7.3.13	GRARE Improvements	7-7

TABLE OF CONTENTS (CONTINUED)

	<u>Page</u>
A COMMAND LINK ANALYSIS	
A.1 INTRODUCTION	A-1
A.1.1 Purpose	A-1
A.1.2 Scope	A-1
A.2 TECHNICAL SUMMARY AND CONCLUSIONS	A-2
A.3 SYSTEM DESCRIPTION	A-4
A.3.1 Overall Configuration	A-4
A.3.2 Ground Equipment Configuration	A-5
A.3.3 Space Vehicle Equipment Configuration (Reference 2)	A-6
A.4 ANALYSIS	A-8
A.4.1 Model One (High Bit Rate)	A-9
A.4.2 Model Two (Low and Medium Bit Rates)	A-10
A.4.3 Results of Prior Analysis	A-10
A.4.4 Postdetection Filter Analysis	A-11
A.5 GROUND EQUIPMENT DELAY SETTING	A-16
A.6 CONCLUSIONS	A-17
REFERENCES	A-18
B DATA DISTORTION DUE TO PHASE NONLINEARITIES AND AMPLITUDE RIPPLE	
B.1 GENERAL	B-1
B.2 METHOD OF ANALYSIS	B-1
B.2.1 Selection of Approach	B-1
B.2.2 FM/PM Computer Program	B-3
B.2.3 Distortion Criteria	B-3
B.3 SGLS CONFIGURATION AND CHARACTERISTICS	B-5
B.3.1 Configuration for Analysis	B-5
B.3.2 Phase and Gain Characteristics of Tandem Components	B-5
B.4 RESULTS OF ANALYSIS	B-6
B.5 CONCLUSIONS	B-10
B.6 THE FM/PM SPECTRUM ANALYSIS COMPUTER PROGRAM	B-10
B.6.1 General	B-10
B.6.2 Spectral Analysis of Transmitted Signal	B-11
B.6.3 Spectrum Modification	B-13
B.6.4 Demodulation	B-14
B.6.5 Spectral Analysis of Output Signal	B-15

TABLE OF CONTENTS (CONTINUED)

	<u>Page</u>
C ANGLE TRACKING ACCURACY	
C.1 INTRODUCTION	C-1
C.2 GENERAL DESCRIPTION	C-2
C.2.1 Sources and Types	C-2
C.2.2 Combinative Methods	C-2
C.3 SUMMARY OF TRACKING ERRORS	C-4
C.4 THERMAL ERRORS	C-8
C.4.1 High-Gain Configuration	C-8
C.4.2 Low-Gain Configuration	C-15
C.4.3 Angle Tracking Error Due to Phase Shift and Amplitude Unbalance	C-19
C.5 PROPAGATION ERRORS	C-20
C.5.1 The Atmosphere and Its Effect on Propagation	C-20
C.5.2 Angle Tracking Errors Caused by Multipath at 5° Elevation Angle	C-24
C.5.3 Radome Refraction	C-26
C.6 SERVO ERRORS	C-28
C.6.1 Servo Lag	C-28
C.6.2 Servo Bias Error	C-37
C.7 MECHANICAL ERRORS	C-38
C.7.1 Structural Effects	C-38
C.7.2 Error Due to Antenna Acceleration	C-40
C.8 CALIBRATION ERROR	C-42
C.8.1 Mislevel and Orthogonality	C-42
C.8.2 Encoder Linearity	C-43
C.8.3 RF Beam Collimation	C-44
C.8.4 Site Location Errors	C-45
C.8.5 Polarization Boresight Shift	C-46
REFERENCES	C-48
D EFFECTS OF PHASE SHIFT AND GAIN VARIATIONS ON ANGLE-TRACKING ACCURACY	D-1
D.1 INTRODUCTION	D-2
D.2 PHASE-LOCK TRACKING	D-2
D.2.1 Tracking Model	D-9
D.2.2 Effects of Differential Phase Shift	D-10
D.2.3 Effects of Amplitude Unbalance	D-11
D.3 CROSSCORRELATION TRACKING	D-11
D.3.1 Tracking Model	D-15
D.3.2 Effect of Differential Time Delay	D-18
D.3.3 Summary of Tracking Errors	

LIST OF ILLUSTRATIONS

<u>Figure</u>		<u>Page</u>
1-1	SCLS System, Simplified Block Diagram	1-2
1-2	SGLS Data Links	1-8
2-1	High-Gain Antenna Feed and Comparator	2-2
2-2	Ranging, Simplified Block Diagram	2-4
2-3	Range-Rate Processing, Simplified Block Diagram	2-7
2-4	Azimuth Error vs Elevation Angle (High-Gain Antenna)	2-11
2-5	Elevation Error vs Elevation Angle (High-Gain Antenna)	2-11
2-6	Azimuth Error vs Elevation Angle (Low-Gain Antenna)	2-11
2-7	Elevation Error vs Elevation Angle (Low-Gain Antenna)	2-11
2-8	Range-Code Acquisition Time for 99.9% Probability of Acquisition	2-14
2-9	Clock-Loop Noise Bandwidth vs Ranging Signal Power	2-14
3-1	SGLS Downlink Services	3-2
3-2	Downlink Baseband	3-4
3-3	SGLS Ground Receiver Simplified Block Diagram	3-7
3-4	PCM Decommunication Equipment Block Diagram	3-12
3-5	PCM Codes	3-13
3-6	IM Distortion Model	3-18
3-7	SGLS High-Gain RF Configuration	35/36
3-8	SGLS Low-Gain RF Configuration	35/36
3-9	SGLS High-Gain Noise Temperature Model	3-37
3-10	SGLS Low-Gain Noise Temperature Model	3-37
3-11	Noise Temperature of a Typical Directional Antenna	3-39
3-12	SGLS High-Gain Dynamic Range	3-40
3-13	SGLS Low-Gain Dynamic Range	3-41
3-14	Space Loss vs Vehicle Range	3-52
3-15	Downlink Carrier 1 Performance (High-Gain Antenna-FM Services)	3-55/3-56
3-16	Downlink Carrier 1 Performance (High-Gain Antenna-PCM Services)	3-55/3-56
3-17	Downlink Carrier 2 Performance (High-Gain Antenna-PCM Services)	3-55/3-56
3-18	Downlink Carrier 2 Performance (High-Gain Antenna-FM Services)	3-55/3-56

LIST OF ILLUSTRATIONS (CONTINUED)

<u>Figure</u>		<u>Page</u>
4-1	Characteristics of Uplink Baseband	4-3
4-2	Typical Command Signal Waveform	4-4
4-3	Klystron and TWT Envelope Delay Curves	4-11
4-4	TWT Output vs Load VSWR	4-13
4-5	Transmitter-Receiver Interface, High-Gain SGLS	4-14
4-6	Transmitter-Receiver Interface, Low-Gain SGLS	4-15
4-7	High-Gain Configuration	4-18
4-8	Low-Gain Configuration	4-18
4-9	Space Loss for 1.8 GHz Uplink	4-19
5-1	SGLS System Functional Schematic Block Diagram	5-3
5-2	60-Foot High-Gain (TT&C) Antenna	5-5
5-3	Selective Filter	5-5
5-4	2-GHz Parametric Amplifier	5-6
5-5	Down Converter	5-7
5-6	2-GHz Noise Source	5-7
5-7	S-Band Vertex Horn	5-7
5-8	SGLS Antenna Panel	5-8
5-9	Echo Check/Receiver Test Control Unit	5-8
5-10	Transmitting Filter	5-8
5-11	14-Foot Low-Gain (Prelort) Antenna	5-9
5-12	Diplexer	5-9
5-13	SGLS Antenna Panel	5-10
5-14	Spectral Filter	5-11
5-15	Transmitting Equipment Block Diagram	5-11
5-16	Baseband Assembly Unit	5-12
5-17	Baseband Control	5-12
5-18	Transmitter Exciter	5-13
5-19	Transmitter Driver	5-13
5-20	S-Band Power Amplifier	5-14
5-21	Radiation Warning Control	5-15
5-22	Receiving Equipment Block Diagram	5-16
5-23	GRARE	5-17
5-24	Frequency Synthesizer	5-18
5-26	Baseband Separation Unit	5-19
5-27	1.7-MHz Demodulator	5-19
5-29	Digital Ranging Equipment Block Diagram	5-20
5-30	Doppler Frequency Converter	5-21

LIST OF ILLUSTRATIONS (CONTINUED)

<u>Figure</u>		<u>Page</u>
5-31	Range Rate Extractor	5-21
5-32	Telemetry Equipment Block Diagram	5-22
5-33	PCM Demodulator	5-23
5-34	PCM Simulator	5-23
5-35	Control & Display Equipment (SGLS)	5-25
5-36	Data Terminal Equipment (SGLS)	5-27
5-37	Data Terminal Equipment Block Diagram	5-28
5-38	Signal Switching Facility	5-29
5-39	Signal Switching Facility Block Diagram	5-30
5-40	Recording/Playback Block Diagram	5-31
5-41	Ampex FR1600 Magnetic Tape Recorder	5-31
5-42	COMSEC Equipment	5-32
5-43	COMSEC Equipment Block Diagram	5-32
5-44	Analog Test Unit A	5-33
5-45	Analog Test Unit B	5-34
5-46	Test Transponder & Uplink Monitor	5-34
5-47	Test Transponder	5-35
5-48	Test Transponder Transmitter	5-35
5-49	1.7-MHz Biphasic Modulator	5-36
5-50	Uplink Monitor	5-36
5-51	Equipment Location at the RTS	5-38
5-52	Typical Arrangement of Equipment in the RF Area	5-39
5-53	Preamplifier Transmitter Test Transponder GRARE Driver Type 1	5-41
5-54	Uplink Equipment, Data Terminal A, Type 1, Demodulator, Digital Ranging Equipment	5-42
5-55	High Voltage Power Supply, RF Unit, Beam Control Unit, Heat Exchanger	5-44
5-56	Diplexer, Spectral Filter	5-45
5-57	RWS Control Unit, RDT Status Interface Unit	5-46
5-58	SGLS Control and Display Panels	5-47
5-59	Typical Arrangement of Equipment in the Data Processing Area	5-48
5-60	PCM Equipment	5-49
5-61	Switching and Recording Equipment	5-50
5-62	Data Terminal and Downlink Equipment	5-51
5-63	COMSEC Equipment	5-52
5-64	Antenna-Mounted Equipment - SGLS-60	5-54

LIST OF ILLUSTRATIONS (CONTINUED)

<u>Figure</u>		<u>Page</u>
5-65	Test Transponder and Noise Figure Test Equipment - SGLS-60	5-55
5-66	Transmitting Filter for SGLS-60	5-56
5-67	Typical SGLS Low-Gain Configuration	5-59
5-68	Typical SGLS High-Gain Configuration	5-61
5-69	Tracking Test Configuration	5-69
5-70	Uplink Test Configuration	5-70
5-71	Downlink Test Configuration	5-71
A-1	Statistical Model	A-3
A-2	The Command System	A-4
A-3	Major Components of Baseband Assembly Unit (Ground Equipment)	A-5
A-4	Typical Signal Conditioner for Low and Medium Bit Rates	A-7
A-5	Typical Signal Conditioner for High Bit Rate	A-7
A-6	Typical Command Signal Waveform	A-9
A-7	Model One (for 100-kbaud Bit Rate)	A-9
A-8	Model Two (for Bit Rates of 10 kbauds and Less)	A-10
A-9	Waveform at Lowpass Filter Output for Model One	A-12
A-10	System Degradation vs Sync Uncertainty for Model One	A-13
A-11	Signal at Output of Lowpass Filter for Model Two	A-14
A-12	System Degradation vs Sync Uncertainty for Model Two	A-15
B-1	Calculated Phase Characteristic of 5-Pole Chebyshev Preselector Filter	B-8
B-2	Measured and Calculated Phase Characteristic of 3-Pole Chebyshev Predetection Filter Assembly with $B_{3dB} = 2.716$ MHz	B-9
B-3	Partitioning of Integrant Waveform	B-12
C-1	Azimuth Error vs Elevation Angle (High-Gain Antenna)	C-7
C-2	Elevation Error vs Elevation Angle (High-Gain Antenna)	C-7
C-3	Azimuth Error vs Elevation Angle (Low-Gain Antenna)	C-7
C-4	Elevation Error vs Elevation Angle (Low-Gain Antenna)	C-7
C-5	Tracking Loop for Simultaneous Lobing (Coherent Detection)	C-9
C-6	Typical Amplitudes for Sum and Individual Lobe Patterns	C-9
C-7	Carrier-to-Noise Ratio vs Rms Angle Error (High-Gain Antenna - Coherent Detection)	C-12
C-8	Receiver rms Noise Error vs Antenna Elevation Angle (High-Gain Antenna)	C-12
C-9	Tracking Loop for Simultaneous Lobing (Correlation Detection)	C-13

LIST OF ILLUSTRATIONS (CONTINUED)

C-10	IF Bandwidth SNR vs Rms Angle Error (High-Gain Antenna - Correlation Detection)	C-14
C-11	Tracking Loop for Conical Scan Angle Tracking	C-15
C-12	Carrier-to-Noise Ratio vs Rms Angle Error (Low-Gain Antenna - Coherent Detection)	C-17
C-13	Receiver RMS Noise Error vs Antenna Elevation Angle (Low-Gain Antenna)	C-17
C-14	IF Bandwidth SNR vs RMS Angle Error (Low-Gain Antenna-Square Law Detection)	C-18
C-15	Phase Shift and Amplitude Unbalance Tracking Errors (Azimuth Axis) vs Elevation Angle (High-Gain Antenna)	C-19
C-16	Typical Ray-Path Trajectory	C-22
C-17	Tropospheric Refraction Error for a Standard Atmosphere	C-23
C-18	Total RMS Error in the Predicted Fraction at 2-GHz	C-23
C-19	Ionospheric Refraction Errors	C-24
C-20	Allowable Radome Boresight Shift (High-Gain Antenna)	C-26
C-21	Geometry of Vehicle-to-Tracking-Antenna Relationship	C-29
C-22	Error Curves for 131-nmi Orbit (Azimuth Error vs Time)	C-33/C-34
C-23	Error Curves for 500-nmi Orbit (Azimuth Error vs Time)	C-33/C-34
C-24	Error Curves for 1,000-nmi Orbit (Azimuth Error vs Time)	C-33/C-34
C-25	Error Curve for 500 mni Orbit (Azimuth Error vs Elevation Angle)	C-33/C-34
C-26	Error Curves for 131-nmi Orbit (Elevation Error vs Time)	C-33/C-34
C-27	Error Curves for 500-nmi Orbit (Elevation Error vs Time)	C-33/C-34
C-28	Error Curves for 1,000-nmi Orbit (Elevation Error vs Time)	C-33/C-34
C-29	Error Curve for 500-nmi Orbit (Elevation Error vs Elevation Angle)	C-33/C-34
C-30	Error Curves for 100-nmi Orbit (Azimuth Error vs Time)	C-35/C-36
C-31	Error Curves for 500-nmi Orbit (Azimuth Error vs Time)	C-35/C-36
C-32	Error Curve for 100-nmi Orbit (Elevation Error vs Time)	C-35/C-36
C-33	Error Curves for 100-nmi Orbit (Elevation Error vs Time)	C-35/C-36
C-34	Error Curves for 500-nmi Orbit (Elevation Error vs (Time))	C-35/C-36
C-35	Error Curve for 100-nmi Orbit (Elevation Error vs Elevation Angle)	C-35/C-36
C-36	Tracking Error Due to Feed Sag (Simplified Model)	C-38
C-37	Tracking Error Due to Azimuth Acceleration (High-Gain Antenna)	C-40
C-38	Tracking Error Due to Elevation Acceleration (High-Gain Antenna)	C-40

LIST OF ILLUSTRATIONS (CONTINUED)

<u>Figure</u>		<u>Page</u>
D-1	Model for Phase-Lock Tracking	D-2
D-2	Sum Channel (Σ) Vector Diagram	D-3
D-3	Difference Channel (Δ) Vector Diagram	D-4
D-4	Typical Product Detector	D-5
D-5	Individual Feed Patterns	D-7
D-6	Detector Output Voltage vs Off-Boresight Angle	D-8
D-7	Angle-Tracking Error Due to Phase Shift	D-9
D-8	Boresight Angle Variation Due to Feed Amplitude Unbalance	D-10
D-9	Crosscorrelation Tracking Model	D-11
D-10	Product Detector	D-14
D-11	Error Voltage vs Off-Boresight Angle (Crosscorrelation Tracking)	D-16
D-12	Angle-Error Voltage vs Differential Time Delay (Crosscorrelation Tracking)	D-17

LIST OF TABLES

<u>Table</u>		<u>Page</u>
1-1	Typical Tracking Performance	1-4
1-2	SGLS Command Rates	1-5
1-3	Uplink Baseband Structure	1-6
1-4	Downlink Baseband Structure	1-9
2-1	Orbital Types and Parameters	2-9
2-2	Ranging Error RMS values (ft)	2-13
2-3	Range-Rate Error RMS Values (Ft/Sec)	2-16
3-1	PCM/PM Telemetry Data Rates (kbps)	3-4
3-2	Receiver Sweep Ranges and Rates	3-10
3-3	Carrier 3 Demodulation Options	3-11
3-4	Signal Switching Facility Options	3-16
3-5	SGLS Tape Recorder Capabilities Summary	3-17
3-6	Downlink Distortion Objectives	3-21
3-7	PRN Code Components	3-23
3-8	Computer Intermodulation Program Cases	3-24
3-9	Signal-To-Interference (Intermodulation) Ratio Various Services	3-26
3-10	Signal-To-Interference Calculations at Optimum Modulation Indices	3-32
3-11	System Noise Temperatures	3-33
3-12	SGLS High-Gain Temperature Characteristics	3-38
3-13	SGLS Low-Gain Noise Temperature Characteristics	3-39
3-14	FM Subcarrier Services - Subcarrier Threshold Power Calculations	3-47
3-15	Downlink Service Thresholds, Carrier 1: 1.024-MHz Subcarrier	3-48
3-16	Downlink Service Thresholds, Carrier 1: 1.7-MHz Subcarrier	3-48
3-17	PRN Ranging Threshold	3-49
3-18	Carrier 2 Thresholds	3-50
3-19	Carrier 3 Thresholds	3-50
3-20	Downlink Power Budget, Typical System	3-52
3-21	Carrier 1 Configuration	3-57
4-1	Uplink Baseband Characteristics	4-5
4-2	Command Thresholds	4-5
4-2A	Command Sync Uncertainty	4-6
4-3	Klystron and TWT Envelope Delay Curves	4-11
4-4	Effective Radiated Power (High-Gain SGLS)	4-17
4-5	Effective Radiated Power (Low Gain SGLS)	4-18

LIST OF TABLES (CONTINUED)

4-6	Typical Uplink Power Budget	4-20
4-7	Uplink Power Distribution	4-21
4-8	Bessel and Trigonometric Functions of Modulation Angle	4-22
4-9	Typical Uplink Threshold Levels	4-22
6-1	SGIS Equipment Mean-Time-Between-Failures (MTBF)	6-2
6-2	Matrix of Equipment Required for Operational Functions (High-Gain Configuration)	6-4
6-3	Matrix of Equipment Required for Operational Functions (Low-Gain Configuration)	6-5
6-4	Mean-Time-Between-Failures (MTBF) For SGIS Functions (High-Gain Configuration)	6-6
6-5	Mean-Time-Between-Failures (MTBF) For SGIS Functions (Low-Gain Configuration)	6-6
6-6	SGIS Equipment Corrective Maintenance Downtime (M_{ct}) and Failure Rates (λ)	6-10
6-7	Mean-Time-To-Repair (MTTR) for SGIS Functions (High-Gain Configuration)	6-12
6-8	Mean-Time-To-Repair (MTTR) for SGIS Functions (Low-Gain Configuration)	6-12
A-1	IF Signal-to-Noise Ratio and Sync Jitter	A-10
B-1	Measured Phase and Loss Characteristics of Predetection Filter Assembly	B-7
C-1	Angle Tracking Accuracy	C-1
C-2	High-Gain Antenna	C-5/C-6
C-3	High-Gain Antenna	C-5/C-6
C-4	Low-Gain Antenna	C-5/C-6
C-5	Low-Gain Antenna	C-5/C-6
C-6	Coherent Detection (High-Gain Configuration)	C-10
C-7	Crosscorrelation Detection (High-Gain Configuration)	C-14
C-8	Coherent Detection (Low-Gain Configuration)	C-16
C-9	Summary of Angle Tracking Errors Due to Phase Shift and Amplitude Unbalance (High-Gain Antenna)	C-19
D-1	Summary of Angle-Tracking Errors Due to Differential Phase Shift and Amplitude Unbalance	D-18

INTRODUCTION

This volume, in two parts, contains a technical description of the Space-Ground Link Subsystem (SGLS) ground station. "Part 1, Ground Station Design" presents an overview (Section 1) of the entire system. This is followed by a presentation (Sections 2, 3, and 4) of SGLS functional services and their interrelationships. Section 5 describes the ground station equipment items (including their typical arrangement at a remote tracking station) and the SGLS self-test capability. Section 6 contains reliability and maintainability analyses. Recommendations related to future SGLS system developments are presented in Section 7.

"Part 2, Appendices" includes analyses that support Part 1 but are considered too detailed for inclusion in the main body of the volume.

LIST OF ABBREVIATIONS

AFSCF	Air Force Satellite Control Facility
Bi ϕ	biphase
bps	bits per second
CAD	correlation amplitude detector
CCP	cross-connect panel
CDRL	contract data requirement list
CNR	carrier-to-noise ratio
C/N	(same as CNR)
COMSEC	communication security
DCB	digital command buffer
DCBSU	digital command buffer switching unit
DRE	digital ranging equipment
ERP	effective radiated power
FDM	frequency division multiplex
FSK	frequency shift key
GHz	gigahertz (10^9 Hz)
GRARE	ground receiver and analog ranging equipment
Hz	hertz
IM	intermodulation
IOB	input-output buffer
I-Q	in-phase quadrature
IRIG	Inter-Range Instrumentation Group
kbps	kilobits per second (10^3 bps)
kHz	kilohertz (10^3 Hz)
LO	local oscillator
LRU	line-replaceable unit
MHz	megahertz (10^6 Hz)
MPF	multipurpose feed
MPP	master patch panel
MTBF	mean time between failures
NRZ	nonreturn to zero
O&M	operation and maintenance



WDL Division

PLL	phase lock loop
p/o	part of
PRN	pseudorandom noise
PSK	phase shift key
RAT	receiver-antenna-transmitter
RDT	remote data terminal
RTS	remote tracking station
RTU	receiver test unit
RZ	return to zero
SCF	(see AFSCF)
SDU	spectrum display unit
SGLS	Space-Ground Link Subsystem
S/I	signal-to-interference ratio
SNR	signal-to-noise ratio
S/N	(same as SNR)
SOC	station operator's console
SSF	signal switching facility
SPB	station program board
STC	Satellite Test Center
TDP	telemetry data processor
TLM	telemetry
TOR	technical operating report
TSRE	terminal send and receive equipment
TT&C	tracking, telemetry, and command
TTR	test transponder receiver
TTT	test transponder transmitter
VCO	voltage-controlled oscillator
VCXO	voltage-controlled crystal oscillator
VFO	variable frequency oscillator
VPG	verification pulse generator
VSWR	voltage standing wave ratio

SECTION 1

SYSTEM OVERVIEW

The Space-Ground Link Subsystem (SGLS) communication link includes tracking, telemetry, and command capability multiplexed on RF carriers that utilize a common antenna for both uplink transmission and downlink reception. The system (see Figure 1-1) operates in a CW mode with either of two types of antenna subsystems: a low-gain configuration with a 14-foot parabolic reflector (Prelort antenna) or a high-gain configuration with a 60-foot parabolic reflector (TT&C antenna). Overall system performance is essentially the same, except for the additional gain the 60-foot antenna provides.

This section reviews the general requirements for SGLS, provides an overview of the system, and summarizes the ground station command and control capability. Since the design of the spacecraft subsystem was accomplished under other Air Force contracts, only a brief discussion of the vehicle is included here to show the general relationship between ground-to-space (uplink) and space-to-ground (downlink) links. Subsequent sections of the report are concerned with the ground station equipment.

1.1 REQUIREMENTS SUMMARY

Aerospace Report No. TOR-669 (6110-01)-54, Satellite Control Facility Design Criteria: Overall Space-Ground Link Subsystem, defines the general design requirements for the ground station equipment. The more significant of these requirements are briefly summarized below.

- a. The Space-Ground Link Subsystem (SGLS) will be the major subsystem to be used as a prime source of tracking, telemetry data, and command and control capability in support of all satellite programs that are serviced by the Air Force Satellite Control Facility (AFSCF).

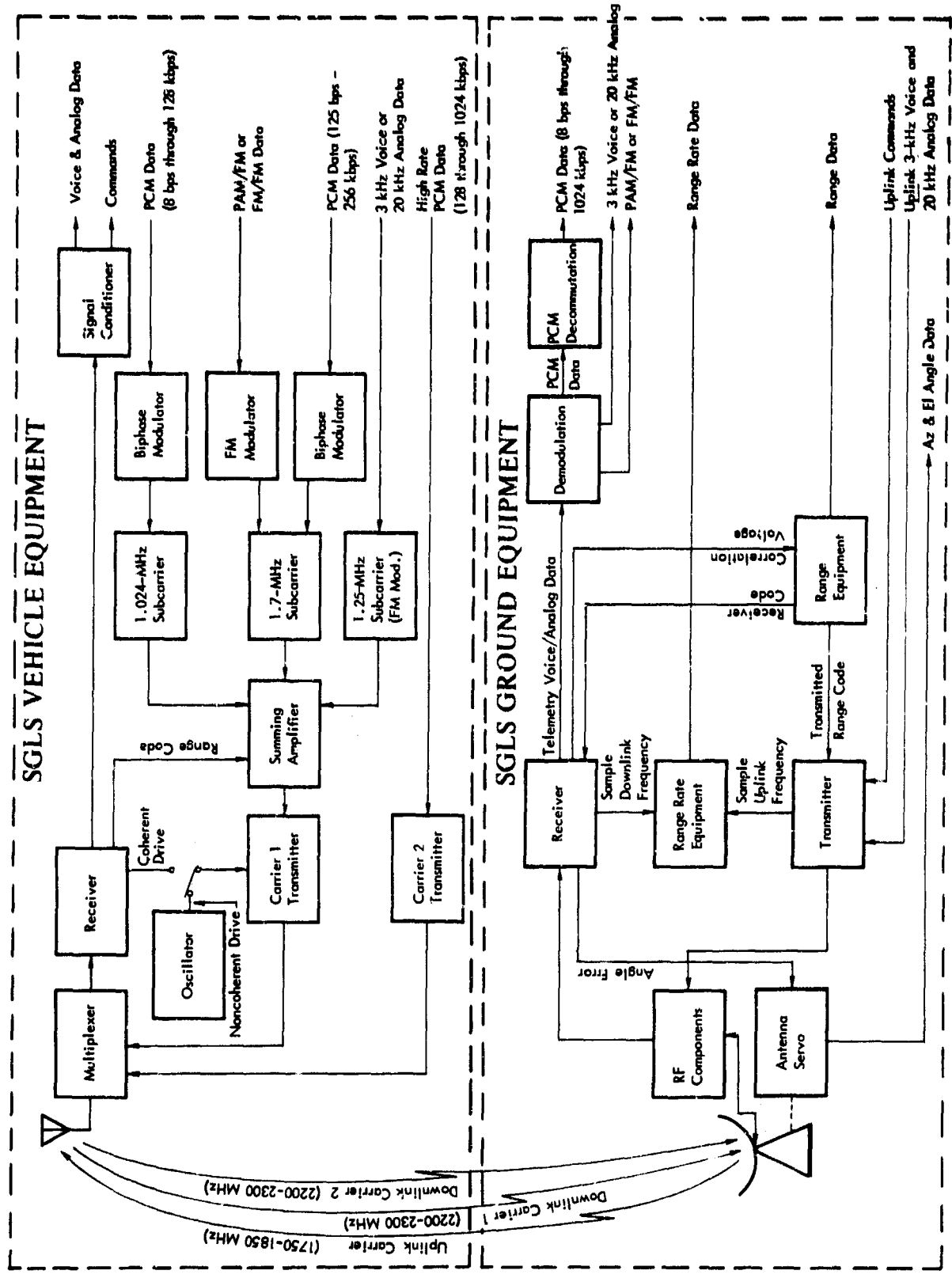


Figure 1-1 SGLS System, Simplified Block Diagram

- b. The uplink services must include:
 - Commanding in a digital format, as well as a means for verifying correct command transmission
 - Analog data and voice communication channels to the spacecraft
- c. The downlink services to be provided must include:
 - PCM telemetry data reception, demodulation, and decommutation
 - PAM/FM or FM/FM telemetry data reception
 - Analog-data or voice-communication channels from the spacecraft
- d. The subsystem must (1) provide for automatic tracking of the spacecraft and (2) output the following:
 - Azimuth and elevation angle data
 - Spacecraft range and range rate
- e. The subsystem must interface with, and perform in conjunction with, other equipment items at the remote tracking stations (RTS) of the Satellite Control Facility (SCF).
- f. The subsystem must provide a secure communication link with the spacecraft.

Detailed requirements are contained in General Specification WDL-SS-167211B,
Performance and Design Requirements for the Space-Ground Link Subsystem
Ground Station.

1.2 TRACKING

Both high- and low-gain SGLS configurations provide an automatic tracking capability in either a phase-locked or crosscorrelation mode of operation. The high-gain antenna uses simultaneous lobing techniques, while the low-gain antenna uses conical scanning. Automatic signal acquisition is accomplished by simultaneous space and frequency search using variable sector and frequency scan widths and rates. Measurement of range rates requires a coherent relationship between the

signal transmitted to the spacecraft and the return signal received by the ground station. This relationship is discussed briefly in Paragraphs 1.3 and 1.4 and more fully described in Section 2. Typical tracking capability is tabulated in Table 1-1.

TABLE 1-1
TYPICAL TRACKING PERFORMANCE

Parameter	Phase Lock Mode	Wideband (Crosscorrelation) Mode
Tracking Bandwidth	1.0 kHz 0.8 kHz	35 MHz 3 MHz 0.5 MHz
Frequency Tracking Range	+200 kHz (max)	N/A
Frequency Tracking Rate	14 kHz/sec (max)	N/A
Angle		
Rate	at least 3 deg/sec	
Error	1 mrad rms (typical for elevation angles below 70°)	
Readout	16 bits or 17 bits	
Resolution	10 sec or 20 sec	
Range		
Error	30 ft rms (-120 dBm at receiver input, neglecting propagation effects)	
Readout	30 bits, 10 samples/sec max	
Maximum Unambiguous Range	at least 400,000 nmi	
Resolution	7.8 ft	
Range Rate		
Error	0.2 ft/sec rms	
Readout	24 bits at 1 sample/sec	
Resolution	0.036 ft/sec	
Maximum Range Rate	49,000 ft/sec	

1.3 UPLINK

The uplink operates on one of 20 preset channels in the 1750- to 1850-MHz frequency band and uses a single carrier for transmission of multiplexed commands, pseudo-random noise (PRN) ranging code, and analog data to the spacecraft.

1.3.1 Commanding

Uplink commands are transmitted in ternary digital formats. Command data is transmitted by frequency shift keying (FSK) three-command tone oscillators corresponding to the "1", "0", and "S" pulses of the ternary format. Table 1-2 shows the baud rates for the low, medium, and high command rates. A clock, or command sync signal, is also transmitted by amplitude modulation of the tone oscillator output.

TABLE 1-2

SGLS COMMAND RATES

Command Rate	Bauds
Low	1, 20
Medium	100, 1000, 2000
High	10,000 & 100,000

To provide a means of confirming that no errors were introduced in the transmitted commands, the uplink carrier is sampled and command data detected to permit an echo check (bit-by-bit comparison) of the commands initiated versus the commands transmitted. This comparison is accomplished in the RTS data handling complex.

1.3.2 Analog and Ranging Data

In addition to digital commands, analog data and voice signals can be relayed from the RTS control complex to the spacecraft via the SGLS uplink. One analog channel with a 20-kHz information bandwidth and one voice channel with a 3-kHz information bandwidth are available. Analog data frequency modulates a 1.25-MHz subcarrier while voice signals frequency modulate a 30-kHz subcarrier.

The FSK command signals, the 1.25-MHz analog subcarrier, and the 30-kHz voice subcarrier are combined with a PRN ranging code; the resulting composite baseband is phase modulated on the uplink carrier. Figure 1-2 depicts this uplink frequency spectrum and Table 1-3 summarizes the uplink baseband structure.

TABLE 1-3
UPLINK BASEBAND STRUCTURE

Data Type	Data Bandwidth or Bit Rate	Subcarrier Frequency	Subcarrier Modulation	Subcarrier Deviation
Voice	0.2 to 3 kHz	30 kHz	Frequency modulation	±3 kHz maximum
Analog	0.1 to 20 kHz	1.25 MHz	Frequency modulation	±30 kHz
PRN Range Code or Range Clock Commands	1 Mbps 0.5 MHz 1 bps-100 kbps	N/A N/A 2.05 kHz-1.073 MHz	N/A N/A Frequency shift keyed	N/A N/A Variable *
Command Sync	N/A	N/A	Amplitude modulation	N/A

*See Table 4-1 for subcarrier frequencies.

In the vehicle, the multiplexed information is recovered and processed to accomplish the various spacecraft control functions. In addition, the uplink carrier is sampled in the vehicle receiver to derive a coherent drive for the Carrier 1 downlink transmitter.

Further, the ranging code is detected, multiplexed with other vehicle data, and retransmitted on Carrier 1 for subsequent range measurement in the ground station.

1.4 DOWNLINK

The downlink operates in the 2200- to 2300-MHz frequency band and provides for transmission of PCM telemetry, wideband analog data, and either one 3-kHz voice channel or one 20-kHz analog channel. Two downlink carriers are used. Carrier 1 is phase coherent with the uplink carrier, Carrier 2 is noncoherent and is centered 5 MHz below the frequency of Carrier 1. Figure 1-2 illustrates these relationships.

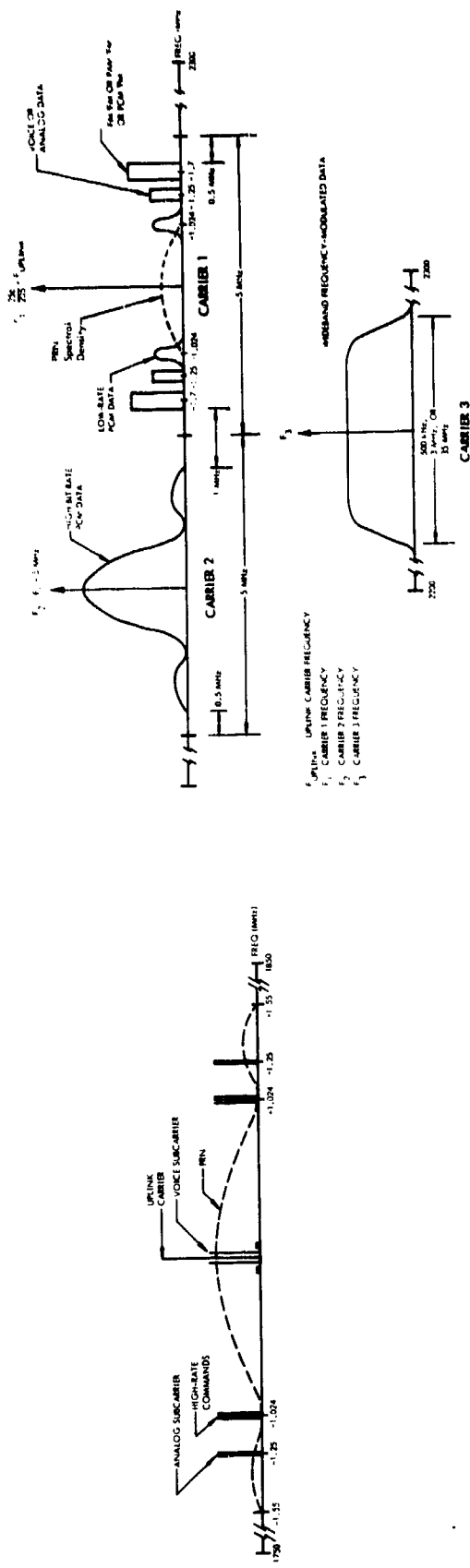
1.4.1 Carrier 1

Data multiplexed on Carrier 1 includes the following:

- PCM telemetry data biphase modulated on a 1.024-MHz subcarrier with rates ranging from 8 bps through 128 kbps
- Wideband analog data (PAM/FM or FM/FM) frequency modulated on a 1.7-MHz subcarrier (The 1.7-MHz subcarrier may provide additional PCM telemetry instead of PAM/FM or FM/FM through biphase modulation of the subcarrier at rates ranging from 125 bps through 256 kbps.)
- One 3-kHz voice channel or one 20-kHz analog data channel frequency modulated on a 1.25-MHz subcarrier.

The PRN ranging code is combined with this data and the resulting composite baseband phase modulates the Carrier 1 transmitter. Table 1-4 summarizes the baseband structure of Carrier 1.

In the ground station, the received range code is compared with the original transmitted code to determine the round trip delay. The latter is then converted to vehicle range. Range rate is derived from a measurement of the two-way doppler shift on coherent Carrier 1.



DOWNLINK

FREQUENCY:	1750 to 1850 MHz; 20 preset channels
POWER:	10 to 10,000 W, adjustable
POLARIZATION:	High gain (60 ft), right-hand circular; low gain (14 ft), selectable, right-hand or left-hand circular, or vertical linear
COMMAND:	Ternary PCM/FSK/PM
COMMUNICATIONS:	Analog FM/PM and Voice-FM/PM
RANGE:	PRN
ANTENNA GAIN:	High gain (60 ft), 46 dB minimum; low gain (14 ft), 34 dB minimum

FREQUENCY:	2200 to 2300 MHz, coherent		
POWER (TYPICAL):	50 mW, 2 W, 20 W		
CARRIER 1	(Coherent with Uplink) Low rate PCM/PSK/FM PAM/FM/PM, FM/PCM/PM, or PCM/PSK/PM		
TELEMETRY:	Analog-FM/PM or Voices-FM/PM		
COMMUNICATIONS:	RANGE AND RANGE UPDATE: RANGE RATE:		
CARRIER 2	(Noncoherent, 5 MHz below C) High-rate PCM/PSK/PM		
TELEMETRY:	TELEMETRY: ANTENNA GAIN:		
CARRIER 3	Wideband data link FM modulator High gain, 48 dB; low gain, 34 dB		

Figure 1-2 SGLS Data Links

TABLE 1-4
DOWNLINK BASEBAND STRUCTURE

CARRIER 1				
Data Type	Data Bandwidth or Bit Rate	Nominal Subcarrier Frequency	Subcarrier Modulation	Subcarrier Deviation
Voice or Analog	0.1 to 3.5 kHz 0.1 to 20 kHz	1.25 MHz	FM	3.0 kHz peak to peak voice 18 kHz peak to peak analog
IRIG Telemetry or PAM or PCM	Channels 1-21 and A-H to 20 kHz 0.125 to 256 kbps	1.7 MHz 1.7 MHz 1.7 MHz	FM FM PSK (biphase)	75 kHz peak to peak 75 kHz peak to peak ±90°
PCM	0.0076 to 128 kbps	1.024 MHz	PSK (biphase)	±90°
PRN Ranging Code or Range Clock	1 Mbps 0.5 MHz	N/A N/A	N/A N/A	N/A N/A
CARRIER 2				
Data Type	Data Bandwidth or Bit Rate	Carrier Frequency	Carrier Modulation	
PCM	128 to 1024 kbps	5 MHz below Carrier 1	Direct biphase	
CARRIER 3				
Data Type	Data Bandwidth or Bit Rate	Carrier Frequency Band	Carrier Modulation	
Wideband Data	30 Hz to 200 kHz 30 Hz to 1 MHz 30 Hz to 10 MHz	2200 MHz to 2300 MHz	FM	

1.4.2 Carriers 2 and 3

The Carrier 2 transmitter is directly biphase modulated by PCM telemetry data at rates ranging from 128 through 1024 kbps. Provision is also made for noncoherent tracking and demodulation of a very wideband direct modulation carrier (designated as Carrier 3) with information bandwidths ranging from 200 kHz to 10 MHz available. Table 1-4 also summarizes the baseband structure of Carriers 2 and 3.

1.4.3 PCM Telemetry

Two bit streams can be processed simultaneously by using two identical PCM decommutation equipment items. Data processing control is provided by the RTS data handling and control/display subsystems that operate in conjunction with computer programs stored in the magnetic core memory of each decommutation equipment item. Processed data is outputted to the RTS data handling subsystem for further reduction and subsequent transmission to the Satellite Test Center (STC). PCM data in various standard IRIG formats can be decommutated and processed by the ground station.

In addition to the digital information provided to the RTS data handling subsystem, each decommutator provides 20 analog and 32 discrete (relay) outputs to the RTS FM/FM ground station. These RTS interfaces are discussed further in Paragraph 3.1.3.

To facilitate prepass checkout and aid in maintenance activity, a PCM simulator that duplicates the function of a spacecraft PCM telemetry package is provided. The simulator, which contains a separate magnetic core memory, may be loaded with diagnostic programs to permit fault isolation on the primary data paths within each decommutator.

1.4.4 Data Recording

In addition to handling a full complement of data in real time from a SGLS instrumented spacecraft, signals may be recorded on magnetic tape for non-real-time processing. Two identical seven-track recorders, with selection of input and output signals controlled by prepunched IBM cards, make available a wide variety of recording and playback configurations to satisfy diversified program requirements.

1.4.5 Analog Data

As shown in Table 1-4, Carrier 1 has either PCM data or PAM/FM or FM/FM telemetry data available on the 1.7-MHz subcarrier. Ground station processing is limited to one of the three data types since they use a common subcarrier. PAM/FM (or FM/FM) data are translated from the subcarrier frequency (1.7 MHz) to 10 MHz and provided to the RTS FM/FM subsystem for subsequent demodulation and data processing. PCM data on the 1.7-MHz subcarrier are demodulated, decommutated, and outputted to the RTS data handling subsystem.

Carrier 1 also provides a 3-kHz voice channel or a 20-kHz analog data channel frequency modulated on a 1.25-MHz subcarrier. Following demodulation in the SGLS ground station, these signals are available to the RTS.

1.4.6 Communications Security

The SGLS ground station design is compatible with Communications Security (COMSEC) equipment to permit either clear or encrypted uplink command transmission and processing of either clear or encrypted downlink telemetry data. Selection of secure or clear modes of operation is controlled by the RTS data handling subsystem.

SECTION 2

TRACKING SUPPORT

SGLS tracking support permits determination of spacecraft ephemeris through measurement of the relative position and motion of the vehicle. This support consists of azimuth and elevation angle tracking, range tracking, and range-rate determination. This section describes how each of these support functions is accomplished and summarizes the results of analyses that were conducted to determine their expected performance.

2.1 TRACKING FUNCTIONAL DESCRIPTION

2.1.1 Angle Tracking

Each of the two antenna types that interface with SGLS uses a different technique for developing angle-error signals. The high-gain antenna uses simultaneous lobing, while the low-gain antenna uses conical scan. The receiver is designed for operation with either technique.

Simultaneous Lobing

Angle-error signals are generated in the high-gain antenna by an amplitude-comparison simultaneous-lobing feed and comparator. The feed arrangement and comparator network combine the signals from two pairs of feed horns to form a sum (or reference) signal and two orthogonal error (or difference) signals.

Figure 2-1 shows the arrangement of this equipment. When the antenna is pointed at the source, the output of the sum channel is at a maximum, and the outputs of the error channels are zero. Misalignment of the antenna produces error-channel signals whose phase, relative to the reference channel, indicates the direction of displacement, and whose amplitude, for small displacements, is directly proportional to the angular misalignment. These signals are fed to the three-channel

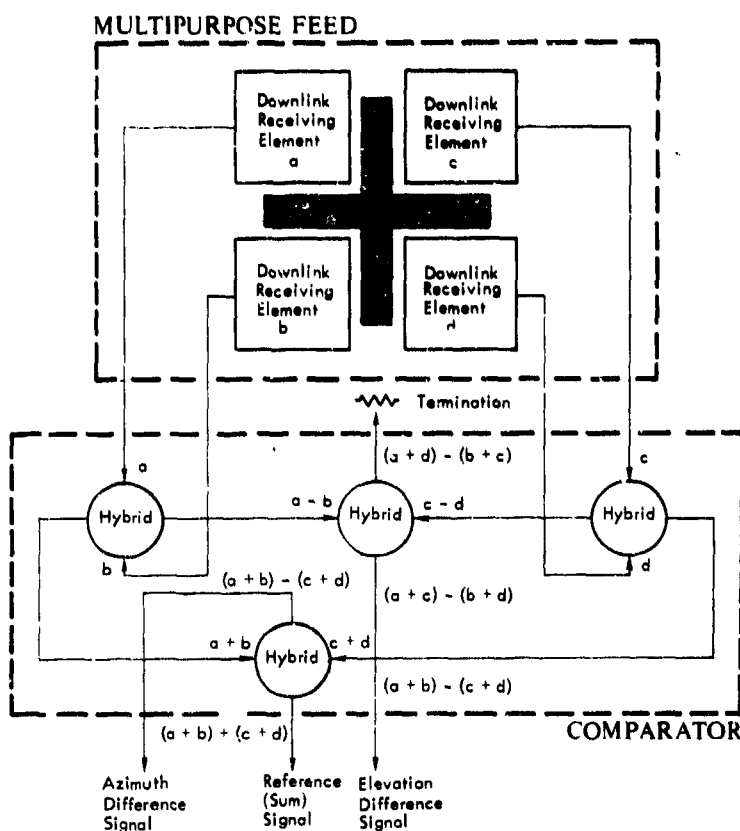


Figure 2-1 High-Gain Antenna Feed and Comparator

receiver. The sum channel (reference) receiver is a triple-conversion phase-lock design. The error-channel receivers are similar with gains normalized to the sum channel gain by AGC.

The output of the two error-signal demodulators are voltages whose polarity represents direction of angle error and whose amplitude represents the magnitude of the error. These voltages are applied to the azimuth and elevation control inputs of the antenna servo system. Angle data for entry into the RTS computer are derived from digital encoders on azimuth and elevation axes of the antenna.

Conical Scan

The low-gain antenna is a conical-scan tracking antenna. A nutator in the feed causes the electrical axis to describe a cone about the antenna's mechanical axis. Any signal not on the antenna axis will be amplitude-modulated, with the tracking error magnitude represented by the amplitude, and the error direction by the phase, of the error signal. The sum-channel receiver and one error-channel receiver are used. Both are fed from the conical-scan feed. The output of the error-channel receiver is a sine wave (obtained by demodulating the signal envelope) that carries the relative amplitude and phase of the error modulation.

Narrowband signals are detected in the phase-lock mode and coherently demodulated by the error-channel receiver. Wideband signals are demodulated by an envelope detector. Use of a separate error-sign~~l~~ receiver permits greater flexibility in selection of AGC characteristics.*

The conscan feed has a reference generator coupled to the nutator shaft, which generates voltages in quadrature. These carry the phase reference for conversion of the receiver error signal into servo error inputs having magnitude and direction.

2.1.2 Ranging

The distance between spacecraft and ground station is determined by measuring the round-trip path delay of a radio signal transmitted to the spacecraft and retransmitted to the station. If the transmitted signal is represented by $f(\omega t)$, then the received signal is $f[\omega(t + \tau)]$, where τ represents the path delay. Since the delay time τ is $2r/c$, where r is the range and c is the velocity of propagation, then the received signal is represented by $f[\omega(t + 2r/c)]$.

In principle, the range can be measured by searching for correlation between the received signal and a replica of the transmitted signal incrementally delayed relative to the transmitted signal. Ambiguities (i.e., multiple correlations) can

*Refer to Volume II, Appendix G for a detailed analysis of AGC selection.

be avoided through use of a function that has a period equal to or greater than the maximum range delay to be measured. SGLS uses a PRN function that is derived by a logical combination of a 500-kHz clock and four independent 1-Mbps binary-coded sequences of PRN codes.

Figure 2-2 is a simplified block diagram of the ranging process. The range measurement is made in two steps. First, the 500-kHz clock component of the received signal is acquired by a phase-locked loop. The phase of the locked oscillator relative to that of the transmitter clock is then measured. The phase measurement is made at the 32nd harmonic of the clock (16 MHz), and threshold circuits identify the phase displacement in increments of $\pi/2$ radians. Each time the phase increments by $\pi/2$, an appropriate number is added to a range tally accumulator. As a consequence, the system tracks the spacecraft with a fixed range error equivalent to $2n\pi$ radians at the clock frequency (equivalent to a $4n$ bit displacement between the transmitted and received PRN sequence).

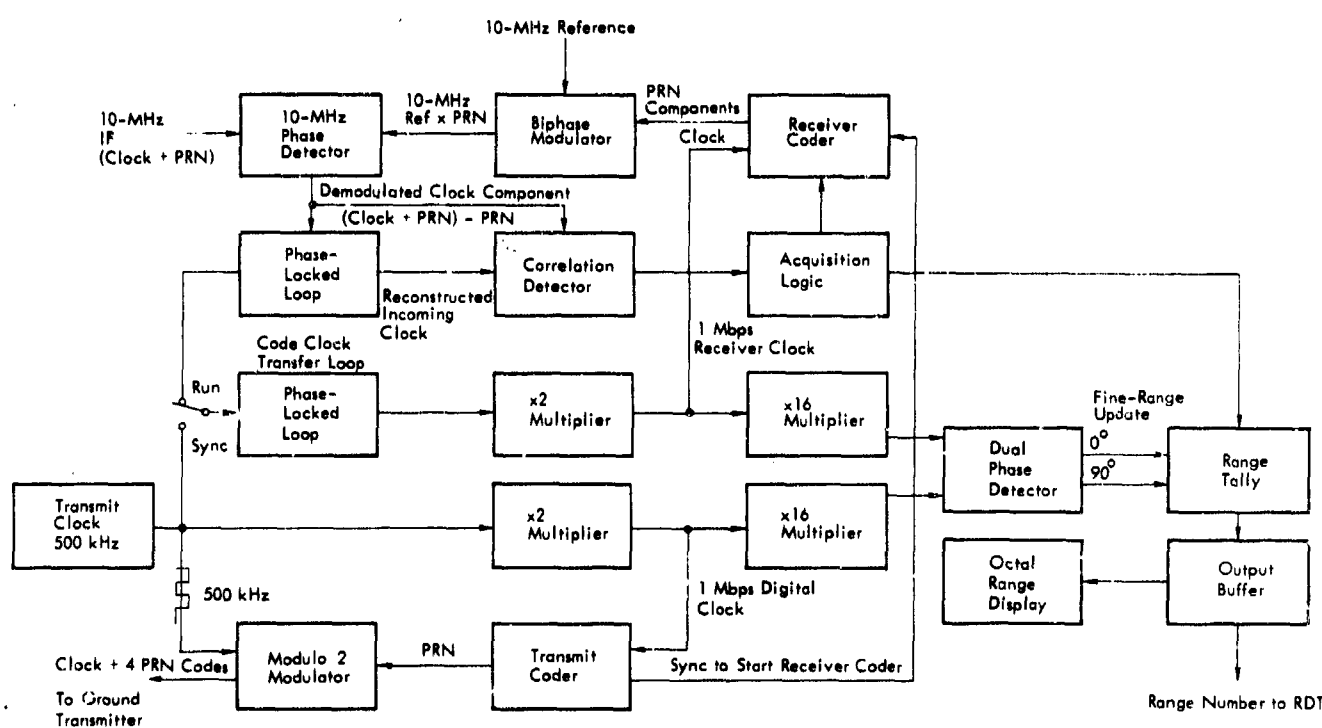


Figure 2-2 Ranging, Simplified Block Diagram

The second step in the range measurement consists of developing a replica of the transmitted code and delaying it long enough to develop maximum correlation of the delayed replica with the received signal. Doppler compression of the received envelope is compensated for by using the locked oscillator (received clock component) for developing the replica. A range number equivalent to this time delay (which is equivalent to the $2n\pi$ radian error previously mentioned) is then added to the accumulator to develop the correct range value.

The SGPS system acquires the received PRN code one sequence at a time, then combines the properly phased sequences in accordance with the same logical function that is used for generating the transmitter code. This technique reduces the acquisition time from a factor proportional to the product of the lengths of the individual sequences to the sum of their lengths.

2.1.3 Range Rate

Range rate is determined by using the vehicle phase-lock transponder, which generates the coherent carrier at a rational fraction of the received frequency (256/205). The vehicle transponder is illuminated by the ground transmitter operating at a frequency of f_t . This produces a received signal at the vehicle of f_t plus one-way doppler shift. This frequency is multiplied by 256/205 and retransmitted to the ground, where it is received with additional one-way doppler. Precise range-rate data may be extracted through appropriate mixing of the received signal with signals from the ground transmitter. Phase-lock techniques are used in the ground receiver to (1) provide an efficient tracking filter for the received carrier, and (2) permit near-optimal demodulation of the telemetry and ranging modulation on this signal.

Figure 2-3 is a simplified block diagram showing the doppler extraction process at the ground station. The doppler frequency is obtained from the reference receiver voltage-controlled oscillator (VCO) output signal. Although this signal is phase-locked to the received frequency, it contains a bias because it is a submultiple of the receiver first local oscillator (LO) frequency.

After down-translation, this signal is mixed with submultiples of the transmitted frequency and then with a multiple of the receiver reference oscillator frequency to remove the bias. The result is a signal that is a function of the transmitted frequency and the two-way doppler shift. This signal, together with a submultiple of the transmitted frequency, is applied to a counting circuit which produces a number that is a function of doppler shift only. This number is treated mathematically by the RTS computer to determine the range rate.

Referring to Figure 2-3, the transmitted frequency is f_t . After multiplication in the space-vehicle transponder and two-way doppler shift, the received frequency (f_{rc}) is

$$f_{rc} = \frac{256}{205} f_t \left(1 - 2 \frac{v}{c} + \frac{v^2}{c^2} \right) \quad (1)$$

Since $c \gg v$, the quadratic term may be neglected, resulting in a frequency (f_r) of

$$f_r = \frac{256}{205} f_t \left(1 - 2 \frac{v}{d} \right) \quad (2)$$

Manipulation of this signal results in an input to counter n_1 with a frequency (f_{n_1}) of

$$f_{n_1} = \frac{f_t}{820} \left(1 + 2048 \frac{v}{c} \right) \quad (3)$$

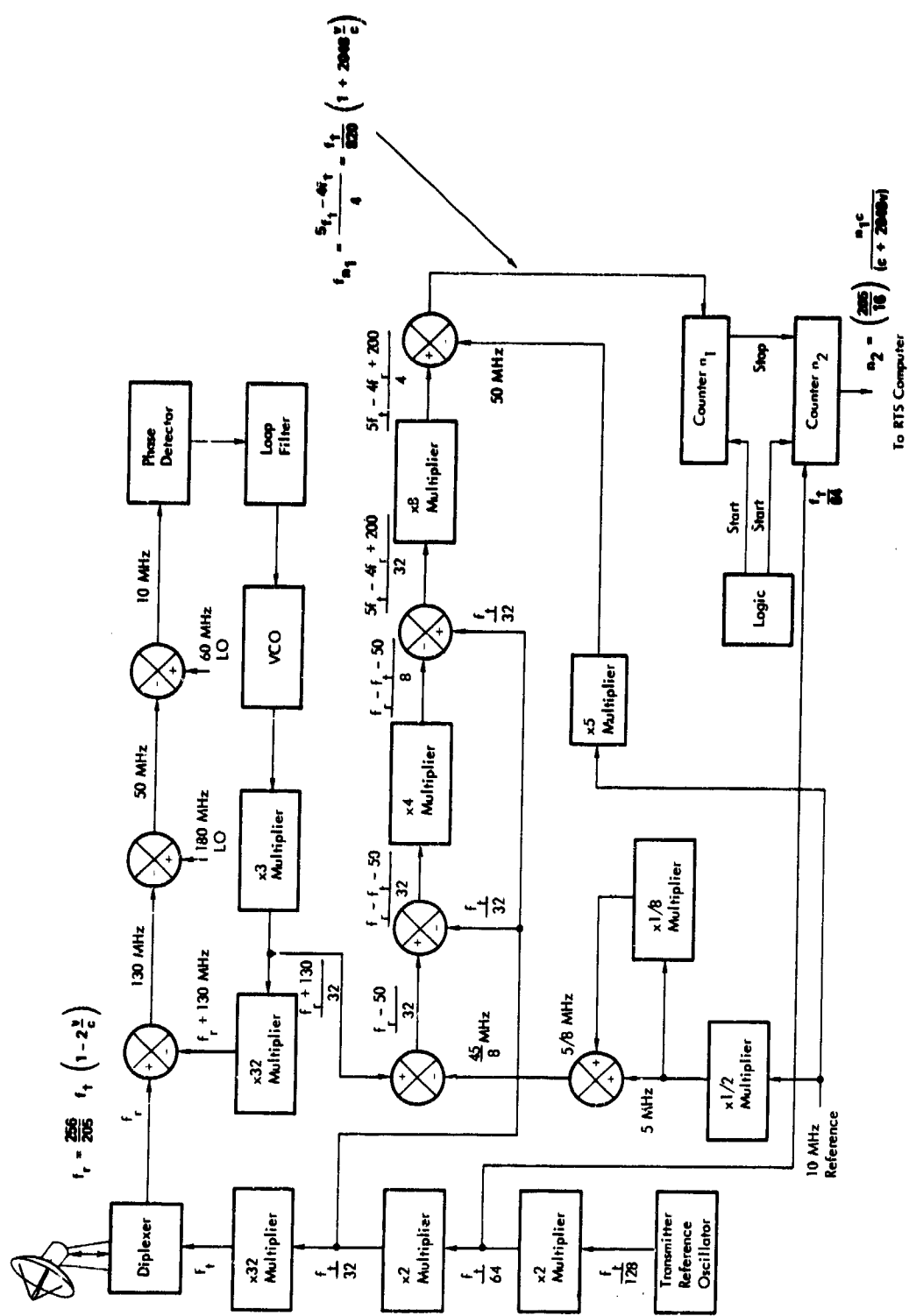


Figure 2-3 Range-Rate Processing, Simplified Block Diagram

The input frequency (f_{n_2}) to counter n_2 is

$$f_{n_2} = \frac{f_t}{64} \quad (4)$$

The counters are arranged such that both counters start simultaneously and counter n_2 is stopped by a signal from counter n_1 . The start of the counters is controlled by switch settings and pulses from the timing terminal unit (TTU). The stop signal for counter n_2 is generated by n_1 when it is filled.

The count contained in n_2 after any period t is

$$n_2 = \frac{f_t}{64} t \quad (5)$$

Now t is determined by the length of time required to fill counter n_1 , which is given by

$$t = \frac{n_1}{f_{n_1}} \quad (6)$$

Substituting this result into Equation (5) gives

$$n_2 = \left(\frac{f_t}{64} \right) \left(\frac{n_1}{f_{n_1}} \right) \quad (7)$$

Again substituting from Equation (3) and collecting terms, we have

$$n_2 = \left(\frac{205}{16} \right) \left(\frac{n_1 c}{c + 2048v} \right) \quad (8)$$

Since n_1 and c are constants, n_2 is a function of velocity only; the effects of transmitted frequency have been eliminated.

2.2 TRACKING PERFORMANCE

Tracking accuracy is affected by error contributions from many sources. Analyses were performed to determine the nature and magnitude of the individual contributors and the overall (rms) error for each tracking function. Since tracking accuracy is also affected by the characteristics of the spacecraft orbit, five examples were considered. Pertinent parameters for the orbits are given in Table 2-1. In summary, the accuracies were determined to be as follows:

- Angle Tracking: less than 1.0 mrad bias error; less than 1.1 mrad rms noise error for both azimuth (secant-corrected below 70°) and elevation
- Ranging: less than 30 ft rms for both bias and noise errors at a carrier power of -120 dBm (referenced to the parametric amplifier input and neglecting the effects of propagation errors)
- Range Rate: less than 0.2 ft/sec rms for both bias and noise errors (neglecting the effects of propagation error)

TABLE 2-1

ORBITAL TYPES AND PARAMETERS

Type of Orbit	Maximum Range (nmi)	Maximum Radial Velocity (10^3 ft/sec)	Maximum Radial Acceleration (ft/sec 2)	Maximum Doppler (kHz)
100,000 nmi (Worst Case)	100,000	40.0	1920	175
50 nmi (Circular)	290	25.4	2150	114
120 nmi (Circular)	600	25.3	1040	114
6000 nmi (Circular)	8,000	6.0	3	26
150 to 60,000 nmi (Elliptical)	60,000	35.4	1430	163

Each of the above tracking functions is discussed in greater detail in the following subparagraphs.

2.2.1 Angle Tracking Accuracy

The basic parameters of interest in a discussion of angle tracking performance are (1) the angular velocity and acceleration requirements for the antenna structure and (2) the system tracking errors.

The peak angular velocity capability (imposed by the servo saturation characteristics) places a fundamental limitation on the ability of a two-axis azimuth-elevation antenna to track vehicles passing close to the zenith. This is the well-known "keyhole effect."

For tracking of low circular orbits to be possible, the approximate inequality

$$\dot{\phi}_{\max} \geq \frac{v}{h} \tan \theta_{el}$$

must hold, where $\dot{\phi}$ is the maximum azimuth angular velocity capability of the antenna, v is the linear velocity and h the altitude of the vehicle. θ_{el} is the maximum elevation angle of the vehicle viewed from the antenna site. To illustrate, for the high-gain antenna, $\dot{\phi}$ is $15^\circ/\text{sec}$, indicating that azimuth tracking capability will be exceeded at elevation angles greater than 81° for a 100-mile circular orbit.

The angular acceleration effect, on the other hand, is a limitation in the sense that acceleration-induced tracking errors in type 2 servo loops can exceed the system angle tracking capability. These considerations are treated in some depth in Part 2 of this volume (Paragraph C.6).

Appendices C and D analyze the various sources of angle tracking errors. These error sources are categorized as: RF, Propagation, Servo, Mechanical, and Calibration, with contributions within these categories originating in some sixteen

sources. Figures 2-4 through 2-7 summarize the error performance of the angle tracking systems for both the high- and low-gain antennas. In all cases, elevation errors are seen to be less than 1 mrad, as are azimuth errors for elevation angles less than about 70°. The rapid increase thereafter is due to the elevation secant correction factor that must be applied to many of the azimuth error terms.

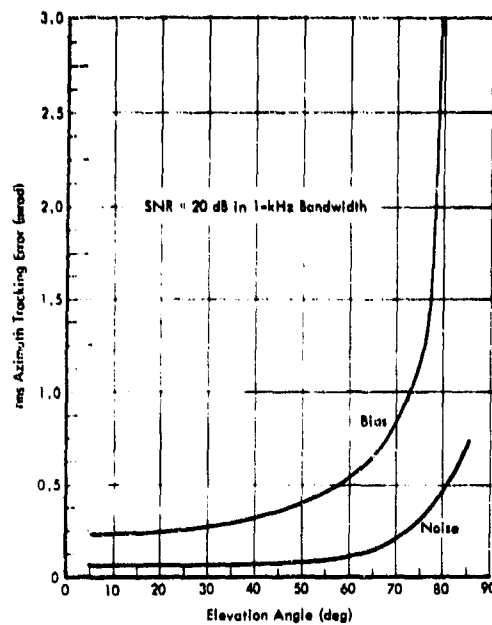


Figure 2-4 Azimuth Error vs Elevation Angle (High-Gain Antenna)

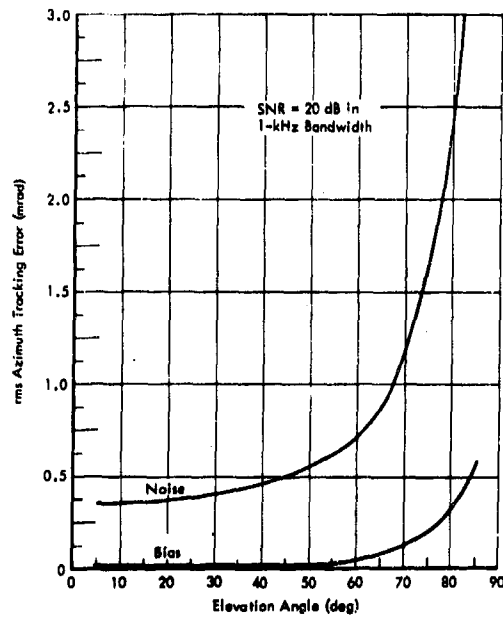


Figure 2-6 Azimuth Error vs Elevation Angle (Low-Gain Antenna)

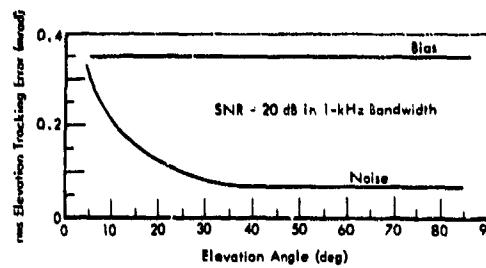


Figure 2-5 Elevation Error vs Elevation Angle (High-Gain Antenna)

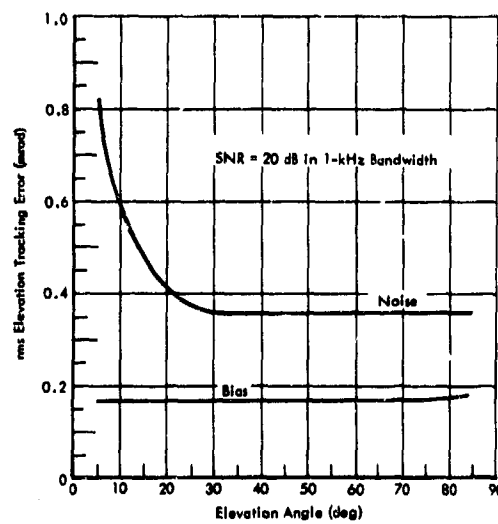


Figure 2-7 Elevation Error vs Elevation Angle (Low-Gain Antenna)

Comparison of the low- and high-gain antennas shows that noise errors exceed bias errors in the low-gain case, whereas the reverse is true for the high-gain antenna. This result is largely due to the collimation and polarization errors assigned to the high-gain antenna, plus the phase and amplitude unbalance errors that apply only to the high-gain simultaneous-lobing tracking antenna.

2.2.2 Ranging Accuracy

PRN ranging system accuracy is affected by the following factors:

- Receiver noise
- Oscillator stability
- Dynamic errors
- Phase instability
- Quantization error
- Time measurement errors
- Propagation errors

Uncertainties in the velocity of light and station location are not included. Some of the error sources produce bias errors that vary slowly with signal level, temperature, and component aging. Others give rise to more rapid fluctuations (noise errors). In Table 2-2, bias and noise error rms values are presented for the orbits listed in Table 2-1. The bias and noise errors for the hypothetical worst case are 36 and 32 ft, respectively.

The random noise analysis (Volume III, Appendix II) shows that at a subcarrier signal-to-noise density ratio of 26.6 dB-Hz, the required accuracy of 30 ft rms can be met. This condition, defined as ranging threshold, includes the effects of uplink noise, which is "turned around" along with the PRN code. For applications that require range and range-rate data only, range and range rate threshold simultaneously when the PRN code deviation is 0.3 rad peak. Acquisition times for the short (5,000 nmi) and long (400,000 nmi) codes are 1 and 4 min, respectively, at threshold (Volume III, Appendix IX). Smaller acquisition times can be traded in direct proportion for increased signal power (Figure 2-8).

TABLE 2-2

RANGING ERROR RMS VALUES (FT)
(Bias and Noise Error rms Values for Orbita of Table 2-1)^a

Error Source	100,000 nmi (Worst Case)		50 nmi (Circular)		120 nmi (Circular)		6,000 nmi (Circular)		150 to 60,000 nmi (Elliptical)	
	Bias	Noise	Bias	Noise	Bias	Noise	Bias	Noise	Bias	Noise
Receiver noise ^b		30.0		----		0.4		4.0		21.0
Oscillator noise	5.0	----	5.0	----	5.0	----	5.0	----	5.0	----
Dynamic errors										
Velocity	10.0		6.3	----			0.1		----	
Acceleration	15.4		----		2.5		----		----	
Phase instability	13.8		13.8		13.8		13.8		13.8	
Quantization		2.3		2.3		2.3		2.3		2.3
Time measurement	10.0	10.0	10.0	10.0	10.0	10.0	10.0	10.0	10.0	10.0
Reflections	7.0		7.0		7.0		7.0		7.0	
Propagations ^c	17.0 ^c	0.3	2.0	0.3	6.0	0.3	17.0 ^c	0.3	8.0	0.3
Total rms error (ft)	36.4	32.0	19.6	10.0	19.6	10.0	25.7	11.0	20.6	23.0

^a Required ranging accuracy: 30 ft (rms) (-120 dBm carrier power at the parametric amplifier input - neglecting propagation error), tropospheric bias error corrected.

^b Downlink Power Budget assumes threshold occurs at 100,000 nmi range.

^c Ionospheric and tropospheric bias errors corrected.

The acquisition times shown do not include the time required for acquiring the 500-kHz clock, which is done automatically. Also, the acquisition times shown in Figure 2-8 are ideal since the integration times for each code phase are available only in binary multiples of a major machine cycle (124 μ sec). These times, therefore, may be optimistic by as much as a factor of 2. Clock-loop bandwidth switching is provided with three bandwidths available; 1, 4, and 12 Hz. The 4-Hz bandwidth would be chosen for normal operation since it combines reasonable dynamic errors with satisfactory noise performance (Volume III, Appendix II). At ranging threshold power levels, the medium bandwidth loop (4 Hz) expands to 28 Hz bandwidth, whereas the wide (12 Hz) loop is about 50 Hz (Figure 2-9). The doppler and frequency uncertainties are in the order of 50 Hz.

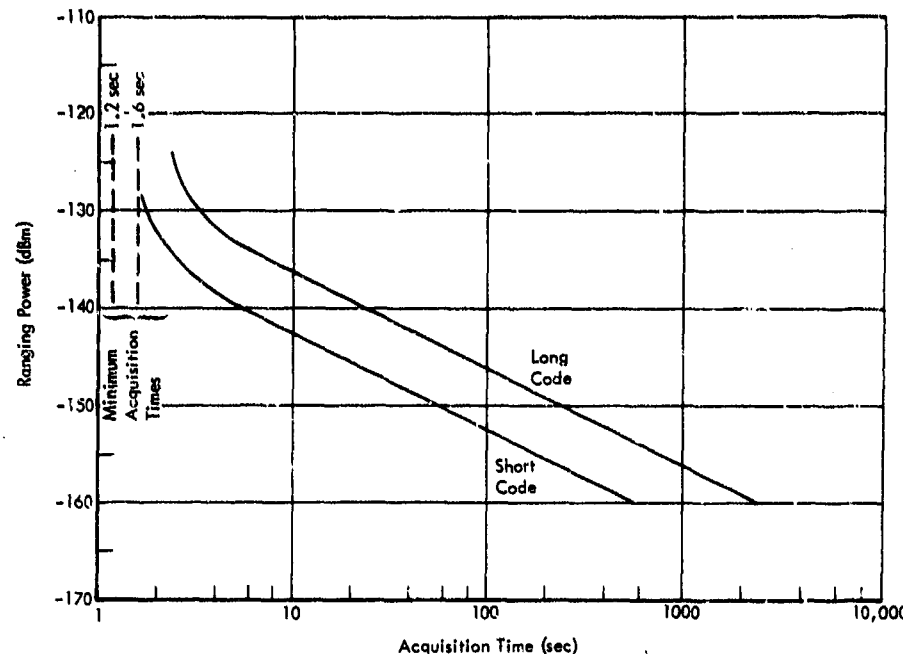


Figure 2-8 Range-Code Acquisition Time for 99.9% Probability of Acquisition

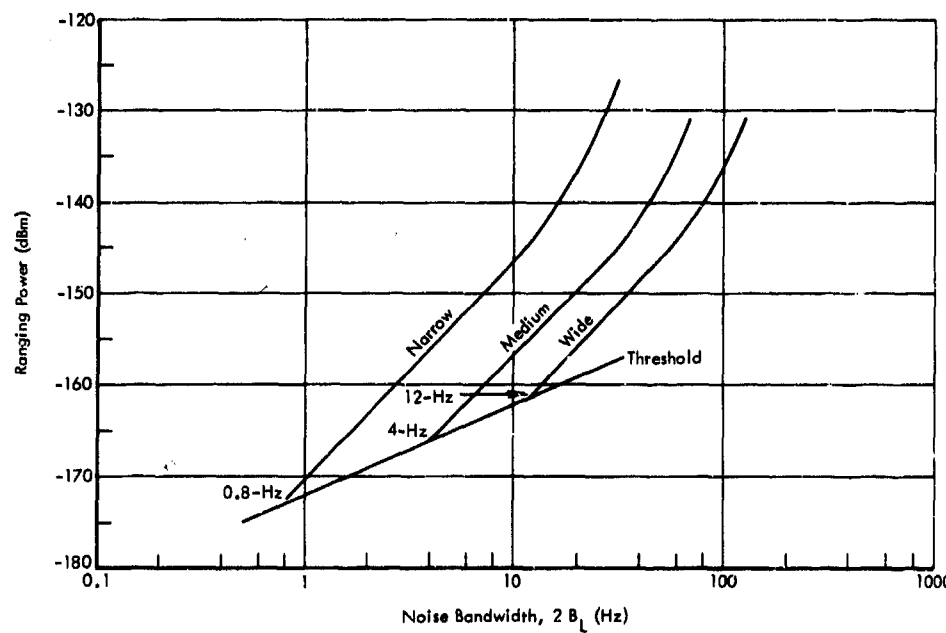


Figure 2-9 Clock-Loop Noise Bandwidth vs Ranging Signal Power

In addition to random noise and dynamic errors, phase instability in the vehicle and ground receivers, quantization, and time measurement errors are important contributors to the total range error. Phase shift variations at 500 kHz have been measured on the SGLS transponder and the ground receiver. The largest contributor (14 ft rms) is the estimated phase error in the analog range extraction equipment (e.g., the range clock loop and code-clock transfer loop) resulting from phase detector unbalance and finite loop gain. Quantization error is in reality the resolution and refers to the smallest time interval which the system can measure. In the error budget, however, the rms value of this quantity is used rather than the maximum value. Timing errors are estimated total values for the digital equipment involved in the range measurement.

Propagation errors caused by the troposphere and ionosphere are significant contributors. The tropospheric bias error may be corrected by measuring the surface refractivity index and assuming a standard refractivity profile. A small residual error should result. The ionospheric error must also be corrected if the desired accuracy is to be achieved; otherwise this error will be about 50 ft for vehicles above 300-nmi altitude. Because of the variability of the ionosphere, the correction is more difficult to make, requiring multiple frequency measurements. A residual error of one-third the bias has been assumed for the higher altitude orbits.

2.2.3 Range-Rate Accuracy

The range-rate error budget involves the definition of the following factors that contribute to the total error (Volume III, Appendix I).

- Thermal noise
- Oscillator noise
- Quantization noise
- Uncertainty in the velocity of light
- Propagation error

WDL-TR3227-1
Volume I, Part 1

TABLE 2-3

RANGE-RATE ERROR RMS VALUES (FT/SEC)
(Bias and Noise Error rms Values for Orbits of Table 2-1)^a

Error Source	100,000 nmi (Worst Case)		50 nmi (Circular)		120 nmi (Circular)		6,000 nmi (Circular)		150 to 60,000 nmi (Elliptical)	
	Bias	Noise	Bias	Noise	Bias	Noise	Bias	Noise	Bias	Noise
Thermal noise		0.018		----		0.0001		0.0002		0.0017
Oscillator noise		0.030		0.0017		0.0018		0.0067		0.0018
Quantization		0.025		0.025		0.025		0.025		0.025
Velocity of light	0.052	0.033	0.034			0.0078		0.049		
Propagation error	0.1 ^b	0.002	0.037 ^b	0.026	0.63 ^b	0.26	0.063 ^b	0.002	0.1 ^c	0.026
Subtotals	0.112	-0.043	0.050	0.036	0.071	0.036	0.063	0.025	0.115	0.036
Total rms error (ft/sec)	0.120		0.062		0.079		0.068		0.120	

^a Required range-rate accuracy: 0.2 ft/sec (rms) neglecting the effects of propagation.

^b Tropospheric bias error corrected.

^c Ionospheric and tropospheric bias errors corrected.

Range-rate errors resulting from these sources are tabulated in Table 2-3 for various orbits.

Total rms errors in all cases satisfy the required range-rate accuracy of 0.2 ft/sec. The worst case and elliptical orbits exhibit the greatest error: 0.12 ft/sec. The greatest contributor in all cases is the propagation error, and in all cases the tropospheric bias error is assumed to be corrected. In addition, for orbits passing near the altitude of the ionospheric F_{max} (160 nmi), the ionospheric bias error must also be corrected in order to achieve the desired overall accuracy. This is the case for the perigee of the elliptical orbit as indicated in Table 2-3. The residual error after correction is assumed to be about one-third of the initial bias. The fluctuation or noise errors caused by the propagation medium are quite acceptable.

Among the other sources of error, uncertainty in the velocity of light is seen to be an important contributor to the bias. Thus, both major error sources are external to SGLS. Furthermore, both are bias errors that are not subject to smoothing over several observations. The SGLS contributions to range-rate errors (thermal noise, oscillator noise, and quantization) are essentially random phenomena, the effects of which can be reduced by repeating sampling. For the worst-case orbit, these three errors are each maximum and about one-tenth of the total accuracy requirement. The thermal and oscillator noise effects are mission-dependent, while quantization error is not.

The quantization error is subject to further reduction should this prove desirable. Since the doppler frequency is measured by counting the cycles (n_2) of a reference oscillator during the time required to complete a predetermined number (n_1) of doppler cycles, the error due to the one-count uncertainty in stopping the reference counter can be reduced by increasing the counting frequency.

SECTION 3

DLWNLINK SERVICES

SGLS downlink services provide for the transmission of telemetry, analog, and voice information from the spacecraft to the ground station. This section describes these services as well as the downlink structure and the signal detection, decommutation, and data distribution functions. This description is followed by an examination of the effects of interference between downlink services and, lastly, by an analysis of downlink performance in terms of system noise temperature, dynamic range, and the various service thresholds. In view of the large number of options available, a procedure is also included to assist the SGLS user in determining the performance of a specific combination of services.

3.1 DOWNLINK FUNCTIONAL DESCRIPTION

3.1.1 Downlink Structure

Downlink services are transmitted on three carriers (Carriers 1, 2, and 3) that are available in a variety of combinations. Services on Carrier 1 are multiplexed on three separate subcarriers, while direct carrier modulation is used on Carriers 2 and 3.

Carrier 1 may be used singly or together with Carrier 2. Carrier 2, however, may not be used except in conjunction with Carrier 1. Use of Carrier 3 precludes the use of the other carriers. These options are illustrated in Figure 3-1.

Carriers 1 and 2 each occupy a 5-MHz RF bandwidth with the Carrier 2 center frequency 5-MHz below the center frequency of Carrier 1. Each of these carriers occupies one of the 20 downlink channels available in the 2200 to 2300-MHz frequency band. A 1-MHz guard band is provided between the two carriers in the adjacent channels.

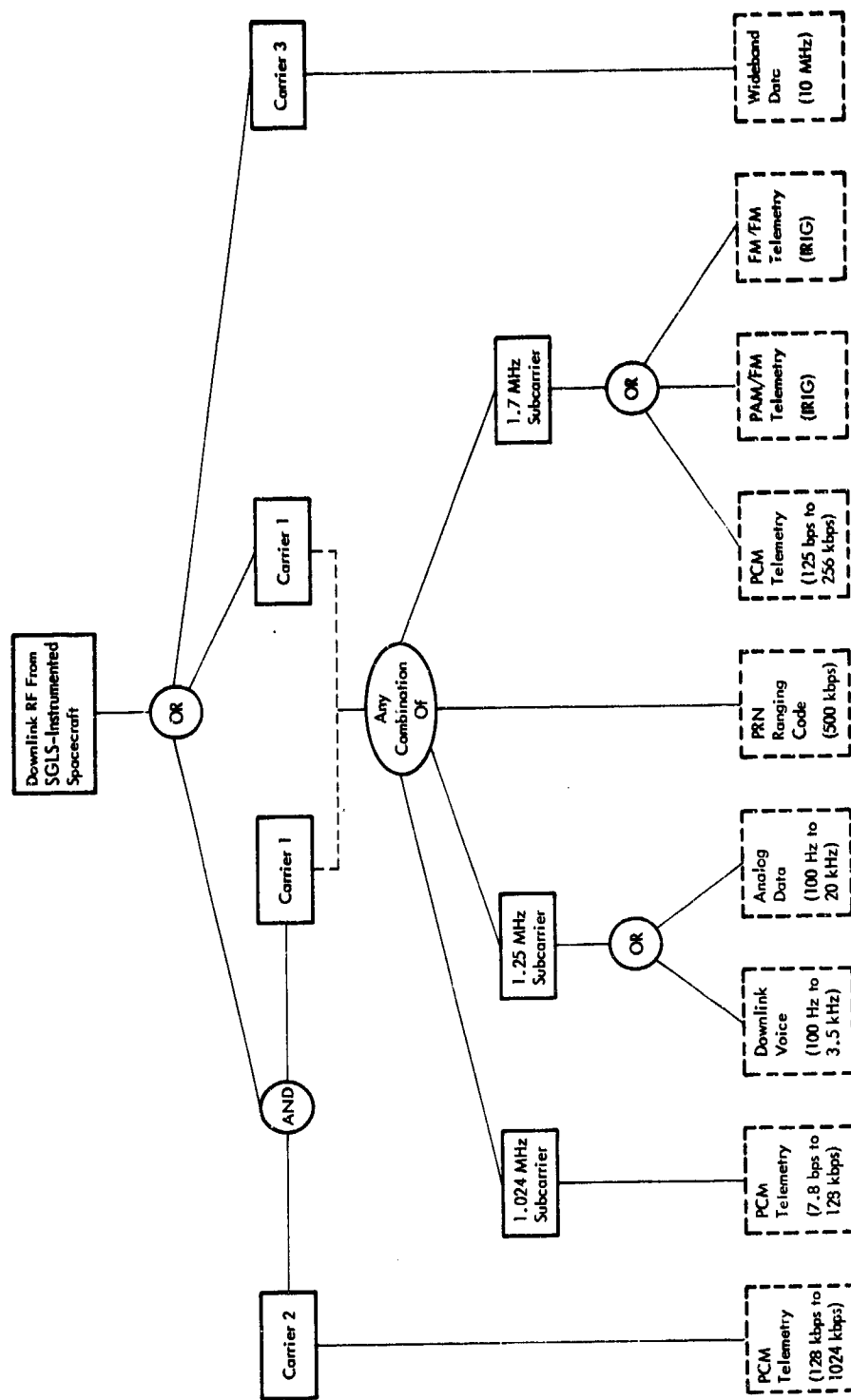


Figure 3-1 SGLS Downlink Services

Carrier 3 occupies up to a 35-MHz RF bandwidth and provides a wideband communication downlink. These frequency relationships are illustrated in Figure 3-2.

Carrier 1

Carrier 1 is a rational fraction (256/205) of, and is phase coherent with, the up-link carrier. (In the absence of an uplink carrier, drive to the Carrier 1 transmitter can be generated locally in spacecraft.)

The baseband of Carrier 1 consists of three subcarriers and the PRN ranging signal. The three subcarriers may be used separately or in any combination. Their center frequencies are 1.024, 1.25 and 1.7 MHz. This baseband, in turn, phase modulates the RF carrier.

1.024-MHz Subcarrier. The 1.024-MHz subcarrier transmits low-rate PCM with bit rates from 7.8 bps through 128 kbps (see Table 3-1). These PCM data phase modulate the subcarrier +90 or -90 degrees in each bit interval.

1.25-MHz Subcarrier. The 1.25-MHz subcarrier is frequency modulated by either voice communications or analog data. The information bandwidth for voice communications is 3.5 kHz with a predetection bandwidth of 25 kHz. For analog data, the information bandwidth is 20 kHz with a predetection bandwidth of 155 kHz.

1.7-MHz Subcarrier. The 1.7-MHz subcarrier has a predetection bandwidth of 660 kHz and is modulated by either PCM, PAM, or FM telemetry data. The PCM data biphase modulates the subcarrier at bit rates from 125 bps through 256 kbps (see Table 3-1), while frequency modulation is used for PAM or FM telemetry data.

PRN Ranging Signal. The PRN ranging signal is either a 1-Mbps PRN code or a 500-kHz clock signal that is extracted from the uplink carrier by the spacecraft receiver and inserted in the Carrier 1 downlink baseband. This signal, as previously noted in Paragraph 2.1.2, is required for range determination by the ground station.

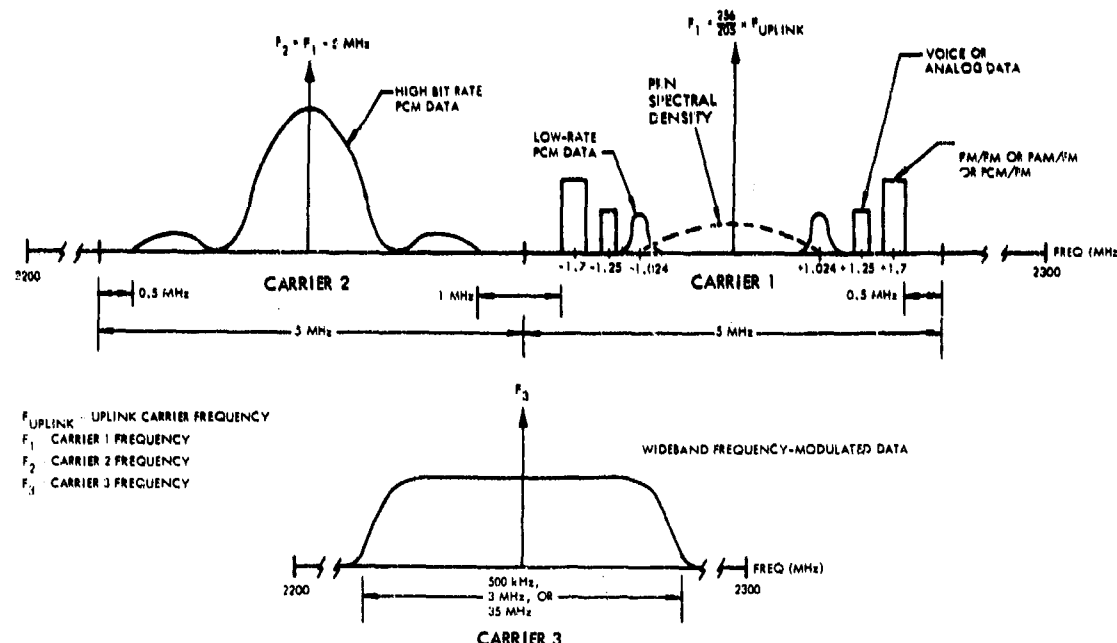


Figure 3-2 Downlink Baseband

TABLE 3-1
PCM/PM TELEMETRY DATA RATES (kbps)

Carrier 1		Carrier 2
1.024 MHz Subcarrier	1.7 MHz Subcarrier	
0.0078125	0.125	128
0.03125	0.25	256
0.0625	0.5	512
0.25	1.0	750
0.5	2.0	1024
1.0	4.0	
1.6	8.0	
4.0	16.0	
8.0	32.0	
32.0	64.0	
51.2	128.0	
64.0	256.0	
128.0		

Carrier 2. Carrier 2 is noncoherent with the uplink and is biphase modulated by high-rate PCM data at bit rates of 128 kbps through 1.024 Mbps (see Table 3-1). As indicated earlier, the center frequency of this carrier is 5 MHz below the center frequency of Carrier 1.

Carrier 3. Carrier 3 is a noncoherent, wideband, frequency modulated service that may be used to transmit either analog or digital data. Information bandwidths of 0.2, 1.0, and 10 MHz are available.

3.1.2 Signal Detection

To accommodate functional requirements imposed by the structure of the downlink, the ground receiver must

- Receive and coherently demodulate to baseband the S-Band PM multiplex carrier (Carrier 1).
- Simultaneously receive and translate to 45 MHz a second wideband signal (Carrier 2) that appears 5 MHz below Carrier 1.
- Receive and noncoherently demodulate to baseband a wideband FM carrier (Carrier 3), Carrier 3 not being present simultaneously with Carriers 1 and 2.

Actual demodulation of Carrier 2 takes place outside the ground receiver in a physically separate unit, as does demultiplexing and subsequent demodulation of the Carrier 1 subcarriers.

These requirements, plus a requirement for computer control of tuning by an external computer, play a determining role in establishing the receiver design concept described below. Additional features of the ground receiver (known as the Ground Receiver and Analog Ranging Equipment - GRARE) provide for angle tracking, ranging, and range-rate determination.

The receiver is a three-channel device that processes sum and difference outputs from the SGLS tracking comparator to yield azimuth and elevation error outputs. In an alternative mode for use with conical-scan antenna systems, the GRARE develops a 30-Hz conical-scan error signal. The GRARE also performs the analog functions associated with the extraction of range information, such as the measurement of range-code correlation and code-clock acquisition. In addition, the GRARE provides a 67.2- to 70.3-MHz signal that contains doppler shift information for use by the range-rate extraction equipment.

Figure 3-3 is a simplified version of the SGLS ground receiver block diagram, illustrating the design features described below.

Receiver Operation

RF and First IF. The receiver RF front end accepts an S-band input from the parametric amplifier and converts it to the of 130-MHz first IF. Preceding the first mixer are an S-band low-pass filter, an isolator, and an S-band preselector. The preselector is a 5-pole Chebyshev filter with a 1-dB bandwidth of approximately 120 MHz that ensures 40-dB minimum first image rejection. Providing a low-loss path for the input signal, the isolator attenuates the local oscillator leakage signal that appears at the RF front end. The lowpass filter further attenuates the first image frequency along with any residual uplink signal that appears as low-level parametric amplifier throughput or as RFI. High-side local-oscillator injection is used in order to minimize the possible spurious output. The first local oscillator is derived from the combination of a voltage-controlled oscillator and a frequency synthesizer, with the resulting signal multiplied X96 to the 2330 to 2430 MHz frequency range.

One of three bandwidths (35, 3.0, and 0.5 MHz) may be selected in the 130-MHz first IF: these defining the noise bandwidth in the reception of the noncoherent Carrier 3. In the coherent Carrier 1 and 2 mode, the 35-MHz bandwidth is automatically selected.

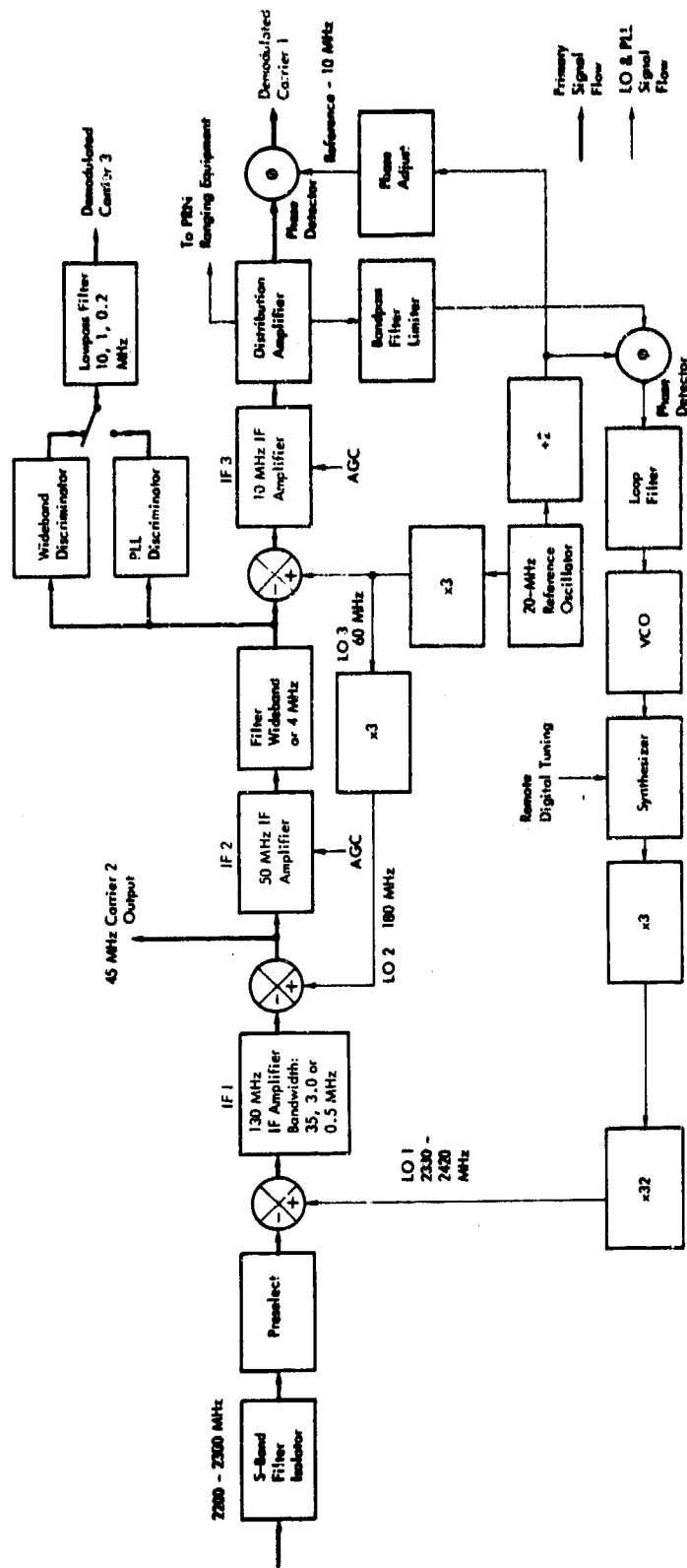


Figure 3-3 SGLS Ground Receiver Simplified Block Diagram

Second IF. The second IF frequency is 50 MHz. High-side local-oscillator injection is again used in the second down-conversion, which results in translation of the Carrier 2 signal frequency to the desired 45 MHz. The 180-MHz local oscillator is derived, along with all other fixed frequency reference signals, from a 20-MHz stable crystal oscillator.

Bandwidth selection also takes place at 50 MHz. A wideband (greater than 35 MHz) filter is selected in the wideband Carrier 3 mode and a 4-MHz bandwidth in the Carrier 1 and 2 mode. The wide bandwidth ensures that Carrier 3 bandwidth control takes place in the preceding (130 MHz) IF, while the 4-MHz bandwidth position separates the 45-MHz Carrier 2 signal from the 50-MHz Carrier 1 signal. Carrier 3 demodulation is performed at 50 MHz, Carrier 1 is passed to a third IF for subsequent demodulation. The gain of the 50-MHz IF amplifier is controlled by an AGC signal derived from the third IF. The AGC loop design is considered in detail in Volume II, Appendix G.

Third IF. The resulting 10-MHz signal is then distributed to the coherent Carrier 1 demodulator, to the phase-lock-loop detector, to the AGC detector, and to the analog ranging section of the receiver. The derived AGC is used to control the gain of both the 50-MHz and the 10-MHz IF amplifiers.

Local Oscillators. The fixed local and reference oscillator frequencies (180, 60, and 10 MHz) are derived from the same stable 20-MHz crystal oscillator source by multiplying X9, X3, and X1/2, respectively. The choice of this configuration was based on information provided in Volume II, Appendix A.

The first local oscillator (180-MHz nominal frequency) completes the feedback path of the reference phase-locked loop. This LO signal is derived by multiplying the output of a frequency synthesizer by a factor of 96 in three stages (X3, X4, X8). The output of the synthesizer, in turn, is developed by using the signal from the VCO in the phase-locked-loop circuit as a base for incrementing the synthesizer output frequency to the nominal frequency of the selected band, the nominal frequency of the VCO is 25 MHz and the synthesizer output is variable from a nominal frequency of 24 MHz to 26 MHz, depending upon the band selected.

The synthesizer is remotely adjustable in 100-Hz increments, giving a remote tuning resolution of 9.6 kHz. The doppler tracking requirements on the VCO are such that a VCO tuning range of ± 2.1 kHz (maximum) will cover the desired doppler range of ± 200 kHz after multiplying the synthesizer output X96.

Reference Phase-Locked Loop. The primary function of the loop is to enable coherent demodulation of Carrier 1, and secondarily, to provide coherent automatic gain control.

Major design features of the reference phase-locked loop are the use of (1) the long-loop concept and (2) the above-mentioned synthesized VCO.

The loop design, chosen as a result of the analysis reported in Volume II, Appendix G, meets the SGLS incremental tuning requirements with low incidental phase noise due to oscillator jitter.

The loop consists essentially of the triple conversion RF/IF chain in the forward path, a bandpass filter-limiter and a loop phase detector, followed by a VCO synthesizer combination forming the feedback path. The loop is closed around the first mixer at S-band. The 15-kHz bandpass filter-limiter combination provides good performance at low signal-to-noise ratios. Noise suppression of the carrier in the limiter results in a decrease in loop bandwidth as the carrier-to-noise ratio is reduced below about 6 dB, thus tending to partially offset the effects of noise.

The loop has an active loop filter that gives a high dc-loop gain, enabling static phase error less than 0.1 rad to be obtained at extreme frequency offsets. The loop is also provided with an automatic acquisition feature. In this mode, the loop filter is pulsed, causing the VCO to perform a sawtooth frequency sweep. The sweep rate is chosen to be compatible with the ability of the loop to lock to the signal without excessive sweep-induced phase error. Once acquired, the presence of the signal is registered by a coherent amplitude detector and the acquisition sweep is disabled. The sweep ranges and sweep rates corresponding to the available phase-lock bandwidths are shown in Table 3-2. The loop damping factor is 0.7 ± 0.2 at high signal-to-noise ratios.

Signal Demodulation

TABLE 3-2

RECEIVER SWEEP RANGES AND RATES

Loop Bandwidth 2B _{LO} (Hz)	Sweep Range (kHz)	Sweep Rate (kHz/sec)
200	±10	1
1000	±100	25
5000	±200	500

Carrier 1. The PM Carrier 1 multiplex is demodulated to baseband in a 10-MHz wideband phase detector. This phase detector uses the same 10-MHz reference source as the phase-locked loop,

except that the demodulator reference requires a phase adjustment to balance out any residual phase offset that is due to the 10-MHz crystal filter in the reference phase-locked loop. The ground receiver outputs the resulting multiplex for baseband separation and subsequent demodulation. Essential performance features of the 1.024-, 1.25-, and 1.7-MHz subcarrier demodulators are described below. The demodulators are physically located in equipment items external to the ground receiver.

1.024-MHz Subcarrier. The 1.024-MHz biphase modulated PCM subcarrier is separated from the Carrier 1 multiplex by one of six bandpass filters. It is then coherently demodulated, the coherent reference being obtained from the suppressed carrier signal by a squaring loop. The demodulated output then feeds a bit synchronizer that regenerates the noisy bit stream using an integrate and dump-matched filter. The predetection bandwidth is selected according to the PCM bit rate, which may range from 8 bps to 128 kbps.

1.25-MHz Subcarrier. The 1.25-MHz subcarrier is also demultiplexed by selecting one of two bandpass filters applicable to narrowband FM voice or general purpose analog FM modulation. The filter bandwidths are 25 kHz and 155 kHz, respectively. The demultiplexed 1.25-MHz signal is applied to a modulation tracking phase lock loop, with one output supplied to the user directly. A second output is supplied via a voice-bandwidth filter. This latter output may be monitored with a loudspeaker.

1.7-MHz Subcarrier. Various techniques may be used to modulate the 1.7-MHz subcarrier subject to the restriction of the 660-kHz wide demultiplexing bandpass

filter. The demultiplexed subcarrier is output directly after translation to 10 MHz, without demodulation although an FM discriminator output also is provided for monitoring purposes. This subcarrier channel is suitable for PAM/FM or IRIG FM/FM telemetry channels.

A second optional application of the 1.7-MHz subcarrier is its use as an additional biphase PCM channel. A 1.7-MHz PCM demodulator, actually operating on the translated 10-MHz output signal of the demultiplexing unit, is also provided for this purpose. The bit-rate capability is from 125 bps to 256 kbps.

Carrier 2. Carrier 2 also carries biphase PCM at rates from 128 kbps to 1024 kbps. A separate Carrier 2 demodulator is provided to operate on the 45-MHz Carrier 2 output of the ground receiver.

The Carrier 2 demodulator extracts the PCM telemetry data by means of a data phase detector, a loop phase detector, an in-phase quadrature (I-Q) multiplier, and a loop amplifier/voltage-controlled crystal oscillator (VCXO). The Carrier 2 demodulator receives the second IF from the reference receiver as an input. Carrier 2 data is centered at 45 MHz, and appropriate filtering used to reject the 50-MHz Carrier 1 signal. Coherent demodulation of the data is accomplished by the conventional loop and data phase detectors, using the coherent 45-MHz VCXO. The I-Q multiplier ensures that the correct polarity of error signal is applied to the loop amplifier and VCXO during phase reversals that are caused by input biphase data modulation. The multiplier effectively switches polarity of the loop error signal as a function of PCM data polarity.

Carrier 3. Carrier 3 FM demodulation takes place within the ground receiver. A conventional FM limiter/discriminator is used in the very wide band mode (35-MHz IF bandwidth)

while a modulation tracking phase-locked loop provides some degree of threshold extension in the two narrower bandwidth modes. Baseband post-discriminator filtering is also provided. Table 3-3 indicates the available bandwidth/demodulator combinations.

TABLE 3-3
CARRIER 3 DEMODULATION OPTIONS

Demodulator	IF Bandwidth (MHz)	Baseband Width (MHz)
Discriminator	35.0	10.0
Phase Locked Loop	3.0	1.0
Phase Locked Loop	0.5	0.2

3.1.3 PCM Decommunication

The PCM decommutation equipment (Figure 3-4) is designed to handle two independent bit streams simultaneously. Handling of PCM data consists of reconstructing the degraded serial data, finding the appropriate synchronization patterns in the serial data, performing a serial-to-parallel conversion, and outputting selected parallel data words to an external computer. To ensure that sensitive data cannot be inadvertently obtained by unauthorized users, precautions have been taken to ensure that radiated and conducted signals are held to very low levels.

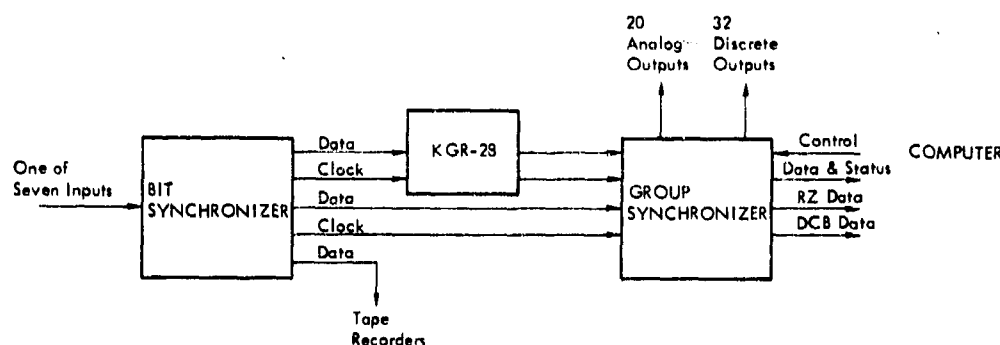


Figure 3-4 PCM Decommutation Equipment Block Diagram

The bit synchronizer accepts a signal degraded by noise, jitter, baseline offset, and other perturbations, and reconstructs the signal, along with generating a clock signal at the input bit rate. Bit synchronizer inputs are selectable from three demodulators, two tape recorders, the simulator, simulated encrypted data, and one auxiliary input. Reconstructed serial data outputs with clocks are provided to the KGR-28 decryption equipment and group synchronizer. An unclocked data output is provided for postdetection recording.

Data inputs to the bit synchronizer may be automatically acquired at any one of 17 discrete rates between 7 bps and 1.2 Mbps. Data rates at other than the discrete frequencies can be accommodated by manual control. Input codes that are accommodated are shown in Figure 3-5. Bit-error-rate performance with any code is within 1 dB of theoretical noise performance for that code. The group synchronizer accepts either the KGR-28 output or clear data directly from the bit synchronizer.

PCM CODE	PULSE PATTERN	EXPLANATION
NRZ-L		NONRETURN-TO-ZERO LEVEL (OR NONRETURN-TO-ZERO CHANGE): "One", one level "Zero", other level
NRZ-M		NONRETURN-TO-ZERO MARK: "One", a change in level "Zero", no change in level
NRZ-S		NONRETURN-TO-ZERO SPACE: "One", no change in level "Zero", a change in level
RZ		RETURN-TO-ZERO: "One", a half-bit-wide pulse "Zero", no-pulse condition
BiΦ-L		BIPHASE LEVEL: "One", a "10" "Zero", a "01"
BiΦ-M		BIPHASE MARK: A transition occurs at the beginning of every bit period "One", a second transition half-bit-period later "Zero", no second transition
BiΦ-S		BIPHASE SPACE: A transition occurs at the beginning of every bit period "One", no second transition "Zero", a second transition half-bit-period later

Figure 3-5 PCM Codes

Mainframe and subframe synchronization pattern search is performed by the group synchronizer. Synchronization patterns may be from 4 to 64 bits in length and may be syllabized into as many as 16 syllables with a minimum of 4 bits per syllable. As many as four asynchronous subframes or sub-subframes may be accommodated. Subframes may be the recycle type (synchronization patterns) or identification type. Main frame length, subframe length, and the number of synchronous subframes are unlimited except that the program to handle them must be stored in 4096 24-bit words of core memory.

After having found the main and subframe synchronization pattern, the group synchronizer divides the serial data stream into data words of 1 to 32 bits and places them in a 32-bit register. If the data word contains less than 32 bits, the least significant bits are set to zeros. Data from the register can then be routed to D/A converters or discrete relays, the computer buffer, or the data can be discarded.

The D/A converters receive the eight most significant bits. The discrete relays receive data from one of four 4-bit syllables that comprise the 16 most significant bits of the 32-bit register. The computer buffer receives the 20 most significant bits. The remaining four bits that comprise the 24-bit word stored in the computer buffer are the status of the group synchronizer.

Data stored in the 512-word computer buffer is output upon demand to the CDC 160A computer in the same order in which it is stored. Each 24-bit word is divided into 12-bit half words prior to transfer to the computer.

An additional output from the group synchronizer is an RZ bipolar coded serial data stream consisting of 48 consecutive bits extracted from each main frame and clocked at 10 kbps.

All of the operating parameters for the bit synchronizer and group synchronizer described above are stored in the group synchronizer core memory. These parameters are normally loaded from the 160A computer. In addition, a paper-tape reader (located at the ground station) can be used, or loading can be accomplished manually. Loading or changing these parameters can only be accomplished when the group synchronizer is stopped.

In addition, by means of function codes, the 160A computer can control several other operations; namely, starting and stopping the transfer of all data via the computer buffer; starting and stopping the decommutator; requesting a group synchronizer status word that is subsequently passed over the same data lines as are the words from the computer buffer; and requesting a digital command buffer (DCB) word that is 36 consecutive bits (from every main frame) transferred to the DCB as three 12-bit words for command authentication. The location of the 36 bits is also specified by the 160A computer via the DCB.

In addition to the two bit synchronizers and two group synchronizers, a simulator is provided for performance testing of the PCM equipment. The simulator can produce any format that the bit synchronizer and group synchronizer can handle, and can provide any of the common forms of signal degradation. In addition,

the simulator can compare the output of the bit synchronizer or group synchronizer with the simulated input data.

The simulator is programmed (except for signal perturbations) by the 160A computer, paper-tape reader, or manually. Outputs are also provided for loop testing additional equipment outside the PCM equipment. All satellite modes of operation, including command authentication and data encryption, can be tested.

3.1.4 Data Distribution

SGLS uplink and downlink signals may be recorded and played back in a variety of formats by two Ampex FR-1600 wideband tape recorders. Each recorder is capable of recording up to seven tracks. By relocating electronic modules within the recorder, signals may be recorded in either a direct or FM mode. The recording and playback head stack configuration is in accordance with IRIG standards. Track assignments for both recording and playback are made by the signal switching facility (SSF), which serves as a recorder tie point for all SGLS data lines. In addition to the reconfiguration function, the SSF also contains necessary line bridging amplifiers to ensure that the recording and playback requirements are met without introducing degradation to the real-time signals.

To satisfy various program recording requirements, the recorders can be operated in either a sequential or simultaneous mode. In the simultaneous mode, redundant real-time recordings can be made. In the sequential mode, data is recorded alternately on each of the tape recorders; in this way, data can be recorded for extended intervals. Automatic control provides recording overlap to ensure no loss of data.

To permit use of the recorders by non-SGLS programs, a switching capability has been incorporated which allows recording and playback of seven data channels from the RTS FM/FM ground station.

Table 3-4 depicts the possible configuration capability within the SSF, where a "●" indicates a permissible connection. The significant characteristics of the FR-1600 recorders are summarized in Table 3-5.

TABLE 3-4
SIGNAL SWITCHING FACILITY OPTIONS

Uplink/Downlink Signals	Track Option													
	Recorder 1							Recorder 2						
	1	2	3	4	5	6	7	1	2	3	4	5	6	7
Record Inputs														
Low-Rate PCM	●			●				●			●			
Uplink Voice	●							●						
RTS Intercom	●													
Fault Isolation Input	●	●	●	●	●	●	●	●	●	●	●	●	●	●
Hi-Rate PCM	●	●							●	●	●			
PCM Ground Station 1 Bit Sync	●				●				●			●		
PCM Ground Station 2 Bit Sync	●				●				●			●		
IRIG Telemetry 1 Baseband (Non-SGLS)		●								●				
IRIG Telemetry 2 Baseband (Non-SGLS)		●								●				
1.7-MHz PCM		●									●			
100-kHz Reference Tone			●								●			
Predetection PCM Baseband				●								●		
Downlink Voice				●								●		
Predetection Analog/Voice				●								●		
Carrier 1 Baseband					●							●		
STCW						●							●	
Downlink Analog					●							●		
Playback Outputs														
PCM Ground Station 1	●	●	●		●	●		●	●	●		●		
PCM Ground Station 2	●	●	●		●	●		●	●	●		●		
BSU					●							●		
SPB					●							●		
Tape Select Unit						●							●	
Fault Isolation Detector	●	●	●	●	●	●	●	●	●	●	●	●	●	●
To RTS MPP			●						●					
Synch Off Tape Circuit				●						●			●	
Analog Test Unit A	●							●						

TABLE 3-5
SGLS TAPE RECORDER CAPABILITIES SUMMARY

Number of Tracks	7
Nominal Configuration	FM/FM Channels: 1, 5, and 7 Direct Channels: 2, 3, 4, and 6
Tape Speeds	240, 180, 120, 60, 30, 15, 7 1/2 and 3 3/4 ips
Direct Frequency Response	± 3 dB, 800 Hz to 2 MHz @ 120 ips
FM/FM Frequency Response	+5, -5.5 dB, dc to 500 kHz @ 120 ips
Signal-to-Noise Ratio	20 dB minimum in direct, 26 to 30 dB minimum in FM/FM (depending on tape speed)
FM/FM Center Frequency	900 kHz
Remote Control	All transport functions can be remotely sensed and/or controlled by a computer. The system can be operated in either a simultaneous or sequential mode.

3.2 SIGNAL-TO-INTERFERENCE ANALYSIS

In view of the complexity of the downlink the S/I ratios in the various services were examined to access their impact on system performance.

Three categories of interference were considered. These are: intermodulation, distortion due to phase nonlinearity and amplitude ripple, and spurious interference due to spectral overlap. The interference of interest is inherent in the system as a result of the baseband structure employed and the associated modulation and demodulation techniques used to provide the required downlink services. Interference introduced prior to modulation and subsequent to demodulation is of lesser concern since the magnitude of such interference is controlled by appropriate circuit design. For this reason, these interference effects are not considered here.

In the discussion that follows, it is shown that worst-case interference levels do not limit downlink performance.

3.2.1 Intermodulation

Phase modulation of the carrier by a composite baseband of subcarriers results in the generation of RF sidebands, some of which are first-order sidebands displaced from the carrier by frequencies equal to the subcarrier frequencies. Others appear as crossproduct terms separated from the carrier by multiples of the sum and difference frequencies, accompanied by higher order terms. Since the demodulation process is coherent, the spectrum of the demodulated output is identical to the spectrum of the composite baseband but additionally contains these cross-product terms introduced by phase modulation of the RF carrier. (Note that, if a phase discriminator were used in the demodulation process, the output of such a discriminator would be a replica of the composite baseband without the cross-products.) This occurs because the coherent phase detector is a linear frequency translation device. To facilitate the analysis of the effects of these crossproducts, the detector is, however, treated as a phase discriminator followed by a sinusoidal nonlinearity. It can be shown that this model is equivalent to the selected coherent phase detector.

Because of the several services arranged in frequency division multiplex (FDM) on Carrier 1, the intermodulation (IM) requirements of this carrier determine the allowable downlink baseband and phase nonlinearities. The uplink is designed such that its contribution to nonlinearity is negligible. A model for determining IM distortion is shown in Figure 3-6. Baseband amplitude nonlinearities are variations from perfect linearity of the modulator- and baseband-amplifier transfer characteristics. Phase nonlinearities are chiefly variations from linearity of the phase-shift versus frequency characteristic for IF and RF portions of the system. This is ordinarily specified and measured as the variation from a constant value of the envelope delay as a function of frequency.

In Volume III, Appendix IV, general expressions are developed for nonlinearities of the model in Figure 3-6, as well as for the IM products they produce. The

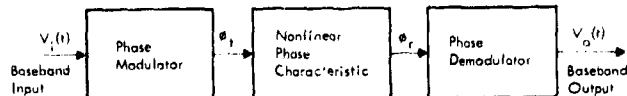


Figure 3-6 IM Distortion Model

product or phase demodulator is unique in that it has a precise mathematical transfer function. The output baseband-amplitude characteristic of the product demodulator is represented by the expression $V_o = c_1 \sin(\phi_r + e)$ where e is the tracking error in the phase-lock loop (this loop reconstructs the coherent carrier reference). The coherent product demodulator is also unique because it determines an optimum schedule of subcarrier deviations which minimizes the total received power required (Volume III, Appendix VI). Deviations so determined are not small in terms of nonlinear sine functions, ranging up to 1.84 radians. Therefore, the phase demodulator becomes the limiting system nonlinearity.

For system design purposes, apportionment of IM objectives begins with the mathematical certainty of the phase demodulator. Presumably, all other contributors can be made linear to any desired degree with sufficient design effort. If the desired IM performance cannot be achieved with the best equipment design, or if the phase-demodulator IM generation is excessive, phase deviations of one or more of the services must be reduced from the optimum; random-noise performance of the affected service(s) will be thereby compromised to some degree. This has not been found to be necessary for SGLS; that is, the optimum phase deviations dictated by random noise give acceptable IM-product levels as well.

Expressions that relate other distortion coefficients to sine nonlinearity in terms of allocated distortion percentages and prescribed phase deviations are developed in Volume III, Appendix IV. The following IM categories were considered in the analysis:

- Second-order baseband-amplitude nonlinearity at the modulator
- Third-order baseband-amplitude nonlinearity at the modulator
- Sinusoidal phase-detector nonlinearity with carrier-tracking loop-phase error (second and third order)

- Second-order IF- and RF-phase nonlinearity (linear envelope delay)
- Third-order IF- and RF-phase nonlinearity (parabolic envelope delay)

Each of the above nonlinearities generates a different type of distortion. Second-order distortion is related to third-order distortion and thus to phase-detector distortion. The distortion percentage allocated to each IM category is a matter of engineering judgment. For instance, because frequency multiplication follows the phase modulator, this element can be easily operated over a linear range, and therefore can be allocated a smaller portion of the overall distortion budget.

Distortion objectives for the downlink are given in Table 3-6. A more detailed treatment and a definition of the distortion parameters is given in Volume III, Appendix IV. Linearity specifications in Table 3-6 were distortion objectives, not firm requirements, for the various SGLS equipment items during the system design phase.

Sine Nonlinearity

A mathematical study of IM products caused by the phase detector (sine nonlinearity) is included in Volume III, Appendix IV of this report. Amplitude and frequency of each product are precisely determinable. To generate useful results, simplified models of the modulating signals are used. Basically, the approach used in the study represented the periodic PRN code by certain of its Fourier components, and the subcarrier modulation by discrete tones or subcarriers.

Analysis of the phase detector output for a known input baseband function indicates that the original baseband frequencies are reproduced with a Bessel function weighting of their amplitudes and a large number of IM-frequency products. To limit the number of IM products considered, all products less than a specified amplitude, or greater than a given order, or all products outside a specified frequency band can be rejected.

TABLE 3-6
DOWNLINK DISTORTION OBJECTIVES

Nonlinear Distortion Sources	Percentage of Total Distortion	Ground Station or Spacecraft Equipment	Percentage of Total Distortion	Linearity Specification
Second-order baseband-amplitude nonlinearity	5	Spacecraft: Baseband assembly equipment and phase modulator	3	$a_2/a_1^2 = 0.035 \text{ rad}^{-1}$
		Ground Station: Baseband separation equipment and phase demodulator	2	$\epsilon = 0.05 \text{ rad}$ phase error of carrier reference
Third-order baseband-amplitude nonlinearity	50	Spacecraft: Baseband assembly equipment and phase modulator	10	$a_3/a_1^3 = 0.06 \text{ rad}^{-2}$
		Ground Station: Baseband separation equipment and phase demodulator	40	Fixed constraint of phase-detector sinusoidal characteristic
Second-order phase nonlinearity (linear envelope delay)	18	Spacecraft: Transmitter IF and RF equipment	9	$T_{DL}^{(pp)} = 88 \text{ ns over 5-MHz BW}$
		Ground Station: Receiver IF and RF equipment	9	$T_{DL}^{(pp)} = 88 \text{ ns over 5-MHz BW}$
Third-order phase nonlinearity (parabolic envelope delay)	25	Spacecraft: Transmitter IF and RF equipment	12.5	$T_{DL}^{(pp)} = 115 \text{ ns over 5-MHz BW}$
		Ground Station: Receiver IF and RF equipment	12.5	$T_{DL}^{(pp)} = 115 \text{ ns over 5-MHz BW}$
RF echoes (equivalent to ripple envelope delay)	2	(Total allowance for transmitter and receiver)	2	Relative voltage amplitude of single echo: $\rho_r = 0.05$

From the expansion of the sine function, the IM effect on the various SGLS multiplex services can be assessed. The amplitude and frequency of IM products falling in each acceptance band can be calculated. For FM and PM subcarriers, a general analysis of the nature of the interference that appears after demodulation is given in Volume III, Appendix IV. Since the ranging phase detector or balanced demodulator normally employs the carrier reference phase-modulated by the local receiver-PRN code, the analysis does not apply to this detector. However, during the first step in the acquisition procedure (acquiring the 500-kHz range clock), the local code is set to zero and the carrier reference is unmodulated. For this special condition, the sine expansion is valid when searching for ranging-system IM products that are in the vicinity of the clock frequency.

The large number of frequency components in the PRN code dictates the use of a digital computer for the calculation of IM products. The PRN short- and long-code lengths are 35,805 bits and 2,728,341 bits, respectively. Expanding each code in terms of the 500-kHz clock frequency yields the lowest frequency, approximately 14 Hz for the short code and approximately 0.2 Hz for the long code. If all multiples of the fundamental frequency are considered up to 2 MHz, and if a reasonable number of baseband carriers and subcarriers are considered, then the number of IM products generated begins to exceed the capacity of even a large digital computer. With these considerations in mind, the Fourier expansion of the short code for the computer analysis consists of multiples of the X component, the B component, and the X times the B component; and the Fourier expansion of the long code consists of multiples of the X component, the A component, and the X times the A component (Table 3-7).

Computer Analysis

The computer program used in the analysis computed the IM products in two steps. First, the program computed the frequency and amplitude, starting with zero order and proceeding to plus and minus fifth order, of all IM products that are above a specified level (-60 dB with respect to the total IF signal in all cases run) and that are contained in a specified frequency interval (0 to 2 MHz in all cases run). Second, the program grouped the IM products by frequencies and combined the products that occur at the same frequency.

TABLE 3-7
PRN CODE COMPONENTS

Component	Code	Length (μs)	Fundamental Frequency (kHz)	Relative Power
x	Short or long	11	45.5	0.0226
a	Short or long	31	16.1	0.0020
b _s	Short	7	71.5	0.0090
b _l	Long	63	7.9	0.0010
c _s	Short	15	33.3	0.0042
c _l	Long	127	3.9	0.0004
x · a	Short or long	11·31	14.7	0.0002
x · b _s	Short	11·7	6.5	0.0008
x · c _s	Short	11·15	3.0	0.0004

NOTES

1. Modulo number

Short code = 35,805; 5000 nmi range

Long code = 2,728,341; 400,000 nmi range

2. Transmitted code

$$cl + \bar{x} \cdot [(a \cdot b + b \cdot c + c \cdot a) \oplus cl] = cl \oplus \bar{x} \cdot (a \cdot b + b \cdot c + c \cdot a)$$

Receiver code (tracking) = $x \cdot (a \cdot b + b \cdot c + c \cdot a)$

$$3. \text{ Fundamental frequency (transmitted)} = \frac{f_{cl}}{L_{comp}}$$

where

f_{cl} = clock frequency = 500 kHz

L_{comp} = length of component in bits

WDL-TR3227-1
Volume I, Part 1

The cases calculated are given in Table 3-8. Only the most significant computer runs are summarized here, since some of the runs yielded very similar results.

Case 4 has a 128-kbps PCM/PM signal, the analog FM subcarrier, and the FM/FM subcarrier with a short PRN-ranging code directly modulating the PM carrier.

This run yielded 338 direct and IM products in the 0- to 2-MHz band and above the -60 dB point relative to the total IF signal power. There were no significant

TABLE 3-8
COMPUTER INTERMODULATION PROGRAM CASES

Case	Service	Subcarrier Frequency (MHz)	Modulation Index on Carrier (rad peak)	Modulating Frequency (kHz)	Modulation Index for Modulating Frequency (rad)	No. of Direct and IM Products
1	PCM/PM Voice/FM PRN	1.024 1.25 0.5	1.55 0.563 0.1	- - -	- - -	162
2	PCM/PM Voice/PM FM/FM PRN	1.024 1.25 1.70 0.5	0.73 0.196 1.35 0.1	- - - -	- - - -	154
3	PCM/PM Voice/FM FM/FM PRN	1.024 1.25 1.70 0.5	0.73 0.196 1.35 0.1	- 3 - -	- 1.53 - -	204
4	PCM/PM Voice/FM FM/FM PRN	1.024 1.25 1.70 0.5	0.73 0.196 1.35 0.1	64 (128 kbps) - - -	1.57 - - -	338
5	PCM/PM Voice/FM FM/FM PRN	1.024 1.25 1.70 0.5	0.73 0.196 1.35 0.1	- 3 - -	- 1.53 - -	204
6	PCM/PM Voice/FM FM/FM PRN	1.024 1.25 1.70 0.5	0.73 0.196 1.35 0.1	- 20 165 (IRIG H) -	- 1.53 0.345 -	262
7	PCM/PM Voice/FM FM/FM PRN	1.024 1.25 1.70 0.5	0.73 0.196 1.35 0.1	- - 93 (IRIG F) 165 (IRIG H)	- - 0.258 0.345	242
8	PCM/PM Voice/FM PRN	1.024 1.25 0.5	1.55 0.56 0.1	64 (128 kbps) 3 -	1.57 1.53 -	610
9	Uplink Voice Command PCM/PM PRN	0.030 0.095 1.024 0.5	0.1 0.1 1.55 0.1	- - 64 (128 kbps) -	- - 1.57 -	240

IM components within several kilohertz of the 500-kHz clock frequency. Two IM products within -3 dB of the clock amplitude were 15 kHz below the clock frequency and 10 kHz above the clock frequency.

Case 6 has the PCM/PM subcarrier, the analog FM subcarrier modulated with a 20-kHz test tone, and FM/FM with IRIG channel H plus the PRN short-ranging code. This run yielded 262 direct and IM products in the 2-MHz band and above the -60 dB point relative to the total IF signal power. The largest component near the clock is 13 kHz from the clock and 4 dB down from the clock power level. A possible problem area in this case is that nine IM products appear in the FM/FM passband with a total power -13 dB below the total sideband power of the FM/FM signal. However, eight of these are actually four pairs of amplitude-modulation products that are removed by the subcarrier limiter. The net predetection signal-to-intermodulation (S/I) ratio becomes 36 dB. The complete printout of Case 6 is given in Volume III, Appendix XIII.

Case 8 is similar to Case 6 except that the FM/FM is dropped from the baseband. This case has a PCM/PM signal modulated at 128 kbps, an analog FM signal modulated by a 3-kHz test tone, and the PRN code. Case 8 yielded a surprising 610 IM products. The reason the two subcarriers and PRN code yielded more than double the number of IM products produced in Case 6 is that the carrier deviation of the two subcarriers has been increased such that the relative amplitude of more IM products is above the -60 dB threshold. Also, the fact that these two subcarriers are only 226 kHz apart allows more of the IM products to fall within the 2-MHz baseband. A larger number of IM products need not be detrimental provided no large components fall near the PRN-clock frequency or near subcarrier frequencies. The closest large IM product to the PRN-clock frequency is 39 kHz away and is 4 dB down from the clock power level. The complete computer printout is given in Volume III, Appendix XIII.

Case 9 considers the problem of the uplink command frequencies that interfere with the 128-kbps PCM/PM signal. The difference between the 30-kHz and 95-kHz command frequencies is 65 kHz, and the combination of 30 kHz and 95 kHz and PCM/PM carrier at 1.024 MHz produces IM products at 65 kHz above and below

the PCM/PM carrier. When the PCM 128-kbps signal is a square wave, that is, a successive one-zero pattern, then the first sidebands of the PCM/PM signal are 64 kHz above and below the PCM/PM carrier. Thus, it is possible that some IM product of a multiple of the command frequencies and the PCM/PM carrier may produce a harmful product that would degrade the PCM-bit error probability.

Turned-around command-frequency deviations for this case are 0.1 radian for a one-to-one turnaround of the uplink. The deviations of the PCM/PM subcarrier and PRN short code are 1.55 radians and 0.1 radian, respectively. Although IM products generated by the analog FM were not computed, power taken by this subcarrier was compensated for by multiplying all direct and IM products by a program constant J_0 (0.56), where the analog FM deviation is 0.56 radian. The run yielded 240 IM products none of which were within several kilohertz of the range-clock frequency. Also, above the -60 db threshold level no IM products were found at multiples of the 65-kHz uplink subcarrier difference frequency above and below the PCM/PM subcarrier frequency.

Worst-case ratios of S/I products are summarized in Table 3-9. The worst-case IM level was found by computing the mean-square subcarrier S/I ratio in the predetection bandwidth for all of the computer runs. Although the 24-dB ratio for the PCM/PM may appear inadequate, an S/I ratio of at least 23 dB will not significantly impair bit error probabilities up to 10^{-6} (see Volume III, Appendix VIII).

TABLE 3-9
SIGNAL-TO-INTERFERENCE (INTERMODULATION)
RATIO FOR VARIOUS SERVICES

Service	Predetection Bandwidth (kHz)	Computer Case	S/I Ratio (dB)
PCM/PM (128 kbps)	256	8	24
FM/FM	550	6	36.4
FM Analog (3 kHz)	25	-	No IM products found

In addition to the predetection S/I ratio, one particular postdetection subcarrier S/I ratio was computed. The IM product for this analysis is from Case 6 and falls in the FM/FM predetection bandwidth. This is the only large IM product that is not eliminated by limiting or predetection filtering. The IM component is 200 kHz away from the carrier. The FM/FM signal was assumed to be modulated with a 165-kHz subcarrier (IRIG Channel 21 or H). The resulting S/I ratio after the frequency demodulator is 28.1 dB. This S/I ratio is entirely adequate since the subcarrier discriminator signal-to-noise threshold is 10 dB.

3.2.2 Phase Nonlinearities and Amplitude Ripple

Tandem-component characteristics in the sum channel of the SGLS receiving subsystem directly limit the quality of the output signal. In particular, phase-response nonlinearity and amplitude-response variations in these components could distort the angle-modulated signal beyond acceptable limits.

To assess the severity of the problem, the nominal configuration, in terms of signal distortion attributable to predetection components was analyzed. Since Carrier 3 bandwidth requirements are much greater than those for Carrier 1 and Carrier 2, Carrier 3 signals should be subject to greater distortion than the signals for the other two carriers. Hence, Carrier 3 in its wideband mode of operation (35-MHz IF bandwidth) was selected for this analysis (see Appendix B in this volume). A 2-MHz sine-wave input with frequency modulation, simulating FM/FM wideband operation, was assumed. To more closely simulate physical conditions, measurements of the phase and amplitude characteristics for contributing tandem components were used.

Results indicate that Carrier 3 power distortion should be much less than one percent at the input to the wideband discriminator for wideband-FM/FM operation with a 2-MHz sine-wave signal when a modulation index (m) of 5 is used. (This value for m was selected because the RF spectrum embraces the IF bandwidth, and there is a rapid decrease in the amplitude of terms outside this bandwidth.)

The overall distortion which may be experienced by Carrier 3 data is more significantly affected by the demodulation process. It is expected that the demodulator will not contribute enough distortion to cause the overall Carrier 3 power distortion to exceed 3%. Carrier 1 will be similarly affected by subsequent demodulation. The harmonic distortion expected, when considering the overall data processing cycle, is not expected to exceed 5%.

Criteria for determining tolerable interference levels (e.g., postdetection signal-to-interference (S/I) ratio, bit-error probability, ranging error, and percent error in data) are measured against performance standards established by the ultimate user. For services such as PCM data and PRN ranging, these standards are objectively measurable. For voice, however, interference effects are subjectively determined by the individual user, and standards must be set by averaging over a large number of users. For both objective and subjective standards, requirements depend to some degree on the nature of the interference. For example, a 1000-Hz interfering tone is judged by some listeners to be more objectionable than an equal power band of white noise. Similar differences in interference tolerance exist in the data services.

3.2.3 Spurious Interference

Interference occurs when spurious spectral components fall within the acceptance band of one of the SGLS services. The spurious components may be caused by direct spectral overlap of an interfering service, or by IM products generated by two or more services interacting in a nonlinear system element.

Adjacent-channel interference occurs when the desired carrier and a reduced-level second carrier are applied to the phase detector. The form of interference appearing at the baseband depends on whether the channel is, or is not, linear (Volume III, Appendix IV). In either case, the interference spectrum is centered at the baseband frequency corresponding to the carrier separation (5 MHz for basic SGLS). For a limiting receiver, the interference spectrum is the convolution of the complex-envelope spectra of the two carriers. For the linear SGLS ground receiver using coherent AGC, the interference is the translated spectrum of the

interfacing carrier. Because spectrum spreading is inherent in the convolution process, interference is minimized by using coherent AGC, rather than limiting, in the ground receiver.

Although the ground receiver is linear, for some missions a saturating traveling-wave-tube (TWT) amplifier may be used as the vehicle transmitter output device. Under these conditions, the adjacent channel interference may take the form of the convolution spectrum. Furthermore, the TWT, while amplifying two carriers simultaneously, is the source of direct adjacent-channel interference, in which the baseband of one carrier is transferred directly to the other carrier. This phenomenon occurs when the signal frequency deviations are converted to amplitude modulation (AM) on passing through circuits with non-constant-gain frequency characteristics. This AM is subsequently converted to phase modulation in the TWT.

Intercarrier Interference

Interference between Carriers 1 and 2 is caused by overlap between the individual spectra. No filtering is supplied in the vehicle because of the close proximity (in terms of percentage bandwidth) of the 2-GHz carriers. Since the receiver is linear (employing coherent AGC rather than limiting) and each carrier is coherently detected, the unfiltered baseband-interference spectrum would be a replica of the RF spectrum translated to baseband. Because of the predetection IF filters, however, the baseband interference spectrum is altered substantially from the RF spectrum. In particular, interfering higher-order sidebands that fall within the width of the baseband cannot be eliminated from the desired carrier. That is, if the desired sidebands are passed, then so also are the interfering sidebands that occupy the same frequency band.

The following observations are taken from the quantitative analysis of intercarrier interference presented in Appendix VIII of Volume III: At 1 Mbps, the fourth-order through seventh-order sidebands of Carrier 2 fall in the 0- to 2-MHz baseband of Carrier 1. The peak interference arises from the fourth-order sideband and occurs at 1.4 MHz in the baseband of Carrier 1. In

terms of predetection S/I density ratio, therefore, carrier 2 interference with the analog FM subcarrier constitutes the worst-case interference in Carrier 1.

Because of the modest FM advantage for this subcarrier (deviation ratio of 1 to 1.5), the postdetection S/I ratio is also worst for this service. For "square" PCM-bit waveforms, the predetection S/I ratio for the 3-kHz voice channel is 19 dB. This is 9 dB greater than the 10-dB SNR at threshold. Therefore, it is concluded that the higher-order sidebands of the 1-Mbps PCM data produce interference at a tolerable level.

Carrier 1 interference with Carrier 2 arises principally from second- and third-order sidebands of the relatively high-level PAM/FM or FM/FM service. Third-order interference is centered 100 kHz from the Carrier 2 frequency; that is: $(3 \times 1.7) - 5.0 = 0.1$ MHz. Therefore, with a nominal bandwidth of ± 250 kHz, substantially all of this sideband falls in the high-rate-PCM acceptance band. The predetection S/I ratio is calculated at 17.8 dB for a maximum FM/FM or PAM/FM deviation of 1.84 radians and equal level carriers ($P_1 = P_2$). The second-order interference appears at 1.6 MHz relative to the Carrier 2 frequency, and is filtered by the PCM matched filter:

$$\begin{aligned} P_{I_2} &= J_2^2 (1.84) \left(\frac{\sin 1.6\pi}{1.6\pi} \right)^2 P_1 \\ &\cong 0.124 \left(\frac{2}{3\pi} \right)^2 P_1 \\ &= 5.6 \times 10^{-3} P_1 \end{aligned}$$

or $P_s/P_{I_2} = P_1/P_{I_2} = 22.6$ dB. Thus, the total PCM S/I ratio is 16.6 dB. The threshold SNR at decision time (after matched filtering in a bandwidth equal to half the bit rate) for the PCM data is 11.6 dB at a 10^{-3} bit-error probability. Therefore, in the worst case, the Carrier 1 interference is only 5 dB below the random noise. The exact effect of the interference on the bit-error rate at threshold depends on the nature of the interference. Some of the effects of discrete tones are

examined in Appendix VIII of Volume III. If the interference approaches random noise, then a total interference of 5 dB below the noise would increase the PCM threshold by about 1 dB.

PCM and Analog FM Subcarriers

The interference under consideration is between the PCM data centered at 1.024 MHz and the analog FM subcarrier at 1.25 MHz using PCM/PM (PSK) modulation. The worst case is for the highest data rate (128 kbps). Also the analog FM subcarrier is assumed to carry the 20-kHz analog information.

The cases of both random and periodic PSK interference with the analog channel are considered in Appendix VIII of Volume III. For equal-level subcarriers, the basic S/I ratio for PCM modulation is about 12 dB. For simultaneous thresholding, the subcarriers are equal in power. To this S/I ratio must be added the rejection characteristics of the subcarrier filter in the vehicle baseband assembly unit. With 30 dB rejection, the total predetection S/I ratio is better than 40 dB. This is more than adequate to make the interference tolerable.

For the reverse case of analog FM interference with the PCM/PM, the 1.25-MHz subcarrier is assumed to have a peak deviation of 30 kHz with a 20-kHz sine wave. Basic interference in the PCM band is down about 40 dB from the signal. Add to this the baseband assembly filter rejection, and the total S/I ratio becomes 70 dB. The analysis (Volume III, Appendix VIII) indicates that single-frequency interference in the PCM demodulator will be quite acceptable if it is only 20 dB below the signal power.

To examine the effect that interference from PCM/PM data (on the 1.7-MHz services) may have on data quality of the 1.024-MHz and 1.25-MHz services, worst-case conditions are selected as follows: data rates of 256 kbps on the 1.7-MHz subcarrier and 64 kbps on the 1.024-MHz subcarrier, and an analog signal of 20 kHz with a peak deviation of ± 30 kHz on the 1.25-MHz subcarrier.

Results of the analysis,* summarized in Table 3-10, indicate that the presence of PCM/PM data on the 1.7-MHz subcarrier gives rise to conservative S/I ratios of 41.2 dB in the 300-kHz predetection bandwidth on the 1.024-MHz subcarrier and 29.5 dB in the 150-kHz predetection bandwidth on the 1.25-MHz subcarrier; these S/I values are based on system operation at optimum modulation indices for each service. Also, the rejection of the 1.7-MHz subcarrier by the post-modulator filter is 32 dB at 1.024 MHz and 18 dB at 1.25 MHz. While maintaining threshold levels for each of the services and optimizing the modulation indices, the quality of the data was not degraded on the 1.024-MHz and 1.25-MHz services in the presence of PCM/PM data on the 1.7-MHz subcarrier.

TABLE 3-10
SIGNAL-TO-INTERFERENCE CALCULATIONS
AT OPTIMUM MODULATION INDICES

Parameter	Subcarrier Service	
	1.024 MHz	1.25 MHz
Predetection Bandwidth (kHz)	300.0	150.0
Bit Rate for 1.7 MHz (bps)	256.0	256.0
Signal to Interference (dB)	41.2	29.5
Rejection of 1.7 MHz (dB)	32.0	18.0

*SGLS Test Transponder 1.7-MHz Post-Modulator Filter Analysis, Philco-Ford WDL-TR3359, Revision 1, 14 June 1968.

3.3 DOWNLINK PERFORMANCE

This section presents the downlink performance in terms of the power required to operate each service at threshold. Ground station parameters of interest are system noise temperature, dynamic range, and the signal thresholds for the various services. In addition to these parameters, information is provided that will assist the SGLS user in optimizing performance for specific missions. A procedure is also outlined for determining performance, and an example is provided for a typical downlink configuration.

3.3.1 System Noise Temperature

System noise temperature has been calculated for the SGLS equipment items operating in conjunction with typical high- and low-gain antenna configurations at the RTS. Variations can be expected due to minor differences in antenna configurations at some sites. These variations are not, however, considered significant.

Table 3-11 summarizes the system noise temperatures (T_s) for the two antennas. Note that these temperatures are referenced to the input of the parametric amplifier. Typical equipment configurations and the associated models used in the analysis are presented in the following paragraphs.

TABLE 3-11
SYSTEM NOISE TEMPERATURES

Antenna Configuration	Noise Temperature* T_s
High Gain	
Sum	336° K
Difference	900° K
Low Gain	290° K

*Referenced to parametric amplifier input

Equipment Configurations

The RF configurations for the high-gain and low-gain SGLS are shown in Figures 3-7 and 3-8. These were developed from the best data available. The RF configuration drawings identify the parameters of concern. These and other parameters are summarized in Tables 3-12 and 3-13 as a convenient reference for the noise temperature models and equations discussed below.

Noise Temperature Models

Noise temperature models for the high- and low-gain configurations are shown in Figures 3-9 and 3-10, respectively. The model consists of three elements; antenna temperature, transmission line, and the receiver. The latter includes the parametric amplifier, GRARE, and interconnecting components, the system noise temperature for this model is given by

$$T_s = T_A + (L_L - 1) T_O + L_L T_R \quad (1)$$

where

T_s = system noise temperature referenced to the antenna aperture

T_A = antenna noise temperature

L_L = total loss contributed by all RF and transmission line components from the antenna to the input to the parametric amplifier.

T_O = standard temperature (290°K)

T_R = noise temperature of the receiver

For the sum channel of the high-gain configuration, we have

$$T_R = T_P + \frac{(L_2 - 1) T_O}{G_P} + \frac{T_{PD} L_2}{G_P} + \frac{(L_3 - 1) L_2 T_O}{G_P G_{PD}} + \frac{T_{GR} L_3 L_2}{G_P G_{PD}} \quad (2)$$

WR430 = 0.38 dB/100 feet @ 2.25 GHz
= 0.0038 dB/foot

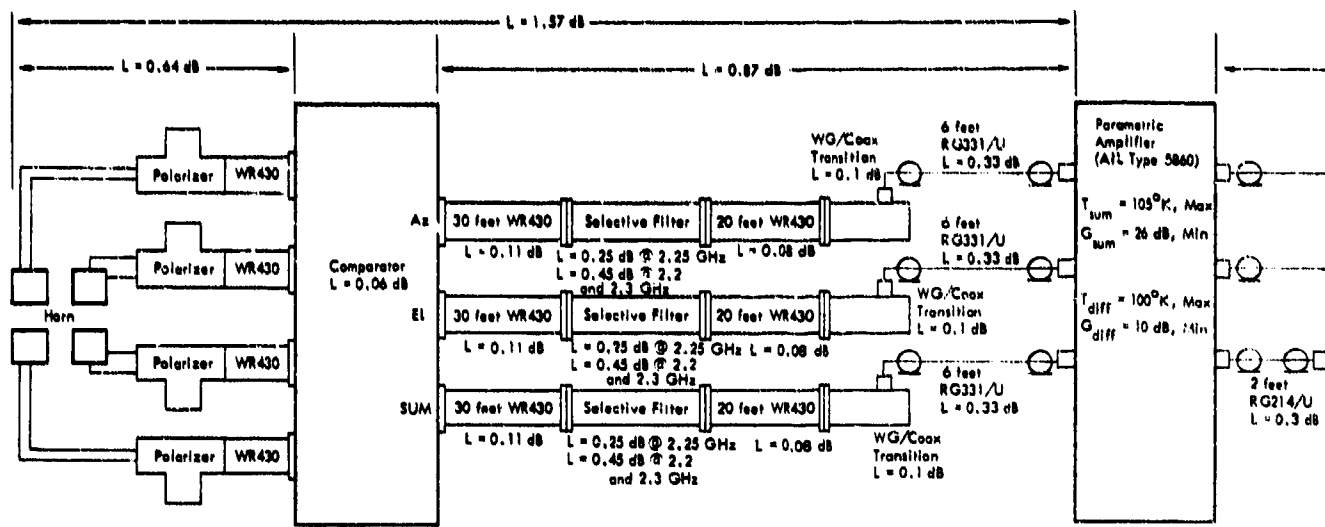
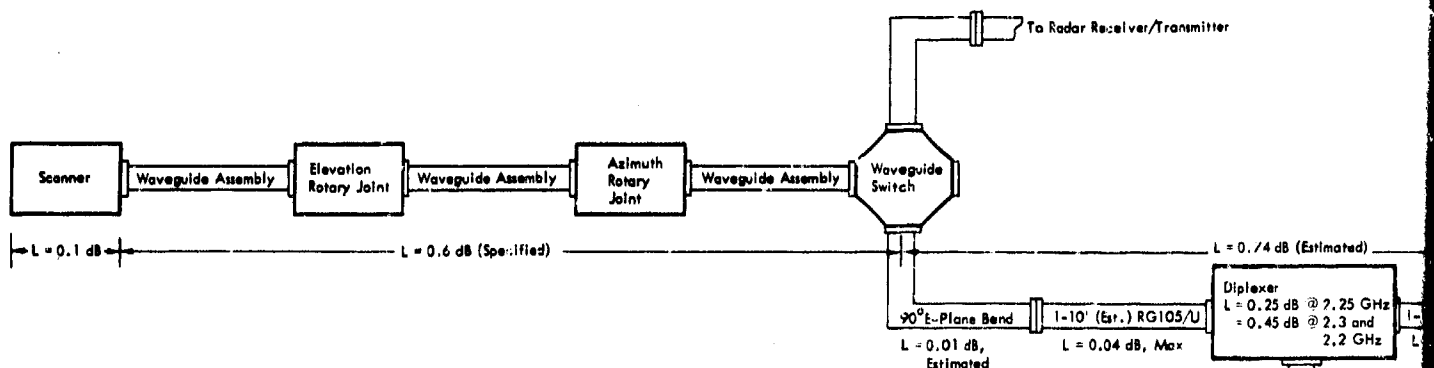


Figure 3-7 SGLS High-Gain RF Configuration



NOTES:

1. Waveguide/Cable lengths shown are approximate.
2. All losses shown evaluated at 2.25 GHz unless otherwise noted.
3. Waveguide/Cable losses:

RG105/U (WR430)	0.38 dB/100 feet	@ 2.25 GHz
RG331/U (1/2 inch Foam)	5.5 dB/100 feet	@ 2.25 GHz
RG (3/8 inch Foam)	6.6 dB/100 feet	@ 2.25 GHz
RG318/U (7/8 inch Air)	2.3 dB/100 feet	@ 2.25 GHz
RG214/U	15 dB/100 feet	@ 2.25 GHz
	2.5 dB/100 feet	@ 130 MHz
RG254/U (1/2 inch Air)	1.4 dB/100 feet	@ 2.25 GHz

Figure 3-8 SGLS Low-Gain RF Configuration

WDL-TR3227-1
Volume I, Part 1

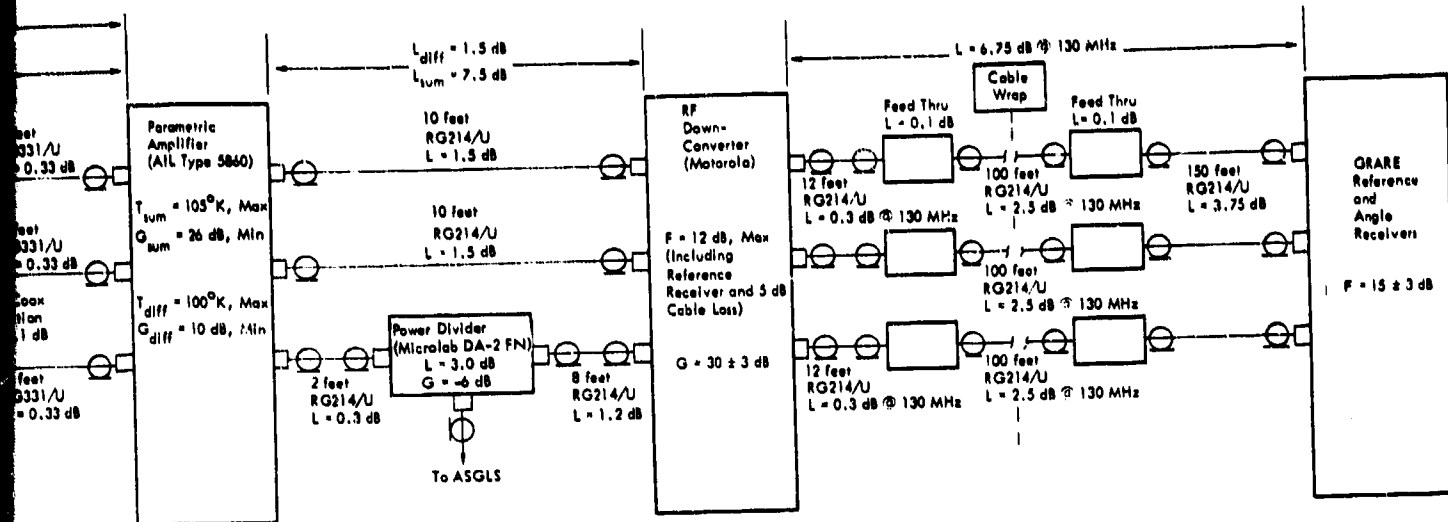


Figure 3-7 SGLS High-Gain RF Configuration

To Radar Receiver/Transmitter

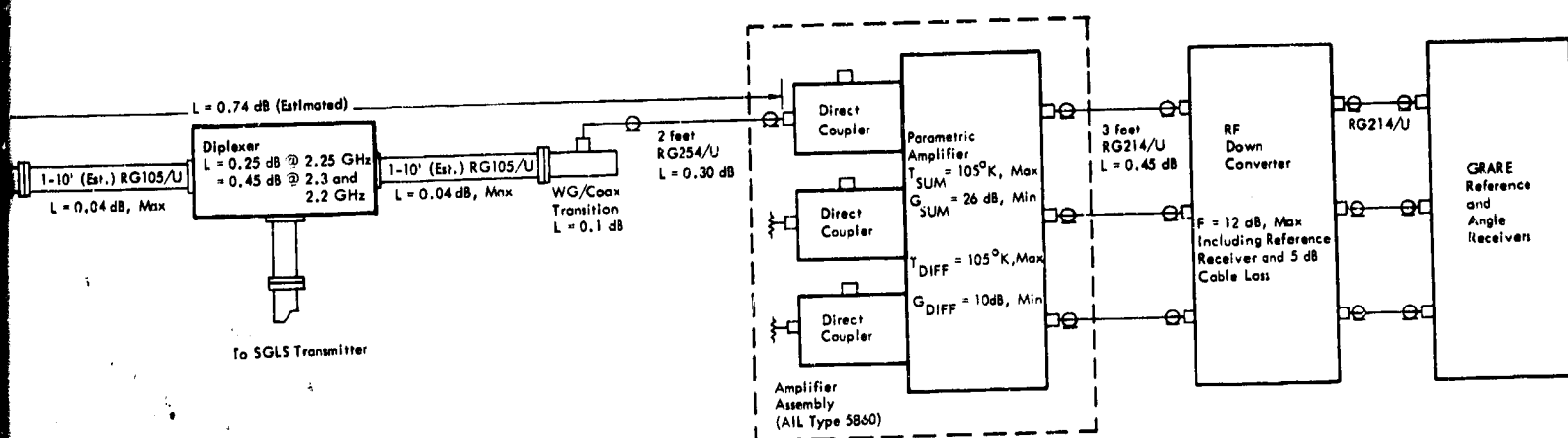


Figure 3-8 SGLS Low-Gain RF Configuration

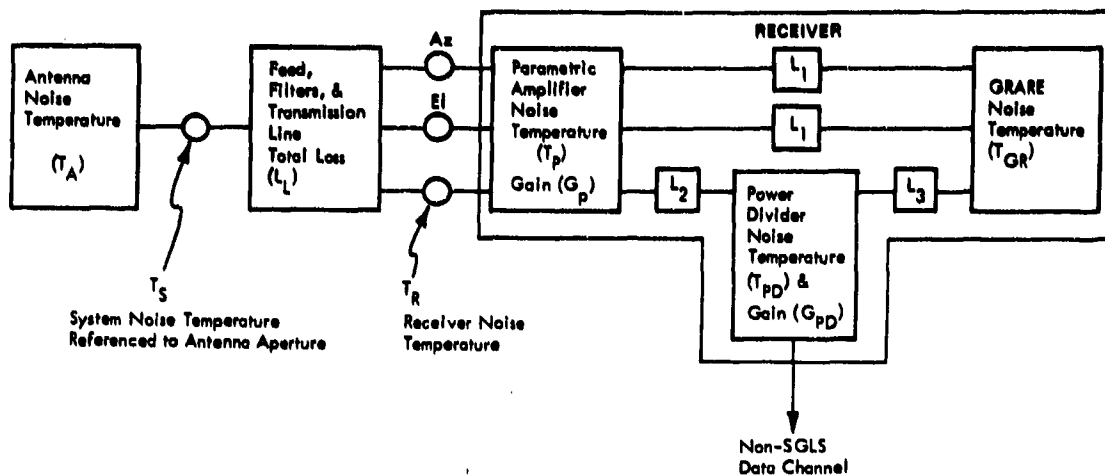


Figure 3-9 SGLS High-Gain Noise Temperature Model

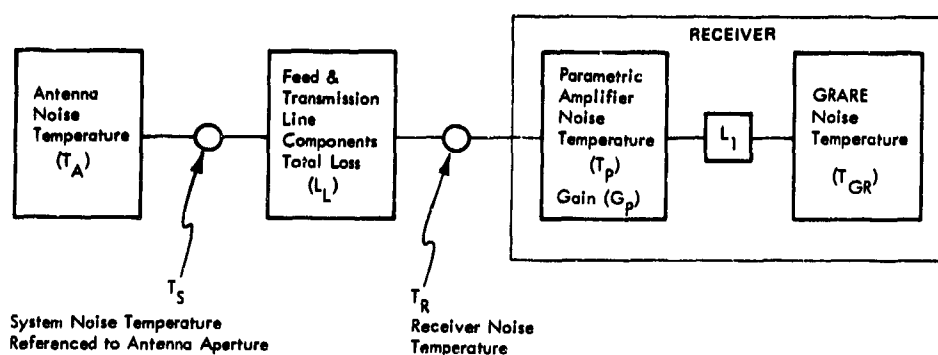


Figure 3-10 SGLS Low-Gain Noise Temperature Model

where

- T_p = noise temperature of the sum channel of the parametric amplifier
- G_p = gain of the parametric amplifier
- L_2 = loss between the output of the parametric amplifier and the power divider
- T_{PD} = noise temperature of the power divider = $(L_{PD} - 1) T_O$, where L_{PD} = the loss in the power divider (3 dB)
- L_3 = loss between the output of the power divider and the input to the GRARE
- T_{GR} = noise temperature of the GRARE
- G_{PD} = gain of the power divider

Substituting the values from Table 3-12 into Equations (1) and (2) gives a system noise temperature in the sum channel (T_s) of 504°K referenced to the antenna aperture. Dividing this result by L_L yields $T_s = 336°K$ referenced to the input to the parametric amplifier.

For the difference channel of the high-gain configuration, we have

$$T_R = T_{P(\text{Difference})} + \frac{(L_1 - 1) T_O}{G_{P(\text{Difference})}} + \frac{T_{GR} L_1}{G_{P(\text{Difference})}} \quad (3)$$

where $T_{P(\text{Difference})}$ is the noise temperature of the difference channel of the parametric amplifier.

TABLE 3-12
SGLS HIGH-GAIN TEMPERATURE CHARACTERISTICS*

Parameter	Value
T_A	67°K
T_O	380°K
L_1	1.50
T_p (Sum)	105°K
G_p (Sum)	282**
T_p (Diff)	100°K
G_p (Diff)	10
T_{PD}	200°K
G_{PD}	0.25
T_{GR}	4310°K
L_1	1.51
L_2	1.07
L_3	1.34

*Includes specified minimum gains, maximum insertion losses and noise temperatures. Coaxial cable and waveguide losses evaluated at 2.25 GHz. Antenna at 5 degrees elevation.

**Includes 1.6-dB anticipated field degradation.

Substituting the values from Table 3-13 into Equations (1) and (3) gives a system noise temperature in the difference channel (T_s) of 1350°K referred to the antenna aperture. Dividing this result by L_L yields $T_s = 900^{\circ}\text{K}$ referred to the input of the parametric amplifier.

For the low-gain configuration (Figure 3-10) the noise temperature of the receiver, T_R , is given by

$$T_R = T_P + \frac{(L_1 - 1)T_O}{G_P} + \frac{T_{GR}L_1}{G_P} \quad (4)$$

Substituting the values from Table 3-13 into Equations (1) and (4) gives a system noise temperature (T_s) of 397°K referenced to antenna aperture. Dividing this result by L_L yields $T_s = 290^{\circ}\text{K}$ referenced to the input of the parametric amplifier.

In the computations above, the effects of mismatch losses are relatively minor and vary as a function of frequency. For this reason, their contribution to system noise temperature has not been included. Further, for the high-gain configuration, antenna temperature (T_A) was obtained

TABLE 3-13
SGLS LOW-GAIN NOISE TEMPERATURE CHARACTERISTICS*

Parameter	Value
T_A	118°K
T_O	290°K
L_L	1.37
T_P	105°K
G_P	282**
T_{GR}	4310°K
L_1	1.1

* Includes specified minimum gains, maximum insertion losses and noise temperatures. Coaxial cable and waveguide losses evaluated at 2.25 GHz with the antenna at 5° elevation.

** Includes 1.5 dB anticipated field degradation.

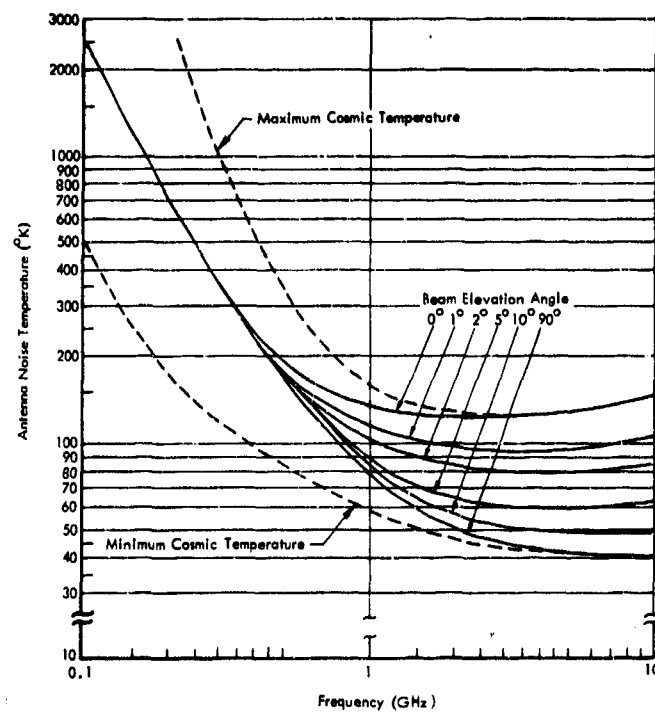
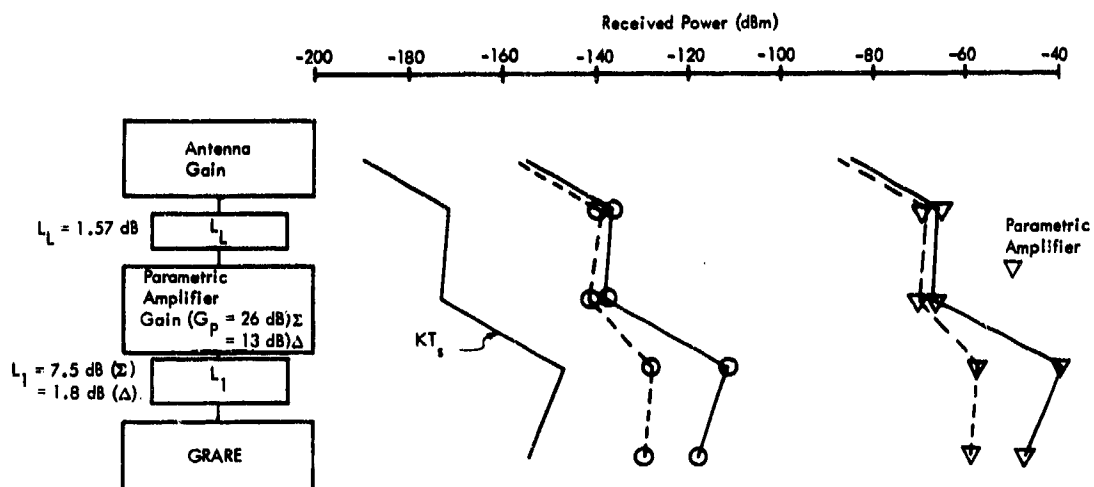


Figure 3-11 Noise Temperature of a Typical Directional Antenna

from the typical antenna temperature curves of Figure 3-11. The low-gain antenna temperature was obtained from measured data.

3.3.2 Dynamic Range

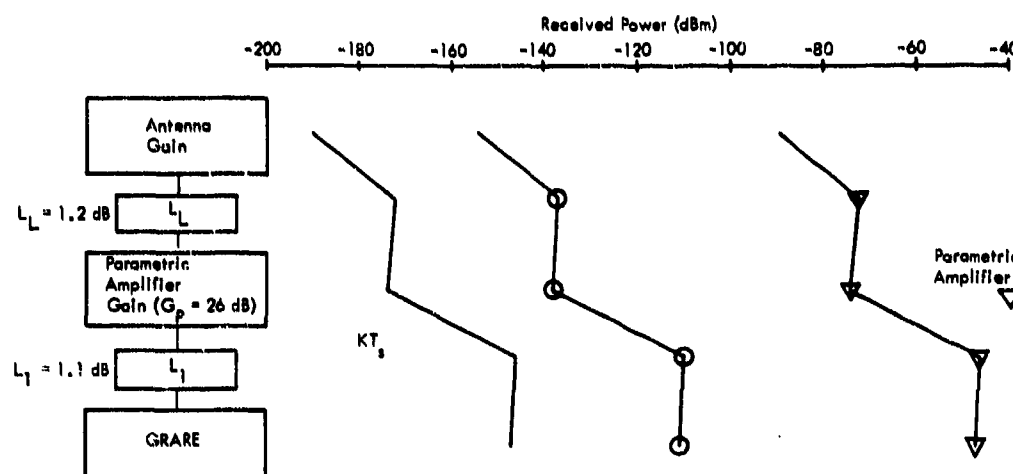
System dynamic range is that range of signal power from threshold signal level (referred to the parametric amplifier input) to a maximum level that results in no more than 1-dB compression in any RF/IF amplifier stage. From this definition, we see that a specific dynamic range exists for each tracking or data demodulation bandwidth considered. Figures 3-12 and 3-13 show system dynamic range associated with phase-lock tracking in the 1-kHz bandwidth. System noise power (dBm/Hz) and threshold carrier power for the 1-kHz phase-lock tracking bandwidth have been plotted, along with the maximum input (saturation) level to the GRARE down-converter.



LEGEND

- threshold levels
- ▽ 1-dB compression levels
- sum channel (1-kHz tracking bandwidth)
- - - difference channel
- KT_s boltzmann's constant
- L_L total loss contributed by all RF and transmission line components from antenna to input of parametric amplifier
- L₁ loss between output of parametric amplifier and input to GRARE

Figure 3-12 SGLS High-Gain Dynamic Range



LEGEND

- threshold levels (1-kHz tracking bandwidth)
- ▽ 1-dB compression levels
- KT_s boltzmann's constant
- L_L total loss contributed by all RF and transmission line components from antenna to input of parametric amplifier
- L_1 loss between output of parametric amplifier and input to GRARE

Figure 3-13 SGLS Low-Gain Dynamic Range

The dynamic range (D) is given by

$$D = P_S - P_T$$

where P_S is saturation power and P_T is threshold power and where all signal levels are referred to the parametric amplifier input. For the example shown in Figure 3-12, dynamic range is

$$\begin{aligned} D &= -65.5 - (-137.3) \\ &= 71.8 \text{ dB} \end{aligned}$$

The dynamic ranges for other GRARE tracking and data demodulation bandwidths may be determined in a similar manner. (For the example shown above, a 336°K system noise temperature, an SNR of +6 dB, and a -47 dBm maximum allowable input are assumed.)

3.3.3 Carrier 1 Thresholds

The downlink Carrier 1 signal uses frequency division multiplex (FDM) to enable simultaneous transmission of multiple services. The FDM is generated in the vehicle by phase modulating the carrier with a baseband mix of subcarriers, each individual premodulation subcarrier level being chosen to yield a specific carrier modulation index. The carrier modulation is essentially narrowband PM, so that, in the RF spectrum, the subcarriers appear as first-order sidebands, higher order sidebands being of negligible power level. The division of total signal power between the various subcarriers and the residual carrier is a function of the pre-modulation subcarrier levels and is discussed further in succeeding paragraphs. This modulation scheme permits the use of a narrowband carrier-tracking phase-locked loop to coherently demodulate the downlink carrier, the resulting spectrum appearing simply as a linear translation of the RF spectrum down to baseband. Extraction of data from the subcarriers is performed in separate subcarrier demodulators.

Under this modulation scheme, the retrieval of data from any subcarrier involves a dual demodulation process, and accordingly, at low SNR's two sources of signal quality degradation are evident because of the imperfections in the operation of the two demodulators. This consideration is in addition to the concept of threshold itself, and the degradation will make itself felt as an effective increase in the required signal power in the receiving equipment to achieve the data quality (SNR or bit error rate) theoretically available at threshold. The system performance computations incorporate empirical degradation figures attributable to these effects. For PCM, a further process is required after the dual demodulation to regenerate the digital data appearing at the noisy subcarrier demodulator output. The process uses an integrate and dump-matched filter and involves phase-lock acquisition of the noisy demodulated bit stream. This takes place in a bit synchronizer and accounts for the third source of performance degradation appearing in the PCM performance tables.

Threshold in an analog subcarrier modulation system is usually defined as the system subcarrier-to-noise ratio (S/N) at which the quality of the demodulated output begins to deteriorate at a disproportionate rate with further reductions in S/N. Efficient design of such a system requires that the system parameters (IF and baseband output bandwidths in FM, for instance) be chosen in such a way that the desired data quality is available at threshold but fails just below threshold. As a result, the threshold subcarrier-to-noise ratio is the important parameter in defining the downlink signal power requirements.

In the case of SGLS PCM services, which use biphase PSK modulation of the subcarrier, the threshold definition differs somewhat in that the coherent demodulation process used exhibits no readily definable threshold, and the important parameter in this case is the SNR theoretically required in a measurement bandwidth that is equal to the bit rate so as to yield a bit error probability of one in 10^5 .

In Tables 3-14 through 3-19 the subcarrier power required to provide the various services under threshold conditions is computed. Performance degradations are included in the calculation to provide a realistic estimate of subcarrier power.

Since subcarrier power and noise density involve absolute power levels rather than ratios, a point must be defined in the RF receiving system (somewhere between the antenna aperture and the subcarrier demodulator) at which the quoted power levels are to be obtained. The input to the parametric amplifier is taken as standard for this report for compatibility with system test procedures. All absolute signal power levels and all RF gain and loss factors, such as antenna gain and system noise temperature, are referred to this point. Subcarrier power levels are not directly measurable at this point but may be accurately inferred from measurements of the total signal power by applying the power division factor discussed in the succeeding paragraph.

Carrier 1 Performance Optimization

In a multiservice system, the transmitted downlink signal power must be divided among the various subcarrier services, preferably in an optimum fashion. This may be accomplished by setting the carrier phase deviation due to each subcarrier according to the principles outlined in Volume III, Appendix VI. The object of this optimization is to minimize the total signal power that must be transmitted, to give specific subcarrier power levels. The actual subcarrier power required is a function of the modulation scheme employed and the bandwidth or bit rate of the transmitted data. The analysis below determines the power levels required at the threshold in the various subcarrier modes. These results may be used as inputs to the optimization procedure in the referenced appendix to obtain the required modulation indices. The procedure, as given in Volume III, Appendix VI, is predicated on the typical requirements that all subcarrier services reach threshold at the same RF power level. Variations from this situation are accommodated by adding the appropriate power margin to each threshold subcarrier power before application of the optimization procedure.

There are many possible choices of subcarrier power division due to the highly diverse choice of operating capabilities offered by the SGLS Carrier 1:

- Choice of number of subcarrier services. Carrier 1 may be modulated by any number or combination of the available subcarriers from one to four.
- Choice of data rates. Bit rates for the 1.024- and 1.7-MHz subcarriers are available between 7.8 bps and 256 kbps, while the analog channel gives dual bandwidth options. In addition, the 1.7-MHz subcarrier may carry either PCM or IRIG telemetry.

- Choice of signal power distribution among the subcarrier services.

Depending on mission requirements, differing signal strength margins may be assigned to the various services. Thus, if high reliability or long range performance is required of one particular service, that service may be allocated a proportionally greater share of the available RF signal power at the expense of the remaining services by proper selection of carrier phase deviations. In such a case, the subcarrier service thresholds will not necessarily occur at the same received RF signal level.

The general relationship between the total Carrier 1 power and the power in a specific sinusoidal subcarrier is given, as a function of modulation indices, by

$$\frac{P_{sc_1}}{P_T} = 2J_1^2(\beta_1) \left[\prod_{i=2}^N J_0^2(\beta_i) \right] \cos^2(\beta_{prn})$$

where

β_i = the carrier modulation index due to the i^{th} sinusoidal subcarrier

β_1 = the carrier modulation index due to the subcarrier in question

P_{sc_1} = the power in the subcarrier in question

P_T = the total unmodulated carrier power

$\frac{P_{sc_1}}{P_T}$ = designated the subcarrier 1 suppression factor when stated in dB's

β_{prn} = the uplink modulation index of the PRN ranging subcarrier for a 1:1 turnaround ratio

N = number of subcarriers

J_0 = bessel functions of the zeroth order

J_1 = bessel functions of the first order

The carrier suppression factor is given by

$$\frac{P_c}{P_T} = \left[\prod_{i=1}^N J_0^2(\beta_i) \right] \cos^2(\beta_{prn})$$

In calculating the performance of a given SGLS configuration, the carrier suppression factor should always be checked to ensure that an SNR well in excess of 6 dB in the carrier tracking phase-locked-loop bandwidth is available in order to assure reliable carrier lock.

Where the PRN ranging subcarrier is of concern, the relationship between the Carrier 1 power and the power in the PRN subcarrier (subcarrier suppression) is

$$\frac{P_{prn}}{P_T} = 8 \left(\frac{\sin}{\pi} \right)^2 (\beta_{prn}) \left[\prod_{i=1}^N J_0^2(\beta_i) \right]$$

The subcarrier suppression equations are used in relating the subcarrier power requirements of an individual subcarrier service to the total received power when other subcarriers are present.

In applying the above equations, certain uplink services are subject to turnaround and will appear as additional subcarriers on the downlink. The uplink analog channel and the low- and medium-rate command channels are on subcarriers of lower frequency than the nominal 800 kHz cutoff frequency of the vehicle-borne turnaround lowpass filter. These subcarriers, when present, must be included in the number (N) of downlink subcarriers in computations of carrier and subcarrier suppression. Turned around subcarriers will appear on the downlink with uplink modulation indices multiplied by the turnaround ratio.

FM Service Thresholds

SGLS offers three downlink FM service capabilities on two of the Carrier 1 subcarriers. In all cases, a threshold SNR of 10 dB is assumed. Additional incidental losses on the order of 1.0 to 2.0 dB are known to occur on all services. The threshold power calculation is listed in Table 3-14.

TABLE 3-14
FM SUBCARRIER SERVICES - SUBCARRIER THRESHOLD POWER CALCULATIONS

Parameter	1.25-MHz Voice	1.25-MHz Analog	1.7-MHz Telemetry
Threshold signal-to-noise ratio	10.0	10.0	10.0
Bandwidth (dB)	44.0	51.9	58.2
Demod. Loss (dB)	1.0	1.0	2.1
S/N (dB)	55.0	62.9	70.3
N _o (336° K) (dBm/Hz)	-173.3	-173.3	-173.3
Subcarrier Threshold Power (dBm)	-118.3	-110.4	-103.0

PCM Service Thresholds

Either the 1.024-MHz or the 1.7-MHz subcarrier may carry PCM data. Tables 3-15 and 3-16 list the respective subcarrier threshold calculations for each bit rate. Threshold SNR's in the tables reflect observed SNR degradations. In addition, the threshold subcarrier powers indicated apply strictly to NRZ-L and BIφ-L codes. Further degradations of 0.3 dB are observed when NRZ-M, NRZ-S, BIφ-M and BIφ-S codes are used. RZ codes effectively operate at double the bit rate and suffer a corresponding 3-dB SNR degradation. Figure 3-5 defines these PCM codes.

The PCM threshold is the operating point for 10^{-5} bit error probability (P_e) at all bit rates.

TABLE 3-15
DLINK SERVICE THRESHOLDS, CARRIER 1: 1.024-MHz SUBCARRIER*

	Bit Rate (kbps)	7.8×10^{-3}	31.2×10^{-3}	62.5×10^{-3}	0.25	0.5	1	1.6	4	8	32	51.2	64	128
Required S/N_0 (dB-Hz)**	9.6	9.6	9.6	9.6	9.6	9.6	9.6	9.6	9.6	9.6	9.6	9.6	9.6	9.6
$P_e = 10^{-5}$														
PCM Degradation (dB)***	1.0	1.0	1.0	1.0	1.0	1.0	1.0	1.0	1.0	1.0	1.0	1.0	1.0	1.0
S/C Demod Degradation (dB)***	4.0	3.0	3.0	3.0	3.0	3.0	3.0	3.0	3.0	3.0	3.0	3.0	3.0	3.0
RF Demod Degradation (dB)***	0.2	0.2	0.2	0.2	0.2	0.2	0.2	0.2	0.2	0.2	0.2	0.2	0.2	0.2
Required S/N_0 (dB-Hz)	14.8	13.8	13.8	13.8	13.8	13.9	13.9	13.9	13.9	13.9	14.0	14.0	14.0	15.1
$N = K T_s B$ (dBm)	-164.4	-159.4	-155.4	-149.4	-146.3	-143.3	-141.3	-137.3	-134.3	-128.3	-126.2	-125.3	-122.3	
Subcarrier Threshold Power (dBm)	-149.6	-144.6	-141.6	-135.6	-132.4	-129.4	-127.4	-123.4	-120.3	-114.3	-112.2	-111.1	-107.2	

*System Noise Temperature = 336°K

** S/N_0 = signal-to-noise density ratio.

*** Empirical degradation (see Paragraph 3.3.3)

TABLE 3-16
DLINK SERVICE THRESHOLDS, CARRIER 1: 1.7-MHz SUBCARRIER*

	Bit Rate (kbps)	0.125	0.250	0.500	1	2	4	8	16	32	64	128	256
Required S/N_0 (dB-Hz)**	9.6	9.6	9.6	9.6	9.6	9.6	9.6	9.6	9.6	9.6	9.6	9.6	9.6
$P_e = 10^{-5}$													
PCM Degradation (dB)***	1.0	1.0	1.0	1.0	1.0	1.0	1.0	1.0	1.0	1.0	1.0	1.0	1.0
S/C Demod Degradation (dB)***	4.5	3.0	2.0	2.0	2.0	2.0	2.0	2.0	2.0	2.0	2.0	2.0	2.5
RF Demod Degradation (dB)***	0.2	0.2	0.2	0.2	0.2	0.2	0.2	0.2	0.2	0.2	0.2	0.2	
Required S/N_0 (dB-Hz)	15.3	13.8	12.8	12.8	12.8	12.9	12.9	12.9	12.9	13.0	13.1	13.1	14.4
$N = K T_s B$ (dBm)	-152.4	-149.4	-146.3	-143.3	-140.3	-137.3	-134.3	-131.3	-128.3	-125.3	-122.3	-119.2	
Subcarrier Threshold Power (dBm)	-137.1	-125.6	-123.5	-120.5	-127.4	-124.4	-121.4	-118.4	-115.3	-112.3	-109.2	-104.6	

*System Noise Temperature = 336°K

** S/N_0 = signal-to-noise density ratio.

*** Empirical degradation (see Paragraph 3.3.3)

PRN Ranging Threshold

The ranging system "threshold" is defined as the operating point at which the rms range error due to downlink noise is 30 ft. The performance of the range clock phase-locked loop is the major factor contributing to thresholding of the ranging system. The code acquisition process is not involved since code acquisition error probability can, in principle, be made arbitrarily low by appropriate choice of integration time.

The analysis in Volume III, Appendix II, indicates that a threshold S/N_0 of 26.6 dB-Hz will produce the 30-ft error when the 4-Hz clock loop bandwidth is used. As indicated in Table 3-17, this results in a PRN threshold power of -146.7 dBm.

TABLE 3-17
PRN RANGING THRESHOLD

Subcarrier signal-to-noise density ratio S/N_0	26.6 dB-Hz
N_0 (336° K)	-173.3 dBm/Hz
Subcarrier threshold power	-146.7 dBm

3.3.4 Carrier 2 Thresholds

Carrier 2 PCM data is regenerated in the same equipment as both Carrier 1 PCM services. In this case, the carrier power at threshold is the parameter of interest since direct PSK modulation of the carrier is used. Also, only a single demodulation process takes place, so that only two sources of performance degradation are evident: the carrier demodulation and the data regeneration. The quoted threshold SNR's in Table 3-18 include the appropriate empirical degradation factor at each bit rate.

3.3.5 Carrier 3 Thresholds

Table 3-19 gives the threshold computation for Carrier 3 operation. Any system SNR degradations are inherent in the threshold SNR figure quoted, since the FM demodulator operates directly on the received carrier. Further signal processing is not assumed since the data form is unspecified.

TABLE 3-18
CARRIER 2 THRESHOLDS

Parameter	Bit Rates				
	128 kbps	256 kbps	512 kbps	768 kbps	1024 kbps
Required C/N ₀ (dB-Hz*) $P_e = 10^{-5}$	9.6	9.6	9.6	9.6	9.6
PCM Degradation (dB)	1.0	1.0	1.0	1.0	1.0
Demodulator Degradation (dB)	3.0	2.9	2.3	2.3	3.1
Required C/N ₀ (dB-Hz)	13.6	13.5	12.9	12.9	13.7
N ₀ ** (dB/Hz)	-173.3	-173.3	-173.3	-173.3	-173.3
Bandwidth (dB)	51.1	54.1	57.1	58.6	60.1
RF Threshold dBm	-108.6	-105.7	-103.3	-101.8	-99.5

*Theoretical for BIΦ-L and NBZ-L codes. Add 0.3 dB to threshold for NRZ-M, NRZ-S, BIΦ-M, and BPS codes. Add 3 dB for RZ code (specification CPRAD-653A, PCM Stored Program Telemetry Ground Station for SGLS).

**Noise power density for 336°K system noise temperature.

TABLE 3-19
CARRIER 3 THRESHOLDS

Mode	500-kHz BW	3-MHz BW	35-MHz BW
Demodulator	Modulation Tracking Phase- Locked Loop	Modulation Tracking Phase- Locked Loop	Conventional Discriminator
Predetection- bandwidth (dB-Hz)	57.0	64.7	75.4
S/N ratio (dB)*	10.0	10.0	10.0
N ₀ (dB/Hz)**	-173.3	-173.3	-173.3
RF Threshold (dBm)	-106.3	-98.6	-87.9

*Measured in predetection bandwidth.

**Noise power density for 336°K system noise temperature.

3.3.6 Typical Performance

Because of the large number of available combinations of downlink signal configurations, it is not feasible to present in this analysis all possible performance data. Instead, a procedure is provided to assist the SGLS user in determining the performance of a specific combination of services. In addition, the performance of a typically configured system is presented.

Procedure for Determining Performance

The procedure for determining downlink performance consists of four steps:

1. Compute the available total received power (P_T)
2. Determine required threshold power (P_R)
3. Compute subcarrier suppression factor (P_S)
4. Compute the power margin (P_M)

Each of these steps is considered in detail in the following paragraphs.

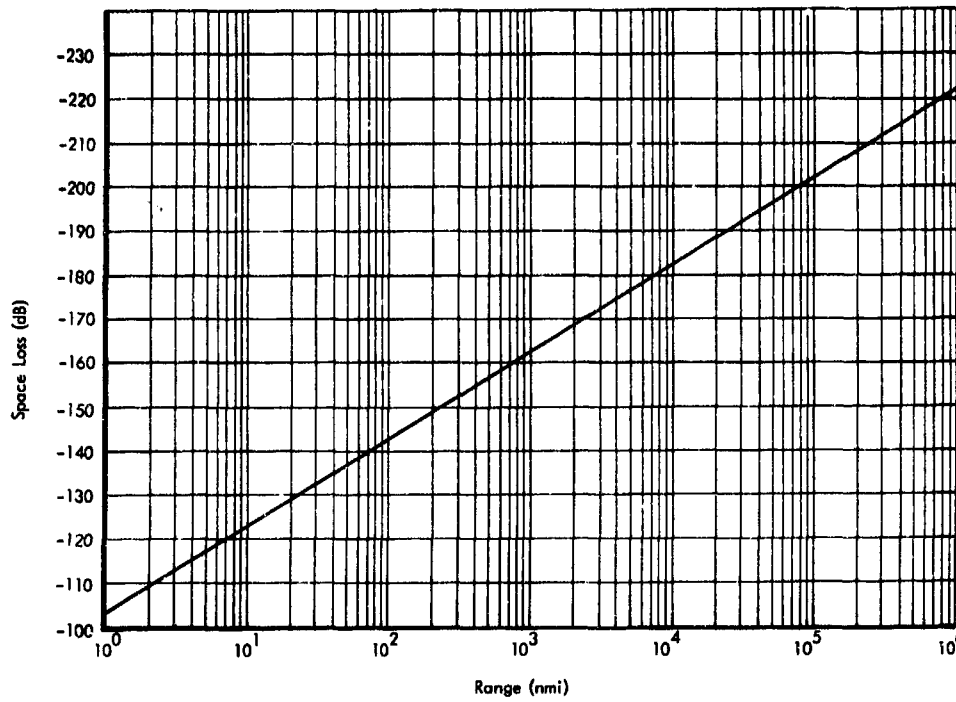
Compute P_T —the available total received power in dBm. As a first step in determining downlink performance, the amount of total received power available at the input reference point (parametric amplifier input) must be determined. This required knowledge of the operating parameters of the spacecraft which, in general, varies from one vehicle to another.

Table 3-20 presents a typical downlink power computation. A 2-W vehicle transmitter is postulated along with an omnidirectional antenna. Space loss is considered the variable in this case. The SGLS high gain antenna, a 60-ft parabola with a multipurpose feed, is assumed. This provides a gain of 48 dB referred to the parametric amplifier input. The received signal power is seen to be $76.2 - L_s$ dBm, where L_s is the space loss in dB for the mission of interest.

TABLE 3-20
DLINK POWER BUDGET, TYPICAL SYSTEM

Parameter	Value
Carrier 1 Vehicle Transmitter Power (2 W)	33.0 dBm
Multiplexer and Cable Loss	-1.8 dB
Vehicle Transmitter Antenna Gain	0 dB
Effective Radiated Power (ERP)	31.2 dBm
Space Loss ($L_s = 104.6 + 20 \log R$ nmi)	$-L_s$ dB
Polarization Loss (linear polarization)	-3.0 dB
Receiver Antenna Gain (referred to paramp input)	48 dB
Total Received Power (P_t)	$76.2 - L_s$ dBm

A graph of space loss vs vehicle range in the downlink frequency band is shown in Figure 3-14. This may be used in lieu of computation to obtain the value of L_s .



Determine P_R - the required threshold power in dBm. This may be determined from Tables 3-14 through 3-19, which show subcarrier and, where appropriate, carrier threshold powers for each downlink service.

Compute P_S - the subcarrier suppression factor. This applies to the subcarrier services on Carrier 1 only, and not to Carriers 2 and 3. Subcarrier suppression is the difference between the total signal power and the effective power in the first-order sidebands. (See "Performance Optimization" under Paragraph 3.3.3 for the computation of this factor.)

Compute P_M - the power margin. This is the margin (in dB) between power available and power required. This margin, a function of vehicle range, is determined as follows:

$$P_M = P_T - (P_R + P_S)$$

A convenient method of expressing this information graphically is shown in Figures 3-15 through 3-18, where P_T is shown plotted against vehicle range in nmi, and $P_R + P_S$ is shown as the minimum usable P_T for operation at threshold.

Typical Performance Curves

Utilizing the procedure outlined in the preceding paragraphs, the performance of a typical SGLS downlink configuration was determined. This performance is illustrated in Figures 3-15 through 3-18. These figures are plots of total received signal power (P_T) for Carriers 1, 2, and 3, shown decreasing with vehicle range, and intersecting horizontal levels that indicate the threshold power level for each particular service. The point of intersection corresponds to the maximum useful vehicle range for that service. At shorter ranges the difference between the received power level and the threshold level is the power margin (P_M) in dB for that service.

For this example, the assumption is that a basic 2 watts of Carrier 1 power and 1/2 watt of Carrier 2 power are diminished by 4.8 dB (due to multiplexing losses prior to radiation) to yield vehicle ERP's of 28.2 dBm and 22.2 dBm, respectively. The downlink power budget calculation of Table 3-20, after modification of the

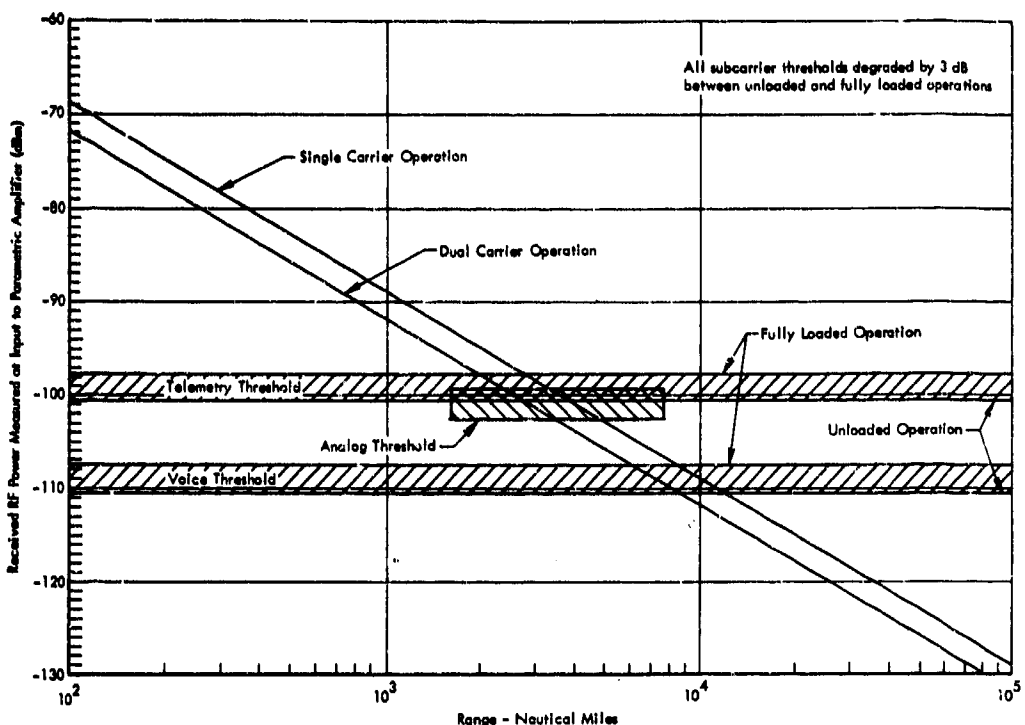


Figure 3-15 Downlink Carrier 1 Performance (High-Gain Antenna - FM Services)

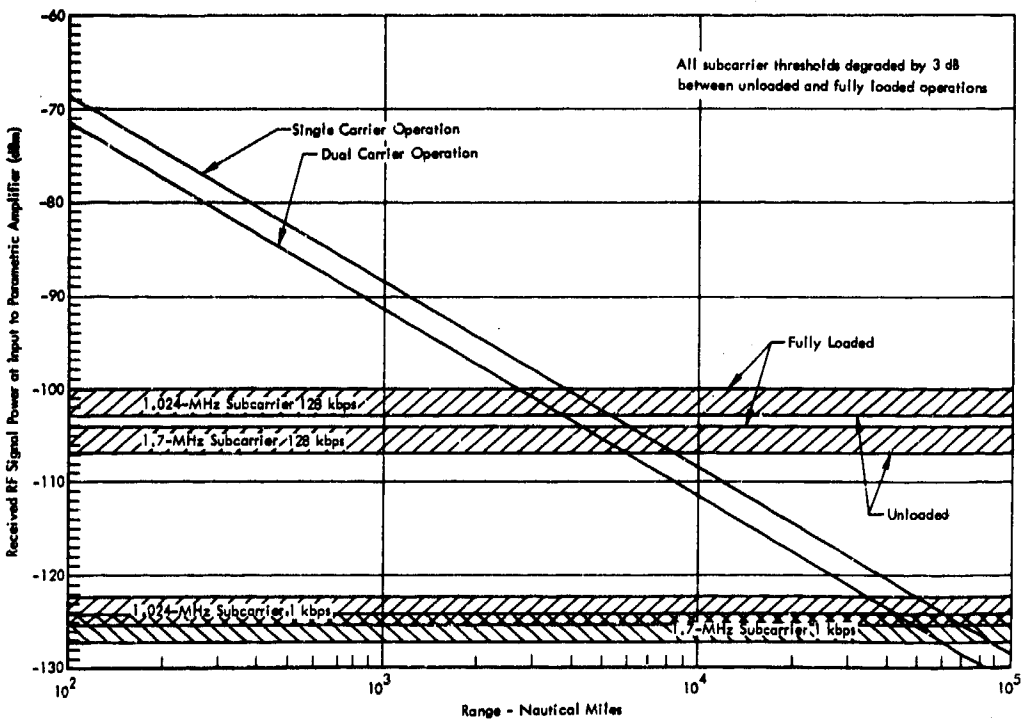
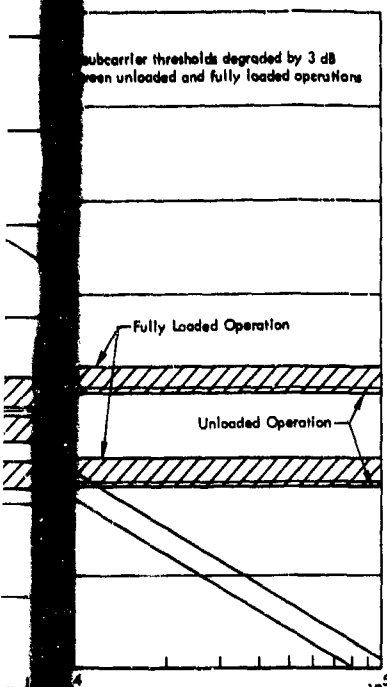


Figure 3-16 Downlink Carrier 1 Performance (High-Gain Antenna - PCM Services)



Antenna - FM Services

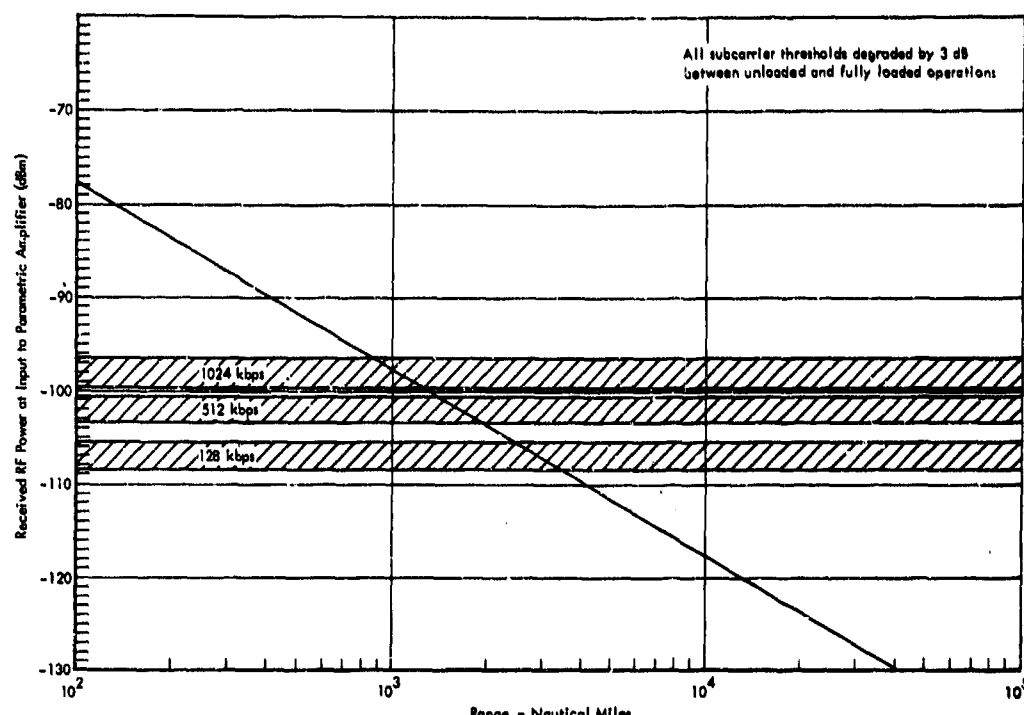
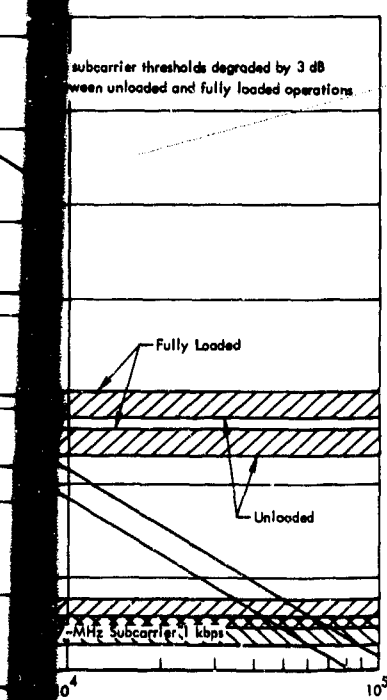


Figure 3-17 Downlink Carrier 2 Performance (High-Gain Antenna - PCM Services)



High-Gain Antenna - PCM Services

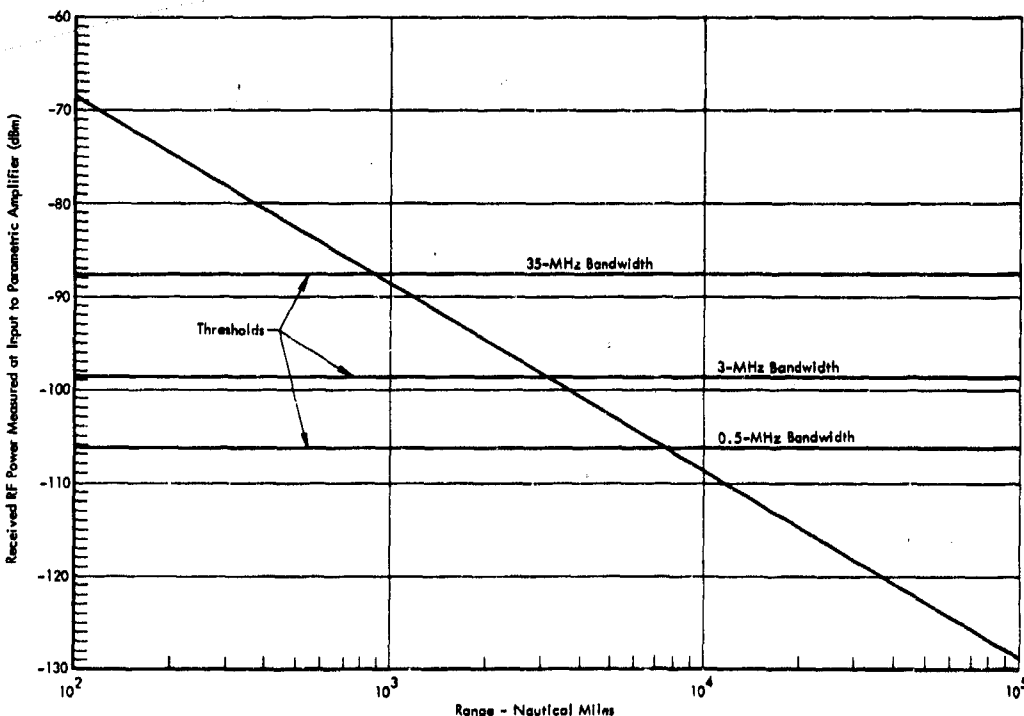


Figure 3-18 Downlink Carrier 2 Performance (High-Gain Antenna - FM Services)

ERP's to the above value, is used as the model for development of the total received power curves. In addition, the configuration indicated in Table 3-21 is also assumed. The division of power among the Carrier 2 subcarriers is therefore dictated by the carrier modulation indices appropriate to that configuration. Please note that the downlink performance represented in Figures 3-15 through 3-18 is in no sense optimum for any particular downlink service, and the configuration chosen is just one in an extremely wide range of choices of subcarrier mix, bit rates, etc.

The Carrier 1 threshold signal levels shown are for "loaded" and "unloaded" operation. These terms imply, respectively, that all uplink and downlink subcarrier services are present simultaneously, or that a single service only is present. In general, a maximum of 3-dB difference in effective received power at threshold is observed for the particular subcarrier mix implied in Table 3-21. Similarly the Carrier 2 threshold level is degraded by a maximum of 3-dB due to interference from Carrier 1.

TABLE 3-21
CARRIER 1 CONFIGURATION

Parameter	Voice/Analog 1.25 MHz	Analog Telemetry 1.7 MHz	PCM 1.024 MHz	PCM 1.7 MHz	Ranging 0.5 MHz
Carrier Mod Index	0.6 rad	1.4 rad	1.0 rad	1.4 rad	0.1 rad
Subcarrier Suppression (single service)	7.8 dB	2.3 dB	4.1 dB	2.3 dB	20.0 dB
Subcarrier Modulation	1/10 kHz FM	75 kHz FM	Biphase PM	Biphase PM	PRN
Subcarrier Deviation	$\pm 3/20$ kHz	± 75 kHz	$\pm \pi/2$ rad	$\pm \pi/2$ rad	Modulo 2
Bit Rate	N/A	N/A	7.8 to 128,000 bps	125 to 256,000 bps	1 Mbps
Predetection Bandwidth	25/155 kHz	660 kHz	N/A	N/A	N/A

SECTION 4

UPLINK SERVICES

SGLS uplink services provide for the transmission of commands, analog data, PRN ranging code, and voice communications from the ground station to the spacecraft. This section describes these services as well as the baseband structure and design characteristics of the uplink. This description is followed by an examination of uplink performance in terms of effective radiated power and carrier power distribution.

4.1 UPLINK FUNCTIONAL DESCRIPTION

Uplink services are provided by signals that have a minimum spectral width consistent with the required information bandwidth. The technique employed uses phase modulation with an index not greater than 1.5 radians. This signal provides a carrier of adequate strength for phase-locked-loop acquisition and lock to assure data demodulation and coherent downlink carrier generation. Information is transmitted by and recovered from the first sidebands. Interference between services is minimized by the proper selection of subcarrier frequencies and modulation indices.

4.1.1 Uplink Baseband Structure

The radio frequency carrier is modulated by the uplink baseband signal, which consists of the PRN ranging code sequence combined with the subcarriers carrying the other uplink services. The amplitudes of individual components of the baseband can be adjusted individually in four steps. After the amplitudes of the individual components are selected, the signals are combined to form the baseband. An adjustment is provided to set the RF modulation index. A peak modulation index of 1.5 radians will not diminish the RF carrier power more than 6 dB below its

unmodulated level. The typical case uses peak deviations ranging from 0.5 to 1.0 radian, which diminish the carrier from 0.6 to 2.4 dB.

The uplink baseband is illustrated in Figure 4-1 wherein the frequency baseline is successively expanded to clarify the fine structure at the lower frequencies and show how they relate to the subcarrier frequencies. Referring to Figure 4-1 low-, medium-, and high-rate commands are transmitted in the form of ternary NRZ digital signals represented by ternary FSK subcarriers. The groups are centered near 2 kHz, 80 kHz, and 1.0 MHz. Only one command-rate group is used at a time.

Analog data is transmitted by frequency-modulating a 1.25-MHz subcarrier, with an information bandwidth up to 20 kHz.

Voice signals frequency-modulate a 30-kHz subcarrier with the modulation signal pre-emphasized at approximately 6 dB per octave to improve the signal-to-noise ratio in the vehicle subcarrier demodulator.

PRN ranging sequences consist of a pseudorandom-coded binary signal, with a 1-Mbps rate. This signal phase-modulates the RF carrier directly. The spectrum for such a signal is a set of spectral lines that have a power density proportional to $(\sin x/x)^2$, with the first minima at ± 1.0 MHz about the carrier. This spectrum makes the selection of subcarrier frequencies near 1.0 MHz most suitable for high-rate commanding and analog data transmission, since minimum interference from PRN will be experienced. The selection of the region around 80 kHz for medium-rate commanding also minimizes interference from PRN by avoiding concentrations of power resulting from the periodic nature of the PRN code.

Table 4-1 summarizes the characteristics of the uplink baseband.

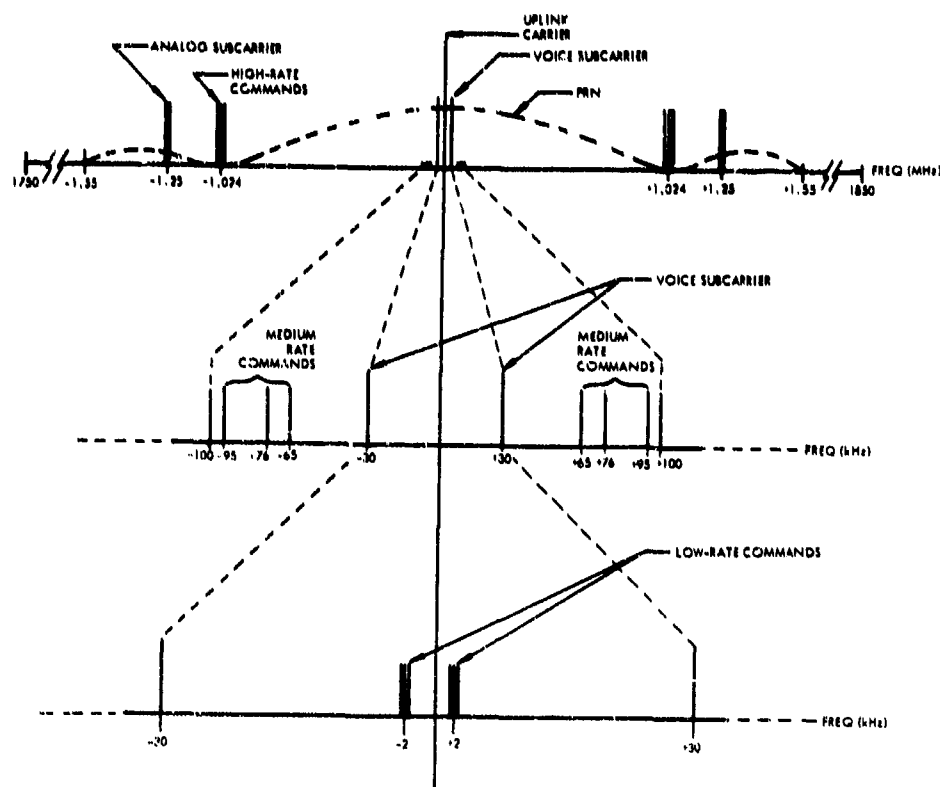


Figure 4-1 Characteristics of Uplink Baseband

Commanding

A noncoherent system is used for SGLS commanding since the demodulation equipment in the spacecraft is more reliable, weighs less, and consumes less power. While analysis (Volume III, Appendix V) indicates that a coherent system would have thresholds 7 dB below a noncoherent system, the higher threshold of the latter is more than offset by the 15 to 40 dB greater margins on the uplink compared to those on the downlink.

Command transmission is performed by a ternary data link, using frequency-shift keyed (FSK) subcarriers to represent the three data states of the ternary system. The data symbols "1", "0", and "S" are each represented by a discrete frequency. Only one frequency is permitted to appear at any time, and at no time may signals be absent. This is a nonreturn-to-zero (NRZ) signal providing a "carrier" for a sync wave amplitude-modulation.

The command signal contribution to the baseband can be varied from zero modulation of the carrier through nominal values of 0.1, 0.3, and 1.0 radian. Figure 4-2 illustrates the ternary FSK command subcarrier amplitude modulated by the sync signal.

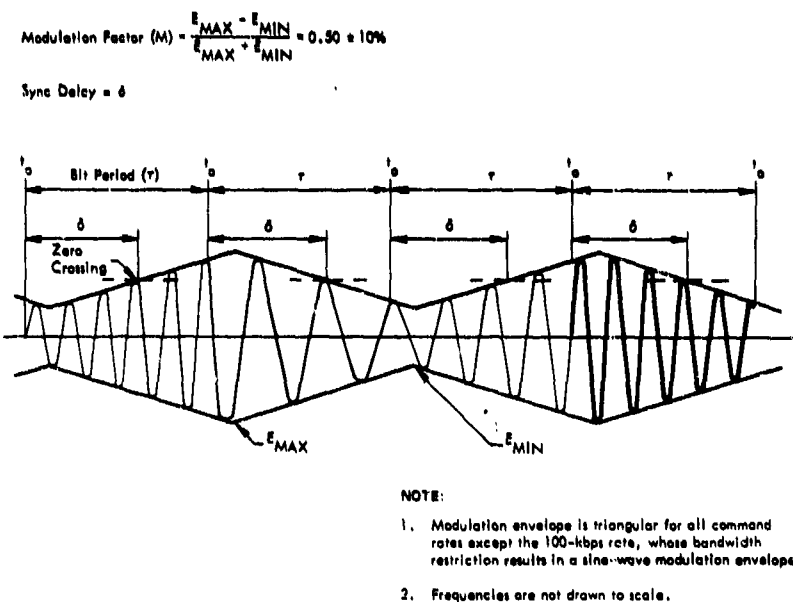


Figure 4-2 Typical Command Signal Waveform

Table 4-1 indicates the ternary frequencies associated with the low-, medium-, and high-rate command signals. At the low- and medium-baud rates, the signals are generated by keying on and off the outputs of constantly running oscillators. Demodulation of low- and medium-rate commands in the vehicle is accomplished by sets of three filters, followed by envelope detectors and logical decision circuits that determine which channel contains the greatest signal-plus-noise. At the high-baud rates, the signals are generated by a voltage-controlled oscillator (VCO) that responds to keyed step-function voltage inputs. This method is used because the spectrum out-of-band drops 12 dB per octave for the VCO versus 6 dB per octave for the keyed oscillators. This minimizes the crosstalk in the 1.25-MHz analog channel.

The limiter-discriminator predetection bandwidth in the vehicle is typically 200 kHz. Thus the 100,000-baud commands will be processed in a narrowband system, but the same system will appear to be a wideband FM system to the 10,000-baud command signal. Analysis (Volume III, Appendix V) shows,

TABLE 4-1
UPLINK BASEBAND CHARACTERISTICS

Service	Information Bandwidth	Modulation	Subcarrier Frequency	Subcarrier Deviation (Peak)
Voice	200 Hz to 3 kHz	FM	30 kHz	± 3.0 kHz
Analog	100 Hz to 20 kHz	FM	1.25 MHz	± 30.0 kHz
Low-Rate Command	1 and 20 bauds	FSK 1 0 S	2.05 kHz 2.40 kHz 2.79 kHz	N/A
Medium-Rate Command	100, 1000, 2000 bauds	FSK S 0 1	65 kHz 76 kHz 95 kHz	N/A
High-Rate Command	10k bauds	FSK 1 0 S	0.975 MHz 1.024 MHz 1.073 MHz	N/A
High-Rate Command	100k bauds	FSK 1 0 S	0.989 MHz 1.024 MHz 1.059 MHz	N/A
Ranging	1 Mbps	Direct Carrier PSK	N/A	N/A

however, that, when optimum frequency deviations are used, the difference in performance of the wideband case compared to the narrowband case is only 0.9 dB. Table 4-2 lists the optimum frequency deviations and associated signal thresholds for a bit-error rate of 10^{-5} .

Based on this analysis, the FSK threshold signal-to-noise ratios (SNR's) for a bit-error rate of 10^{-5} have been established at 20 dB measured in a bandwidth equal to the baud rate.

TABLE 4-2

COMMAND THRESHOLDS

Baud Rate	Deviation	Threshold SNR
10,000	± 49 kHz	19.5 dB
100,000	± 35 kHz	20.4 dB

To minimize the digital error rate in the presence of disturbances such as noise, the command data pulses should be sampled at a time when the pulse amplitude reaches a maximum value. As noted above, the sampling pulse is derived from a synchronizing signal that is amplitude modulated onto the command subcarrier. The phase of the synchronizing signal must be selected such that its zero crossings, which generate the sampling pulses, are coincident with the maximum value of the data pulses. The latter is, however, affected by timing uncertainties introduced by both ground and vehicle equipment as well as sync jitter due to link noise. These sync timing uncertainties were analyzed (Volume I, Appendix A) to determine the optimum total sync delay for the various command rates and the impact on the SNR (in the vehicle signal conditioner) required to maintain a bit error rate of 10^{-5} . In addition, a proposed value for the ground equipment sync delay was established. The results of this analysis are listed in Table 4-2A.

TABLE 4-2A

Parameter	Command Rate	
	100 k baud	Lower Rates
Total sync uncertainty	$\pm 0.113\tau$	$\pm 0.06\tau$
Optimum total sync delay	0.73τ	0.94τ
Increase in SNR for $P_e = 10^{-5}$	0.50 dB	0.18 dB
Sync Delay allocated to Ground Equipment†	0.60τ $\pm 0.10\tau$	0.60τ $\pm 0.03\tau$

τ = bit period

† = this sync delay optimum for 1 kbaud rate

The allocation of sync delay to the ground equipment (0.60τ) is based on a vehicle design which employs a 1 kbaud command rate. Note, however, that the optimum total sync delay is relatively large for both the 100 kbaud rate (0.73τ) as well as the lower rates (0.94τ). Since this is the case, it is proposed that this ground equipment delay (0.60τ) be fixed and system design be optimized by the selection of an appropriate delay in future vehicles for the specific command rates of concern.

Ranging

The PRN ranging code is initiated by the transmitting code generator, and, after shaping, is combined with other uplink services and applied to the transmitter modulator. A four-step attenuator permits selection of modulation indices of 0, 0.1, 0.3, and 1.0 radian by selecting attenuator steps 0, 1, 2, or 3 on the baseband assembly unit. After demodulation of the uplink signal in the spacecraft, the uplink baseband is applied to an 800-kHz lowpass filter. The filter output includes the PRN range signal, as well as low- or medium-rate command signals and the voice subcarrier, if any of the latter uplink services are active. The PRN range signal is retransmitted (on Carrier 1) to the ground station by application of the filter output to the transmitter modulator. Note that any low- or medium-rate command or voice signals present on the uplink will also modulate the downlink transmitter. This latter modulation is undesirable in that it reduces the power available for Carrier 1 downlink services. Since the vehicle transponder has a 1:1 turnaround modulation ratio (Volume III, Appendix X), low-level modulation indices should be used on the uplink to minimize this undesirable modulation of the downlink.

Analog Data

On the uplink, analog data is frequency-modulated on a 1.25-MHz subcarrier, with frequency deviations of up to ± 30 kHz and an information bandwidth of 20 kHz. The nominal modulation index of the analog signal on the RF carrier is adjustable in steps from 0 to 0.2, 0.6, and 1.2 radians.

The analog FM channel is subject to interference from the 100-kbaud ternary FSK command. The derivation of the spectrum of a ternary FSK signal is given in Appendix XI of Volume III. Analysis shows that, with respect to the total PCM/PM power that falls in the 100-kHz predetection bandwidth of the analog FM subcarrier, a single VCO is 9 to 12 dB superior to three separate, gated oscillators

as a modulator (Volume III, Appendix V). Consequently, the VCO is used as the high-rate FSK source to minimize interference from the high-rate command signal in the analog channel.

At the optimum deviation of 35 kHz (Volume III, Appendix V) for 100-kbaud command data, the interference power in the analog channel is 30 dB below the total FSK power. This is a conservative figure by perhaps 3 dB because the envelope (rather than the exact distribution function) of the spectral density lobes was integrated. Finally, the worst ternary case was considered because the probability of occurrence of the 0-pulse was made vanishingly small. This is a worst case because the 0-pulse is transmitted as the center frequency. In the other limiting case, where the probability of occurrence of the 0-pulse is unity, the spectrum is a spike at 1.024 MHz, and, as this probability approaches zero, the spectrum spreads out. As an additional complication, the sync signal is transmitted as amplitude modulation on the FSK subcarrier. The presence of the AM spreads the spectrum, thus enhancing the interference power in the analog channel. Plots of the envelope function that was integrated with the FSK as compared with the amplitude-modulated FSK spectra (Volume III, Appendix XI) indicate that the interference power estimates mentioned above are valid for the amplitude-modulated FSK signal. The interference power estimates are still conservative but the margin of conservatism is somewhat reduced.

Voice

The voice subcarrier is centered at 30 kHz, and is frequency-modulated with a deviation of ± 3 kHz, by pre-emphasized voice signals. The subcarrier level can be adjusted in steps to provide nominal RF carrier modulation indices of 0, 0.1, 0.3, and 1.0 radian. As noted previously, the voice subcarrier is one of the signals unavoidably turned around with the PRN to modulate the downlink. The voice subcarrier power on the downlink interferes with the PRN and uses sideband power that should be devoted to downlink services. Therefore the uplink voice RF modulation index should be no larger than necessary to provide adequate voice communication.

The command and analog channel frequencies were selected to minimize interference from the PRN ranging code. The voice subcarrier, however, was

established at 30 kHz to be compatible with the Unified S-Band System (USB). As a result, many discrete PRN components fall within the passband of the voice subcarrier demodulator.

Analysis indicates that interference from the C component of the short code is generally most serious, because the amplitude of that component is greatest.* Assuming equal peak deviations for the FM voice subcarrier and the PRN signal ($\theta_{FM} = \theta_{PRN}$) and a peak voice frequency deviation of 3 kHz, the S/I is 24 dB for the fundamental of the C_s component. When the deviation is 0.3 radian for the FM subcarrier and 0.1 radian for the PRN signal, the S/I improves to 33 dB.

The next largest interference signal is the product of two PRN-code components, $X \cdot B_s$, but the amplitude of this signal is considerably smaller. Using equal peak deviation for the PRN and FM signals and a peak voice deviation of 4.3 kHz, the S/I is 31 dB. When the deviation is 0.3 radian for the FM signal and 0.1 radian for the PRN signal, the S/I rises to 41 dB.

Interference is most severe where tones fall at the edge of the band; i. e., the frequency difference between subcarrier frequency and the frequency of the interfering PRN component is near the upper limit of the voice passband. This is the case for the C_s fundamental that appears at 33.3 kHz in the baseband. However, because the uplink voice circuit uses pre-emphasis, the de-emphasis circuit in the vehicle signal conditioner reduces this edge-of-channel interference by a factor of 10 dB. Therefore, the overall full-load-tone S/I should be about 33 dB for the worstcase C_s interference.

4.1.2 Uplink Transmission

The current SGLS equipment design includes a new high-power transmitter that uses a TWT amplifier instead of the klystron amplifier used in the initial Demonstration Ground Station (DGS). In addition, the current system interfaces with the

* Final Design Report, Space-Ground Link Subsystem, Volume I - Vehicle, TRW Systems, 1 February 1967.

high-gain as well as the low-gain antenna. The effects of these design changes were evaluated and the results are discussed in the following subparagraphs.

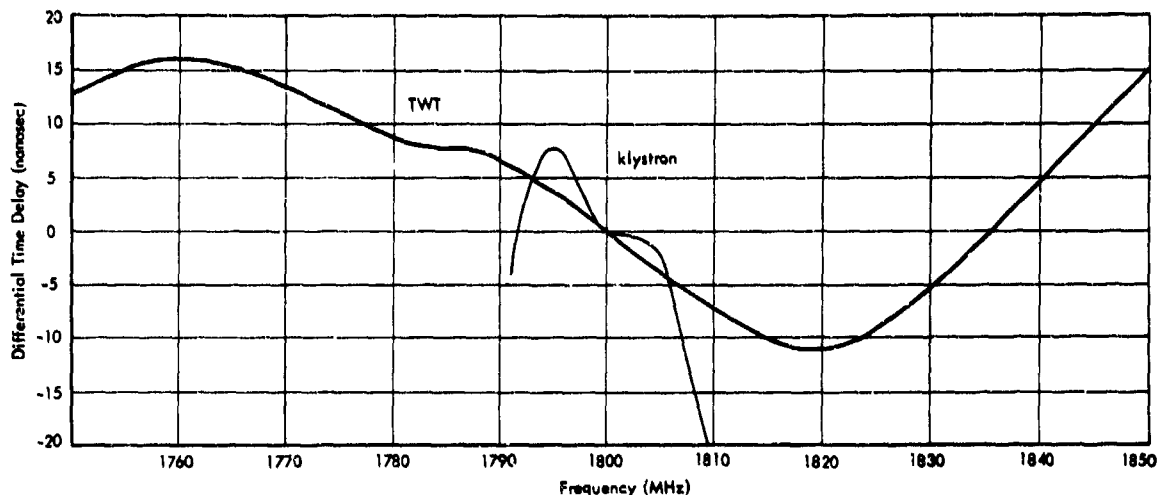
Envelope Delay Distortion

An information-bearing signal has a spectrum consisting of discrete frequency components, each having a specific amplitude and phase as compared to the carrier amplitude and phase. A signal with such a spectrum can be applied to a suitable demodulator and the original information recovered. However, it is essential to faithful reproduction of the original that the amplitudes and phases of all the components be unchanged before reaching the demodulator. Thus, if a signal passes through any device that delays a part of the spectrum more than any other, the differential time delay will manifest itself as phase shift varying over the spectrum, and will cause distortion to appear in the demodulator output (envelope delay distortion).

The effects of changing the envelope time delay in the 10-kW power amplifier were analyzed when the TWT power amplifier was substituted for the klystron used in the DGS. The klystron response curve is typically that of a bandpass filter, which has a strong parabolic component of phase delay near the skirts of the curve. The response of the TWT, on the other hand, is relatively flat, but it has an apparently nonperiodic ripple structure that varies from tube to tube, and that may exceed the 0.2 nanosecond envelope delay permitted by the original transmitter specification. Typical klystron and TWT envelope delay curves are presented in Figure 4-3.

The analysis was performed using a digital computer that was programmed to simulate phase modulation by a 200-kHz sine wave and a 550-kHz sine wave simultaneously, each with 1.0 radian peak modulation index.

The computer program developed the spectrum of the modulated carrier and then systematically applied phase delays in an 8-MHz interval to the individual spectral lines. The resulting spectrum was then demodulated, assuming an ideal phase demodulator, and the resulting two-tone signal (plus distortion components) was compared to the original to evaluate the distortion.



NOTES

1. Klystron delay was scaled from acceptance test data for VA-860.
2. TWT data was obtained from acceptance test for VA-844 Series No. 007.

Figure 4-3 Klystron and TWT Envelope Delay Curves

Three cases were analyzed. Case 1 is for the original differential time delay specified for the TWT transmitter. Case 2 doubles the values in Case 1. Case 3 was an estimate of the probable differential time delay values for the TWT under worst-case conditions. The parameters and analytical results are presented in Table 4-3. It is concluded that differential time delays of the magnitudes evaluated will not degrade the uplink performance to any measurable degree.

TABLE 4-3
TWT ENVELOPE DISTORTION ANALYSIS (8-MHz INTERVAL)

Parameter	Case 1	Case 2	Case 3
Linear Time Delay (ns)	16.5	33.0	13.0
Parabolic Time Delay (ns)	1.5	3.0	26.0
Ripple (ns)	0	0	0
Distortion (dB)	-52	-47	-51

Limits on Transmitted Power vs Frequency

The SGLS 10-kW power amplifier is inherently a broadband device. No problem exists when the transmitter is working in the "dummy load" mode so long as the excitation remains within the frequency range where the high-power circulator is effective. A safe operating range for testing in the "dummy load" mode is 1.7 to 2.0 GHz. The circulator has a high-frequency cutoff near 2.4 GHz, but at this frequency the TWT still has appreciable gain. Therefore, if the drive frequency approaches this region, there is a strong possibility that unstable operation will result, even though the dummy load is presenting a near-unity VSWR. These considerations are of primary interest during tests of transmitter frequency response when a sweeping oscillator may be used for the driving source.

When the transmitter is in "radiate" mode, the presence of the transmitter output filter between the antenna feed and the TWT amplifier restricts the operating frequency to the range of 1750 to 1850 GHz. This restriction is due to the increased reflected power outside the filter passband, which activates protective devices that remove beam power from the TWT.

Transmitter Operation at High VSWR

The transmitter is specified to operate at maximum power without VSWR's not greater than 1.68:1; however, investigation shows that operation at higher VSWR's will not damage the transmitter. In normal operation, the transmitter turns off the beam supply automatically whenever the reflected power measured at the transmitter output exceeds a nominal 3.0 kW. This protects the RF load for the high-power isolator against excessively large power levels. However, a "critical mode" can be initiated in emergency situations, in which the normal 3-kW limit on excess power may be exceeded. Effects of high-VSWR operation were studied and significant results are shown in Figure 4-4.

The TWT must supply circuit losses and a net transmitter output of at least 10 kW. Figure 4-4 shows the relationship between this useful output and the output of the TWT. Below 1.5:1, the useful output can be maintained by increasing the TWT output to make up reflected power loss. Above 1.5:1, the TWT is delivering its power limit, and necessarily, as the reflected power increases, the useful output power falls.

The curve for "reflected power" is above the "reflected power in circulator load" because of circuit losses between the reflected power monitor point and the circulator load. The circulator is rated to dissipate 4.5 kW, as indicated on the curve.

The ability of the transmitter to operate at high VSWR's also depends on the stability of the individual high-power TWT. This factor is not predictable, and must be obtained experimentally for each TWT/circulator pair. The TWT is required to meet specifications when the load VSWR at its output flange is 1.2:1. The isolator (circulator) attenuates reverse power 18 dB, corresponding to a VSWR at the TWT of 1.09 when the load VSWR is near 5:1 on the output port of the isolator.

Transmitter-Receiver Isolation

High-Gain Antenna. The high-gain antenna uses a multipurpose feed (MPF) in which the transmitting and receiving horns are physically separated but electromagnetically coupled due to proximity. The isolation factor is a minimum of 20 dB when the transmitter is in the 1.75- to 1.85-GHz frequency band. The transmitter develops 70-dBm output power, and, allowing for transmission loss to the feed, the

net power at the transmitting feed horn is 68 dBm. After the 20-dB coupling loss to the receiving horns, the net maximum power in the receiving channel is 48 dBm.

The selective filter at the input to the parametric amplifier is designed to provide 170-dB insertion loss to signals in the transmitting frequency band, which results in a transmitter power level at the parametric amplifier input of -122 dBm. Since the GRARE tracking threshold input signal (for a 6-dB S/N ratio is a 200-Hz tracking loop) is approximately -145 dBm at the input to the parametric amplifier, so that the signal-to-interference ratio (S/I) is -23 dB at this point.

A 5-pole Chebyshev bandpass filter between the parametric amplifier output and the down-converter input attenuates the transmitter signal 100 dB without materially reducing the received 2.2-GHz signal. The S/I ratio thus becomes 93 dB at the input to the down-converter, which is the first nonlinear device in the receiving system. Figure 4-5 illustrates the transmitter-receiver interface for the high-gain SGLS.

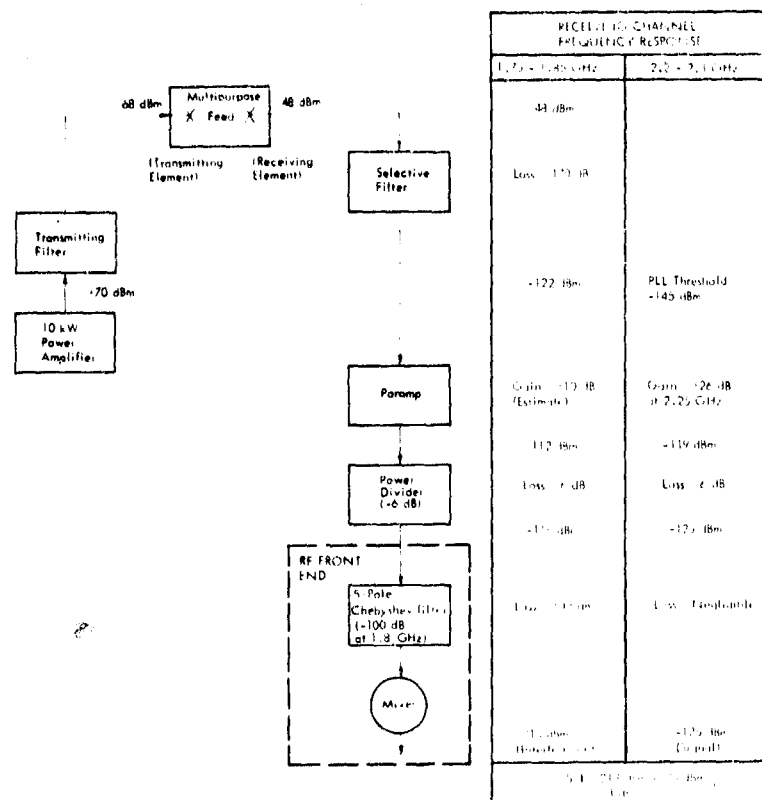


Figure 4-5 Transmitter-Receiver Interface, High-Gain SGLS

Low Gain Antenna. The low-gain SGLS system uses the 14-ft wideband (Prelort) antenna, which has a conical-scanning feed that is used simultaneously for transmission and reception. The transmitter-receiver interface is illustrated in Figure 4-6. The transmitting power level applied to the feed is 68 dBm; the diplexer attenuates this signal at the receiver input port to -102 dBm. The received signal required at the same point for tracking with a 6-dB margin in a 200-Hz phase-locked loop bandwidth is -145 dBm. The parametric amplifier therefore sees -43 dBm S/I ratio at its input.

The transmitter signal level at the input to the 5 pole filter is -92 dBm due to the gain of the Parametric Amplifier (+10 dB). At the same time, the parametric amplifier provides 26-dB gain for the received signal which improves the S/I ratio to -27 dB. The 5-pole filter in the down-converter input further attenuates the transmitter signal by 100 dB, so the net transmitter interference power at the down-converter mixer is -192 dBm. This is 73 dB below the tracking threshold, with intermodulation products in the receiver passband also more than 73 dB below tracking threshold.

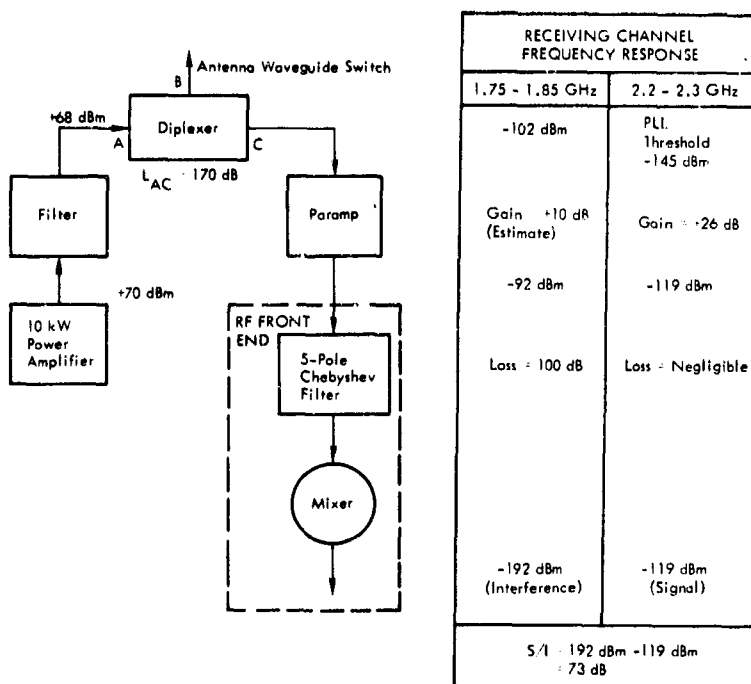


Figure 4-6 Transmitter-Receiver Interface, Low-Gain SGLS

Transmitter Noise

The SGLS 10-kW uplink transmitter generates in-band and out-of-band noise. Noise is also generated by the multipurpose feed (MPF) when it is functioning at high-transmitted-power levels. These effects are discussed in the following paragraphs.

In-Band Noise. In-band noise generated by the transmitter is random phase modulation that is caused by thermal disturbances in the exciter, by amplitude modulation of the beam voltage, and by mechanical disturbance of the equipment by rotary machines and fluid motions. Excursions attributable to all these causes are specified not to exceed 50 milliradians peak. Tests were performed on the 10-kW TWT to determine the power supply ripple, and the resulting phase modulation was computed. Calculations indicate that phase noise in the final amplifier does not exceed the specification value.

Out-of-Band Noise. The SGLS system requires that operation of the 10-kW transmitter will not degrade the system noise temperature by more than 2% compared to the noise temperature when the transmitter is not running. The noise performance of the 60- and 14-ft antennas meets this requirement.

- 60-ft Antenna: The receiving system noise temperature is 336°K, which is a noise density of $4.64 \cdot 10^{-18}$ mW/Hz. The spectral noise density of the transmitter is below -183 dBm/Hz, and this figure is attenuated 20 dB by the coupling loss between transmit and receive channels in the MPF. The noise density from the transmitter seen by the parametric amplifier input is therefore $5 \cdot 10^{-21}$ mW/Hz. This power added to the receiving spectral noise density increases the receiver noise density to $4.695 \cdot 10^{-18}$ mW/Hz, which is equal to 340°K. The specified 2% increase in spectral noise density in the receiving channel would raise the temperature to 342.7°K, leaving a margin of 2.7°K.

- **14-ft Antenna:** The 14-ft antenna has the diplexer transmit arm and the transmitter spectral noise filter in line with the noise path to the receiver input, which provides 80 dB more isolation than that obtained in the high-gain SGLS. Thus the increase in system noise due to transmitter spectral noise density is considerably less than 2%.

4.2 UPLINK PERFORMANCE

This section presents the uplink performance in terms of effective radiated power and typical power budgets. Additional information is provided to assist the SGLS user in optimizing performance for specific uplink configurations.

4.2.1 Effective Radiated Power

The SGLS uplink transmitter is capable of providing 10 kW of RF power to the transmission line over the 1.75 to 1.85 GHz frequency band. The effective radiated power (ERP) varies as a result of site-peculiar differences in the (1) transmission line, (2) RF system losses, and (3) gain of the antenna. Either of two antennas is used with the SGLS system: a 60-ft-diameter parabolic reflector fitted with a multipurpose feed (MPF) to provide 46-dB gain, and a 14-ft diameter parabolic reflector fitted with a conical-scanning feed to provide 34-dB gain. The effective power radiated by each type is discussed in the next two paragraphs. Values shown are the rated maximums; output power can be controlled from nearly zero up to the values derived in the following paragraphs.

TABLE 4-4

EFFECTIVE RADIATED POWER (HIGH-GAIN SGLS)

ERP High-Gain Configuration.

The high-gain configuration (Figure 4-7) uses a 60-ft parabolic reflector illuminated by the MPF S-band transmitting radiator. The performance values (Table 4-4) are typical of the high-gain SGLS uplink.

Parameter	Gains	Losses
Transmitter Output	+70 dBm	
VSWR		-0.3 dB
Waveguide, 105 feet		-0.5 dB
Rotary Joints (2)		-0.2 dB
Radome Loss		-0.6 dB
Antenna Gain	+46 dB	
Totals	+116 dB	-1.6 dB
Effective Radiated Power:	+114.4 dBm	

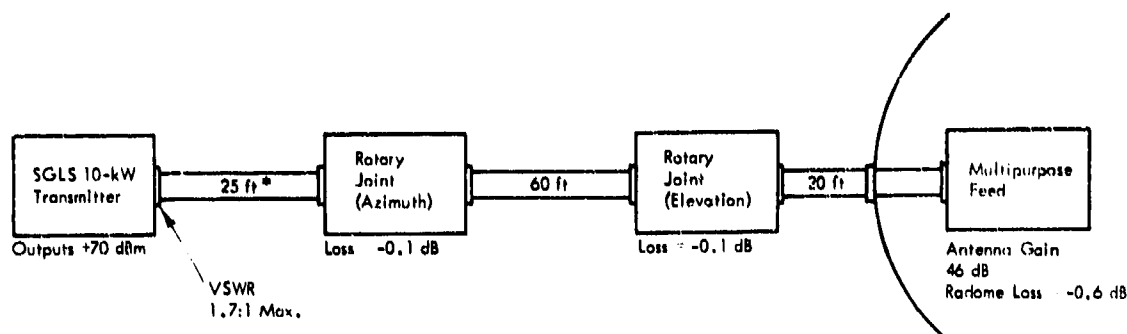


Figure 4-7 High-Gain Configuration

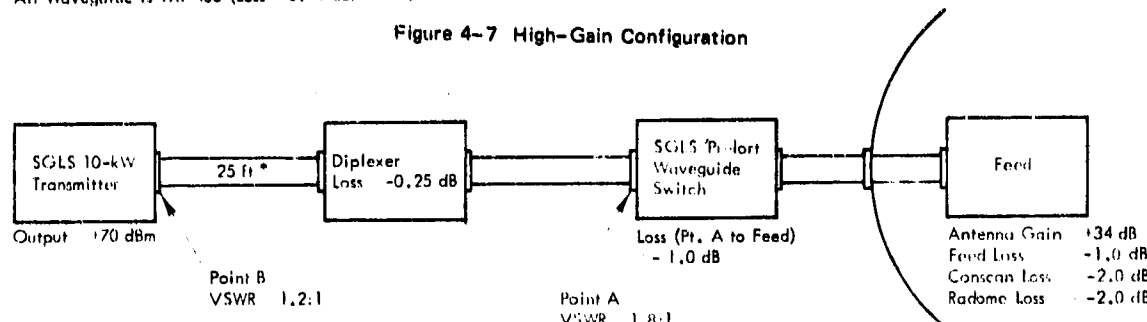


Figure 4-8 Low-Gain Configuration

ERP Low-Gain Configuration. The low-gain configuration (Figure 4-8) uses a 1.4-ft parabolic antenna (the wideband Prelort) illuminated by a conical-scanning feed.

TABLE 4-5
EFFECTIVE RADIATED POWER (LOW GAIN SGLS)

Parameter	Gains	Losses
Transmitter Output	+70 dBm	-0.04 dB
VSWR at "B"		-0.13 dB
Waveguide, 25 Ft		-0.25 dB
Diplexer Loss		-0.38 dB
VSWR at "A"		-1.00 dB
Loss "A" to Feed		-1.00 dB
Feed Loss		-1.00 dB
Conscan Loss		-2.00 dB
Radome Loss		-0.20 dB
Antenna Gain	+34 dBm	
Totals	+104 dBm	-5.00 dB
Effective Radiated Power	+99.0 dBm	

The performance values (Table 4-5) are typical of the low-gain SGLS up-link.

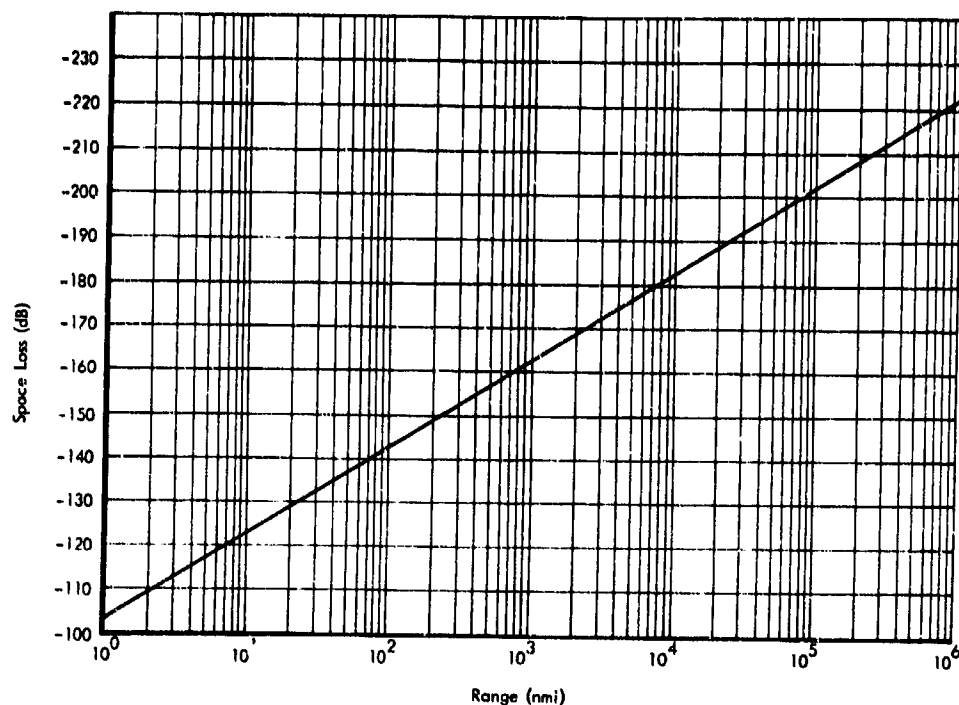


Figure 4-9 Space Loss for 1.8 GHz Uplink

4.2.2 Carrier Power Distribution

Typical Power Budget. High-gain SGLS uplink performance is presented in Table 4-6. This is a typical uplink calculation. Figure 4-9 shows the space loss for the 1.8-GHz uplink signal as a function of range from 1 nmi to 1 million nmi. To find total received power at any range, enter the abscissa on the graph at the desired range, and read the space loss on the ordinate at the left.

The performance for the low-gain SGLS uplink is found by using the values for the high-gain case, then reducing the received power by 15 dB, to account for the reduced ERP of the low-gain configuration.

Subcarrier Power. Once the total power received at the vehicle equipment is known, it is necessary to determine what part of the total can be allocated to each of the four uplink services (ranging, command, analog data, and voice). The SGLS equipment controls the composition of the baseband by pushbutton selection

TABLE 4-6
TYPICAL UPLINK POWER BUDGET

Parameter	Value
Effective Radiated Power, High-Gain SGLS Vehicle (Typical)	114 dBm
Antenna Gain	0 dB
Polarization Loss	-3 dB
Diplexer Loss	-1.5 dB
Cable (3 ft, RG-9)	-0.5 dB
VSWR (2.5:1)	-0.9 dB
Signal Power without Space Loss	108.1 dBm
Typical Space Loss (100,000 nmi)*	-202.9 dB
Total Signal at Vehicle Receiver Input	-94.8 dBm

*To find carrier power for any range, add the space loss from Figure 3-14 algebraically to 108.1 dBm.

of modulation index in four steps. On the analog data channel, the steps are: "off," 0.2, 0.6, and 1.2 radians (nominal values). Steps for the other three services are "off," 0.1, 0.3, and 1.0 radian. Table 4-7, Uplink Power Distribution, shows the effect of selecting different combinations of modulation indices for the various services, and the carrier power remaining in each case. The values are given in decibels below total signal power, and can be applied directly to the total received power.

Combinations shown in Table 4-7 are those considered most probable for normal use. Other modulation index combinations result in different distributions of carrier and sideband power, and can be calculated from

$$P_{sc_1} = P_t \cdot 2 J_1^2(\beta_1) \cdot \cos^2 \beta_{PRN} \cdot \prod_{i=2}^n J_0^2(\beta_i)$$

where

- P_{SC_1} = power in first sidebands of the subcarrier of interest
- J_0 = Bessel function of zero order
- J_1 = Bessel function of first order
- β_i = modulation index for i^{th} service (radians)
- P_t = total signal power

TABLE 4-7
UPLINK POWER DISTRIBUTION

Modulation Steps Selected								Carrier and Subcarrier Power (dB below Total ERP)				
Step	PRN	Command		Analog		Voice		Carrier	PRN	Command	Analog	Voice
0	(0)	0	(0)	0	(0)	0	(0)	0	OFF	OFF	OFF	OFF
1	(0, 1)	0	(0)	0	(0)	0	(0)	0.04	20.0	OFF	OFF	OFF
2	(0, 3)	0	(0)	0	(0)	0	(0)	0.40	10.6	OFF	OFF	OFF
0	(0)	1	(0, 1)	0	(0)	0	(0)	0.02	OFF	23.0	OFF	OFF
0	(0)	2	(0, 3)	0	(0)	0	(0)	0.20	OFF	13.6	OFF	OFF
1	(0, 1)	2	(0, 3)	0	(0)	0	(0)	0.24	20.2	13.6	OFF	OFF
2	(0, 3)	2	(0, 3)	0	(0)	0	(0)	0.60	10.8	14.0	OFF	OFF
1	(0, 1)	2	(0, 3)	1	(0, 2)	0	(0)	0.33	20.3	13.7	17.3	OFF
1	(0, 1)	2	(0, 3)	2	(0, 6)	0	(0)	1.04	21.0	14.4	8.1	OFF
1	(0, 1)	2	(0, 3)	2	(0, 6)	1	(0, 1)	1.06	21.0	14.4	8.1	24.1

Carrier power diminishes with increasing modulation indices, and can be approximated by considering only the first sidebands, as in

$$P_c = P_t \cdot \cos^2 \beta_{PRN} \cdot \prod_{i=1}^n J_0^2 \beta_i$$

When the ranging signal is the only modulation, the power in the sidebands will be

$$P_{PRN} = \sin^2 \beta_{PRN} P_t,$$

and the power in the carrier will be

$$P_{\text{car}} = \cos^2 \beta_{\text{PRN}} \cdot P_t,$$

where

- P_t = total power transmitted
- β_{PRN} = modulation index of the ranging signal
- P_{PRN} = power in PRN sidebands
- P_{car} = power in the transmitted carrier

When the PRN ranging signal is not the exclusive occupant of the uplink, then the power in the ranging spectrum will be

$$P_{\text{PRN}} = \sin^2 \beta_{\text{PRN}} \left[\prod_{i=1}^n J_0^2(\beta_i) \right] P_t$$

Values of β , along with the first Bessel functions and their squares, and values of $\sin(\beta)$, $\sin^2(\beta)$, $\cos(\beta)$, and $\cos^2(\beta)$ are presented in Table 4-8.

TABLE 4-8
BESSEL AND TRIGONOMETRIC FUNCTIONS OF MODULATION ANGLE (β)

Modulation Index (β radians)	Bessel Functions				Trigonometric Functions			
	$J_0(\beta)$	$J_0^2(\beta)$	$J_1(\beta)$	$J_1^2(\beta)$	$\sin(\beta)$	$\sin^2(\beta)$	$\cos(\beta)$	$\cos^2(\beta)$
0	1.0000	1.0000	0.0000	0.0000	0.0000	0.0000	1.0000	1.0000
0.1	0.9975	0.9950	0.0499	0.0025	0.0998	0.0099	0.9950	0.9900
0.2	0.9900	0.9801	0.0995	0.0099	0.1987	0.0395	0.9801	0.9604
0.3	0.9776	0.9557	0.1483	0.0220	0.2955	0.0874	0.9553	0.9121
0.6	0.9120	0.8317	0.2867	0.0822	0.5646	0.3185	0.8253	0.6810
1.0	0.7652	0.5855	0.4401	0.1937	0.8415	0.7080	0.5403	0.2920
1.2	0.6711	0.4504	0.4983	0.2483	0.9320	0.8686	0.3624	0.1313

Uplink Service Thresholds. Typical signal thresholds for the uplink services are shown in Table 4-9. The values listed are based on an assumed signal-to-noise density ratio of -164 dBm/Hz.

TABLE 4-9
TYPICAL UPLINK THRESHOLD LEVELS

Service		Range PRN	Commands - Bit Rates								Data	
			1	20	160	1k	2k	10k	100k	Analog		
Typical Vehicle Parameters	Unit											
Signal-to-Noise Density	dBm/Hz	-164	-164	-164	-164	-164	-164	-164	-164	-164	-164	-164
Bandwidth	dB		0	13	20	30	33	40	50	50	50	13 ^a
Noise in Bandwidth	dBm		-164	-151	-144	-134	-131	-124	-114	-104	-104	-151
Margin												
PRN Demodulator	dB	26.6 ^b	-	-	-	-	-	-	-	-	-	-
Filter-Detector	dB		-	20 ^c	20 ^c	20 ^c	20 ^c	-	-	-	-	-
Discriminator	dB		-	-	-	-	-	20 ^c	20 ^c	10 ^d	10 ^d	-
Required Subcarrier Power	dBm	-137.4	-144	-131	-124	-114	-111	-104	-94	-94	-94	-141

^aCommand bandwidth in Hz assumed equal to signalling rate in bauds.
^bSee Volume III, Appendix II.
^cSee Volume III, Appendix V.
^dThreshold of a conventional FM discriminator.

SECTION 5

GROUND STATION DESCRIPTION

This section describes the equipment items that comprise the SGLS ground station and delineates their physical and functional relationship with each other and with other RTS equipment items. Paragraph 5.1 describes the individual equipment items, Paragraph 5.2 illustrates the equipment arrangement at a typical remote tracking station, and Paragraph 5.3 describes built-in system test capability.

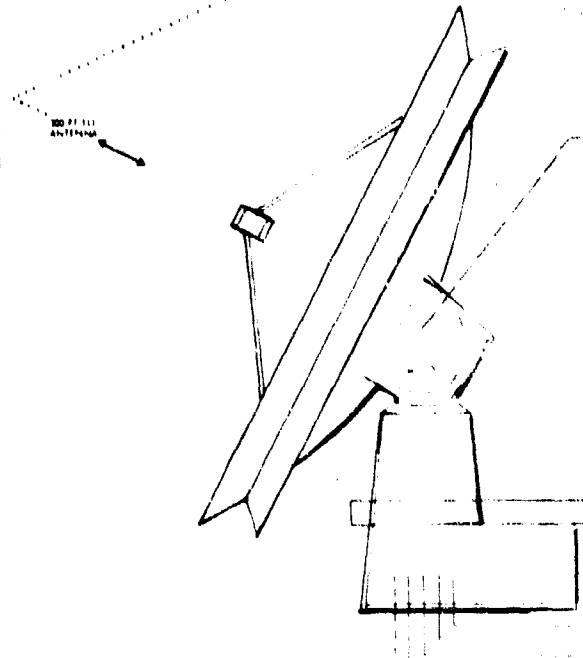
5.1 EQUIPMENT DESCRIPTION

The functional schematic block diagram of the SGLS ground station (Figure 5-1) depicts the interrelationship of the various SGLS equipment items and the interfaces with non-SGLS RTS equipment items. The color coding on the diagram enables the reader to readily distinguish between SGLS equipment items that are common to all stations (black) and those that are unique to a particular antenna configuration (blue or green). The equipment has also been segregated according to the equipment area in which it is located. SGLS equipment is enclosed within heavy red lines to distinguish it from non-SGLS equipment.

5.1.1 Antenna Interface Equipment

Either of two configurations of antenna interface equipment may be installed at the ground station. One configuration is used with the high-gain (TT&C) antenna and the other with the low-gain (Prelort) antenna. Functionally, these equipment configurations are the same in that they provide the necessary isolation, filtering, and attenuation between SGLS transmitting and receiving equipment.

RCS HIGH GAIN TT&C ANTENNA

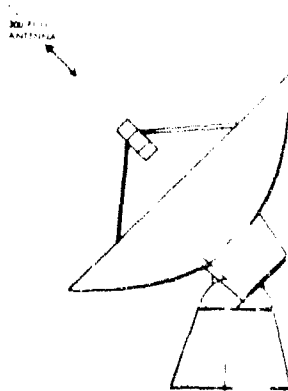


SVC EQUIPMENT - ANTENNA INTERFACE - HIGH GAIN OPTION

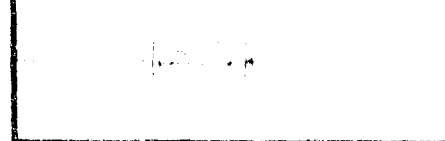


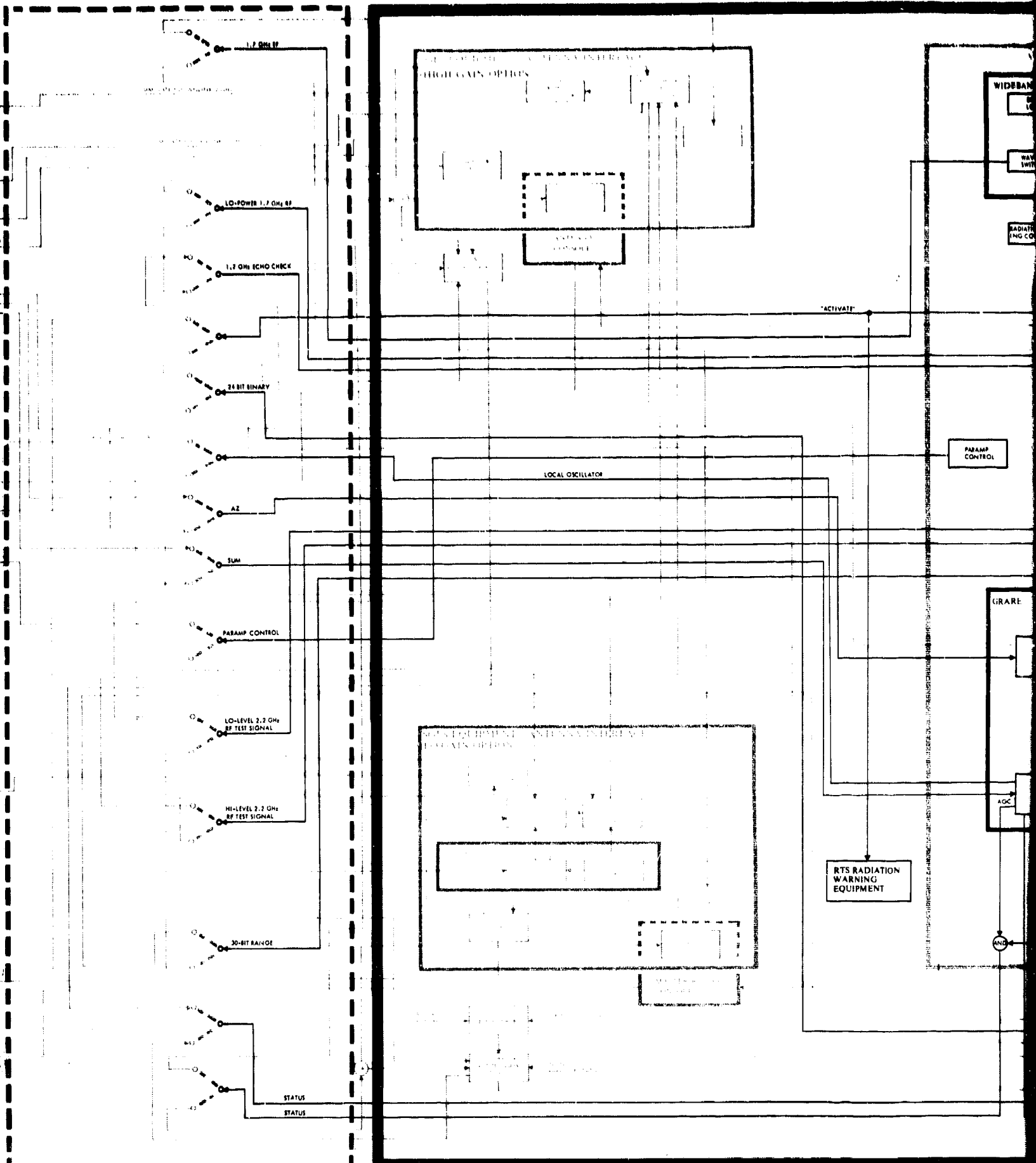
REINSTATEMENT
WARNING
EQUIPMENT

RCS LOW GAIN PREFORE ANTENNA

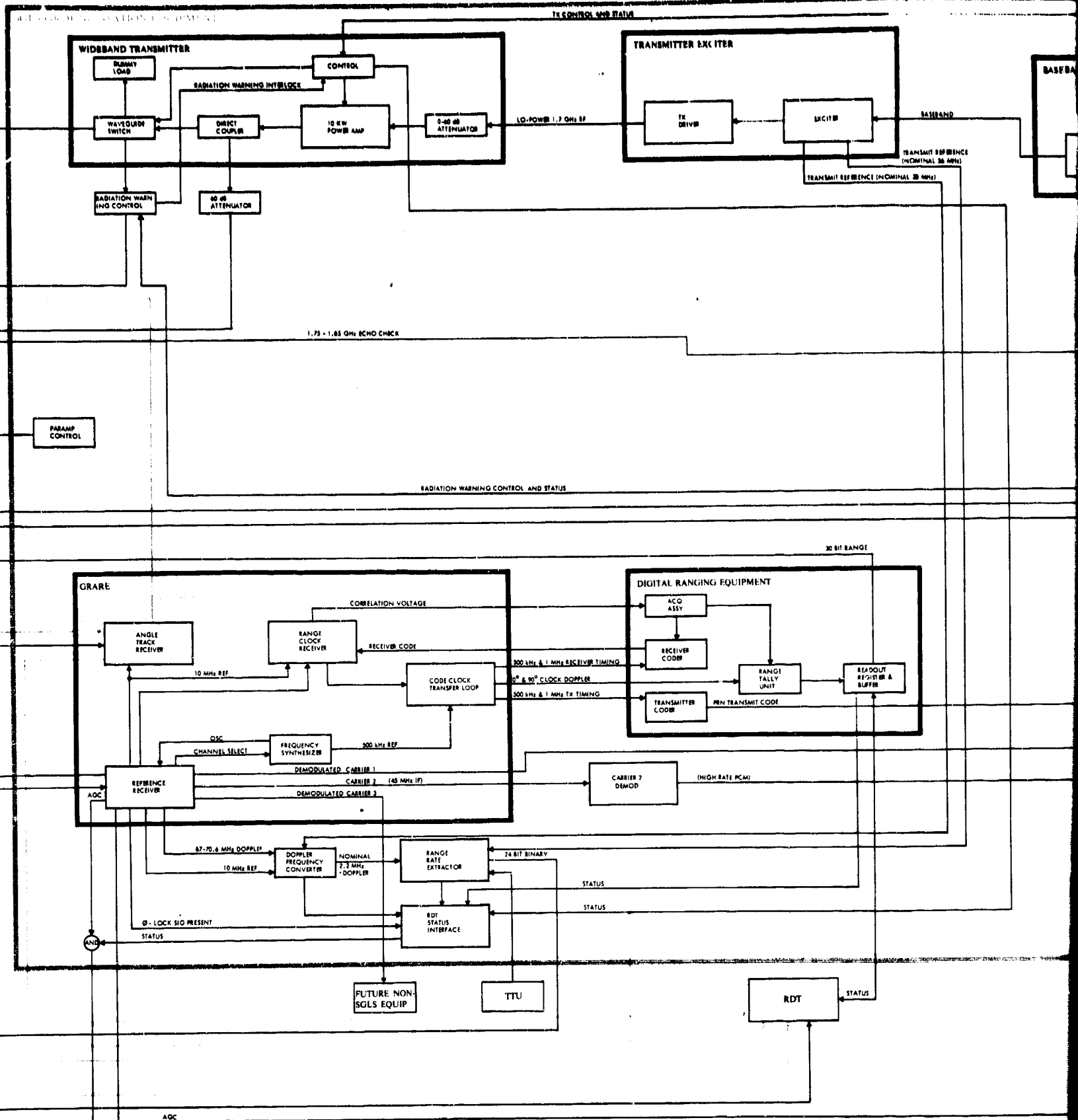


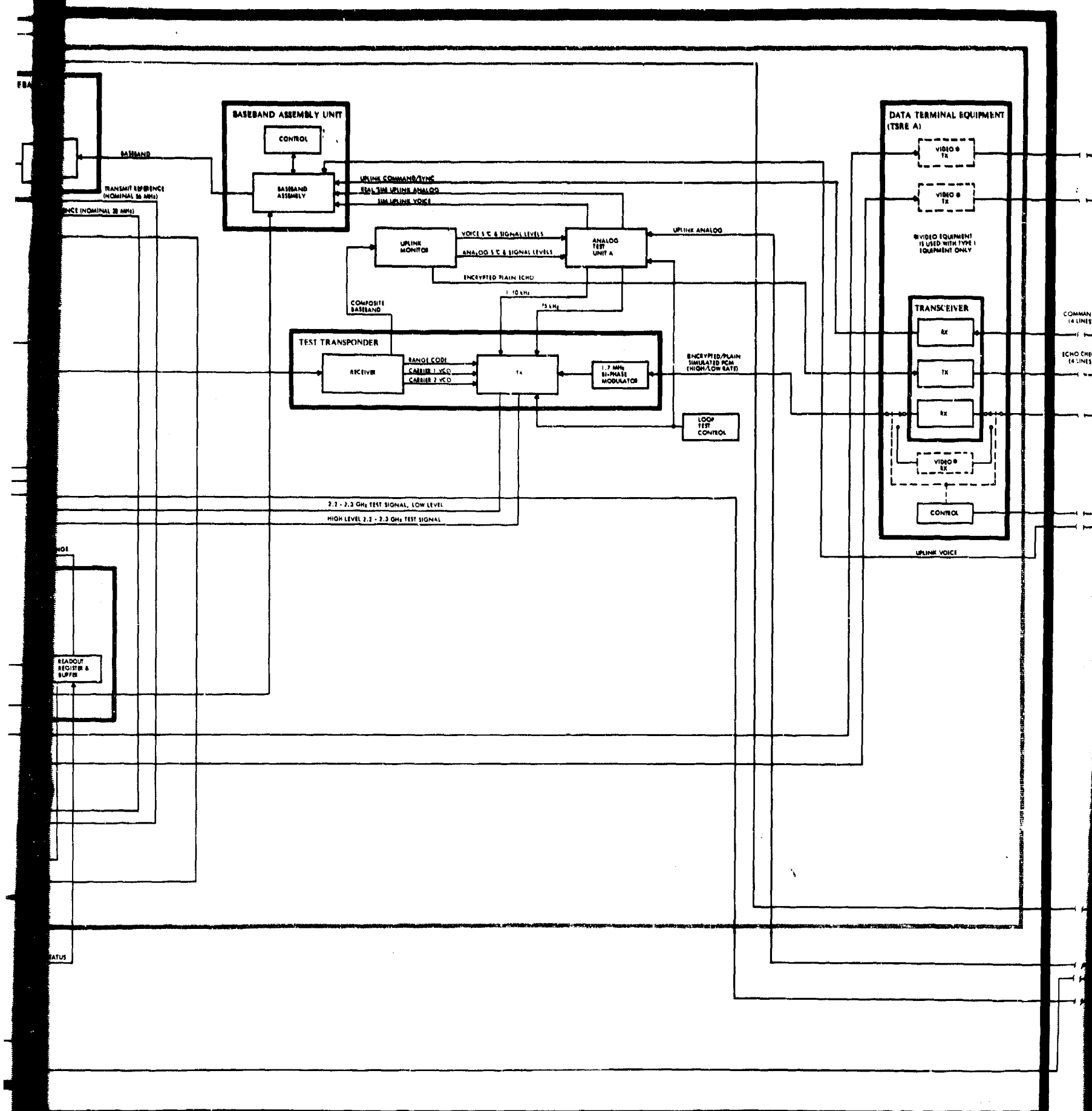
SVC EQUIPMENT - ANTENNA INTERFACE -
LOW GAIN OPTION



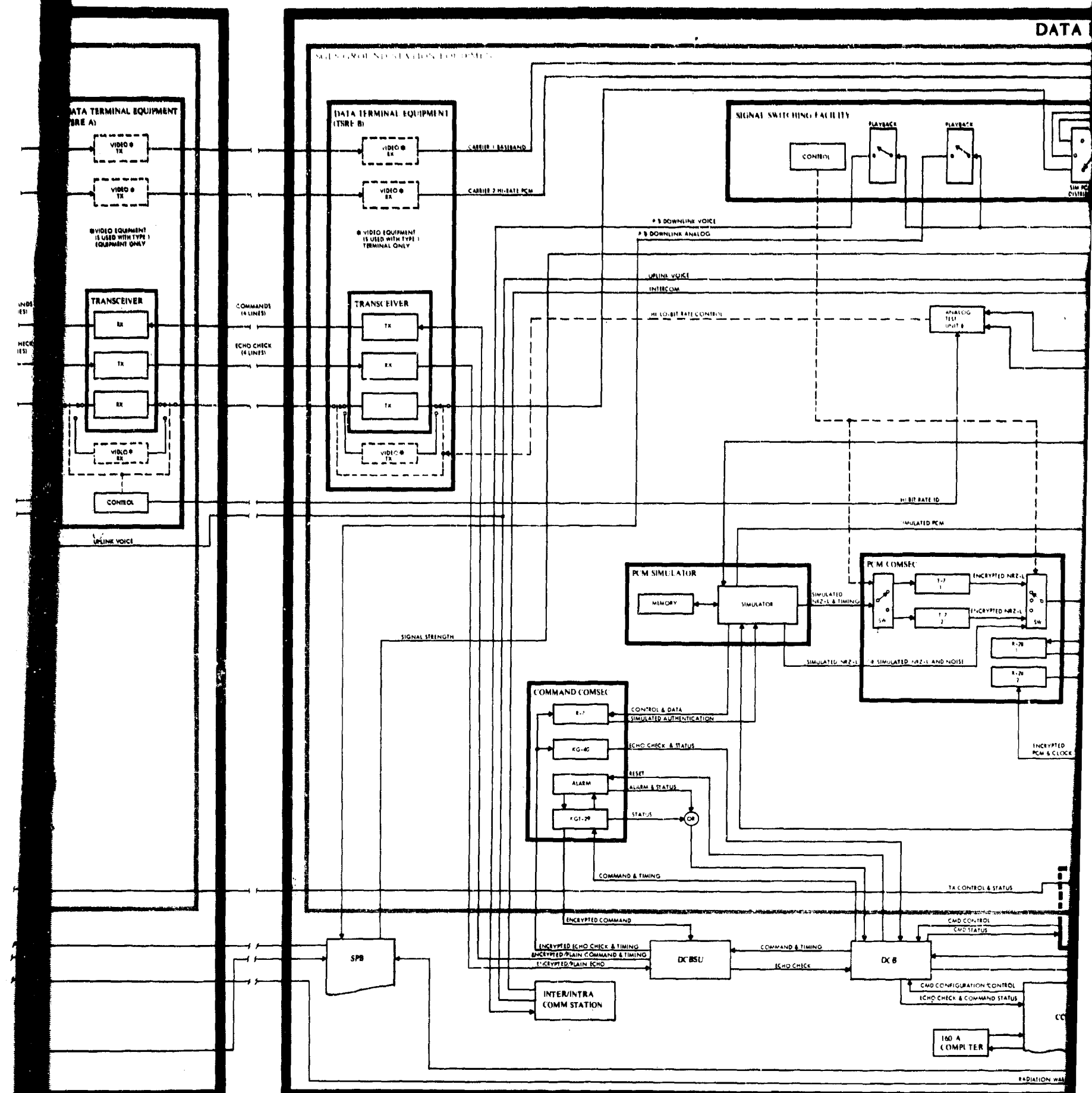


RF EQUIPMENT AREA

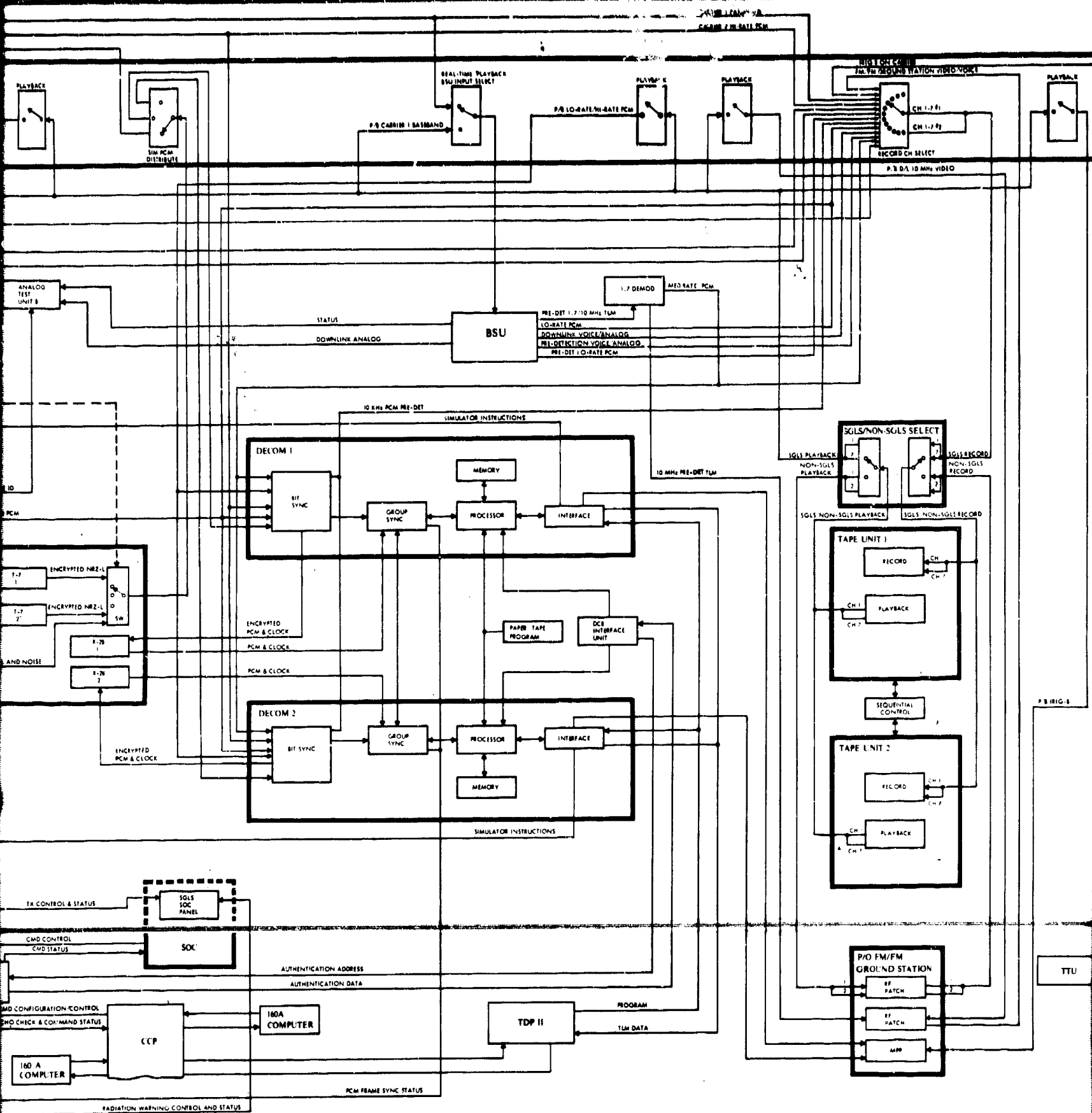


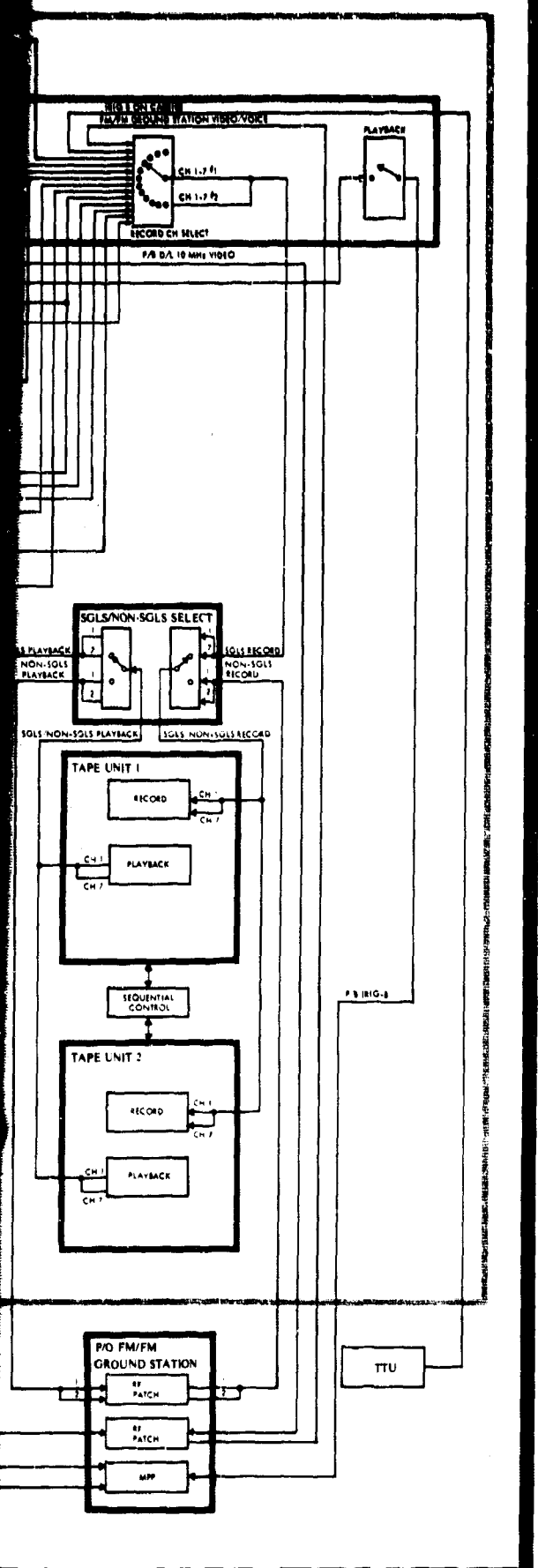


DATA



DATA EQUIPMENT AREA

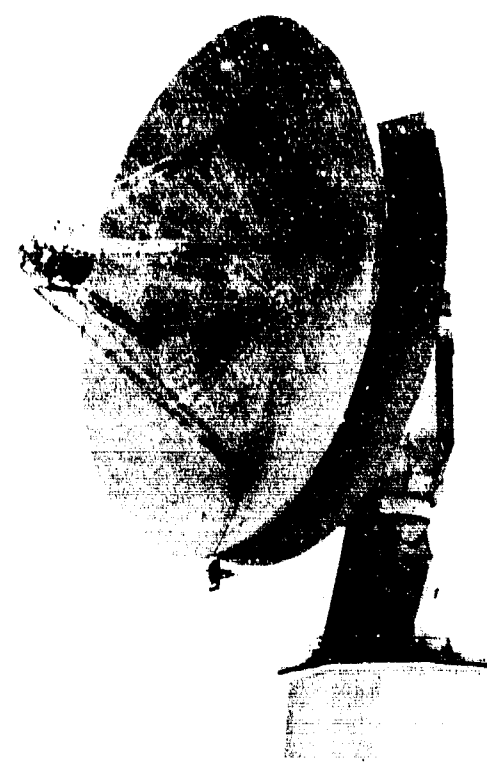




LEGEND

- Equipment Areas**
- SGLS Equipment**
- RTS High-Gain (TT&C) Antenna Configuration**
- RTS Low-Gain (Prefort) Antenna Configuration**
- Configuration Common to Both Options**
- Control Linkage**
 - Mechanical Linkage (High-Gain)
 - Mechanical Linkage (Low Gain)
 - Antenna-to-Boresight Transmission Path (High-Gain)
 - Antenna-to-Boresight Transmission Path (Low Gain)
- Symbolic Representation Only—Connections Are Hard-Wired for Specified Option**

FIGURE 5-1 SGLS SYSTEM FUNCTIONAL SCHEMATIC BLOCK DIAGRAM



High-Gain (TT&C) Antenna Equipment

For those stations equipped with the high-gain (TT&C) antenna (Figure 5-2), the block diagram (Figure 5-1) shows the antenna interface equipment in blue. Two groups of equipment are supplied for this configuration. One of these is antenna-mounted, and the other is installed in the RF equipment area.

Figure 5-2 60-Foot High-Gain (TT&C) Antenna

The antenna-mounted equipment consists of the selective filters, parametric amplifier, down-converter, noise source, and S-band vertex horn. The selective

filters (Figure 5-3) are waveguide coupled-cavity bandpass devices. Three such filters are installed between the multipurpose feed and the parametric amplifier. These filters provide a minimum isolation of 170 dB to prevent the transmitted power from reaching the receiver.

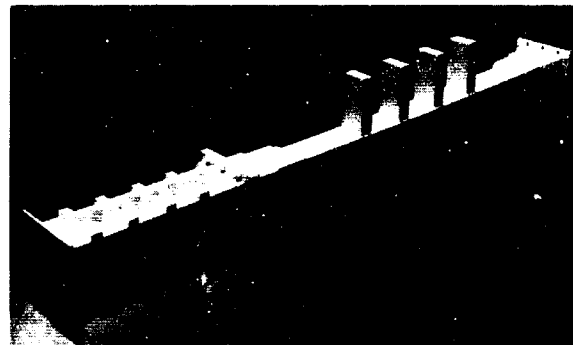


Figure 5-3 Selective Filter

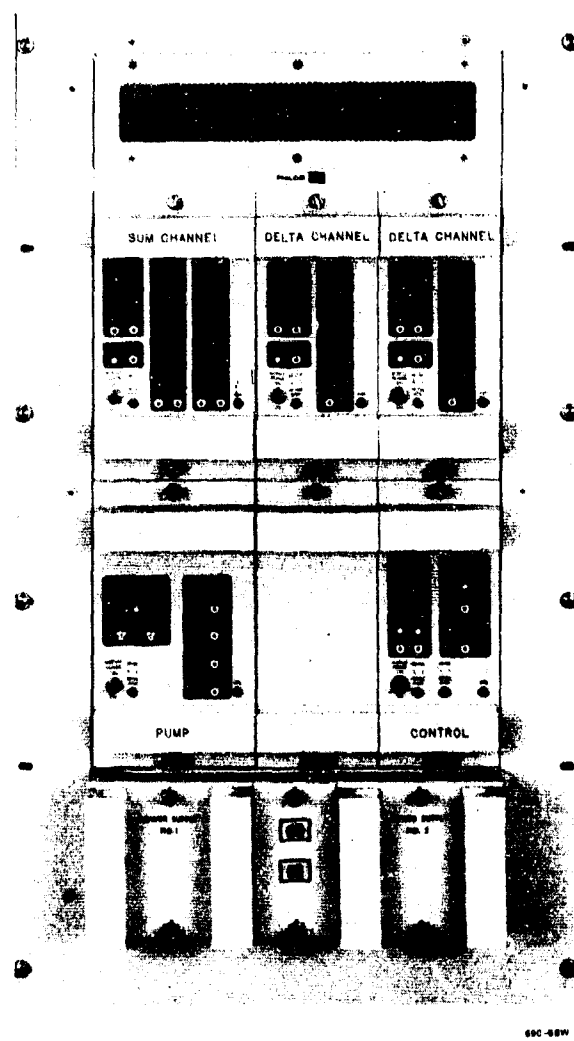


Figure 5-4 2-GHz Parametric Amplifier

The filter outputs are fed to the parametric amplifier (Figure 5-4), which has three channels: one for the sum channel and two for error channels. The sum channel contains two parametric diode amplifiers and a transistor amplifier in cascade to provide a 26-dB gain. The two error channels contain a tunnel diode amplifier followed by a transistor amplifier to provide a 13-dB gain. The parametric amplifier outputs are fed to the down-converter. Whereas the error channels are fed directly, the sum channel is routed through a power divider (non-SGLS) to make this signal available to non-SGLS users.

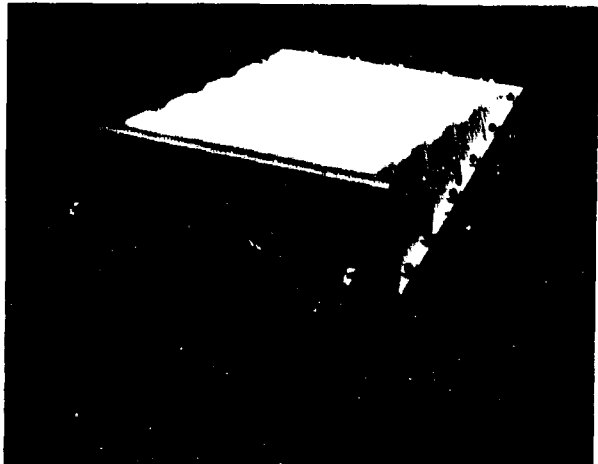


Figure 5-5 Down Converter

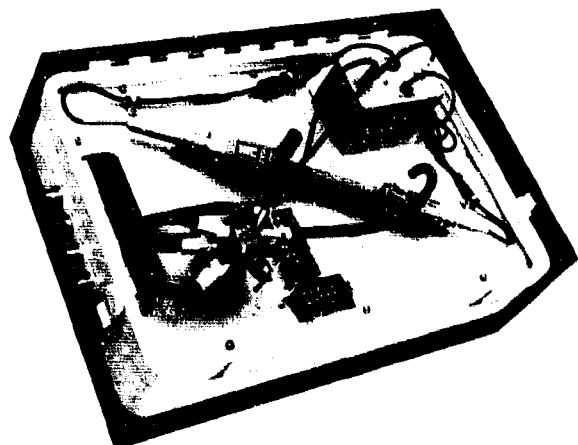


Figure 5-6 2-GHz Noise Source

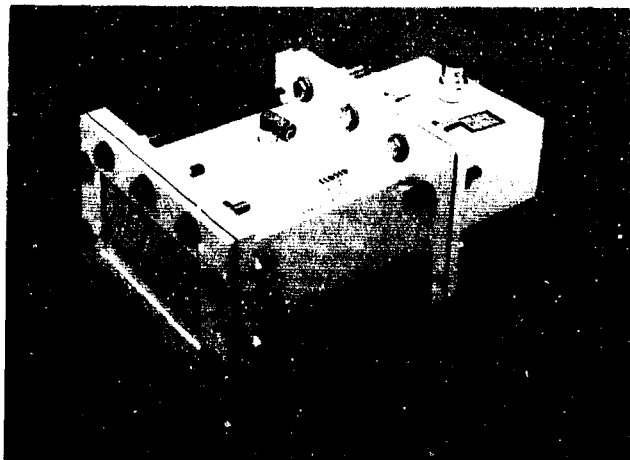


Figure 5-7 S-Band Vertex Horn

The down-converter (Figure 5-5) comprises three identical frequency translators that use a common local oscillator whose frequency is derived from the reference receiver. Each translator comprises a preselection filter, isolator, test signal coupler, bandpass filter, S-band mixer, IF preamplifier, and line driver. The down-converter's three IF outputs are at 130 MHz: the two error channels are routed to the GRARE's angle track receiver, and the sum channel is routed to the GRARE's reference receiver.

The noise source (Figure 5-6) is a test device that injects a noise signal to the parametric amplifier via a directional coupler. This signal permits quantitative determination of system noise performance.

The S-band vertex horn (Figure 5-7) is a waveguide horn that is mounted near the vertex of the antenna reflector. Used as a test antenna, this horn radiates simulated downlink signals for pickup by the multipurpose feed (MPF) or receives uplink signals radiated by the MPF for system monitoring.

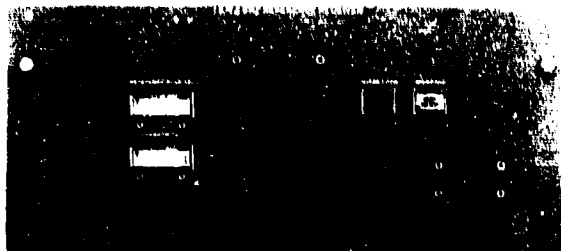


Figure 5-8 SGLS Antenna Panel

uator, and transmitting filter. As shown in Figure 5-8, the SGLS antenna panel (in the antenna control console) contains a reference receiver AGC meter, a signal-present indicator, and a Carrier 1 phase-lock indicator.

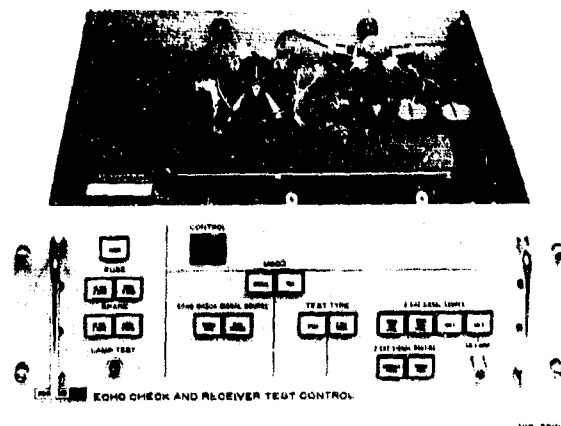


Figure 5-9 Echo Check/Receiver Test Control Unit

The transmitting filter (Figure 5-10) is a bandpass coupled-cavity waveguide device inserted in the 1.8-GHz transmitter output, the filter removes any out-of-band energy generated by the TWT amplifiers in the transmitter. The noise-figure test set (AIL Model 355W) measures the noise figure of the receiver equipment.

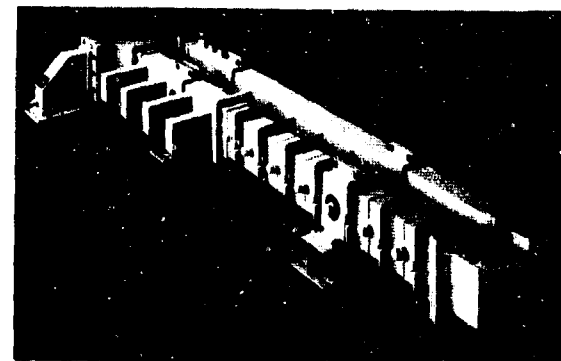


Figure 5-10 Transmitting Filter

The echo check/receiver test control unit (Figure 5-9) provides a means of routing test signals within the subsystem. This unit allows the transmitter output to be monitored or, alternatively, allows simulated downlink signals to be inserted via either the vertex horn or the boresight horn.

The 0- to 100-dB attenuator is inserted in the high-level 2.2-GHz test signal path between the test transponder output and the input to the boresight horn. The attenuator provides positive control over the strength of the test signal received by the system and allows simulation of a variety of reception conditions.

Low-Gain (Prelort) Antenna Equipment

For those stations equipped with low-gain (Prelort) antenna (Figure 5-11), the block diagram (Figure 5-1) shows the antenna interface equipment in green. With the exception of the 2-GHz boresight horn, this equipment is installed in the RF equipment area. Used as a test antenna, the 2-GHz boresight horn (mounted on a structure approximately 300 feet from the Prelort antenna) detects radiating energy for either electrically boresighting the Prelort antenna or performing a loop test of subsystem performance.

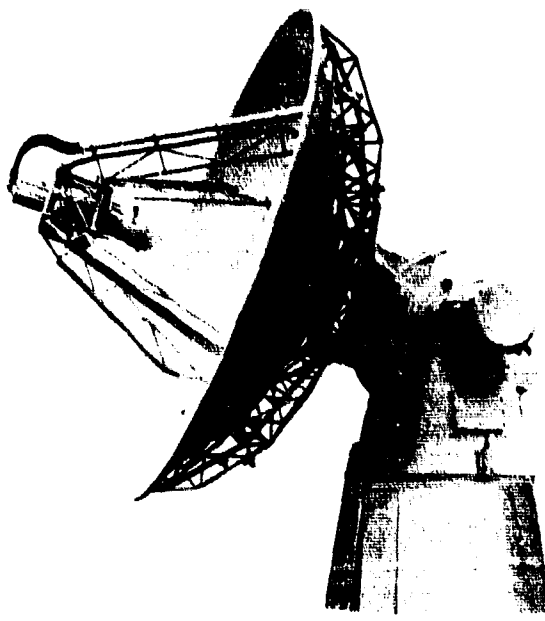


Figure 5-11 14-Foot Low-Gain (Prelort) Antenna

The antenna interface equipment items in the RF equipment area consist of a diplexer, the SGLS antenna panel, parametric amplifier, down-converter, receiver test unit, spectral filter, and variable attenuator.

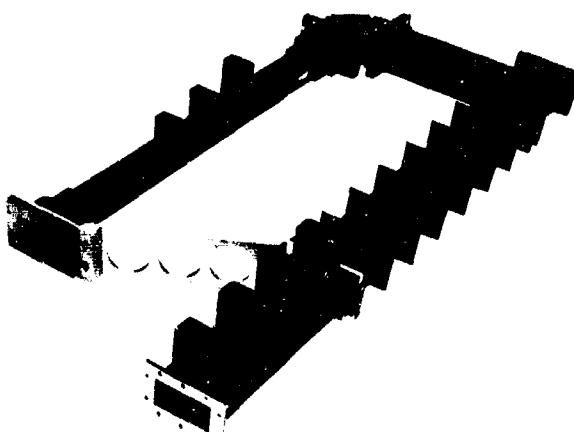


Figure 5-12 Diplexer

The diplexer (Figure 5-12) is a 3-port device that comprises two waveguide filters connected in a Y-configuration. This device allows simultaneous transmission and reception over a common antenna. Isolation between the transmitter and receiver ports is a minimum of 170 dB at 1.75 to 1.85 GHz, and isolation between the antenna port and the receiver port is a minimum of 60 dB at 2.7 to 2.95 GHz.



Figure 5-13 SGLS Antenna Panel

As shown in Figure 5-13, the SGLS antenna panel (in the master radar console) contains a reference receiver AGC meter, a conscan AGC meter, a signal-present indicator, and a carrier phase-lock indicator.

The parametric amplifier is identical to that for the TT&C antenna; however, since conical-scan signals are provided by the Prelort antenna, only the sum-channel amplifier is used in this configuration.

Similarly, the down-converter is identical to that for the TT&C antenna; however, only one frequency translator is used, since only one signal is present in this configuration.

The receiver test unit comprises a 2-GHz noise source and a patch panel. The 2-GHz noise source is a test device that injects a noise signal into the receiver. This signal permits quantitative determination of system noise performance. The output of the noise source is routed to the patch panel along with the low-level RF test signal from the test transponder. The patch panel provides a means of inserting one of these signals into either the parametric amplifier or the down-converter.

The 0- to 100-dB attenuator is inserted in the high-level 2.2-GHz test-signal path between the test transponder output and the input to the boresight horn. The attenuator provides positive control over the strength of the test signal received by the system and allows simulation of a variety of reception conditions.

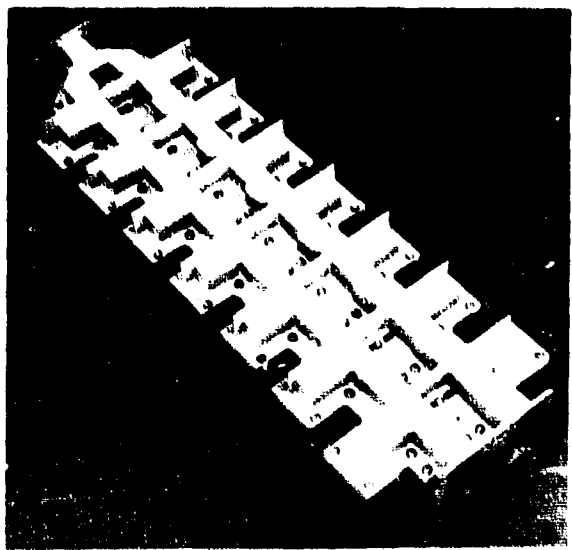


Figure 5-14 Spectral Filter

The spectral filter (Figure 5-14) is a high-pass waveguide device. Inserted in the 1.7-GHz uplink signal path between the transmitter output and the diplexer transmit port, the filter removes any out-of-band energy generated by the TWT amplifiers in the transmitter.

5.1.2 Transmitting Equipment

The transmitting equipment (Figure 5-15) provides the baseband assembly, RF generation, and power amplification for delivery of uplink information to the transmitting antenna. This equipment consists of a baseband assembly unit, a 20-channel transmitter exciter, a transmitter driver, and a 10-kW S-band power amplifier.

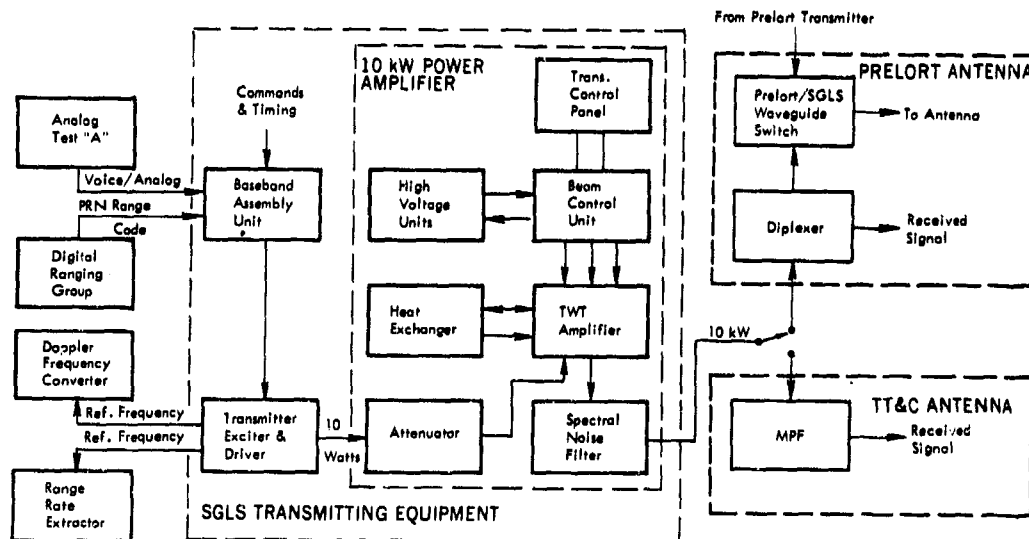


Figure 5-15 Transmitting Equipment Block Diagram

Baseband Assembly and Control Units

The baseband assembly unit (Figure 5-16) and baseband control (Figure 5-17), functionally inseparable units, accept uplink commands, uplink voice and analog data, and pseudorandom noise (PRN) ranging signals, all of which are processed and combined to form the uplink composite baseband.

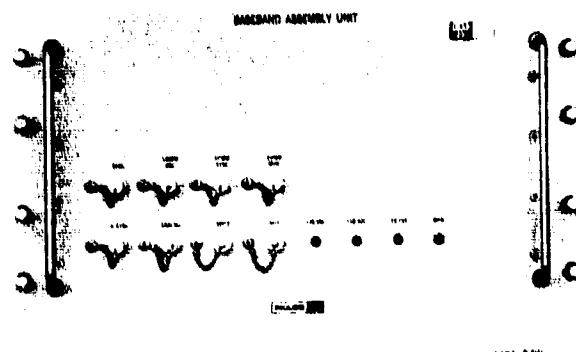


Figure 5-16 Baseband Assembly Unit

The baseband control provides the panel switches, controls, and relays for local and remote selection of the circuit parameters in the baseband assembly unit. The baseband control also contains logic that assures synchronism of the command signals with the command timing signal. The composite baseband is applied to the input of the transmitter exciter.

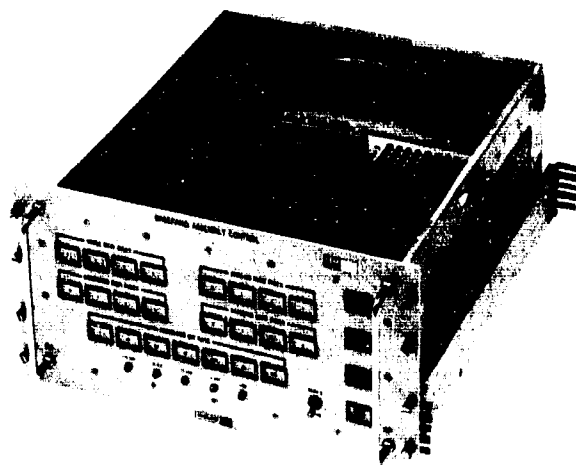


Figure 5-17 Baseband Control

Transmitter Exciter

The transmitter exciter (Figure 5-18) generates the transmitter carrier, modulates this carrier with the composite baseband, and presents the modulated signal to the transmitter driver. The exciter provides a phase-modulated RF output of up to

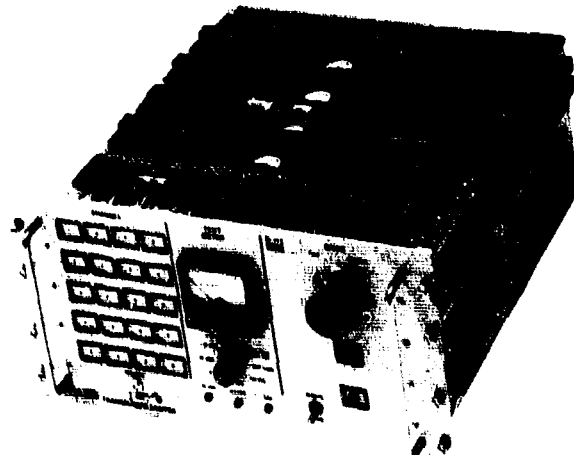


Figure 5-18 Transmitter Exciter

20-mW power at 20 discrete frequencies in the 1750- to 1850-MHz band. It also provides unmodulated reference signals at exactly 1/64 and 1/32 of the selected output frequency for use in the range rate extractor. After receiving the input signal (the composite baseband from the baseband assembly unit), the exciter generates a carrier frequency selected from among a set of 20 crystal oscillators that operate near 14 MHz. The output of the selected oscillator is multiplied in frequency to approximately 112 MHz, and

then phase-modulated by the composite baseband input signal. The modulated signal is doubled, amplified, and multiplied by 8 to produce a phase-modulated, low-level RF signal output at the uplink carrier frequency.

Transmitter Driver

The transmitter driver (Figure 5-19) comprises a traveling wave tube (TWT) amplifier and associated monitor and control circuits. The driver accepts the low-level, phase-modulated signals from the transmitter exciter and amplifies them sufficiently to drive the S-band power amplifier. The nominal 1800-MHz carrier input signal from the transmitter exciter drives the TWT, which amplifies the input signal from the 20-mW level to

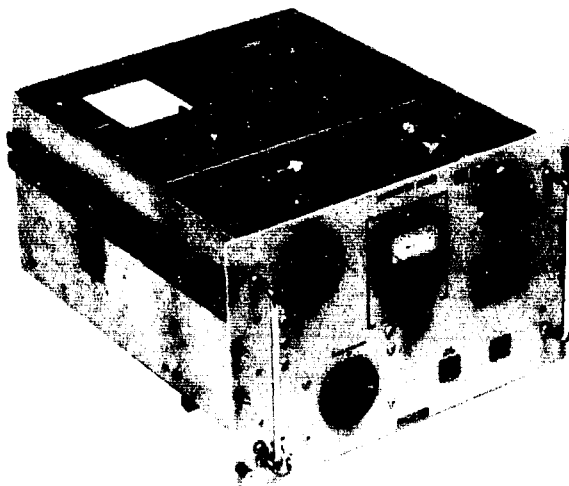


Figure 5-19 Transmitter Driver

1419-67W

a nominal 10 watts. A directional coupler samples the output of the TWT to provide output-level metering, spectrum display, and low-power alarm signals. The carrier signal from the main arm output of the directional coupler is fed via a manually controlled variable attenuator (which provides at least 50-dB continuous attenuation), a marker frequency meter, a hybrid circulator, a through-line power meter, and a coaxial switch to either the input of the S-band power amplifier or to a dummy load.

S-Band Power Amplifier

The S-band power amplifier (Figure 5-20) consists of a liquid-cooled high-power traveling-wave-tube (TWT) amplifier, and the auxiliaries for control, monitoring, and protection. The amplifier accepts the phase-modulated S-band signal from

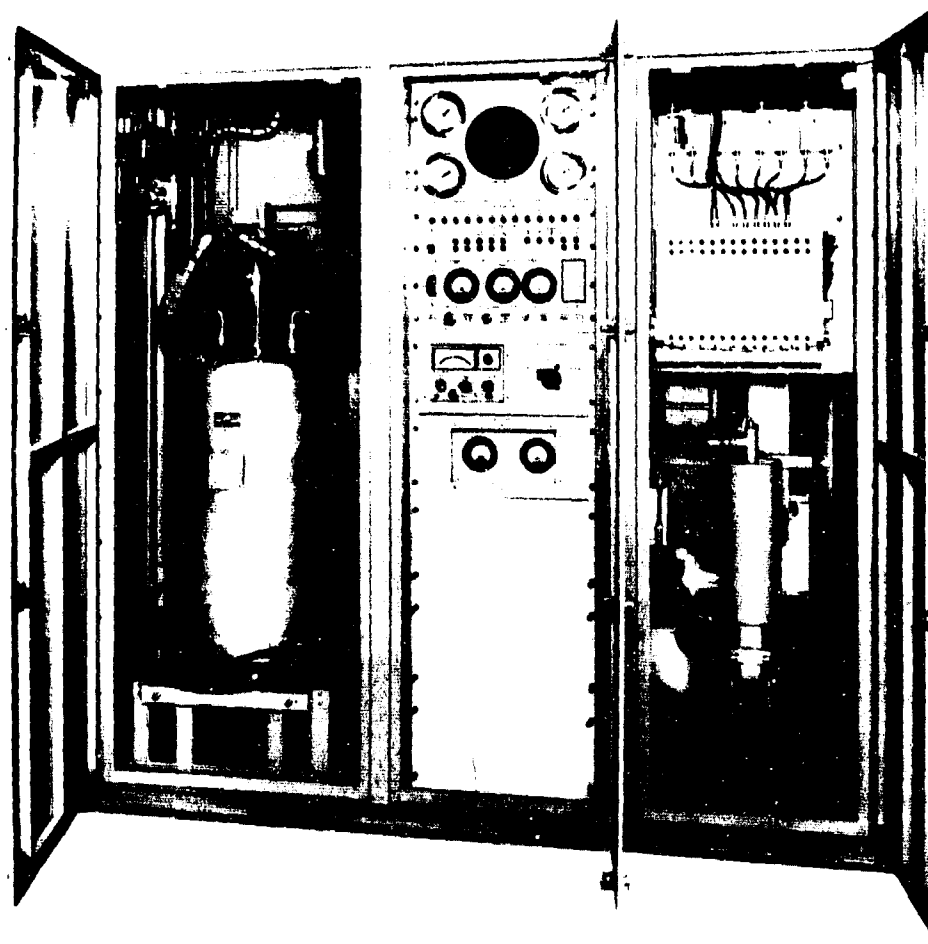


Figure 5-20 S-Band Power Amplifier

210-87W

the transmitter driver and amplifies it to 10 kW. An internal waveguide switch routes the transmitter output to the antenna or, in a test operation, routes the test signal to the internal dummy load.

The drive power from the driver is fed to the TWT via an isolator and a motor-driven attenuator. The TWT amplifies the signal and outputs it to the antenna through a high-power isolator. A filter assures low harmonic output levels. Protective circuitry contains an "electronic crowbar" that discharges the high-voltage filter capacitor harmlessly in the event of an arc or overload. (The crowbar circuits sense various faults and cause a high-power thyratron to short-circuit the high-voltage supply within 10 microseconds or less, thereby preventing damage.) An automatic sensing system gives a visual fault indication, and a keylock system enables single point control of transmitter turn-on to prevent safety hazards during maintenance.

Control of the power amplifier is accomplished from a master control panel that is mounted in a standard 19-inch rack anywhere within 500 feet of the transmitter.

Radiation Warning Control Equipment

This equipment (Figure 5-21) consists of control-logic circuitry that interconnects the transmitter, SOC, and various visual and aural warning devices located in radiation-hazard areas. This equipment is interlocked with the transmitter and interfaces with the RTS radiation warning equipment to allow sufficient time for personnel to clear hazard areas before high-power RF is radiated.



Figure 5-21 Radiation Warning Control

5.1.3 Receiving Equipment

The receiving equipment (Figure 5-22) provides signal detection demodulation, demultiplexing, and frequency tracking. After receiving downlink signals, the receiving equipment outputs voice/analog data, telemetry (PCM and/or PAM/FM, FM/FM), angle-tracking error signals, and range and range-rate data. The equipment consists of the ground receiver and analog ranging equipment (GRARE) and the Carrier 2 demodulator, baseband separation unit, and the 1.7-MHz demodulator. The GRARE (Figure 5-23) contains the reference receiver, angle track receiver, range receiver, and frequency synthesizer.

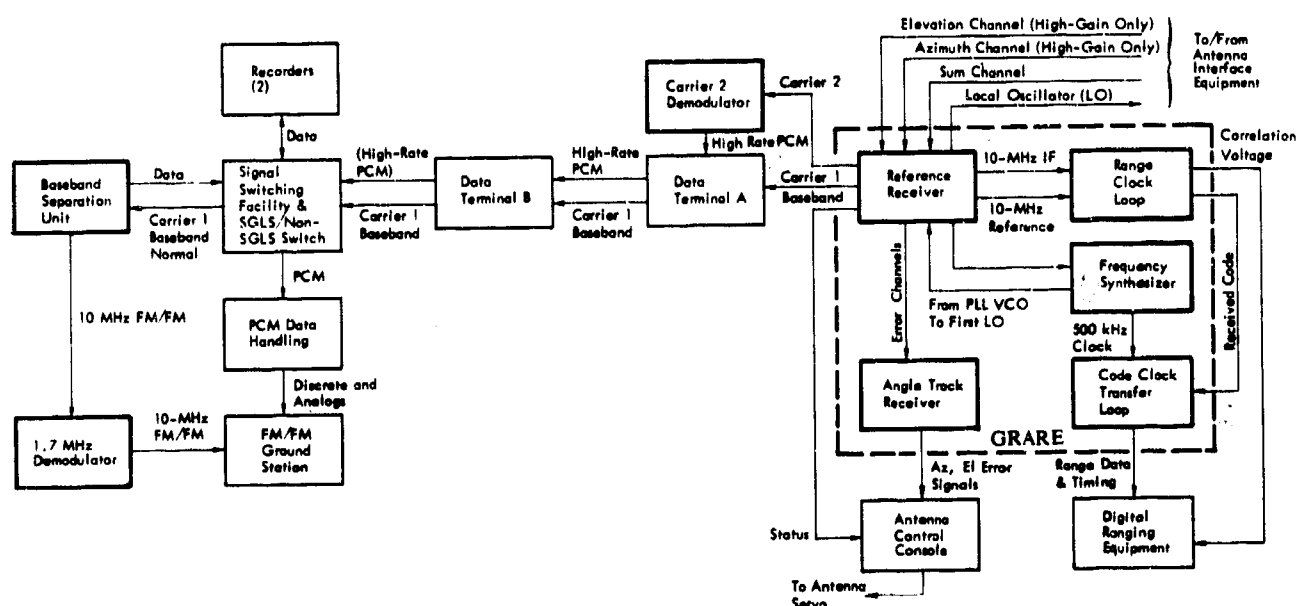


Figure 5-22 Receiving Equipment Block Diagram

Reference Receiver

The reference receiver is a dual conversion device capable of operating in either phase-lock or crosscorrelation modes. It accepts the 130-MHz inputs(s) from the down-converter and produces as outputs the downlink baseband(s), ranging data, doppler data, and reference signals for use by the angle track receiver and the doppler frequency converter.

Angle Track Receiver

The angle track receiver is a dual-channel dual-conversion device. In the high-gain antenna configuration, the receiver detects angle-tracking errors and converts these to error voltages for feedback to the antenna servo system. Receiver inputs are the azimuth and elevation error channel outputs of the MPF. Both receiver channels are used, one for each input. In the low-gain (Prelort) antenna configuration, however, only one channel is used (to recover the conical-scan amplitude modulation from the receiver input).

Range Receiver

In conjunction with digital ranging equipment, the range receiver initially determines and continuously updates the slant range of the space vehicle from the tracking station. During initial range determination, the range receiver compares the receiver PRN code with the transmitter PRN code and produces a signal (correlation voltage) that

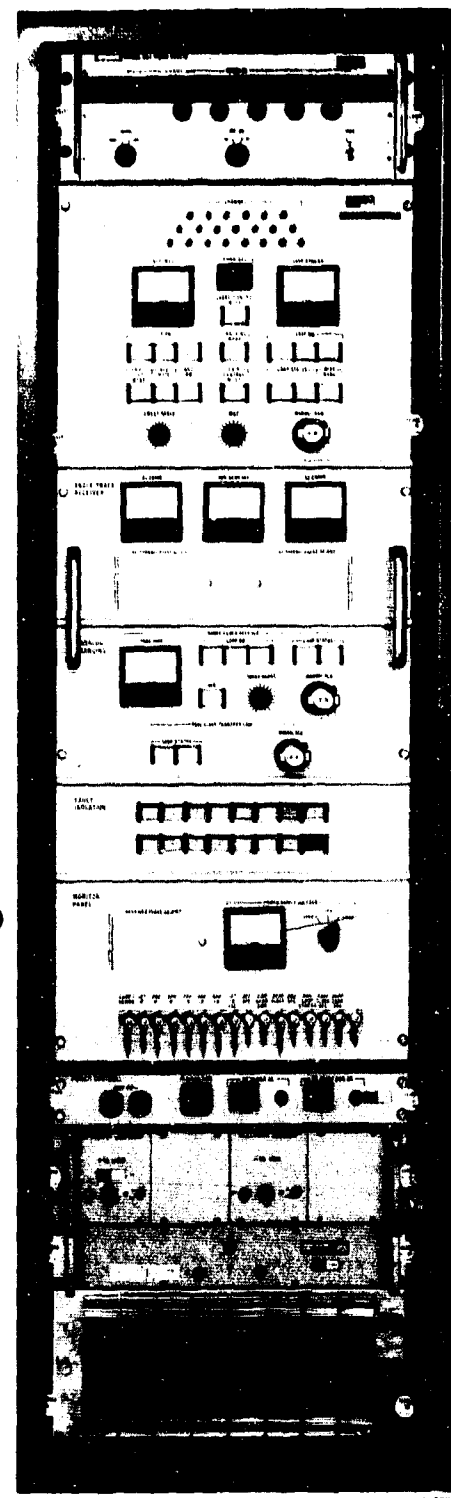


Figure 5-23 GRARE

is a measure of the degree of correlation between these codes. (The digital ranging equipment uses this signal to establish the initial vehicle range.) The range receiver also compares the received clock signal with the transmitter clock and produces the doppler of the two signals. When initial determination is complete, the digital ranging equipment uses this doppler signal to update the vehicle range.

Frequency Synthesizer

The frequency synthesizer (Figure 5-24) accepts the signal from the reference receiver VCO and produces an internally synthesized frequency output that tracks

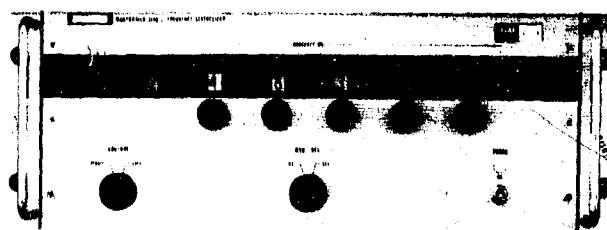


Figure 5-24 Frequency Synthesizer

the input frequency. After X96 multiplication, this output is used as the first LO frequency in the down-converter. The synthesizer also internally produces the 500-kHz reference frequency output for use by the PRN-ranging equipment.

Carrier 2 Demodulator

The Carrier 2 (Figure 5-25) demodulator comprises an IF amplifier, two phase detectors, filters, automatic search and acquisition circuits, and associated circuitry. The demodulator accepts the Carrier 2 baseband signal from the reference receiver and provides the high-rate PCM bit stream output.

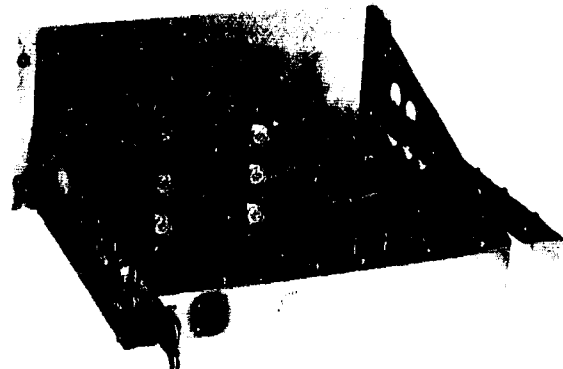


Figure 5-25 Carrier 2 Demodulator

Baseband Separation Unit (BSU)

This equipment (Figure 5-26) comprises the filters, phase detectors, and amplifiers that are needed to separate the three subcarriers from the composite Carrier 1

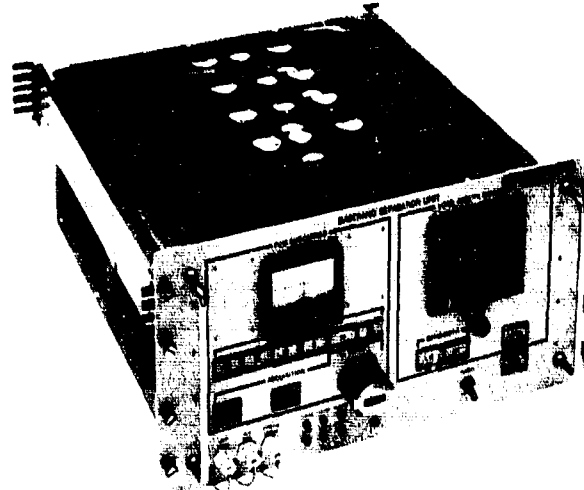


Figure 5-26 Baseband Separation Unit

baseband. After separating the subcarriers, the BSU demodulates the analog data from the 1.25-MHz subcarrier and the PCM data from the 1.024-MHz subcarrier. The BSU upconverts the 1.7-MHz subcarrier to 10 MHz for processing by the 1.7-MHz demodulator. BSU outputs are voice/analog, predetection voice/analog, low-rate PCM, predetection low-rate PCM, and the 1.7-MHz subcarrier upconverted to 10 MHz.

1.7-MHz Demodulator

This unit (Figure 5-27) accepts a 10-MHz, biphase modulated signal from the baseband separator. The subcarrier may be modulated either by PCM or PAM/FM. For PCM, the unit provides coherent signal demodulation and a PCM data-stream output. For PAM/FM, the 10-MHz signal is throughput without demodulation.

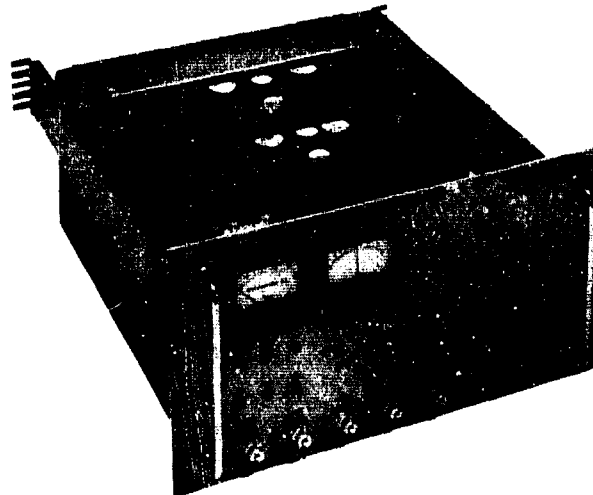


Figure 5-27 1.7-MHz Demodulator

5.1.4 Digital Ranging Equipment (DRE)

The DRE (Figures 5-28 and 5-29) comprises the acquisition assembly, receiver and transmitter coders, range tally unit, readout register/buffer, and internal simulator. This equipment, in conjunction with the range receiver in the GRARE, initially determines and continuously updates the range of the space vehicle from the station. Inputs to the DRE are timing, clock, and correlation voltages from the GRARE; data outputs to the RTS are space vehicle range (in the form of a 30-bit binary word) and status information.

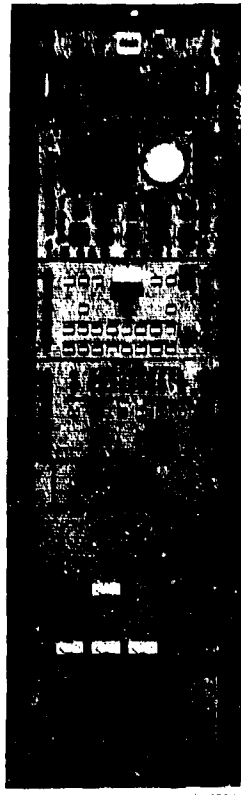


Figure 5-28 Digital Ranging Equipment

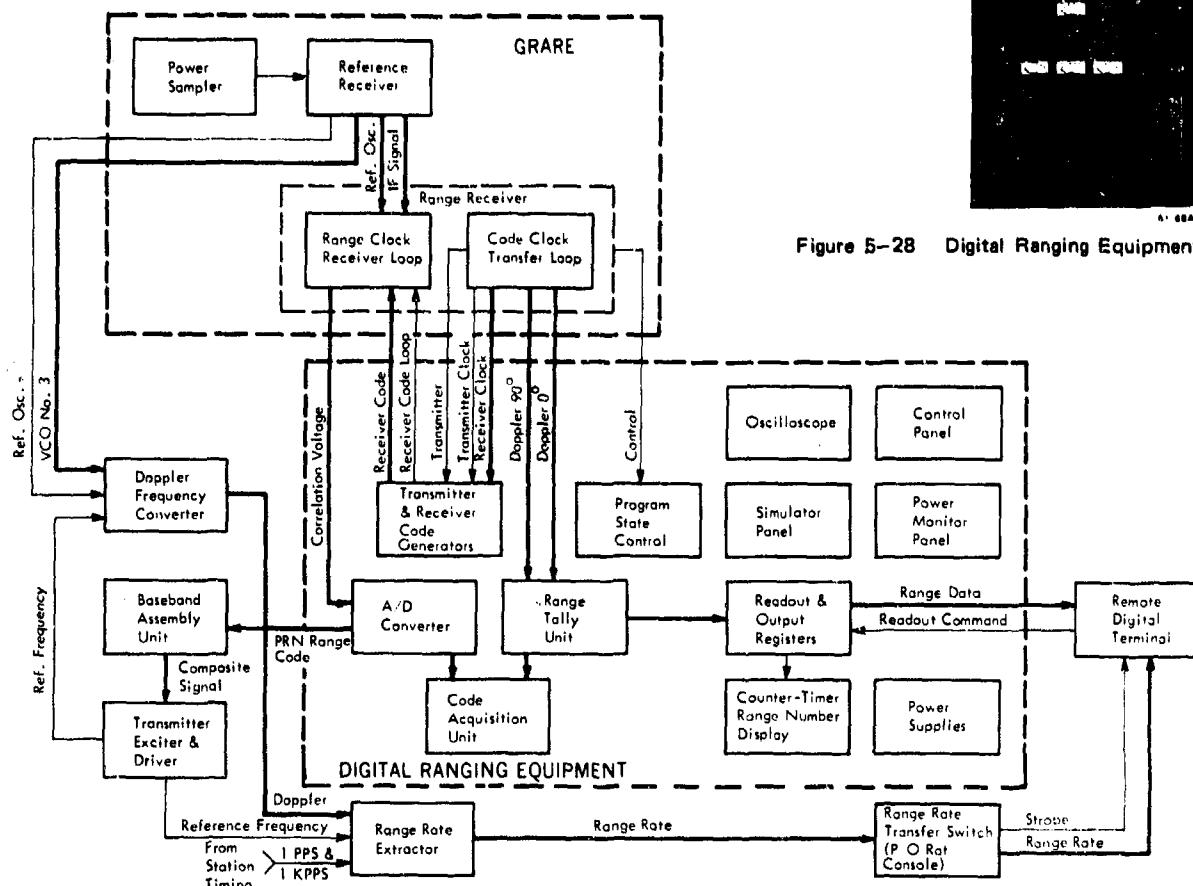


Figure 5-29 Digital Ranging Equipment Block Diagram

6.1.5 Range-Rate Equipment

The range-rate equipment accepts output signals from the receiving equipment and reference signals from the transmitting equipment and provides an analog or doppler frequency output. This equipment comprises the doppler frequency converter and the range-rate extractor.

Doppler Frequency Converter

The doppler frequency converter (Figure 5-30) compares the frequency of the received carrier with that of the transmitted carrier to produce an output signal that corresponds with the spacecraft range rate. Three input signals are supplied to the converter: (1) the transmitter signal frequency, which is 1/32 of the uplink frequency; (2) the receiver reference oscillator frequency of 10 MHz; and (3) the receiver voltage-controlled oscillator (VCO) frequency, which is 1/32 of the first

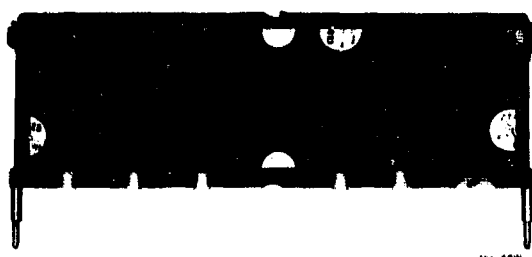


Figure 5-30 Doppler Frequency Converter

LO frequency minus 5.625 MHz. After comparing these signals, the doppler frequency converter produces an output signal (2.20 MHz plus or minus the two-way doppler shift) which is routed to the range-rate extractor.

Range-Rate Extractor

The range-rate extractor (Figure 5-31) accepts the doppler output of the doppler frequency converter and, after comparing it with a transmitter reference signal, produces an output (a 24-bit binary word) that corresponds with the doppler shift.

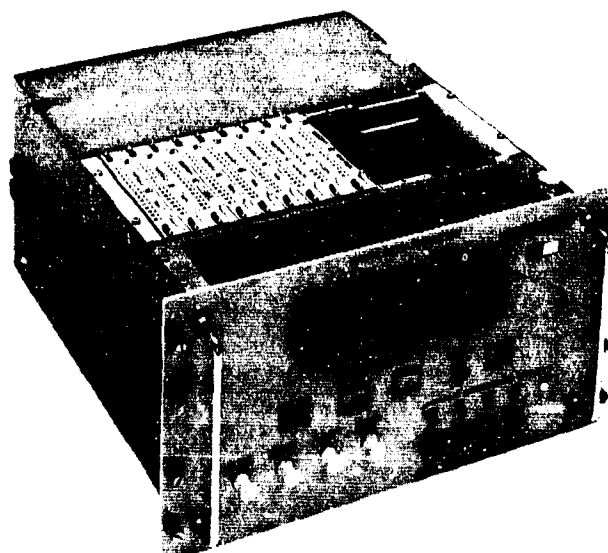


Figure 5-31 Range Rate Extractor

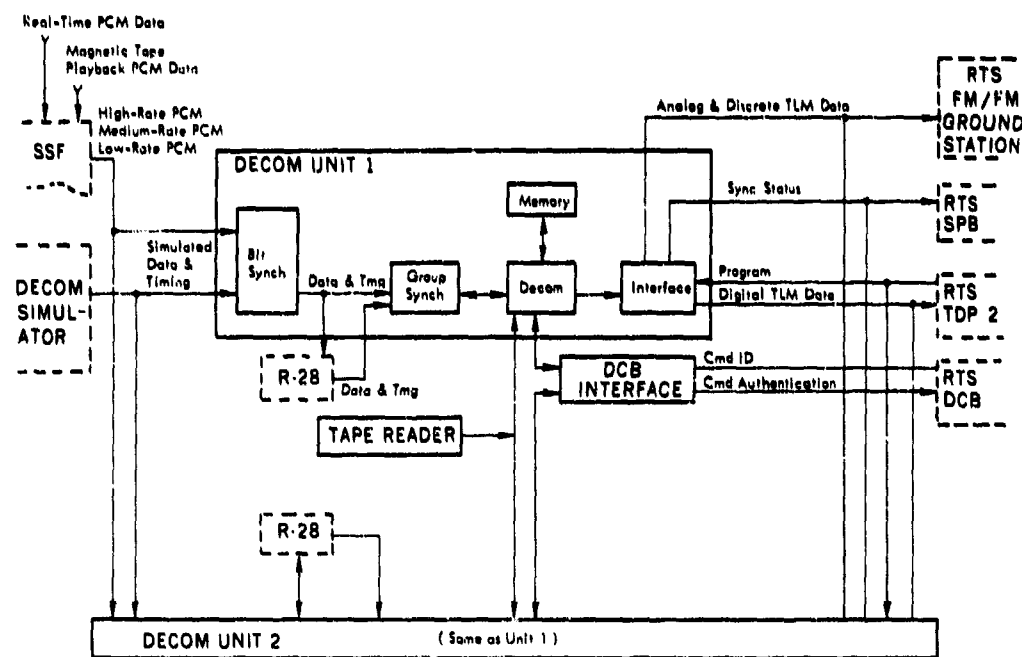


Figure 5-32 Telemetry Equipment Block Diagram

5.1.6 Telemetry Equipment

The telemetry equipment (Figure 5-32), also called the "PCM Ground Station," converts the PCM bit streams from the receiver demodulators into telemetry data words for computer use. The equipment comprises two PCM decommutators and a PCM simulator that is used in test and checkout of the subsystem.

Setup and configuration of the PCM equipment may be accomplished by one of the following means:

- Computer input from the RTS computer
- Punched paper tape via the tape reader provided as part of the PCM equipment
- Manual manipulation of the front panel controls

PCM Decommutators

Since the two PCM decommutators are identical, only one is described here. This unit is a stored program device whose control logic and circuitry is designed to extract the data from the incoming bit stream, reconstruct this data into parallel binary words, and transfer them to the RTS computer. In addition, this device converts selected words (analog functions) from digital to analog, and makes them available for display or recording by up to 20 analog devices (meters, chart recorders, etc.). The PCM decommutator can also convert up to 24 discrete data bits and make them available for driving a status display.

The decommutators are arranged for either single or independent simultaneous operation. When both units are used simultaneously, two PCM bit streams may be processed at one time.

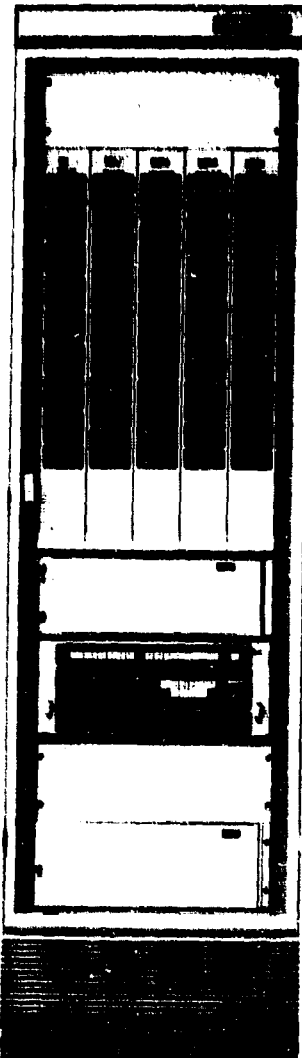


Figure 5-33 PCM Decommutator

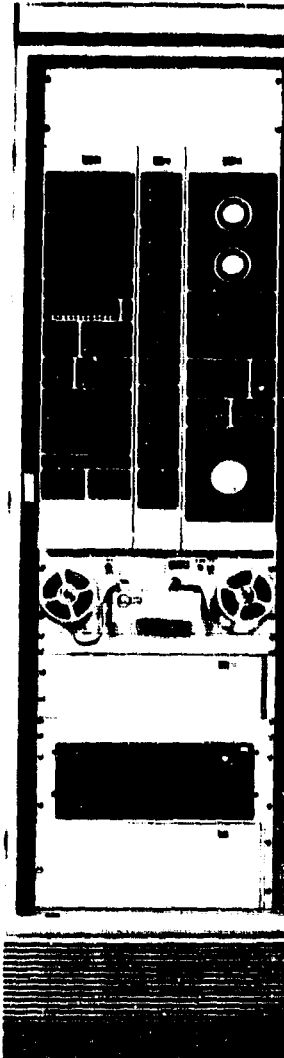


Figure 5-34 PCM Simulator

PCM Simulator

The PCM simulator is a stored program device that can generate either a serial PCM signal with clock or a parallel data word. The serial output signal may include, if desired, noise, rate, jitter, and blanking. The stored program determines the simulator's processing format. The simulator provides outputs to the test transponder (via the PCM COMSEC equipment) for loop test and to the PCM decommutators for maintenance.

5.1.7 Control and Display Equipment

The control and display equipment (Figure 5-35) enables the operator to control and monitor certain SGLS equipment from remote positions. The control and display equipment comprises the SGLS SOC panel, SGLS antenna panel, loop test panel, TSRE amplifier select panel, and the RDT status interface unit.

SGLS SOC Panel

The SGLS SOC panel is located in the SOC console. The controls and displays on this panel enable the operator to activate the radiation warning system and control radiation from the 10-kW S-band transmitter.

SGLS Antenna Panel

This panel is located in the antenna control console and contains a reference-receiver AGC meter, a signal-present indicator, and a Carrier 1 phase-lock indicator. For subsystems interfaced with the low-gain Prelort antenna, a conical-scan AGC meter is also provided.

Loop Test Panel

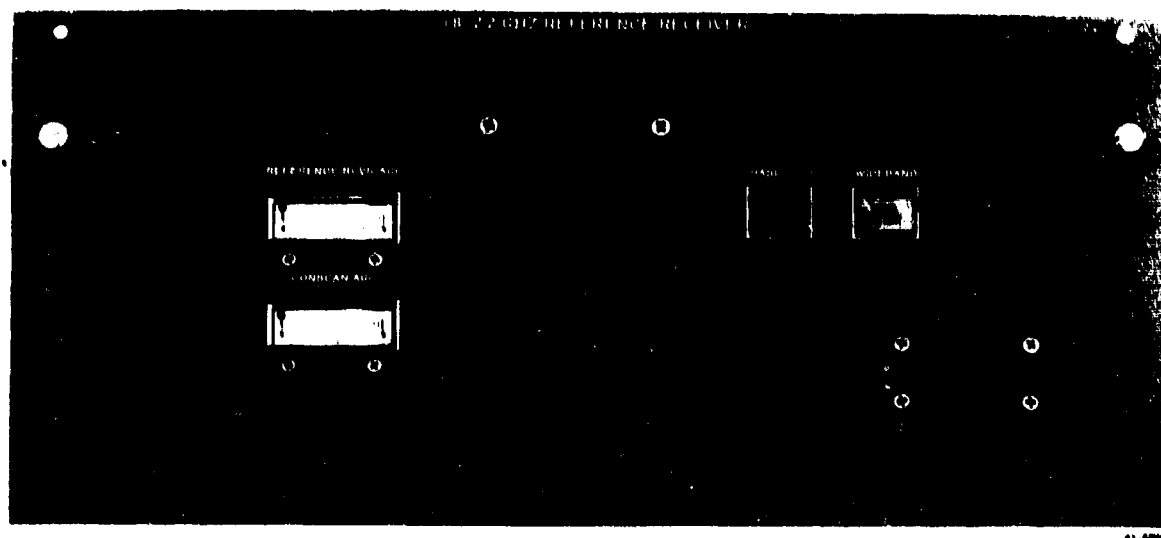
The loop test panel is located in the uplink equipment rack. This panel contains controls for starting and stopping the loop-test function, and a split-legends control for selecting the ATU-A output for downlink loop testing.

TSRE Amplifier Select Panel

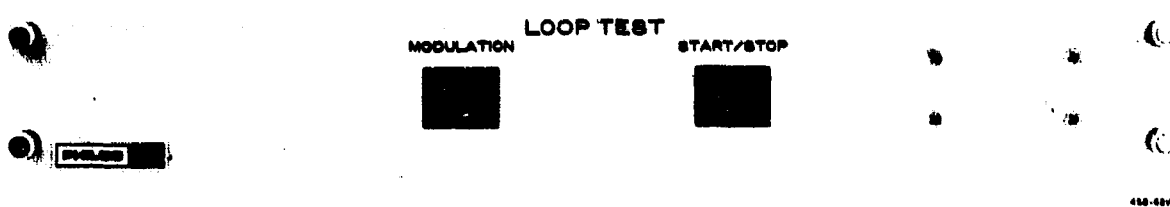
This panel is located in the data terminal A rack and contains controls for selecting the proper transmitter and receiver combination in data terminals A and B.

RDT Status Interface Unit

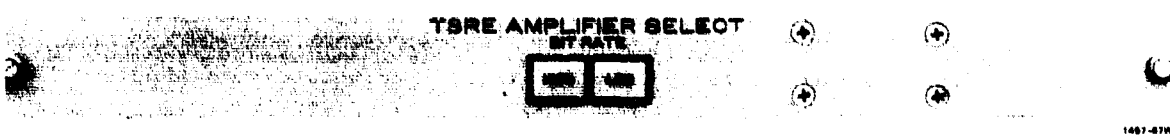
This unit accepts status indications from the various SGLS equipment items in the RF equipment area and provides these indications to the RDT.



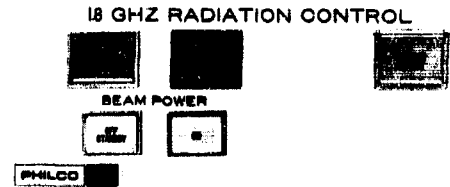
SGLS Antenna Panel



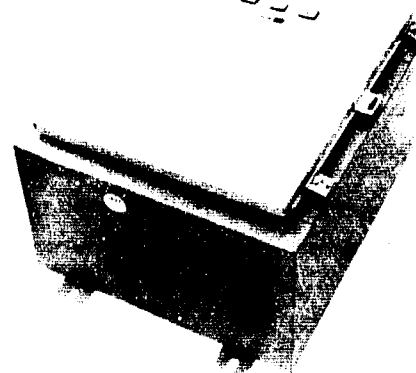
Loop Test Panel



TSRE Amplifier Select Panel



SGLS SOC Panel



RDT Status Interface Unit

FIGURE 5-35 CONTROL & DISPLAY EQUIPMENT (SGLS)

5-25

5.1.8 Data Terminal Equipment

This equipment provides a data link between the RF and data equipment areas. One terminal is located in each area and is equipped with data transceivers for transmitting to and receiving from the other terminal. One of two configurations is used, depending upon the distance between the RF and data equipment areas. Where the distance between the RF and data equipment areas is greater than 500 feet, type 1 terminal is used, and where the distance is less than 500 feet, type 2 terminal is used.

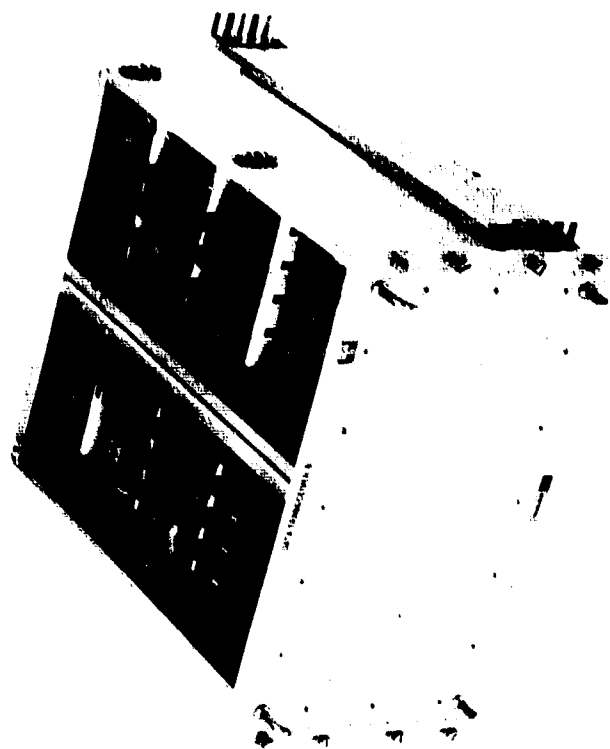
The data terminal equipment (Figures 5-36 and 5-37) consists of two data transceiver terminals (labeled A and B) located in the RF equipment area and the data equipment area, respectively. The terminals are connected by shielded twisted pair cable. Collectively, this equipment provides three telemetry channels and eight command data channels between the two locations.

Data Terminal A

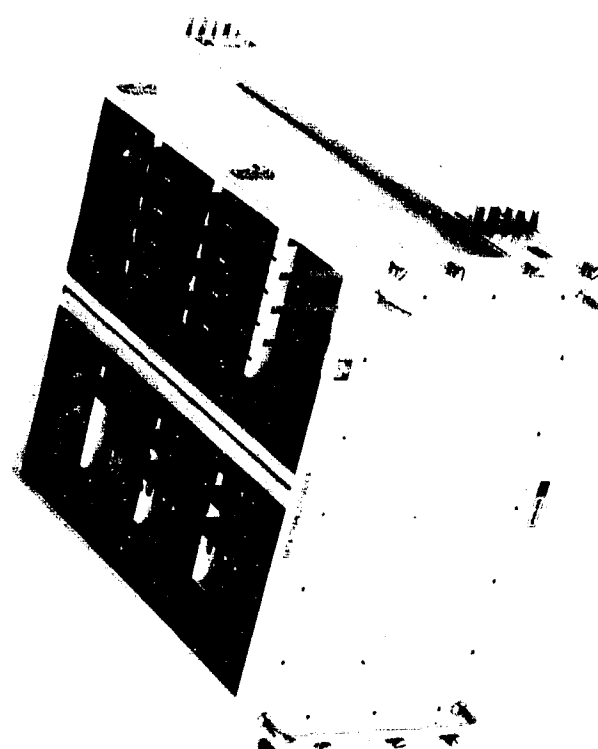
Type 1 data terminal A comprises a command data transceiver that contains one transmitter and two receivers for handling ternary digital data, as well as two wideband video transmitters and one wideband video receiver for handling telemetry data. Type 2 data terminal A contains only the command data transceiver.

Data Terminal B

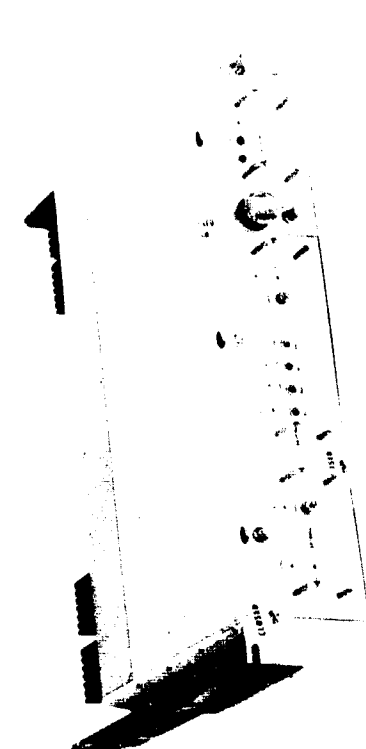
Type 1 data terminal B comprises a command data transceiver that contains two transmitters and one receiver for handling ternary digital data, as well as one wideband video transmitter and two wideband video receivers for handling telemetry data. Type 2 data terminal B contains only the command transceiver.



Data Transceiver B



Data Transceiver A



Wideband Video Transmitter



Wideband Video Receiver

FIGURE 5-36 DATA TERMINAL EQUIPMENT (SGLS)

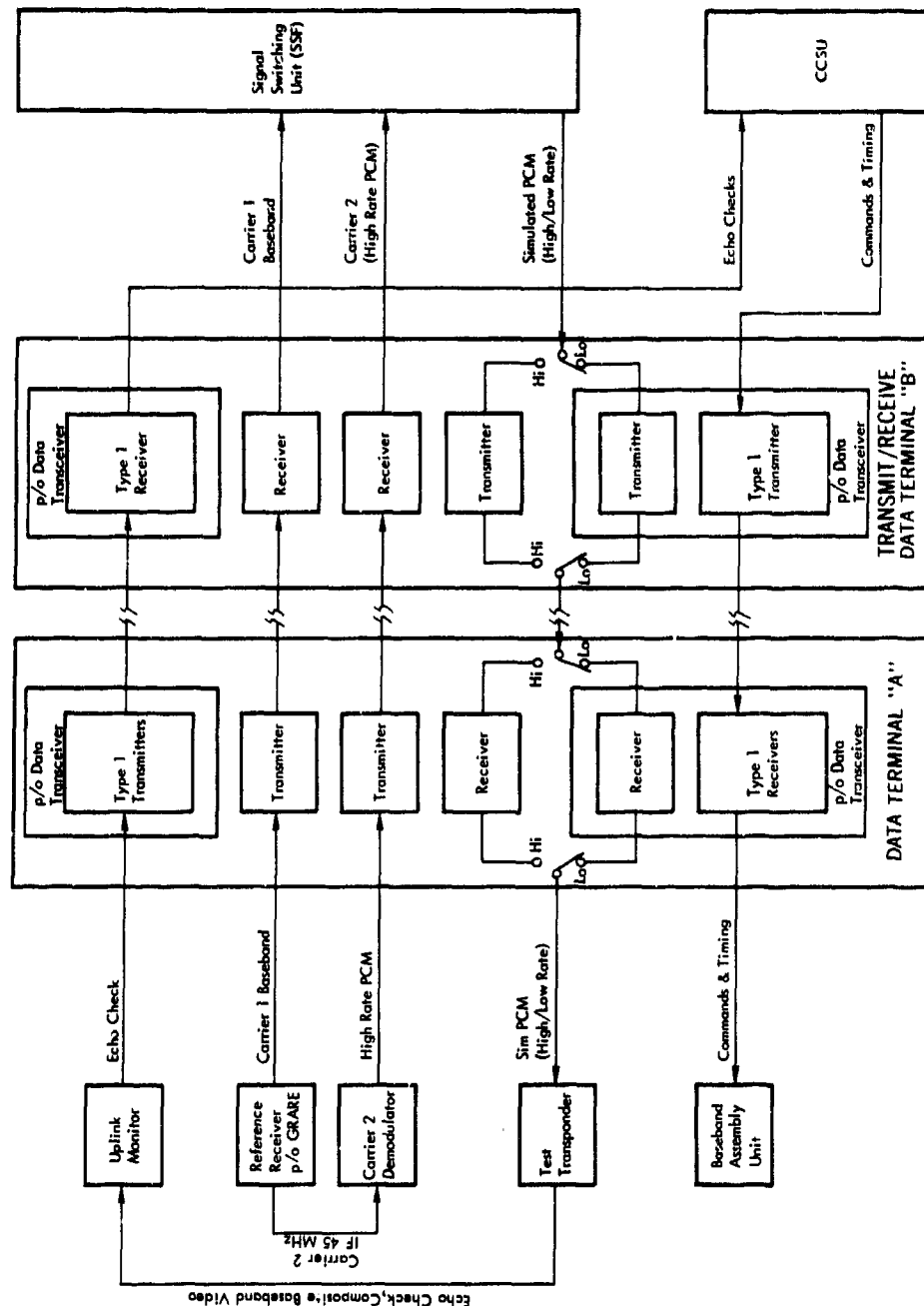


Figure 5-37 Data Terminal Equipment Block Diagram

5.1.9 Signal Switching Equipment

This equipment (Figures 5-38 and 5-39), also called the signal switching facility (SSF), determines the routing of signals (for recording and/or playback) in the data equipment area. The SSF comprises a switch matrix and display; an SSF test unit, recorder fault detector display, sequential control, and card reader; and a signal conditioning unit. The SSF capability includes the:

- Performing of signal line switching and interface matching for SGLS equipment.
- Routing data to external interfacing equipment or to the recording equipment.
- Directing of playback signals from recorders to other external equipment.

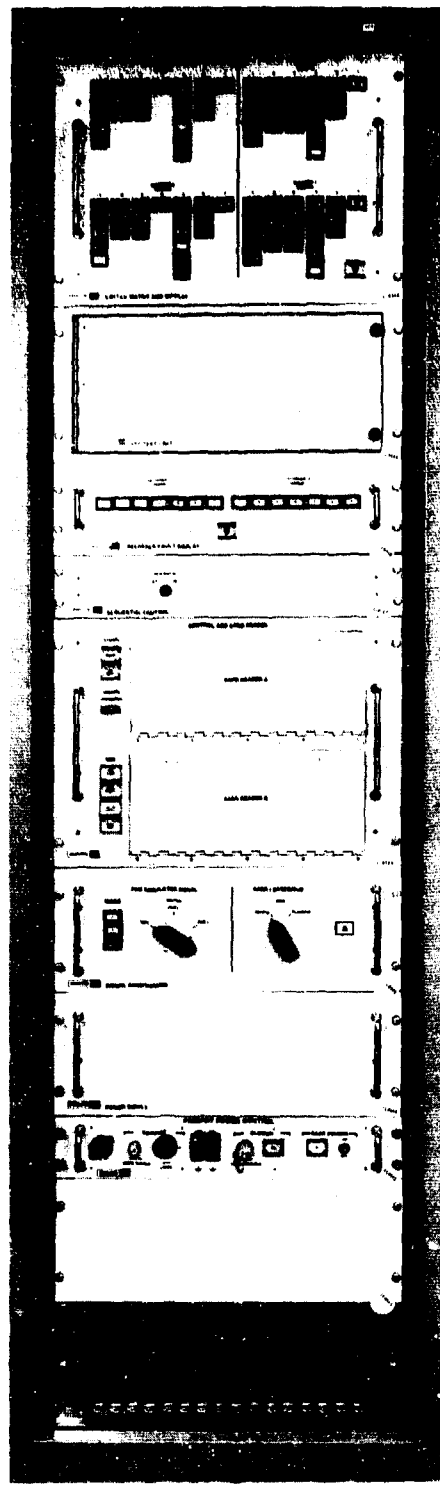


Figure 5-38 Signal Switching Facility

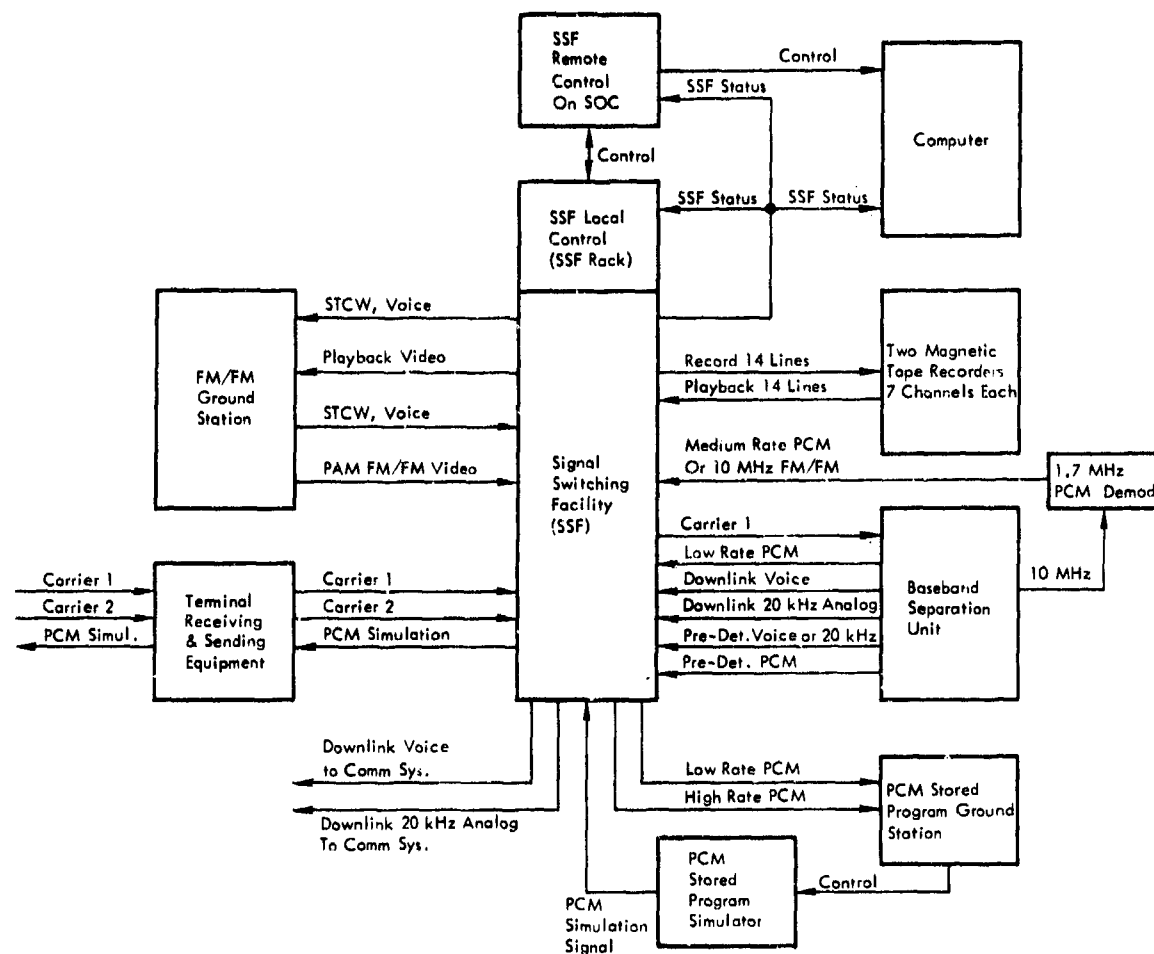


Figure 5-39 Signal Switching Facility Block Diagram

5.1.10 Recording/Playback Equipment

This equipment (Figures 5-40 and 5-41) comprises two AMPEX FR-1600 magnetic tape recorders (together with their associated record and playback amplifiers, equalizers, and automatic sequential controller) that provide the facilities for recording and playback of selected data received from the space vehicle. Each recorder can record/playback on seven tracks. They are interconnected with other equipment items via the signal switching facility.

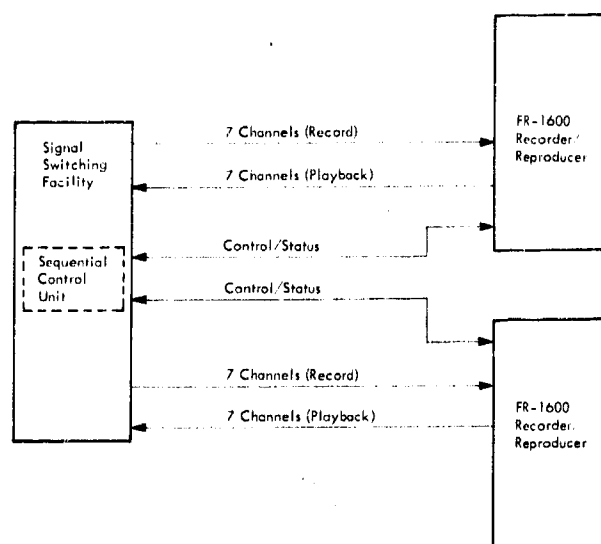


Figure 5-40 Recording/Playback Block Diagram

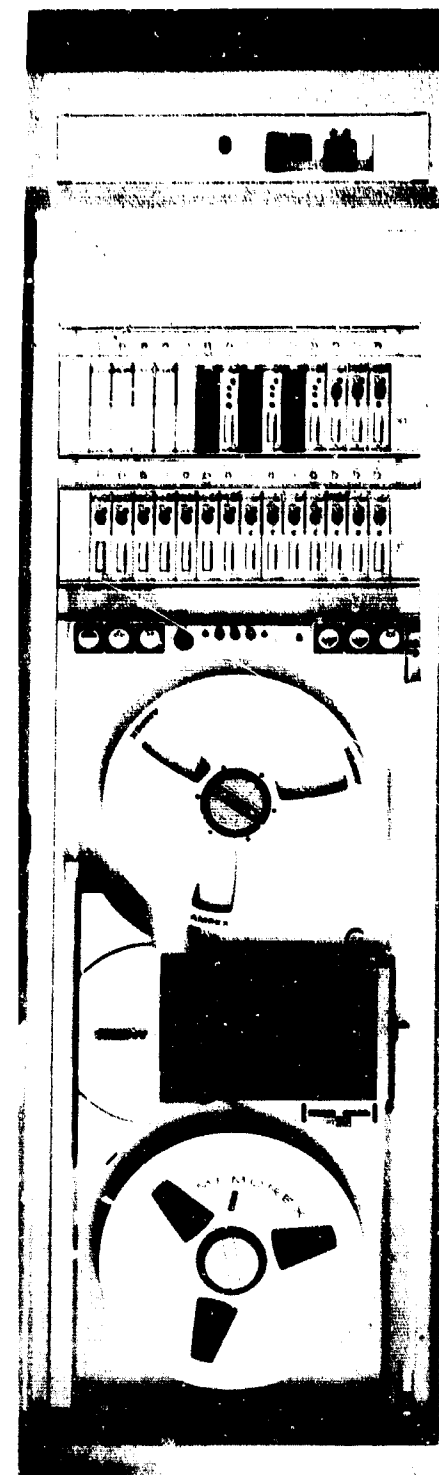


Figure 5-41 Ampex FR1600 Magnetic Tape Recorder

5.1.11 COMSEC Equipment

This equipment, comprising the command COMSEC equipment and the PCM COMSEC equipment (Figures 5-42 and 5-43), provides the facility for encrypting command data prior to transmission and decrypting secure telemetry data received from the space vehicle. Since the equipment is classified, it is pictured in the closed door condition.

Command COMSEC Equipment

This equipment accepts as inputs plain command data, encrypted echo check data, and timing. The outputs consist of encrypted command data, decrypted echo check data, and various status and alarm signals. Upon request from the PCM equipment, the command COMSEC equipment provides command authentication signals.

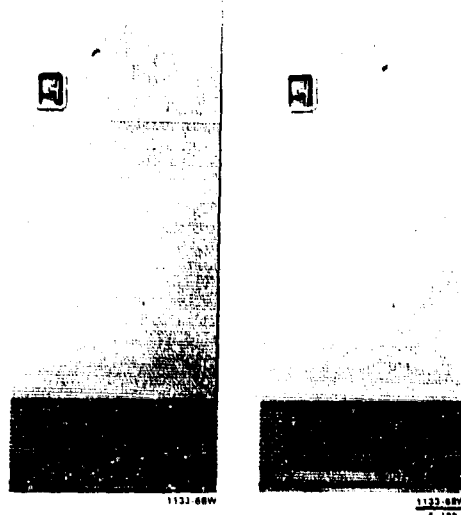


Figure 5-42 COMSEC Equipment

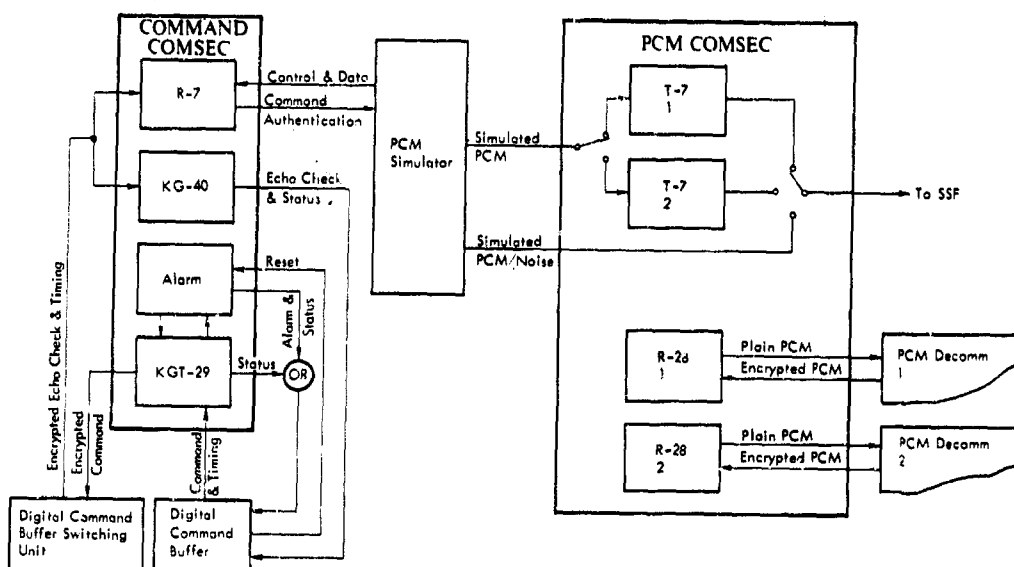


Figure 5-43 COMSEC Equipment Block Diagram

PCM COMSEC Equipment

This equipment accepts as inputs encrypted PCM data and plain simulated PCM data. The outputs consist of decrypted PCM data and encrypted simulated PCM data.

5.1.12 Integration and Checkout Equipment

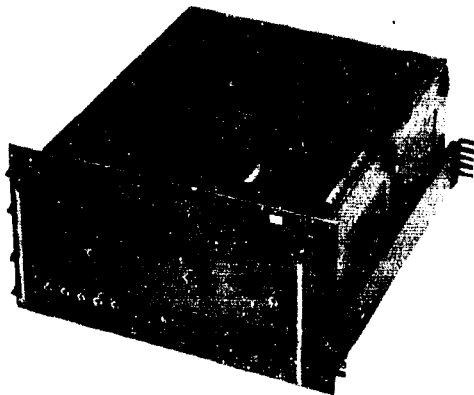
This equipment constitutes the system test equipment necessary for performing loop tests, performance tests and subsystem monitoring during operational missions.

It comprises the receiver test unit (RTU), analog test unit A, analog test unit B, and a set of commercial test equipment.

Receiver Test Unit

For those subsystems interfaced with the high-gain (TT&C) antenna, the RTU comprises an AIL 355W Noise Figure Test Set, a 2-GHz noise source (Figure 5-6), and the echo check and receiver test control unit (Figure 5-9) previously described in Paragraph 5.1.1.

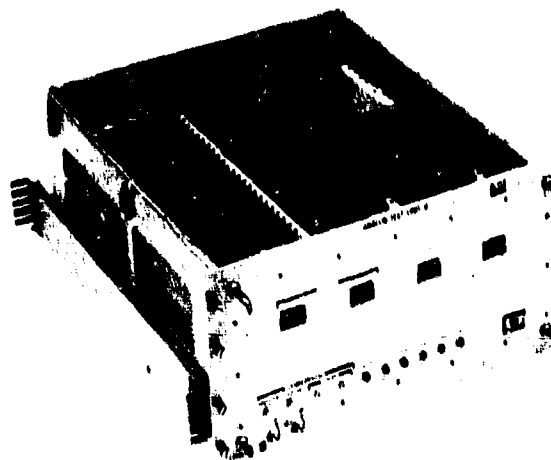
For subsystems interfaced with the low-gain (Prelort) antenna, the receiver test unit comprises a 2-GHz noise source and a patch panel for routing the output of this device (also described in Section 5.1.1).



Analog Test Unit A

Analog test unit A (Figure 5-44) provides simulated voice and analog test signals to the baseband assembly unit and simulated PAM/FM and voice or analog signals to the test transponder transmitter during loop tests. It also monitors the outputs of the uplink monitor.

Figure 5-44 Analog Test Unit A



Analog Test Unit B

Analog test unit B (Figure 5-45) provides on-line monitoring of downlink analog test signals. The unit monitors outputs from the baseband separation unit and provides status indications of the types of signals present.

Figure 5-45 Analog Test Unit B

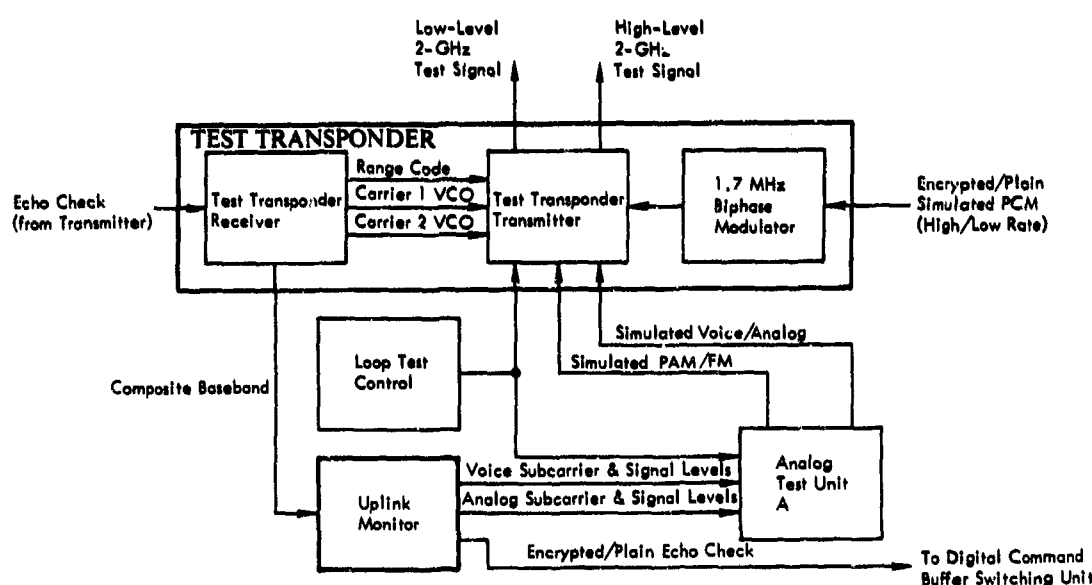


Figure 5-46 Test Transponder & Uplink Monitor

5.1.18 Test Transponder and Uplink Monitor

The test transponder and uplink monitor (Figure 5-46) are units arranged to monitor uplink command transmission during actual operation, and to simulate space vehicle equipment during loop tests.

Test Transponder

This equipment (Figure 5-47) comprises a receiver, transmitter, and a biphase modulator.

The test transponder receiver is a dual-conversion superheterodyne receiver. A phase-locked tracking loop acquires the uplink carrier and provides for synchronous demodulation of the uplink frequency-multiplexed baseband signal. This unit also supplies a coherent RF drive signal, a noncoherent RF drive signal, and the recovered multiplexed baseband to the test transponder transmitter for loop-test purposes.

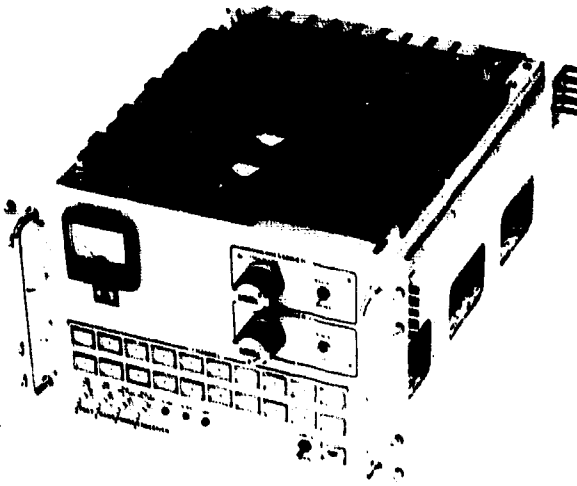


Figure 5-47 Test Transponder

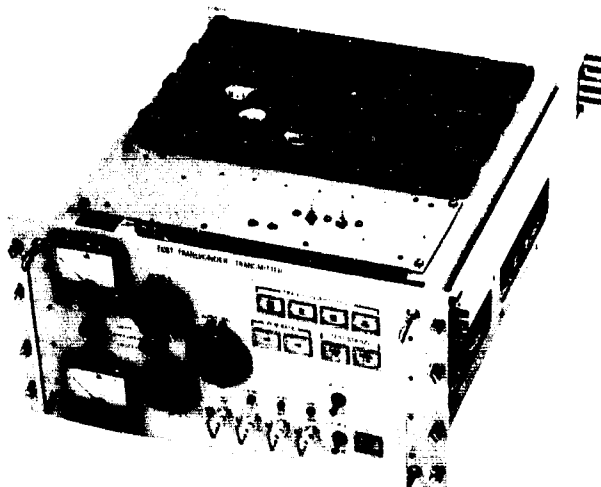


Figure 5-48 Test Transponder Transmitter

The test transponder transmitter (Figure 5-48) is used with the test transponder receiver to simulate vehicle transponders in the Space Ground Link Subsystem (SGLS); it can also be used independently as a specialized signal generator. It accepts simulated voice, analog, PCM, PRN ranging signals and provides an output both a high- and low-level simulated downlink test signal in the 2.2- to 2.3-GHz frequency band. The high-level output is routed to the boresight horn.

WDL-1R3227-1
Volume I, Part 1

For subsystems interfaced with the high-gain (TT&C) antenna, the low-level output is routed to the vertex horn via the echo check/receiver test central unit, and for subsystems interfaced with the low-gain (Prelort) antenna, the low-level signal is inserted into the parametric amplifier via the receiver test unit.

The biphasic modulator (Figure 5-49) receives the simulated PCM signal from data terminal A and provides a biphasic modulated 1.7-MHz output to the test transmitter.

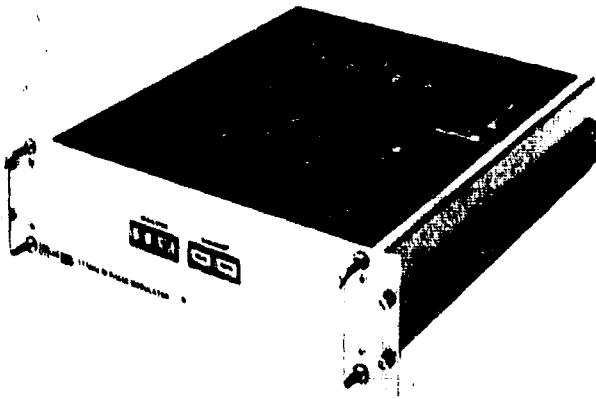


Figure 5-49 1.7-MGHz Biphasic Modulator

1418-67W

Uplink Monitor

This equipment (Figure 5-50) separates and demodulates the composite uplink baseband signals recovered by the test transponder and routes them to analog test unit A for monitoring. It also recovers commands from the uplink baseband and routes them to the data equipment area for command echo check.

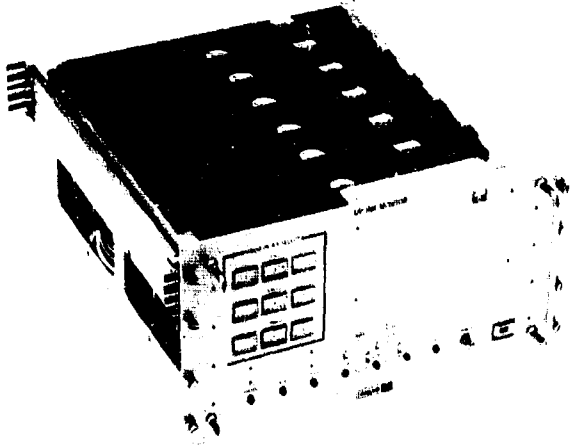


Figure 5-50 Uplink Monitor

1418-67W

5.2 EQUIPMENT ARRANGEMENT

The following paragraphs in this section describe the physical configuration of the SGLS equipment and illustrate the equipment arrangement at the remote tracking stations (RTS). Pointed out is the high degree of commonality among the 10 installations as well as the inevitable differences caused by variations in existing station geography and the differing requirements for the low-gain (Prelort) and high-gain (TT&C) installations.

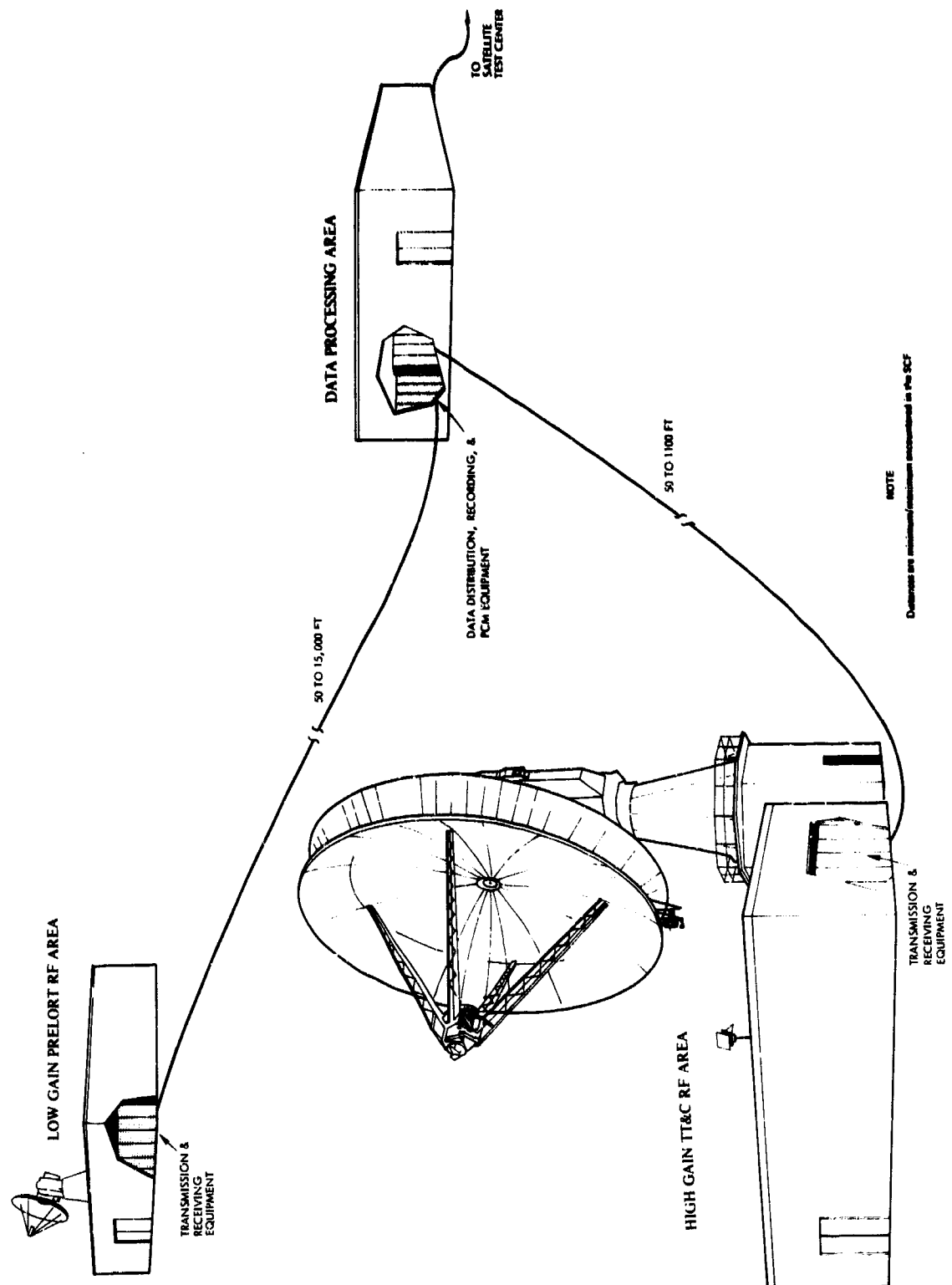
Figure 5-51 is a conceptual view of a dual RTS, showing the general relationship of the two SGLS ground stations to the existing RTS and the range of distances separating them.

To minimize installation, training, operation and maintenance, and documentation requirements, the SGLS installations at the 10 RTS's were designed as nearly carbon copies from the standpoint of rack makeup and room arrangement of the SGLS equipment. Certain multiple standards of rack makeup and equipment arrangement are created by requirements peculiar to the high-gain TT&C antenna (as against those of the low-gain Prelort antenna) and by requirements peculiar to a compact site where all equipment is necessarily close together (as opposed to a scattered site where the antenna may be located miles from the data processing area). The results of these multiple standards are illustrated and described in the following paragraphs.

A typical low-gain (Prelort) SGLS installation consists of 22 racks of equipment, odd-size units for the transmitter, and equipment items that install in other equipment or on the walls and ceilings of buildings. A typical high-gain (TT&C) SGLS installation is similar, with certain items installed on the antenna instead of in racks. The sequence of the racks is the same at all sites as one proceeds from one end of a row of SGLS racks to the other.

5.2.1 Equipment in the RF Area

SGLS equipment in the RF area at stations equipped with the Prelort antenna is typically arranged as shown in the floor plan (Figure 5-52) where the SGLS equipment (shaded) is shown with other RTS equipment.



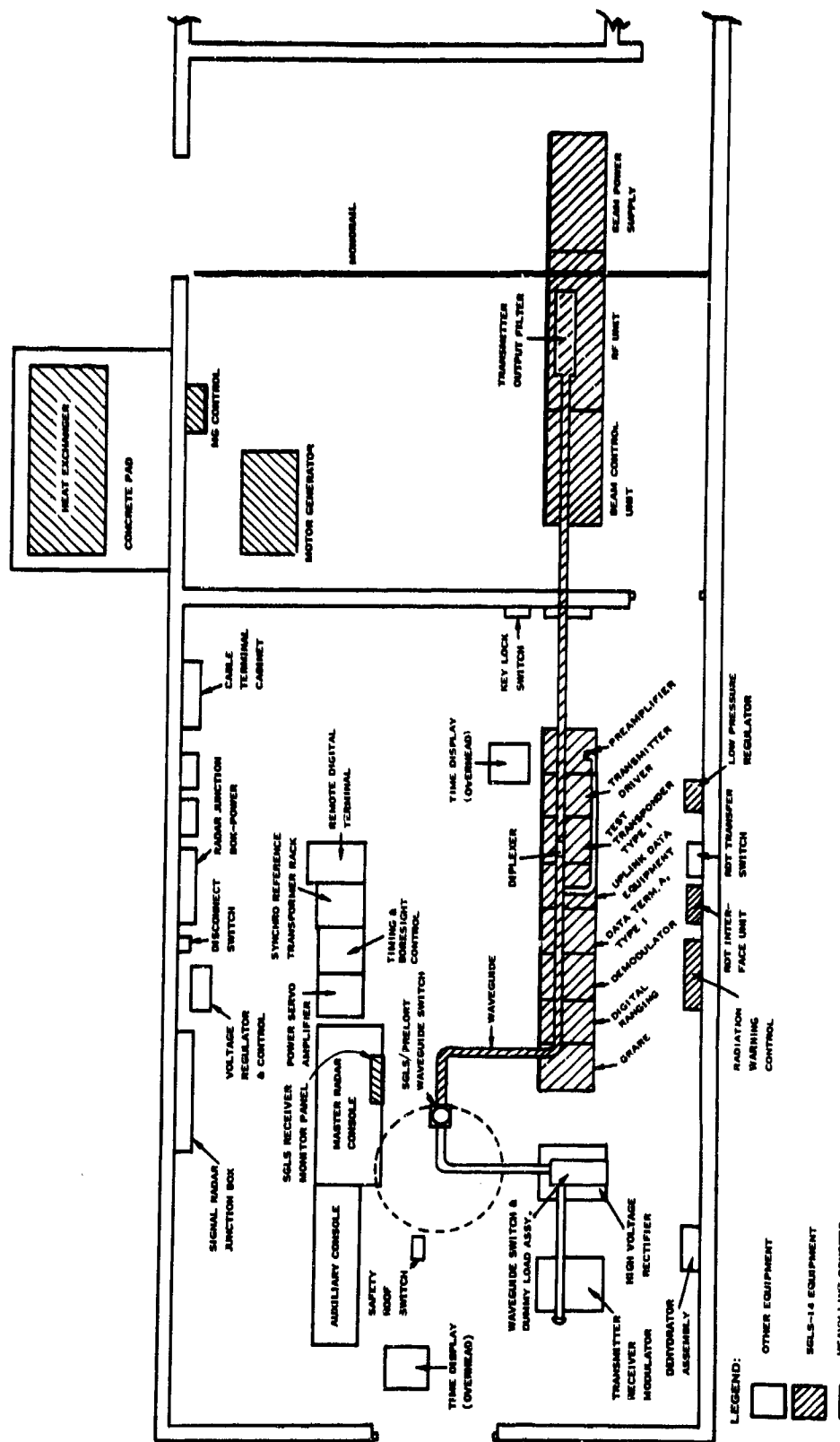


Figure 5-52 Typical Arrangement of Equipment in the RF Areas

Positions of wall-mounted and ceiling-mounted items, plus the heat exchanger outside the building, are indicated along with racks and consoles. The SGLS antenna panel shown in the Prelort console has been exaggerated to identify it as SGLS.

The following photographs illustrate these equipment items and show the palletizing that was employed to simplify installation in the field.

Low-power equipment racks are illustrated in Figures 5-53 and 5-54, and the high-power transmitter equipment is shown in Figure 5-55.

The spectral filter for the transmitter mounts atop the transmitter RF unit (Figure 5-55) and the diplexer is ceiling mounted. Both are shown in Figure 5-56. The RDT status interface unit and the radiation warning control equipment are wall mounted (Figure 5-57).

The four control and display panels are illustrated in Figure 5-58. The SOC panel installs in the data processing area and the other three panels install in the RF equipment area.

5.2.2 Equipment in the Data Processing Area

The equipment in the data processing area is the same type for either a high-gain (TT&C) or a low-gain (Prelort) installation. A typical floor plan, showing the SGLS equipment (shaded) with other RTS equipment, is given in Figure 5-59. Note that a second set of SGLS equipment (not shaded) is included in the floor plan as it might be arranged at a dual station.

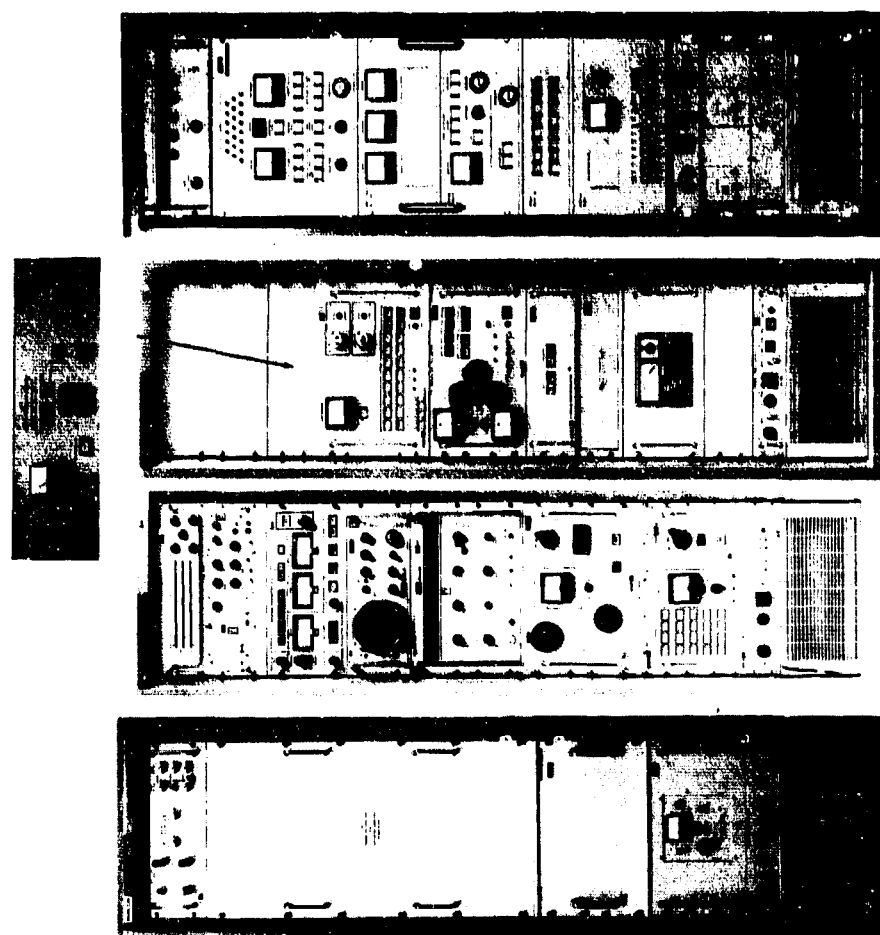
The PCM equipment, the only five-rack pallet in SGLS, is shown in Figure 5-60 in an open-door condition; the switching and recording racks are shown in Figure 5-61.

The data terminal and downlink racks are illustrated in Figure 5-62.

Since the COMSEC equipment items are classified, they are illustrated in their normal closed-door condition in Figure 5-63.

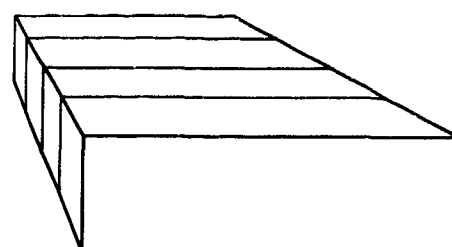
- Installed in RF equipment area
- Arranged in 1- and 2-rack pallets as illustrated
- Each rack 24 inches wide, 28 inches deep, 83 inches high

RF EQUIPMENT



PREAMPLIFIER TRANSMITTER TEST TRANSPONDER GRADE
DRIVER TYPE 1

FIGURE 5-53



- Installed in RF equipment area
- Arranged in a 4-rack pallet
- Each rack 24 inches wide, 28 inches deep, 83 inches high

DATA TRANSMISSION AND MODULATION EQUIPMENT

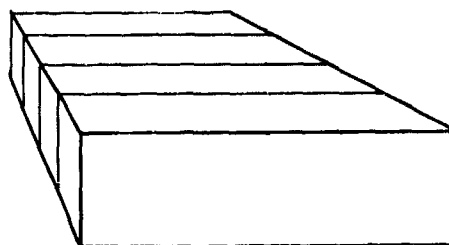
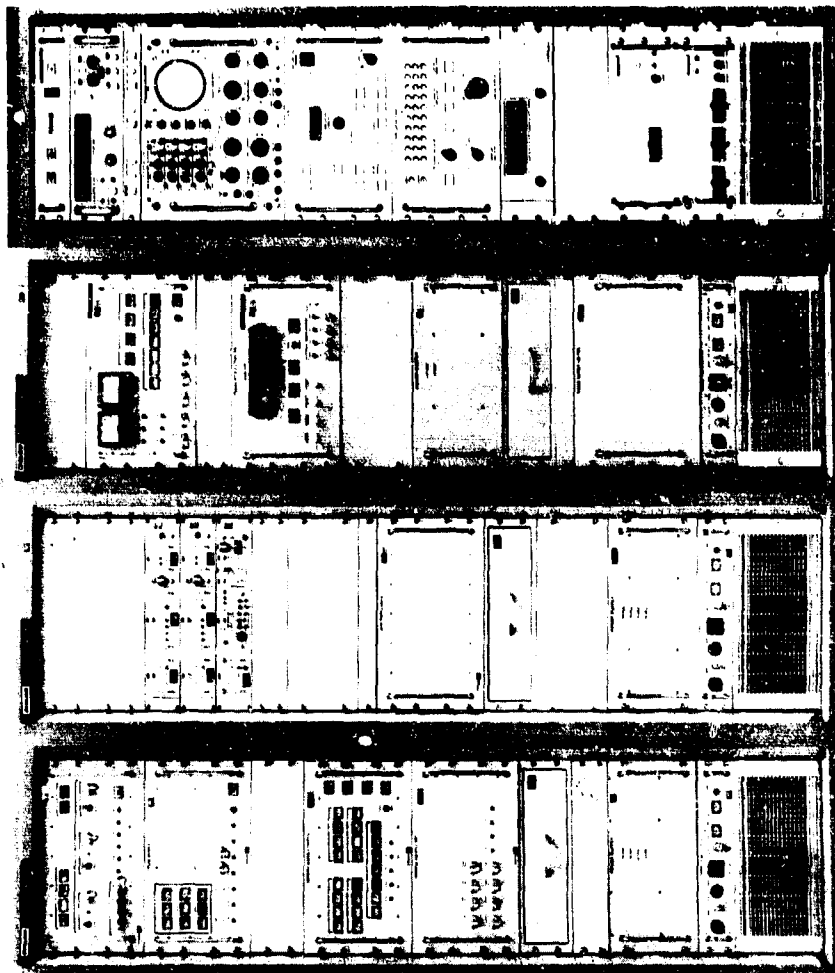
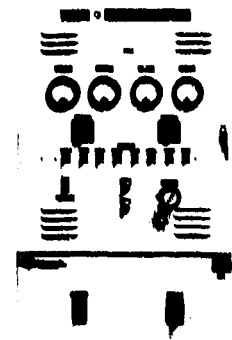


FIGURE 5-54

UPLINK DATA TERMINAL A, DEMODULATOR DIGITAL RANGING EQUIPMENT TYPE 1

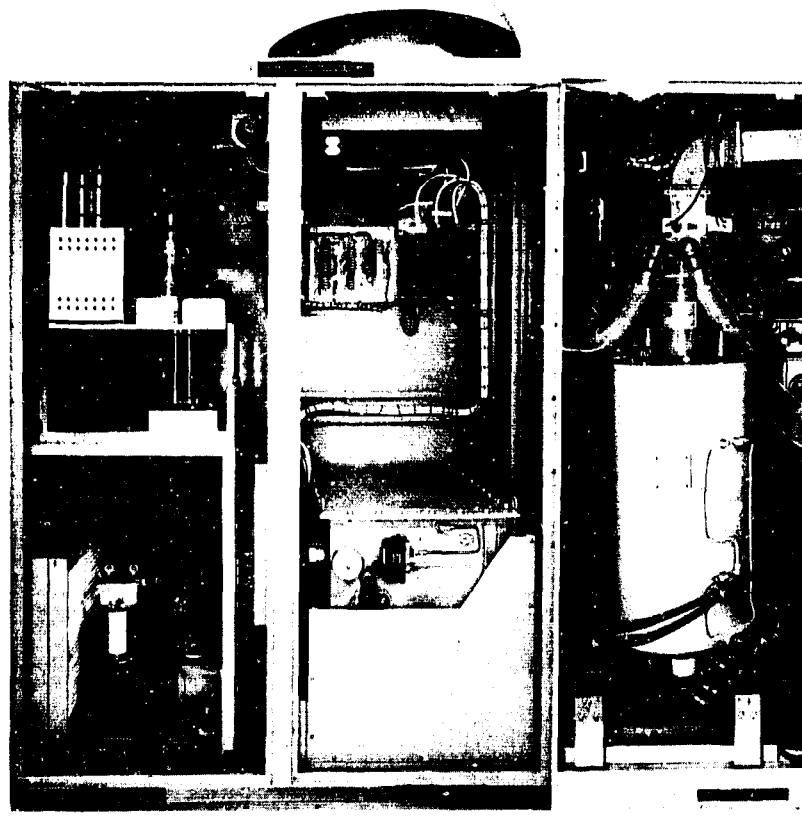
10-kW WIDEBAND GROUND TRANSMITTER

- Installed in antenna area
- Dimensions are shown beneath respective figures



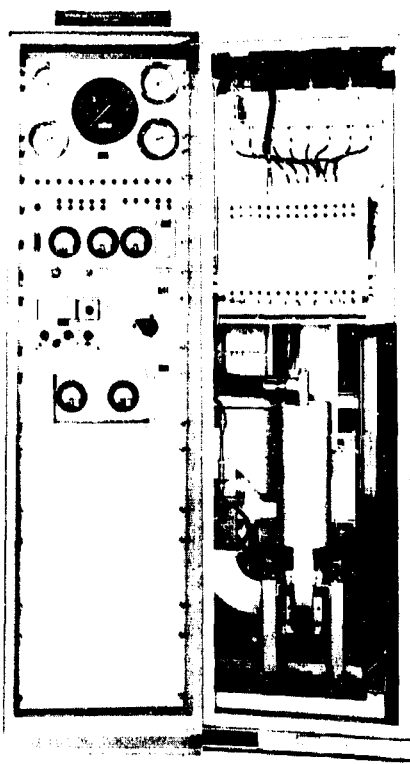
MOTOR GENERATOR CONTROL

(32 inches wide, 17 inches deep, 64 inches high)



HIGH VOLTAGE POWER SUPPLY

(64 inches wide, 36 inches deep, 86 inches high)



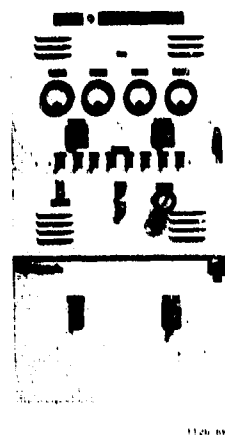
RF UNIT

(84 inches wide, 36 inches deep, 86 inches high)

BEAM

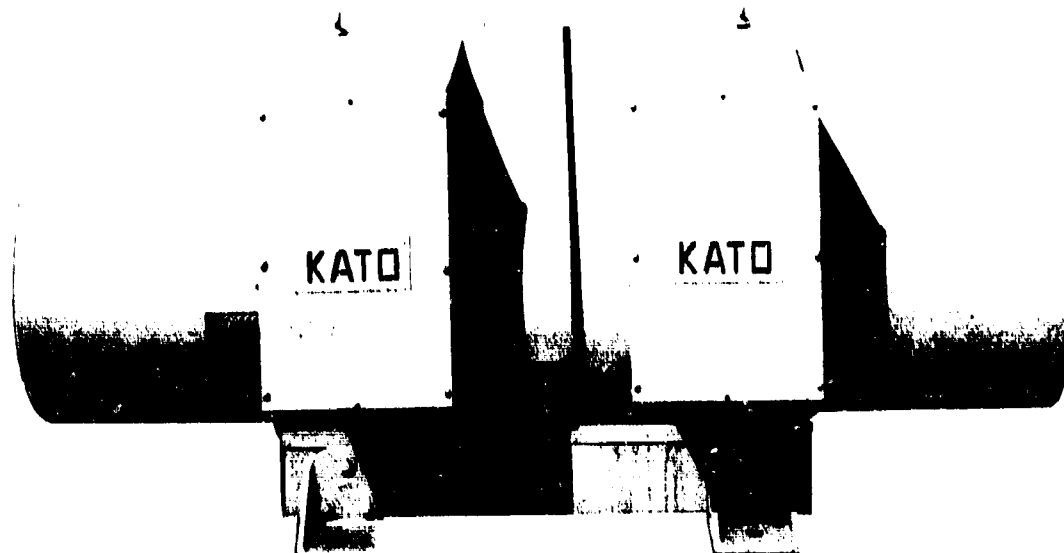
(64 inches wide, 36 inches deep, 86 inches high)

FIGURE 5-55



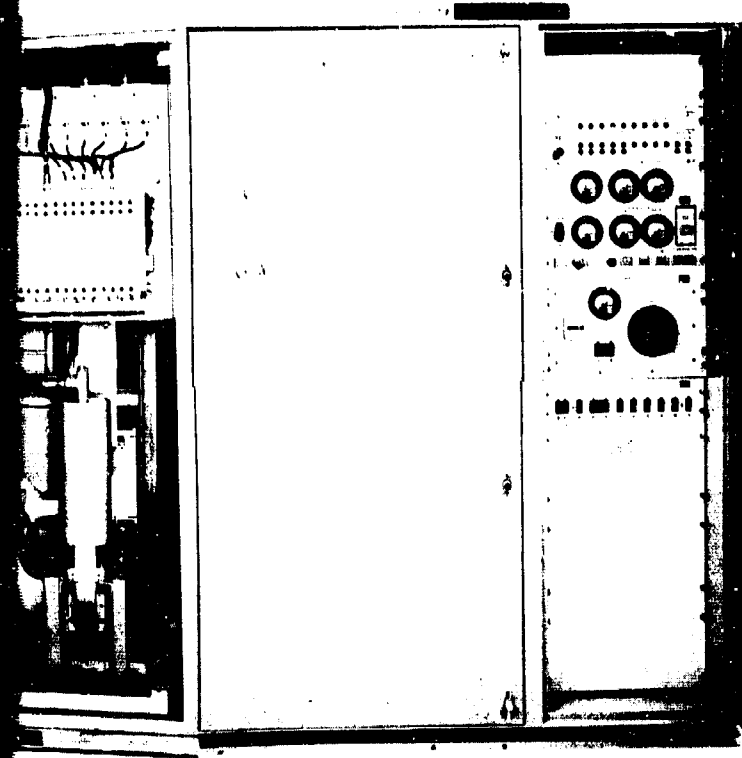
GENERATOR CONTROL

(17 inches deep, 64 inches high)



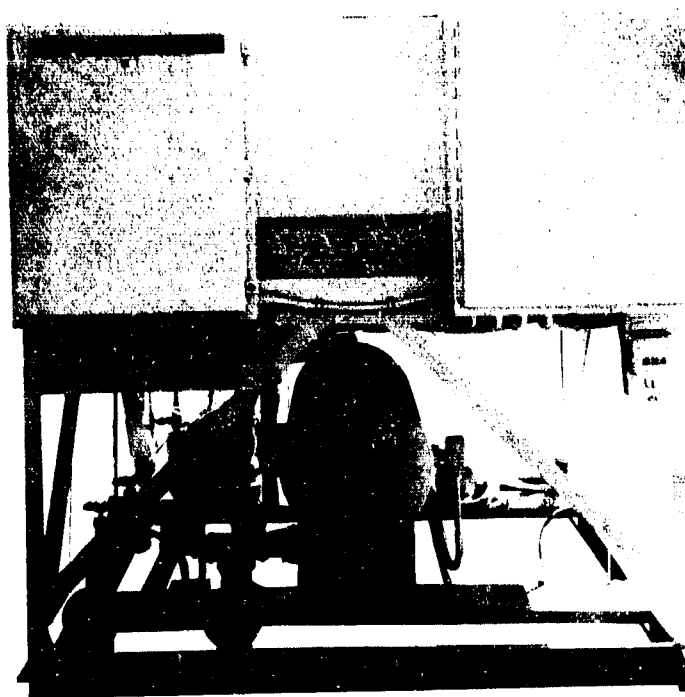
MOTOR GENERATOR

(43 inches wide, 77 inches deep, 37 inches high)



BEAM CONTROL UNIT

(ches high) (64 inches wide, 36 inches deep, 86 inches high)



HEAT EXCHANGER

(69 inches wide, 114 inches deep, 77 inches high)

FIGURE 5-55

5-43/5-44

- Installed in RF equipment area
- RF FILTER, DIPLEXER • Arranged as described in text
- Dimensions are shown beneath respective figures

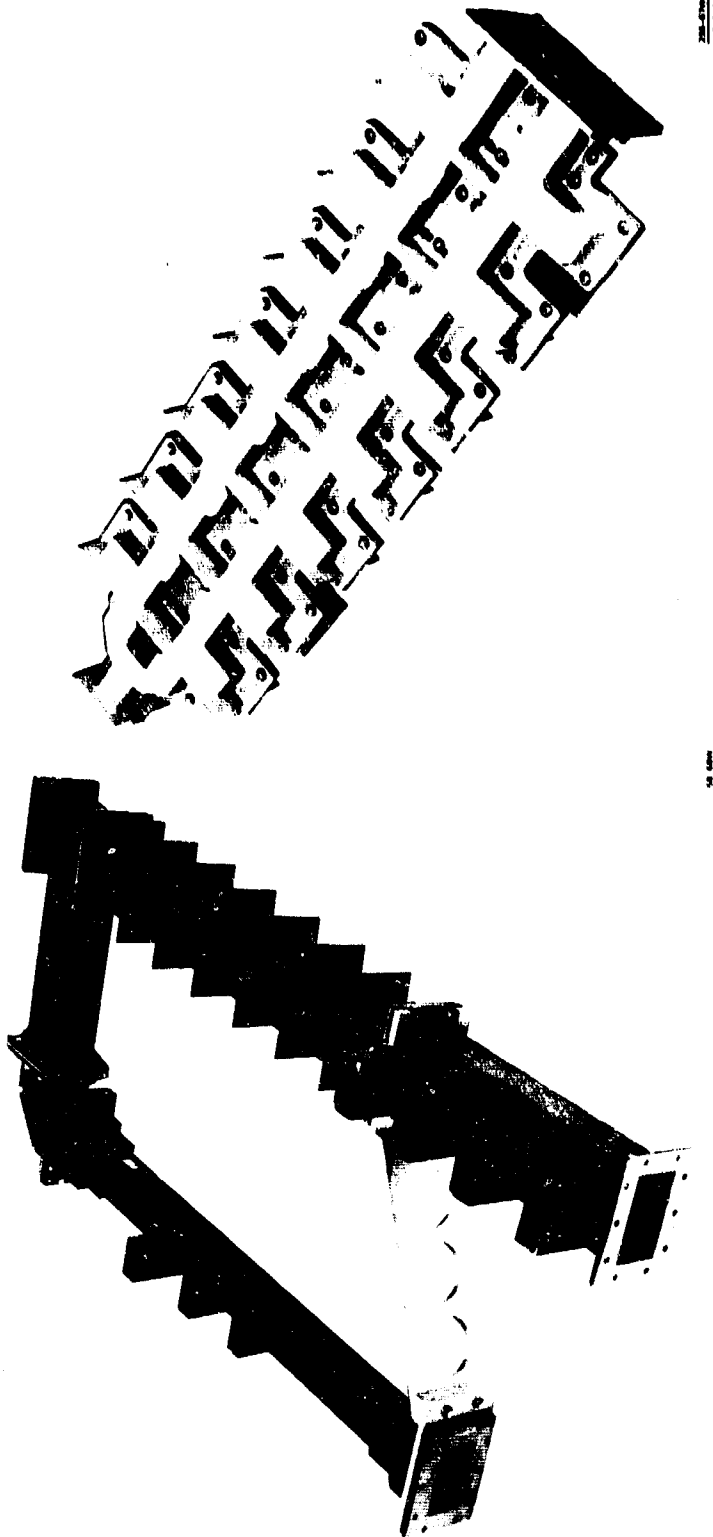
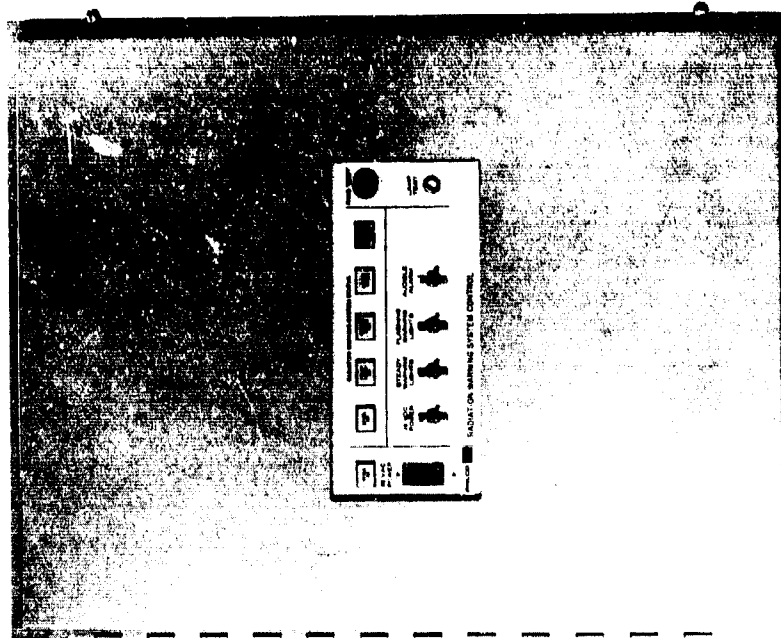


FIGURE 5-56

5-45

- Installed RF equipment area
- Arranged in 2 cabinets and dimensioned as shown beneath respective figures

WALL-MOUNTED EQUIPMENT



RWS CONTROL UNIT

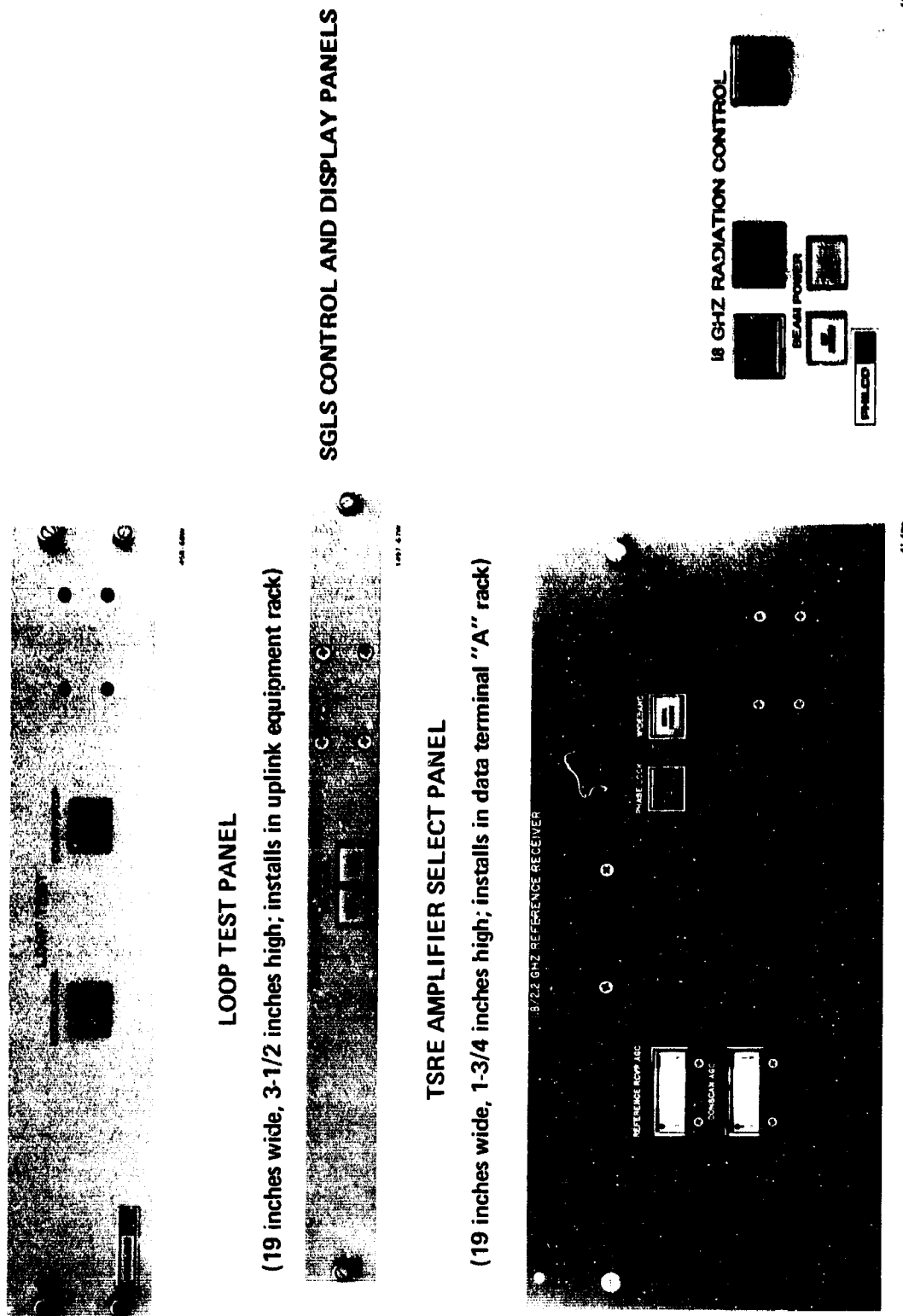
(24 inches wide, 10 inches deep, 30 inches high)



RDT STATUS INTERFACE UNIT

(16 inches wide, 10 inches deep, 20 inches high)

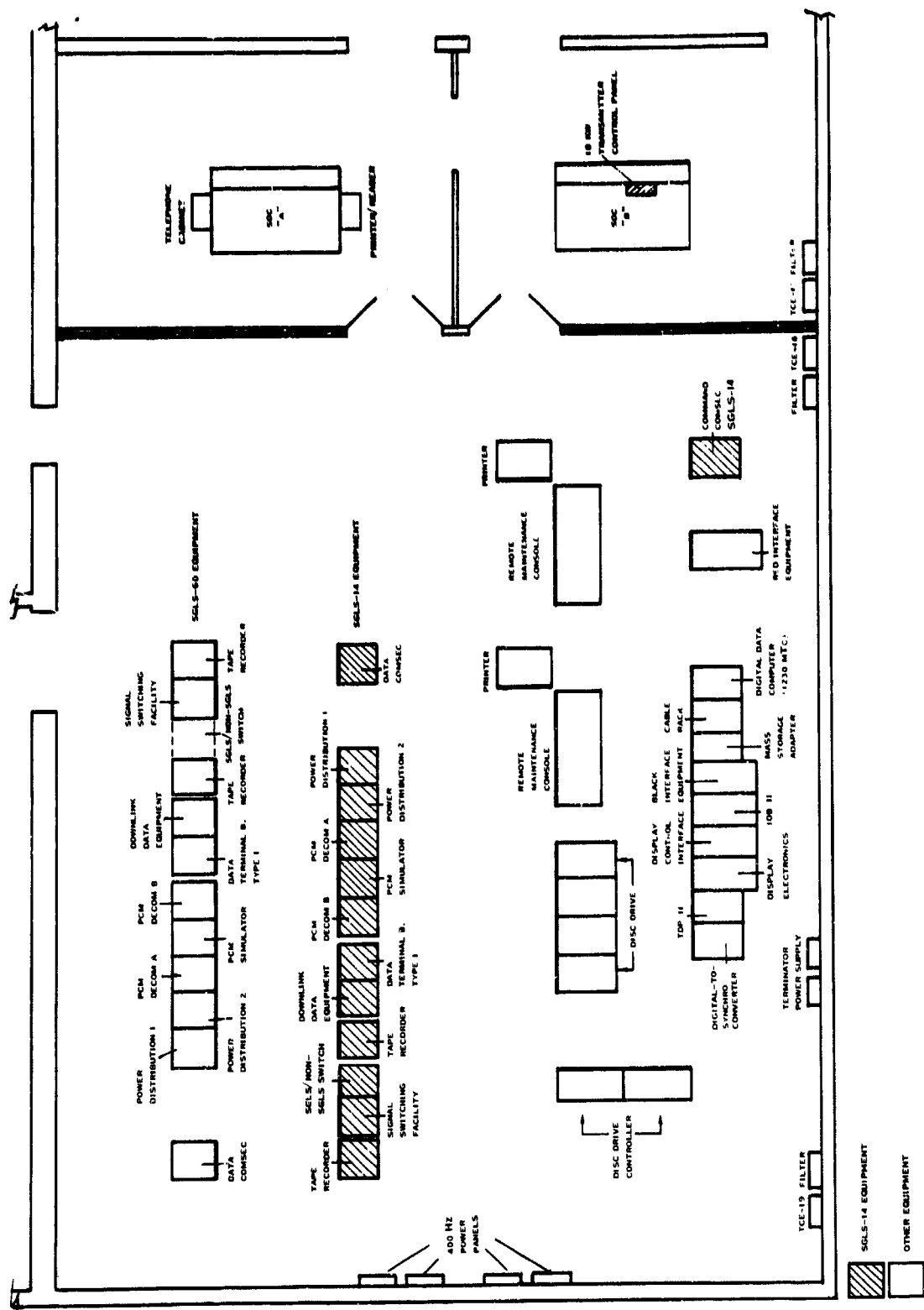
FIGURE 5-57



(9-1/2 inches wide, 7 inches high; installs in antenna control console)

FIGURE 5-58

WDL-TR3227-1
Volume I, Part 1



5-48



WDL Division

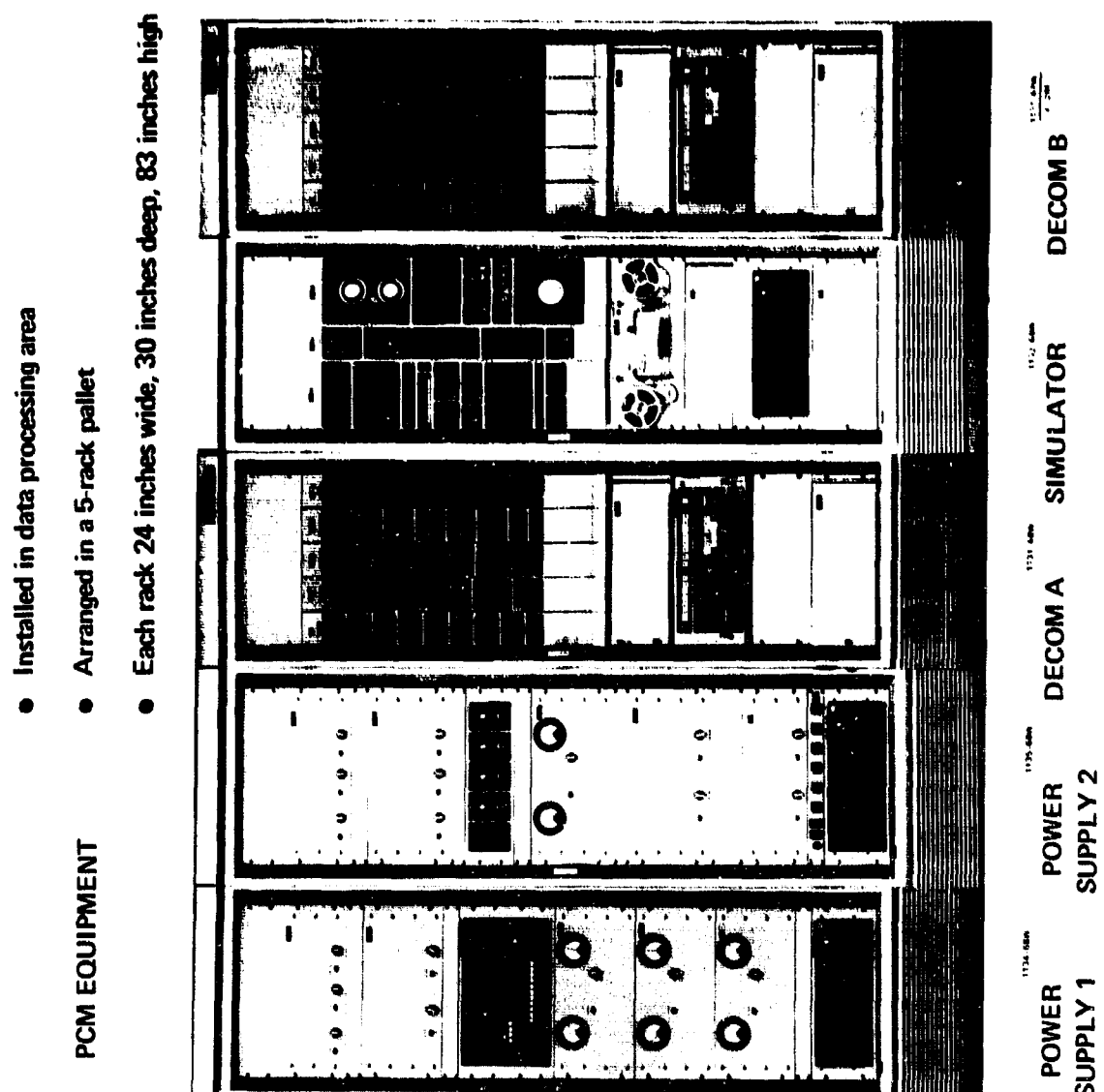
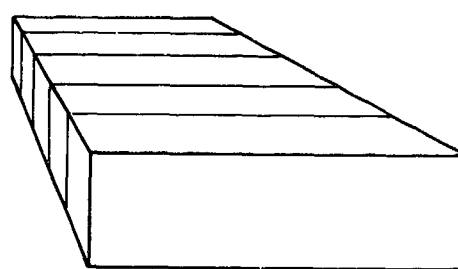


FIGURE 5-60



5-49

- Installed in data processing area

SWITCHING AND RECORDING EQUIPMENT

- Arranged in a 4-rack pallet

- Each rack 24 inches wide, 28 inches deep, 83 inches high or 77 inches high

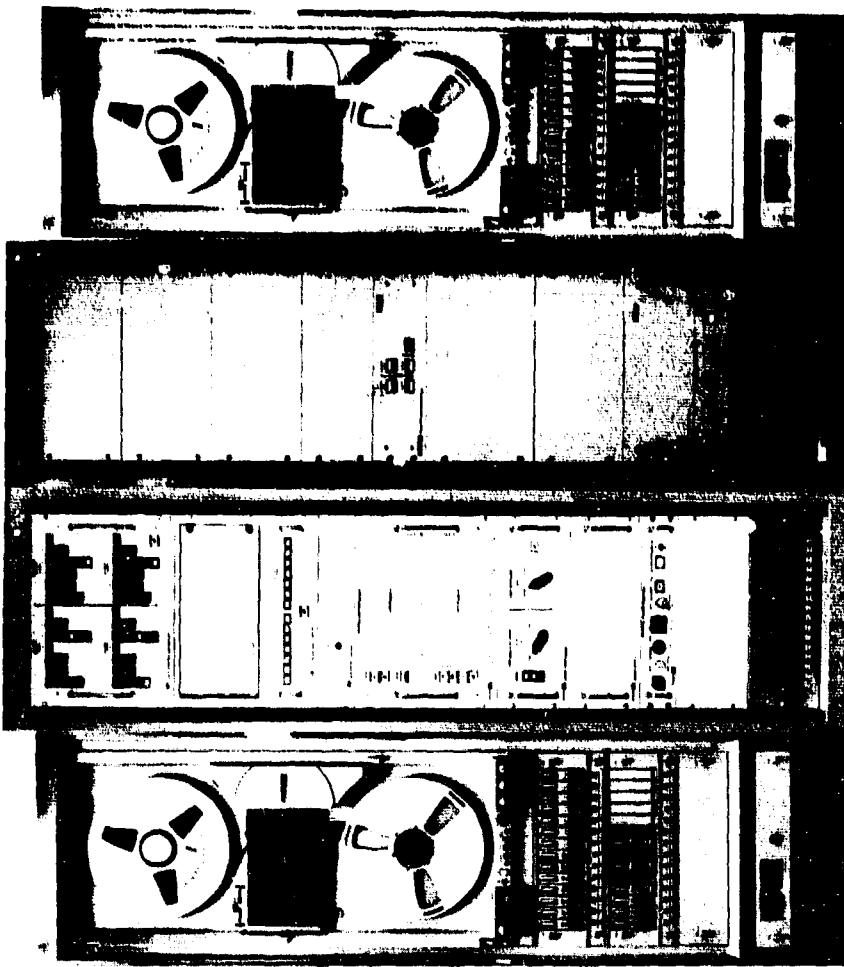
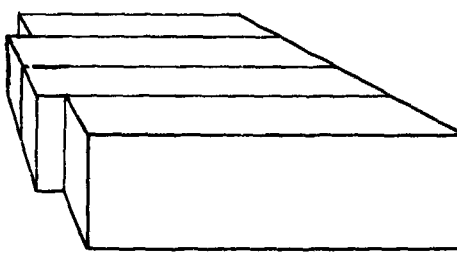


FIGURE 5-61

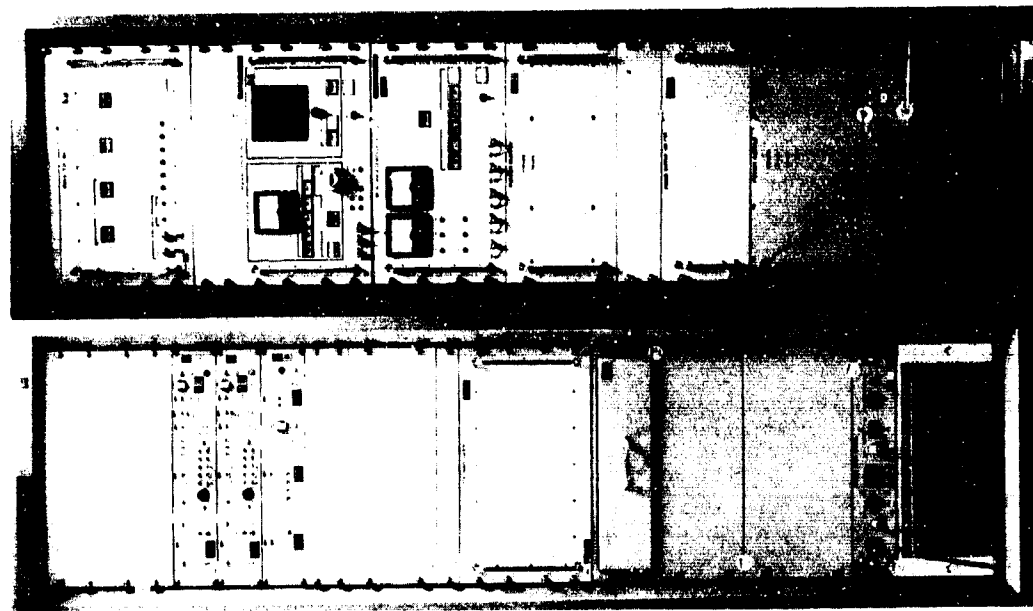
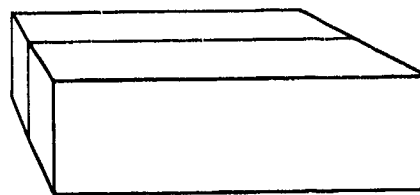
FR1600 SGLS/NON-SGLS SIGNAL FR1600
SWITCH SWITCHING FACILITY



5-50

DATA TERMINAL AND DOWNLINK EQUIPMENT

- Installed in data processing area
- Arranged in a 2-rack pallet
- Each rack 24 inches wide, 28 inches deep, 83 inches high



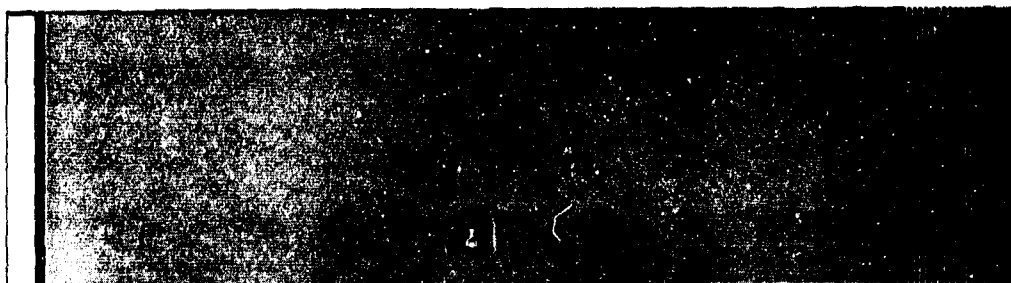
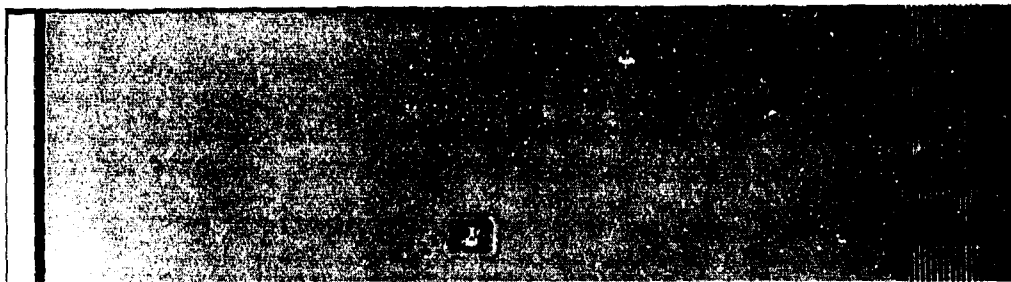
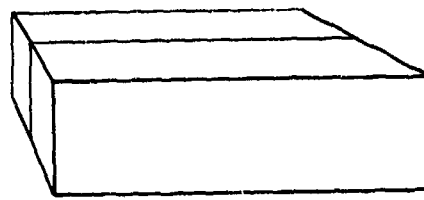
DATA TERMINAL B
DOWNLINK
EQUIPMENT

FIGURE 5-62

5-51

COMSEC EQUIPMENT

- Installed in data processing area
- Arranged in 2 single-rack pallets
- Each rack 24 inches wide, 28 inches deep, 83 inches high



1122-4000
1122-5000
COMMAND COMSEC DATA COMSEC

FIGURE 5-63

5-52

5.2.3 Equipment Peculiar to the High-Gain (TT&C) Installation

The equipment arrangement for a high-gain (TT&C) installation is largely the same as for the low-gain (Prelort) illustrated in Paragraph 5.2.1. All equipment in the data processing area is the same for both configurations. The floor plan for the RF equipment area is also the same except that there is no preamplifier rack (Figure 5-52) in a high-gain installation. The 2-GHz parametric amplifier and the GRARE RF front end (down-converter) from the preamp rack are mounted on the antenna to minimize S-band cable runs. These items are shown in Figure 5-64 along with the selective filter (which replaces the diplexer used in the low-gain configuration), the 2-GHz vertex horn, and the 2-GHz noise source.

The test transponder rack (Figure 5-65) also differs from that for the low-gain configuration (Figure 5-53): the parametric amplifier control panel is omitted and a different set of noise-figure test equipment substituted. The parametric amplifier control panel (Figure 5-65) is mounted in an existing non-SGLS rack at the station.

The high-gain (TT&C) peculiar transmitting filter shown in Figure 5-66 (with waveguide) replaces the spectral filter used with the low-gain (Prelort) configuration. This filter also mounts on top of the 10-kW transmitter RF unit (Figure 5-55).

5.2.4 Data Terminal Types 1 and 2

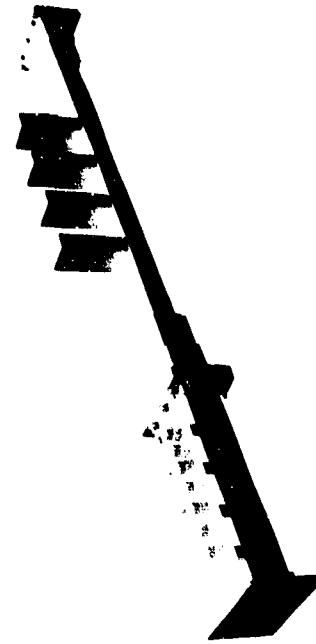
Data terminal type 1 (Figures 5-36 and 5-54) is used at sites where the antenna area is more than 500 ft from the data processing area. At the more compact sites, where some data can be transmitted directly by cable line without amplification, data terminal type 2 is used. These racks are the same as type 1 racks, except that the three wideband video units are omitted from the upper part of the rack, and are replaced with blank panels.

5.2.5 Other Equipment

SGLS equipment not included in the foregoing illustrations includes RF attenuators, a 2-GHz boresight horn, a low-pressure regulator for maintaining air pressure in the waveguide, and installation material, such as waveguides and cables.

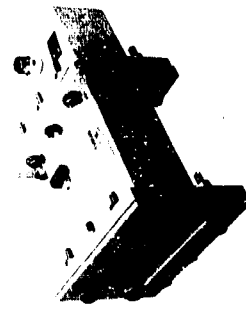
ANTENNA-MOUNTED EQUIPMENT – SGLS-60

- Arranged as described in text
- Dimensions are shown beneath figures



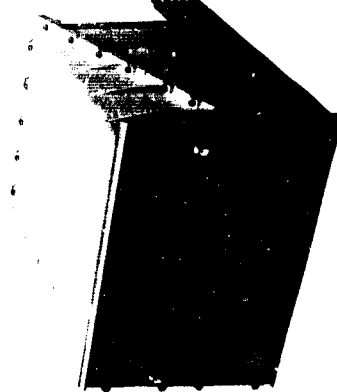
SELECTIVE FILTER

(4.2 inches high, 6.3 inches wide, 56.2 inches long)



2-GHz VERTEX HORN

(4.1 inches high, 6.3 inches wide, 10.4 inches long)



2-GHz PARAMETRIC AMPLIFIER

(32-15/16 inches wide, 20 inches deep, 16-15/16 inches high)

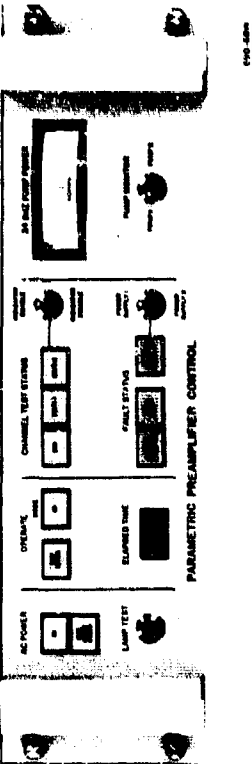
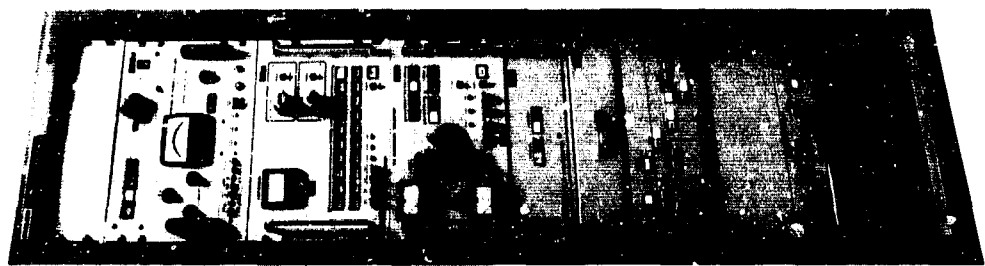
GRARE RF FRONT END

(19 inches wide, 21 inches deep, 15.5 inches high)

FIGURE 5-64

TEST TRANSPONDER AND NOISE FIGURE TEST EQUIPMENT – SGSS-60

- Both install in antenna area
- Noise source installs on the 60-foot TT&C antenna



PARAMETRIC AMPLIFIER CONTROL PANEL

(19 inches wide, 9 1/4 inches deep, 5 1/4 inches high)

TEST TRANSPONDER RACK, TYPE 2
(24 inches wide, 28 inches deep, 84 inches high)

FIGURE 5-65

TRANSMITTING FILTER FOR SGLS-60

- Installs atop 10kW RF unit in RF Equipment area
- Dimensions are 4.2 inches high, 6.2 inches wide, 50.5 inches long

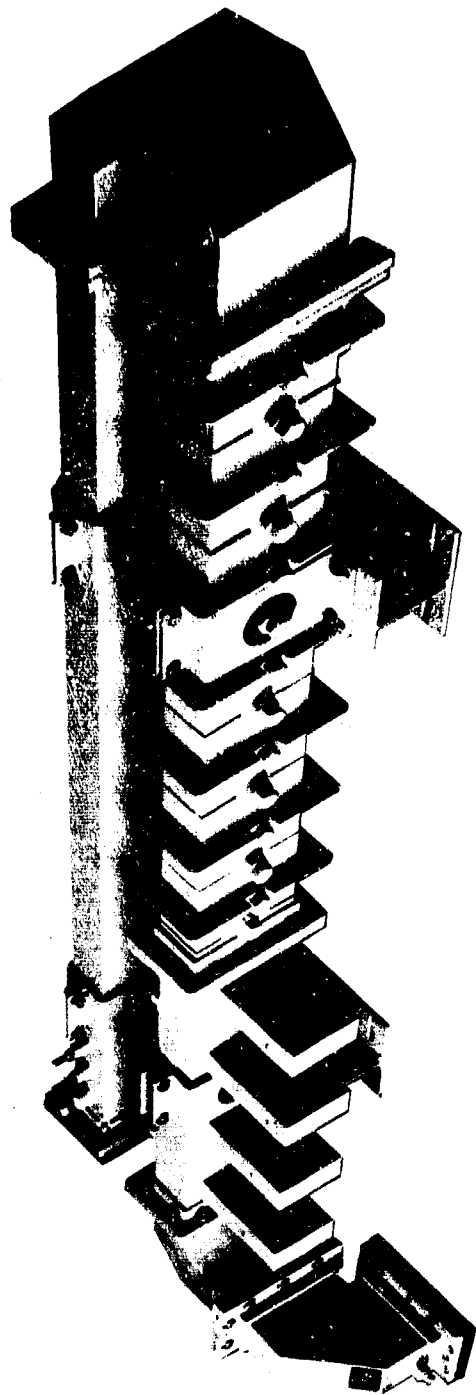


FIGURE 5-66

5-56

5.3 TEST CAPABILITY

Included in the SGLS ground system are test equipment items required for configuration, operation, and monitoring of the system. In addition to system tests, the test equipment can be used for preventive and nonscheduled maintenance.

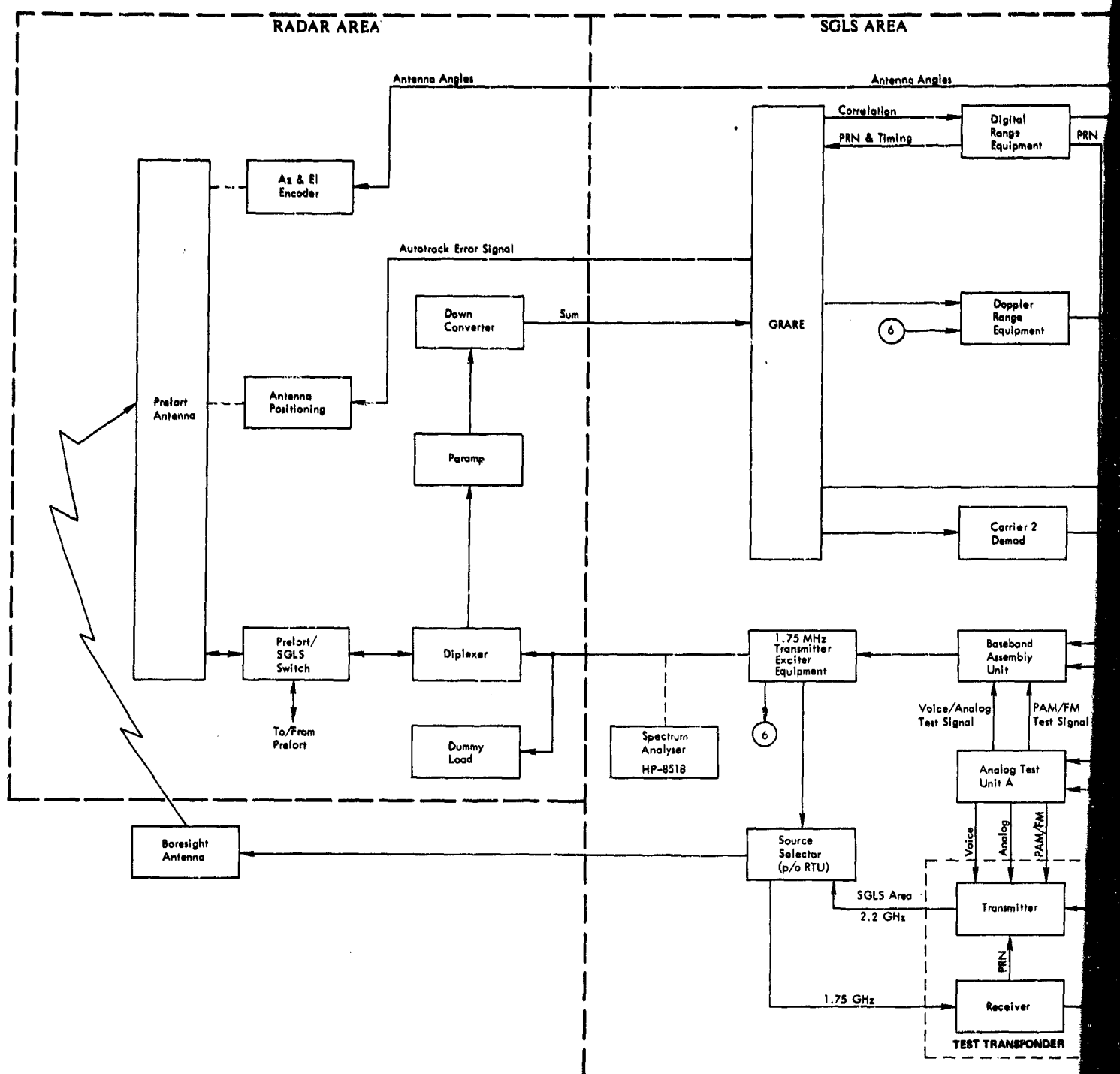
The SGLS test equipment items are as follows:

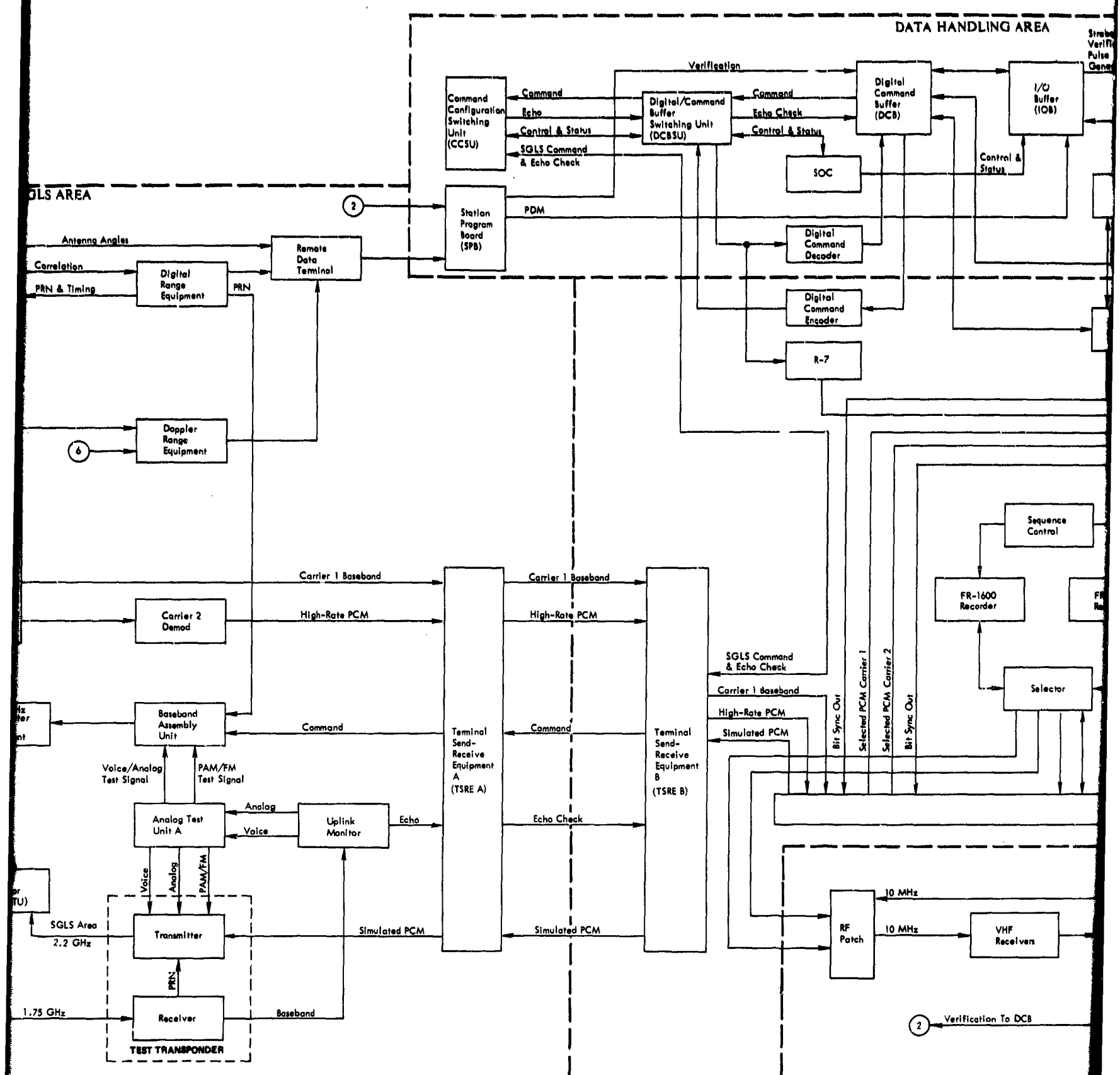
- RF Sweep Generator
- Spectrum Analyzer
- Test Transponder Receiver
- Test Transponder Transmitter
- RF Power Meter
- Receiver Noise Power Test Set (High-Gain Only)
- Analog Test Unit A
- Uplink Monitor
- Loop Test Panel
- Oscilloscope
- Universal Counter-Timer
- PCM Simulator
- Echo Check/Receiver Test Control Unit (High-Gain Only)
- Analog Test Unit B
- Receiver Test Unit (Low-Gain Only)
- Noise Generator
- COMSEC Loop Check Equipment

5.3.1 System Checkout

SGLS ground station checkout is performed with self-contained test equipment that is used for any system configuration.

A complete loop test configuration is used to verify system performance characteristics and station readiness. Typical low-gain and high-gain SGLS ground systems and associated RTS equipment items are shown in Figures 5-67 and 5-68, respectively. The primary difference between the two configurations is the method used





2

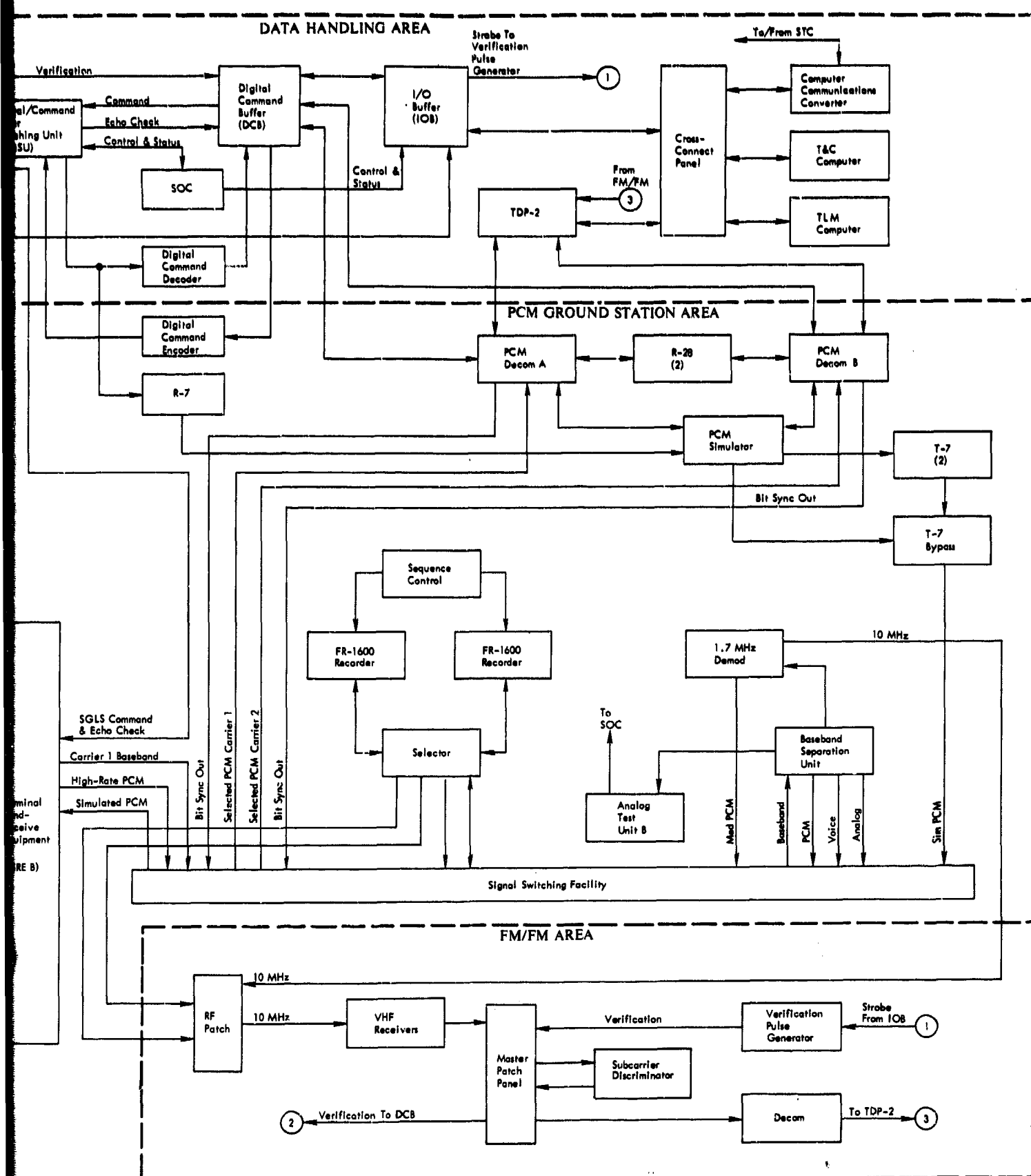
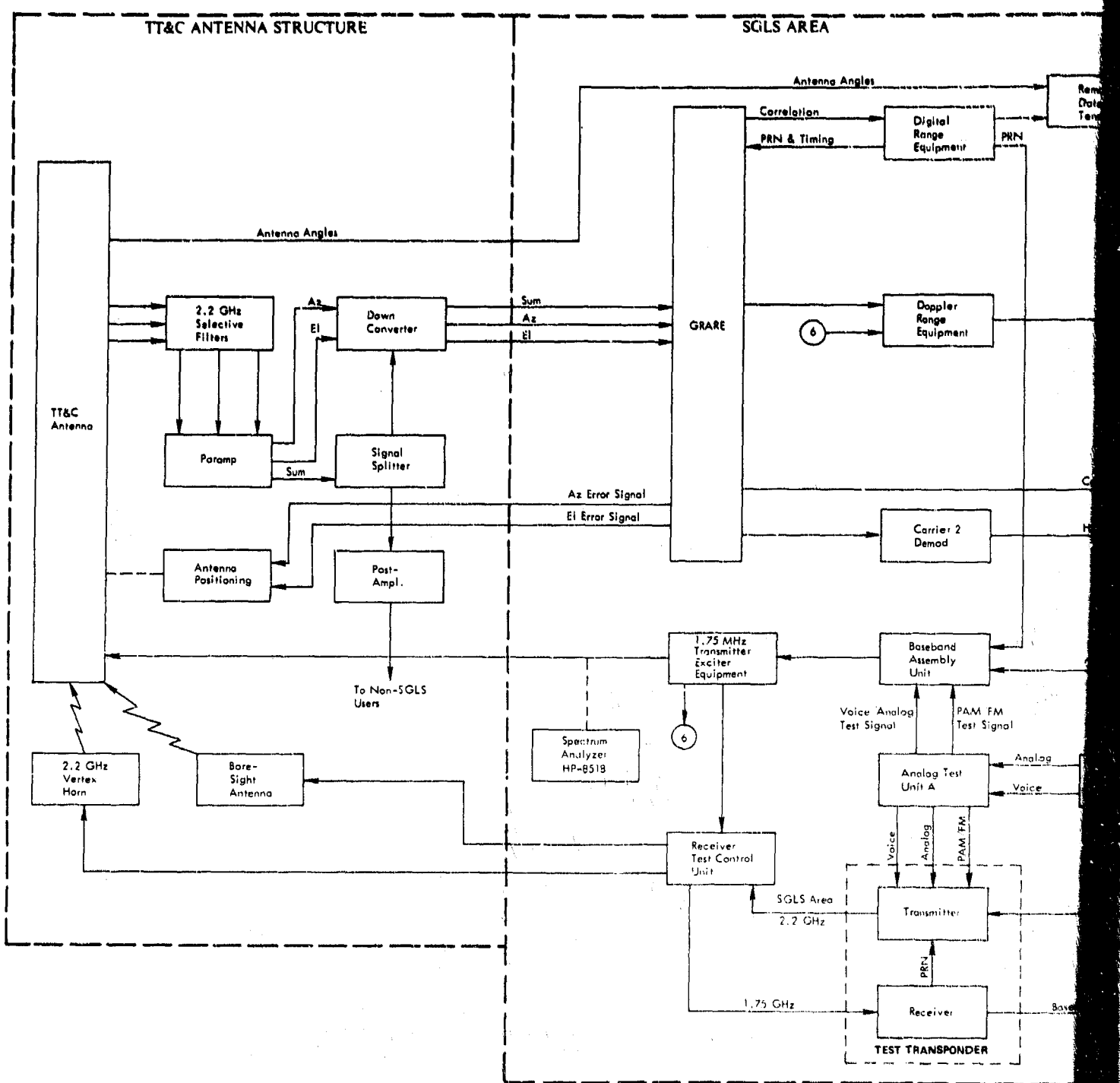
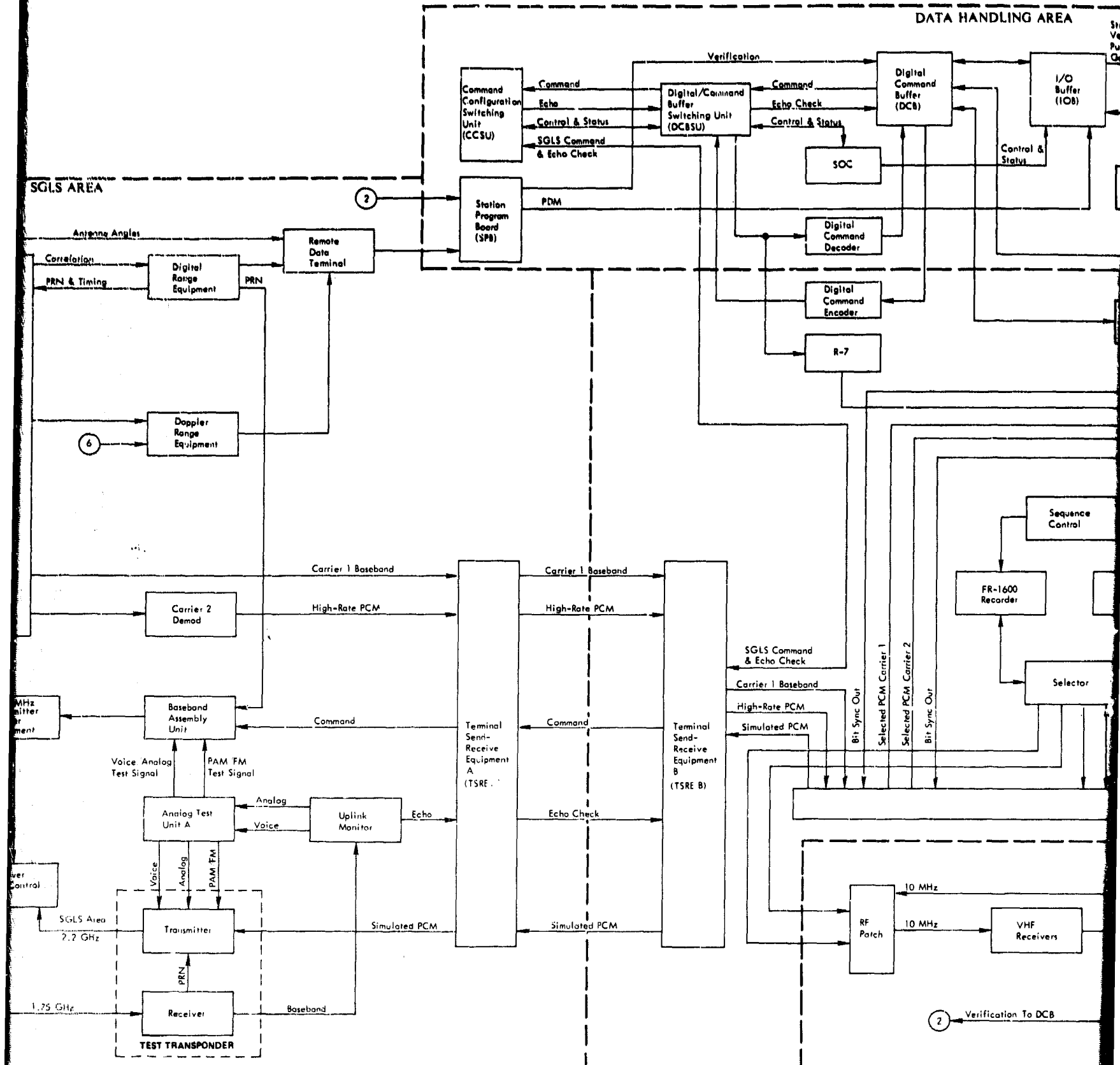


Figure 5-67 Typical SGLS Low-Gain Configuration





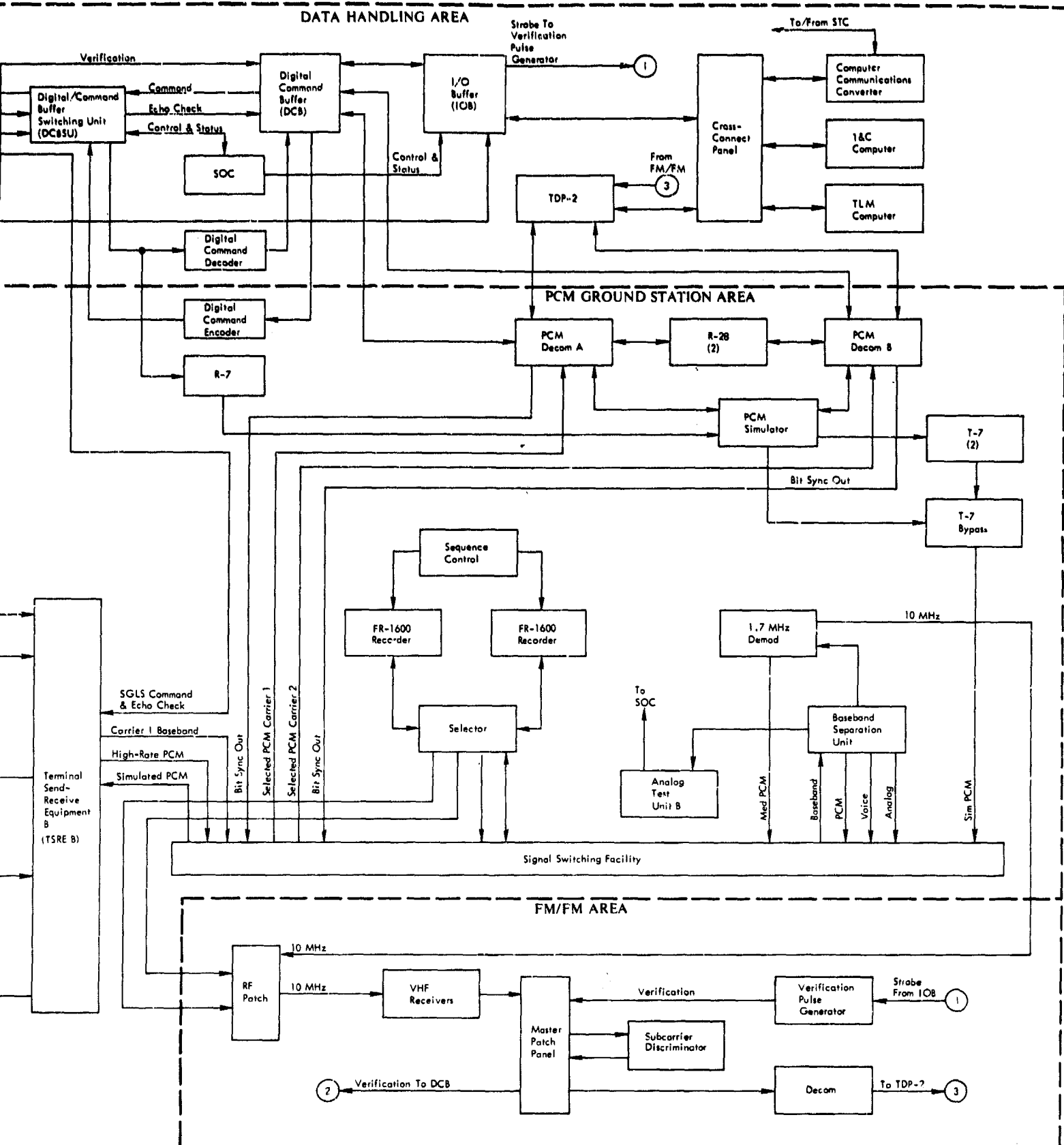


Figure 5-68 Typical SGLS High-Gain Configuration

in developing error signals for antenna positioning for either a conical-scan or monopulse antenna system. The SGLS system loop test described herein is referenced to figures showing the high-gain system but also applies to the SGLS system using the low-gain antenna.

System loop tests are accomplished with the test transponder and analog test units. The test transponder comprises a receiver and transmitter designed to simulate the vehicle receiver, transmitter, and baseband assembly unit. The test transponder receives uplink transmission on the operational channel, extracts the range code, adds simulated PCM signals, and coherently sends a test signal to the ground station at the operational frequency. The downlink test signal contains the range code, the simulated PCM signal, and test tones simulating the voice and analog telemetry channels. The test tones are processed by the ground station (in the same manner as spacecraft signals are) to provide data readouts to determine station readiness. The test transponder also has provisions for power adjustments to simulate marginal link conditions.

In the high-gain configuration, the simulated downlink signals can be transmitted from the boresight tower or the vertex horn. In the low-gain configuration, test signals may be transmitted from the boresight tower or injected into the parametric amplifier or down-converter from the receiver test unit.

In addition to providing test tones for all the services, analog test units A and B evaluate the received test signals.

In the test loop configuration, the tracking, uplink, and downlink functions of the SGLS ground station can be verified. Details of the testing of the specific functions in the loop test configuration are given in the following paragraphs.

Tracking. Testing of the tracking and ranging functions is accomplished with the test transponder transmitter signal radiated from the boresight tower, as shown in Figure 5-69. In the coherent mode of operation, an attenuated sample of the uplink carrier from the transmitter power amplifier is fed into the test transponder receiver. The test transponder receiver locks onto the uplink carrier and produces a coherent

VCO output that is applied as a coherent drive to the Carrier 1 modulator multiplier in the test transponder transmitter. In addition to the coherent mode of operation, a front panel control on the test transponder permits manual frequency adjustment of the carrier.

During system test, the tracking loop test provides a method for verifying combined antenna and SGLS receiver tracking capability for acquisition and autotracking. Test transponder power output adjustment is provided for use in measuring system tracking thresholds.

Ranging loop operation is also verified with the same test configuration as that used for tracking test. The PRN range code signal from the digital ranging equipment is fed through the baseband assembly unit to modulate the uplink carrier. Proper operation is verified by a stable display of the site-peculiar octal range readout.

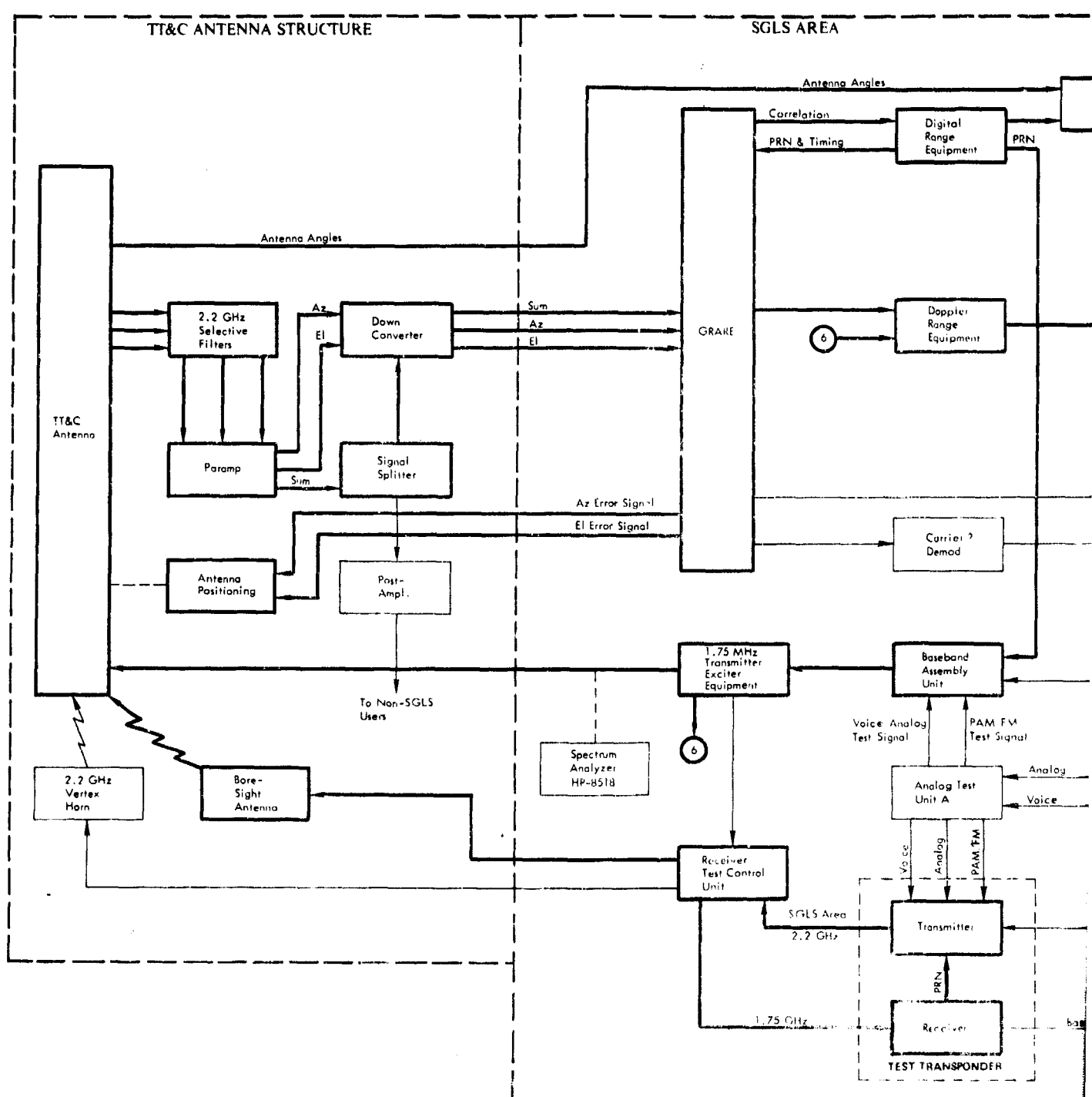
Range rate data is obtained from the range/range rate loop signal by the range rate extractor and proper operation verified by stable (zero) range rate display.

Uplink. Uplink test instrumentation provides for verification of the SGLS uplink during system closed loop test. The test configuration and instrumentation is shown in Figure 5-70. The spectrum analyzer displays the uplink spectrum for verification of frequency, modulation indices, and presence of baseband.

System closed loop testing of the SGLS uplink is accomplished with the test transponder receiver, analog test unit A, and uplink monitor.

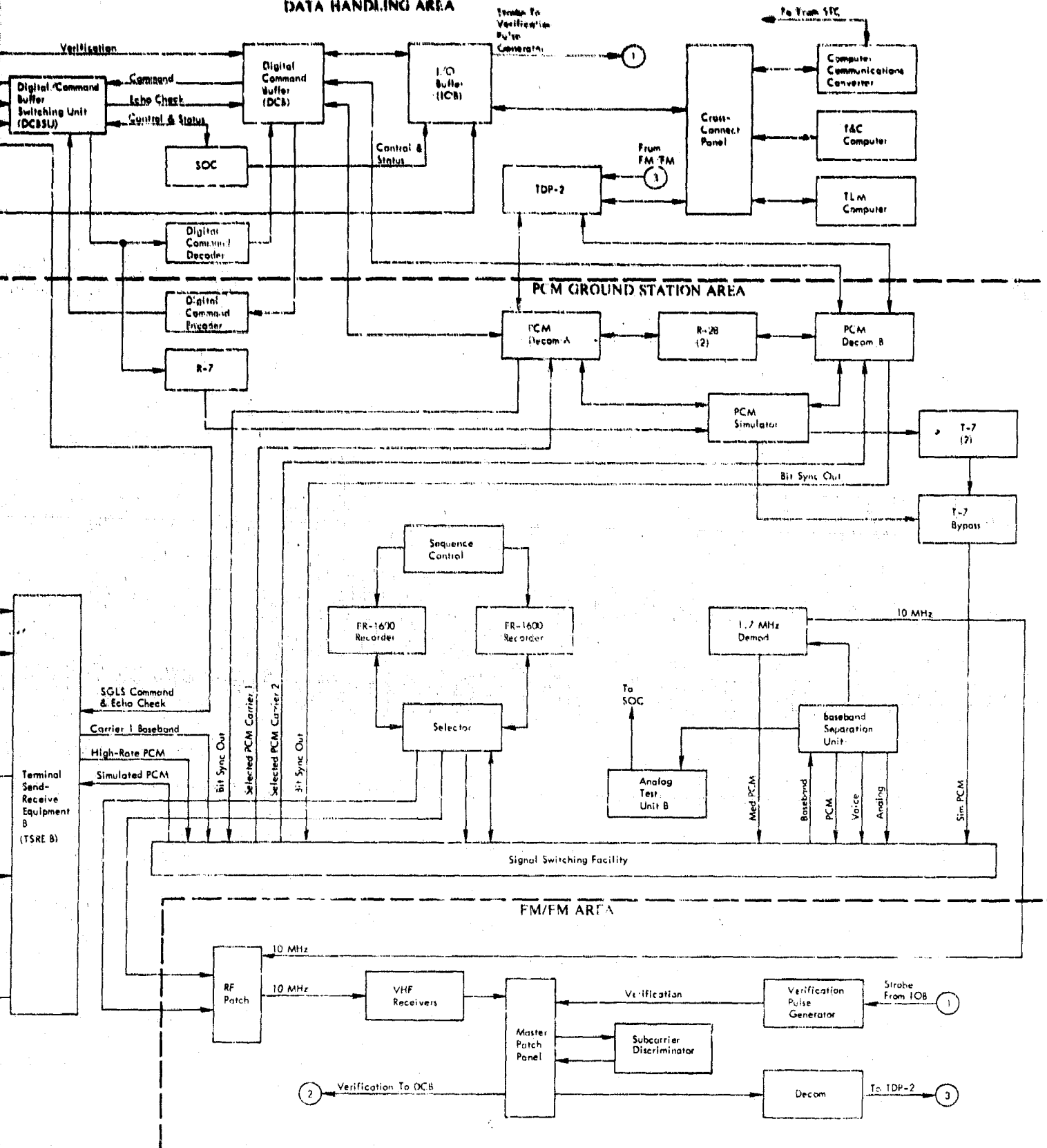
Test Transponder Receiver. In the uplink loop test, the test transponder receiver, acting as the monitor receiver, demodulates the RF carrier and furnishes the input to the uplink monitor.

Uplink Monitor. The uplink monitor separates and demodulates the recovered composite baseband from the test transponder receiver. The baseband signal consists of a maximum of three subcarriers and a PRN ranging code. The possible subcarriers are: three FSK command subcarriers, a 30-kHz subcarrier frequency-modulated by voice, and a 1.25-MHz subcarrier modulated by analog information.



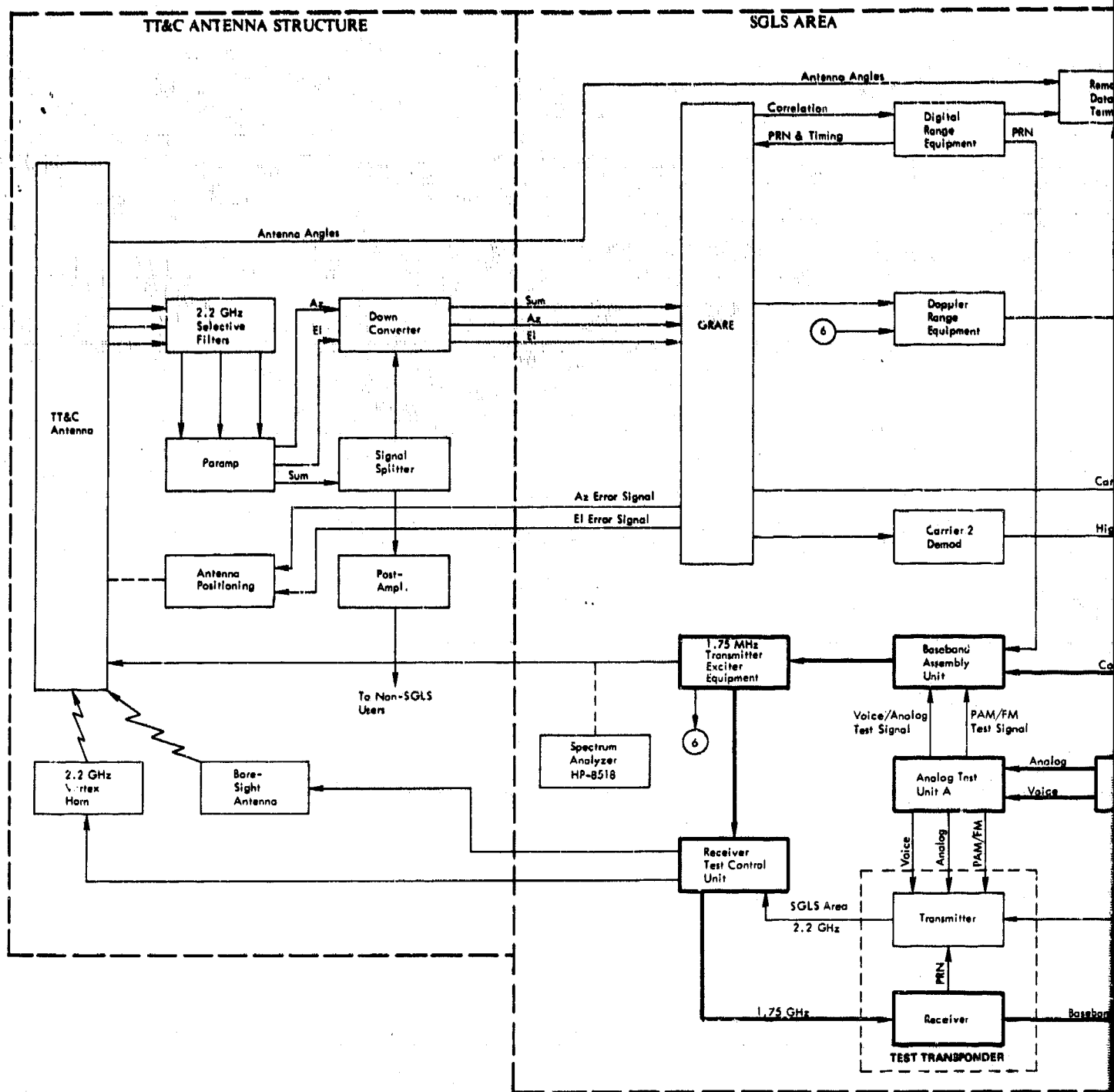
DATA HANDLING AREA

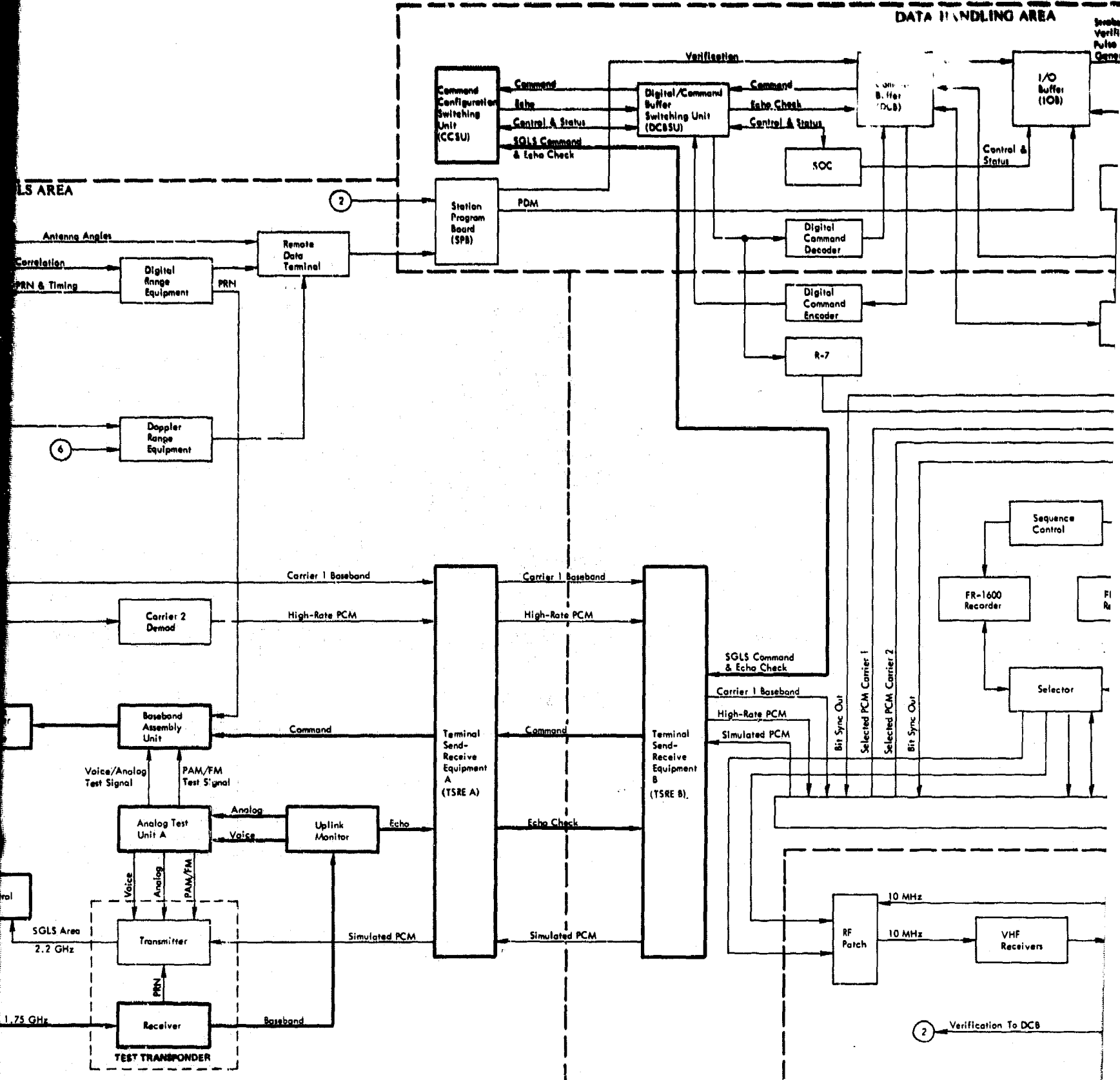
Star Line Inlet > Configuration for Test Four



3

Figure 5-69 Tracking Test Configuration





2

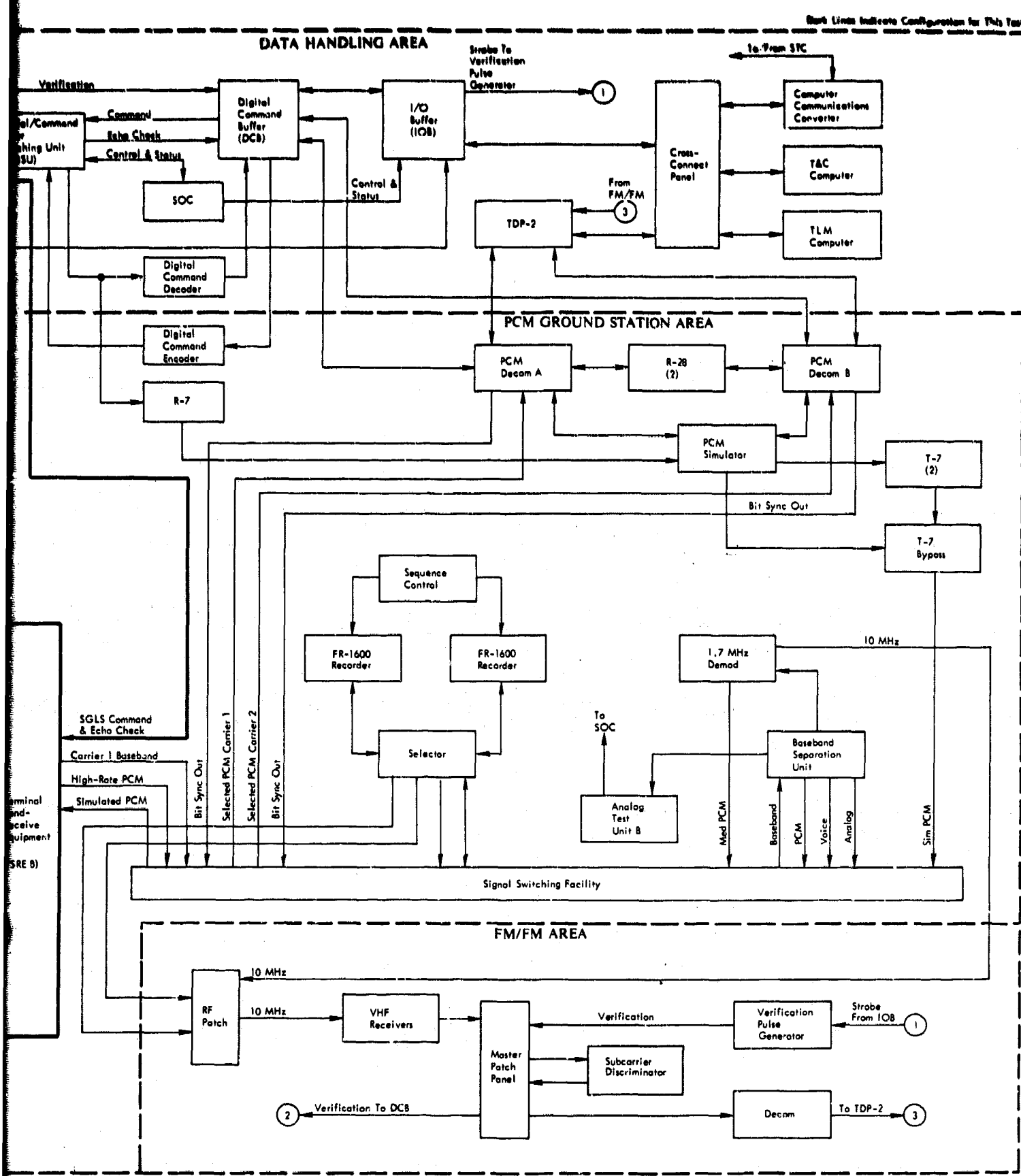


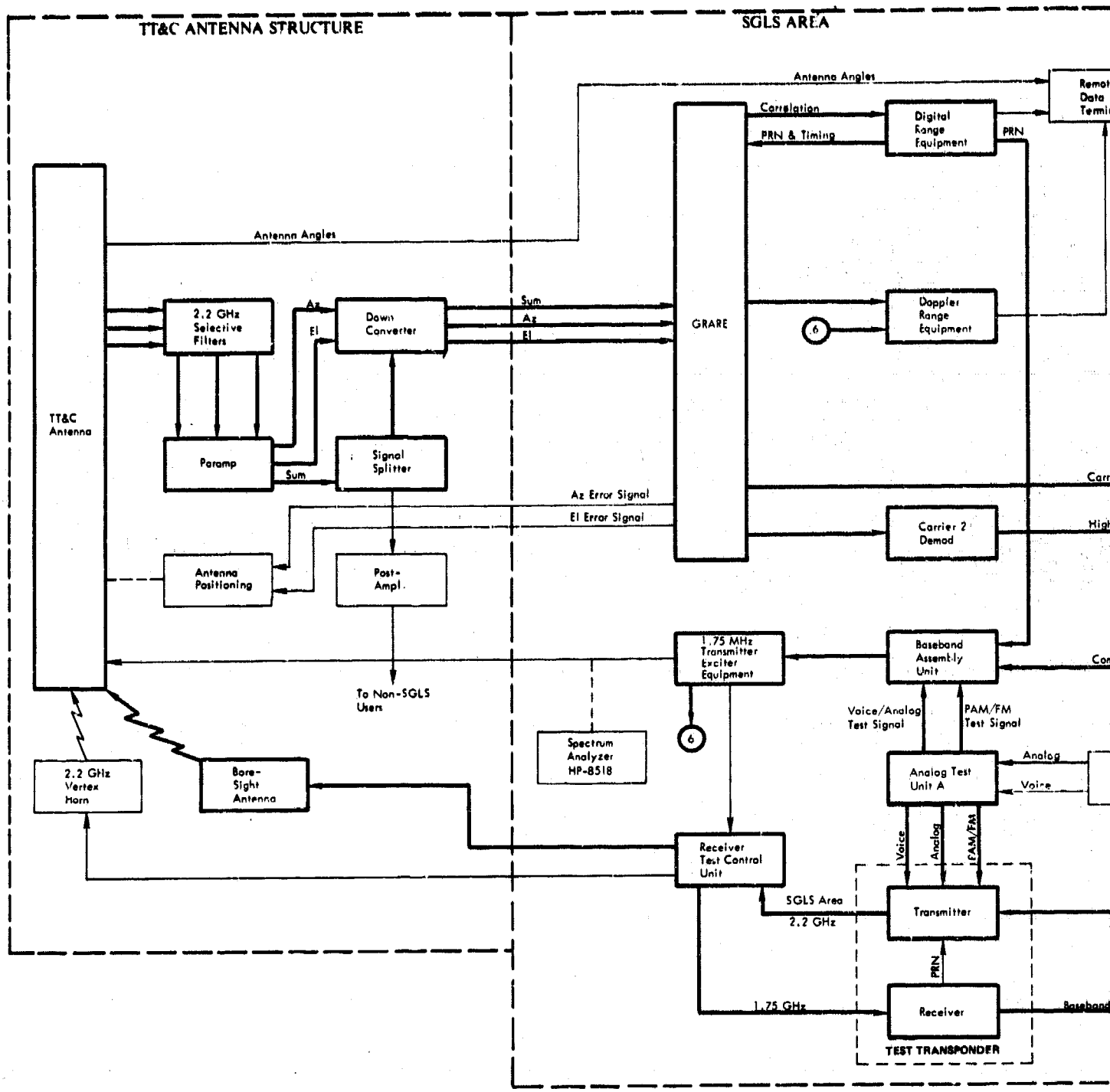
Figure 5-70 Uplink Test Configuration

The uplink monitor accepts the baseband signal from the test transponder, demultiplexes the baseband, and demodulates the command, voice, and analog data. Output signals representing the command "1", "0", and "S" bits, along with the sync signal, are sent via the command data transceivers to the RTS command subsystem for verification. Output signals proportional to the analog signal level, the analog subcarrier level, the voice signal level, and the voice subcarrier level are sent to analog test unit A for monitoring.

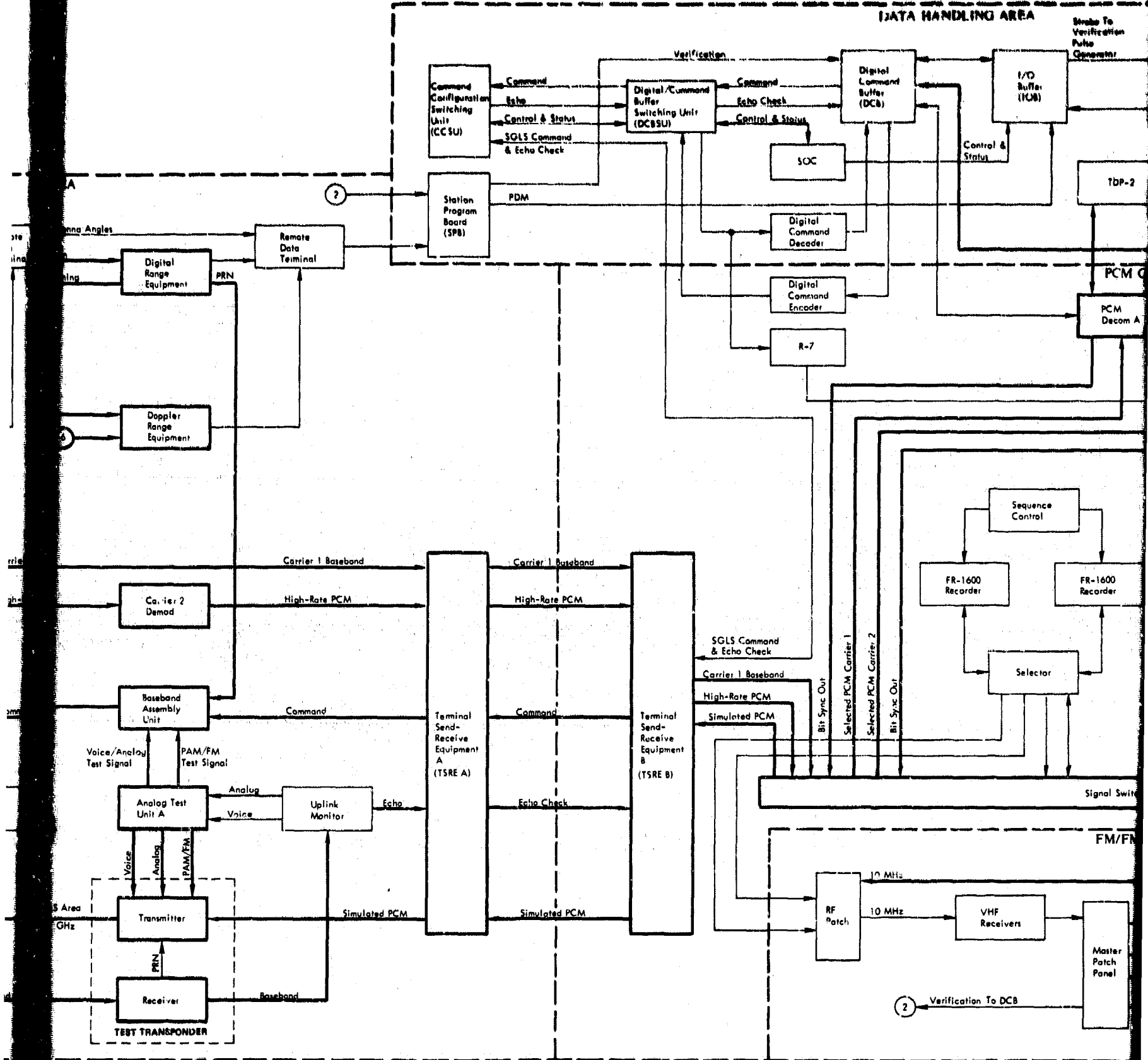
Analog Test Unit A. Analog test unit A accepts signals that represent the demodulated uplink voice and analog test signals (and their respective subcarriers) from the uplink monitor, and provides GO/NO GO information to the status indicators on the ATU. The unit also provides simulated voice (1 kHz) and analog (10 kHz) signals to the baseband assembly unit for uplink test.

Downlink. The downlink test equipment provides for verification of the SGLS ground system performance in a closed loop configuration. The system test configuration is shown in Figure 5-71. SGLS ground station test equipment used in the downlink system loop test includes the test transponder, analog test units A and B, and PCM simulator.

Test Transponder Transmitter. Two RF excitation driver signals and four modulation signals are applied to the test transponder transmitter. The RF drive signals are obtained from the two channel-selected voltage-controlled crystal oscillators in the test transponder receiver. One output from the oscillators is applied to Carrier 1 in the transmitter and the other, which is 5 MHz lower, is applied to the Carrier 2 channel. The four modulating signals are a 1-kHz or 10-kHz simulated voice/analog signal, a 75-kHz simulated PAM/FM signal, a PRN ranging code, and either low-bit-rate or high-bit-rate PCM data. The voice/analog and PAM/FM signals originate in the analog test unit A. The PRN ranging code is contained in the recovered uplink baseband output signal from the test transponder receiver. The simulated PCM signal is obtained from the PCM simulator and is fed either to the Carrier 1 channel of the test transponder transmitter or to the Carrier 2 channel, depending on which carrier channel is programmed for test. In the Carrier 1 channel, the simulated PAM/FM, simulated analog, PRN ranging code, and simulated



DATA HANDLING AREA



2

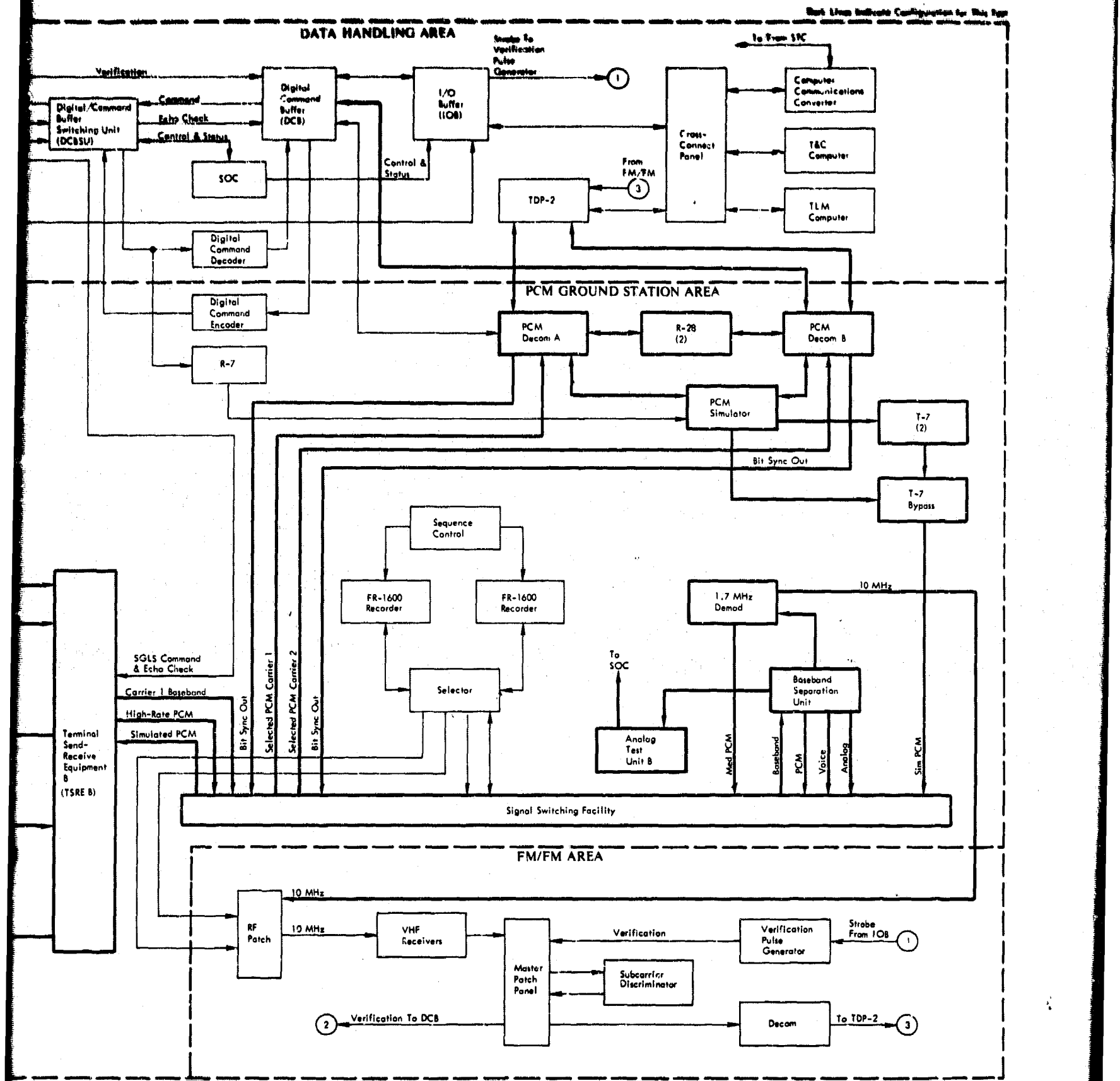


Figure 5-71 Downlink Test Configuration

PCM data are frequency-division multiplexed into a composite baseband signal that phase modulates the Carrier 1 channel RF signal. Carrier 2 simulated PCM data directly biphasic modulates the Carrier 2 channel RF signal.

PCM Simulator. The PCM simulator generates digital signals from data programmed into the self-contained memory for use in testing data processing equipment. One of seven PCM codes (NRZ-L, NRZ-M, NRZ-S, RZ, Bi ϕ -L, Bi ϕ -M, and Bi ϕ -S) may be selected from the PCM simulator. Bit rates may be programmed at a rate from 7.8 Hz to 1.024 MHz.

The PCM simulator also includes circuitry for serial and parallel comparison of the PCM data generated by the PCM simulator and the data returned from the decommutator. The comparator can be programmed for serial or parallel loop test. A bit/word counter functions (counting each bit or word compared by the serial or parallel comparator circuits) during the loop test, generates a stop signal to the simulator processor when a preset number of comparisons have been made, and displays the number of errors detected.

Analog Test Unit B. Analog test unit B provides a means of (1) on-line monitoring of the analog test signals, and (2) handling of control and status signals. The unit provides GO/NO GO status of the demodulated telemetry and voice/analog test signals from the baseband separation unit.

5.3.2 System Configuration Checkout

System configuration checkout verifies the system operation after the operating parameters have been reconfigured to suit a given mission profile. The checkout is normally performed in conjunction with the turnaround test mode of operation. The test is performed by simultaneously initiating the loop tests and monitoring the GO/NO GO indicators and test equipment monitor points. Each command or telemetry test may be performed in either the secure or clear modes of operation.

The following services and performance are verified during the configuration checkout:

Uplink Voice/Analog Loop. This loop verifies the proper operation of the voice and analog subcarriers' (S/C's) modulation indices and signal levels, and is accomplished by application of test modulation signals to the uplink carriers. Proper operation is indicated by the following indicators on analog test unit A:

- UP VOICE GO
- UP VOICE S/C GO
- UP ANALOG GO
- UP ANALOG S/C GO

Command Loop. In the loop test, the uplink monitor separates and demodulates the command subcarrier's portion of the recovered composite baseband from the test transponder receiver. Output signals that represent the command "1", "0", and "S" bits, along with the sync signal, are sent via the command data transceivers to the RTS data handling equipment for comparison with the generated command signals to verify proper uplink command transmission.

Range-Rate Loop. The verification of proper two-way coherent operation and proper extraction of range data is indicated by stable (zero) readout of range-rate data during the system loop test.

Ranging Loop. Proper configuration and operation of the ranging system are verified during the system loop test. Verification and calibration are readily indicated by a site-peculiar octal data readout.

Downlink Voice and Analog Telemetry. Operation of the voice/analog and analog telemetry demodulators is verified by appropriate modulation of the downlink carrier. Proper operation is indicated by detecting the output signals from the baseband separation unit and activating the following indicators on analog test unit B:

- DOWN ANALOG GO
- ANALOG TLM GO
- BASEBAND SEPARATOR READY

Additional verification of downlink equipment readiness is made by measuring the system noise figure. The noise source located in the receiver test unit inserts a known amount of noise into the parametric amplifier. The increase in receiver noise output as observed with the RF power meter or noise figure meter provides an indication of the overall system performance.

PCM Bit Comparison. Proper operation of each downlink PCM channel is verified by means of a bit-by-bit comparison of the PCM input data with demodulated data. Indication of proper operation is given on the PCM equipment front panel.

Antenna Tracking Tests. Proper operation of the antenna tracking system in the SGLS ground system configuration is verified in the boresight loop test. Functions verified during antenna tracking tests are as follows:

- Acquisition
- Dynamic range
- Autotrack
- Error gradients

It should be noted that all command and telemetry tests can be performed in either the secure or clear modes of operation.

SECTION 6

RELIABILITY AND MAINTAINABILITY

Early analyses (Reference 1) of mean-time-between failure (MTBF) and mean-time-to-repair (MTTR) indicated an estimated system point availability of 0.995929 based on a functional MTBF of 117.3 hours and a functional MTTR of 28.8 minutes. The MTBF estimates were at variance with the initial system requirement (Reference 2), which specified an overall point availability of not less than 0.9980 (the MTTR of 28.8 minutes was within the specified 30 minutes).

These early predictions were, however, based on preliminary data and were updated in subsequent publications (References 3, 4, and 5) as more accurate data became available. The following analysis utilizes final MTBF and MTTR data obtained from cognizant government agencies and equipment contractors (Reference 6).

6.1 RELIABILITY ANALYSIS

The SGLS equipment items and their associated MTBF's are listed in Table 6-1. Low-gain and high-gain MTBF data are shown for two cases:

- Case 1 (Functional Equipment Prediction) includes only SGLS equipment that is required for operations (excluding checkout and similar equipment items not essential for pass support).
- Case 2 (Total Equipment Prediction) includes all SGLS equipment regardless of function or usage.

Differences indicated between the low-gain and high-gain configurations are negligible.

TABLE 6-1
SGLS EQUIPMENT MEAN-TIME-BEFORE-FAILURES (MTBF)

Equipment	MTBF			
	Low-Gain Configuration		High-Gain Configuration	
	Case 1 Functional Equipment Prediction (Hours)	Case 2 Total Equipment Prediction (Hours)	Case 1 Functional Equipment Prediction (Hours)	Case 2 Total Equipment Prediction (Hours)
Signal Switching Facility	6,033	1,591	6,033	1,591
Doppler Frequency Converter	74,996	74,996	74,996	74,996
Carrier 2 Demodulator	23,186	21,724	23,186	21,724
Diplexer	200,000	200,000	N/A	N/A
Terminal Sending and Receiving	1,726	1,726	1,726	1,726
Integration and Checkout	2,052	712	2,052	712
Baseband Separation Unit	9,179	9,179	9,179	9,179
Baseband Assembly Unit	4,878	4,827	4,878	4,827
Transmitter Exciter	3,748	3,474	3,748	3,474
Digital Ranging Equipment	2,783	1,257	2,783	1,257
Test Transponder	5,059	5,059	5,059	5,059
Parametric Preamplifier (Klystron)	11,535	9,315	11,315	9,315
Receiver (GRARE)	4,276	2,908	4,276	2,908
Selective Filter	N/A	N/A	500,000	500,000
Range Rate Extractor	6,454	6,099	6,454	6,099
Wideband Transmitter	4,398	2,194	4,398	2,194
Uplink Monitor	8,493	8,237	8,493	8,237
PCM Ground Station (2 each)	310	218	310	218
PCM Simulator	1,315	780	1,315	780
Tape Recorder (2 each)	638	403	638	403
Radiation Alarm System	16,180	16,180	16,180	16,180
CCN's and ECP's (Installed Modifications)	9,709	9,709	10,144	10,144
Total MTBF (Hours)	112	72	113	72

The functional equipment prediction (Case 1) is of primary concern, however. By taking the MTBF for the low-gain configuration as worst-case (i.e., 112 hours versus 113 hours for the high-gain configuration) and allowing a 5% margin for near-term subsequent equipment modifications, a figure of 105 hours is obtained as the functional SGLS MTBF.

The analysis of SGLS reliability also considered the subsets of equipment required to perform each of the primary operational functions listed below:

- Tracking Support: includes signal acquisition, range and range-rate measurement, and automatic angle tracking
- Uplink Support: includes transmission of commands, voice, and range data to the vehicle
- Downlink Support: includes vehicle-to-ground PCM telemetry and analog services

Except for the antenna subsystems and certain communication equipment, RTS equipment items that interface with SGLS (e.g., timing, data handling, etc.) are excluded. The matrix for the high-gain configuration (Table 6-2) and the matrix for the low-gain configuration (Table 6-3) show the equipment items required for each function, associated failure rates, and predicted MTTR. Failure rates (λ) are the number of failures in 10^6 hours.

Non-SGLES equipment items are indicated by an asterisk. MTTR's are in minutes. Paragraph 6.2 discusses the MTTR's in greater detail.

The resulting MTTR's for each function are summarized in Tables 6-4 and 6-5 for the two antenna configurations. Two values of MTBF are given. Values under "Functional Equipment Total" include the contribution of the antenna subsystems and the communication equipment; values under "Functional Equipment SGLES Only" do not. As before, only equipment essential to the indicated operational functions is considered. All equipment items are considered in series such that

TABLE 6-2
MATRIX OF EQUIPMENT REQUIRED FOR OPERATIONAL FUNCTIONS
(HIGH-GAIN CONFIGURATION)

Equipment	Function			Failure Rate (λ) Per 10^6 Hours	Predicted MTTR In Minutes
	Tracking	Uplink	Downlink		
Reflector and Pedestal*	●	●	●	44.34	90
Servos*	●	●	●	1455.00	60
Selective Filter	●	●	●	2.00	90
Parametric Preamplifier (Klystron)	●		●	86.69	60
Reference Receiver (GRARE)	●		●	118.51	13
Receiver Test Unit	●		●	100.47	22
Boresight Antenna*	●		●	25.00	60
Wideband Transmitter	●	●	●	227.16	37
Transmitter Exciter-Driver	●	●	●	287.85	25
Radiation Warning System	●	●	●	24.82	45
Baseband Assembly Unit	●	●	●	207.17	22
Digital Ranging Equipment	●	●	●	359.26	23
RDT Transfer Switch*	●	●	●	24.07	60
Doppler Frequency Converter	●			13.33	20
Range Rate Extractor	●			163.96	23
Frequency Synthesizer	●		●	98.84	30
Carrier 2 Demodulator			●	43.13	22
Terminal Sending and Receiving		●	●	432.02	15
Signal Switching Facility		●	●	165.25	28
Baseband Separation Unit			●	74.58	36
1.7-MHz PCM Demodulator			●	34.38	57
Tape Recorders 1 and 2 (Record Mode)		●	●	1567.39	30
PCM Ground Station (2 each)			●	3221.38	30
Test Transponder		●	●	185.23	25
Analog Test Unit "A"		●	●	46.33	34
Uplink Monitor		●	●	117.74	28
Communications Networks*	●	●	●	182.80	30
dc Power Supplies	●	●	●	214.94	24
dc Power Supplies	●	●	●	156.16	24
ac Power Panels	●	●	●	49.04	24
Blowers	●	●	●	44.32	24
Connector Panels	●	●	●	33.35	22
Interim Control and Display	●	●	●	38.54	60
CCN's and ECP's (Installed Modifications)	●	●	●	38.93	45

* Non-SGLS Equipment

TABLE 6-3
MATRIX OF EQUIPMENT REQUIRED FOR OPERATIONAL FUNCTIONS
(LOW-GAIN CONFIGURATION)

Equipment	Function			Failure Rate (λ) Per 10 ⁶ Hours	Predicted MTTR In Minutes
	Tracking	Uplink	Downlink		
Prelort Reflector*	●	●	●		
Nutating Scanner*	●	●	●		
Rotary Joints and Slip Rings*	●	●	●		
Prelort/SGLS Waveguide Switch*	●	●	●		
Diplexer	●	●	●	5.00	76
Parametric Preamp (Klystron)	●	●	●	86.69	45
Reference Receiver (GRARE)	●	●	●	118.51	13
Receiver Test Unit	●	●	●	76.19	22
Boresight Antenna*	●	●	●	25.00	60
Wideband Transmitter	●	●	●	227.16	37
Transmitter Exciter-Driver	●	●	●	287.85	25
Radiation Warning System	●	●	●	24.82	45
Baseband Assembly Unit	●	●	●	207.17	22
Digital Ranging Equipment	●	●	●	359.26	23
RDT Transfer Switch	●	●	●	24.07	60
Doppler Frequency Converter	●	●		13.33	20
Range Rate Extractor	●	●		163.96	23
Frequency Synthesizer	●		●	98.84	30
Carrier 2 Demodulator			●	43.13	22
Terminal Sending and Receiving		●	●	432.02	15
Signal Switching Facility		●	●	165.25	28
Baseband Separation Unit		●	●	74.58	36
1.7-MHz PCM Demodulator		●	●	34.38	57
Tape Recorder 1 and 2		●	●	1567.39	30
PCM Ground Station (2 each)		●	●	3221.38	30
Prelort Servo*	●	●	●	1089.60	60
Communications Networks*	●	●	●	182.80	30
Test Transponder	●	●	●	185.23	25
Analog Test Unit "A"	●	●	●	46.33	34
Uplink Monitor	●	●		117.74	28
dc Power Supplies	●	●	●	214.94	24
dc Power Supplies	●	●	●	156.16	24
ac Power Panels	●	●	●	49.04	24
Blowers	●	●	●	44.32	24
Connector Panels	●	●	●	33.35	22
Interim Control & Display	●	●	●	33.64	60
CCN's and ECP's (Installed Modifications)	●	●	●	9.75	45

*Non-SGLS Equipment

TABLE 6-4

MEAN-TIME-BETWEEN-FAILURES (MTBF) FOR SGLS FUNCTIONS
(HIGH-GAIN CONFIGURATION)

Operational Function	MTBF (Hours)	
	Functional Equipment Total	Functional Equipment SGLS Only
Tracking Support	284	535
Uplink Support	177	248
Downlink Support	108	131

TABLE 6-5

MEAN-TIME-BETWEEN-FAILURES (MTBF) FOR SGLS FUNCTIONS
(LOW-GAIN CONFIGURATION)

Operational Function	MTBF (Hours)	
	Functional Equipment Total	Functional Equipment SGLS Only
Tracking Support	275	526
Uplink Support	174	247
Downlink Support	104	127

$\lambda_{\text{total}} = \lambda_1 + \lambda_2 + \dots + \lambda_n$. Further, the failure rates used assume that all parts having an identifiable wear-out mechanism will be replaced prior to failure.

6.2 MAINTAINABILITY ANALYSIS

The maintenance concept at the RTS provides for three levels of maintenance:

- Organization Maintenance: performed directly on equipment in its operational configuration and setting.
- Field Maintenance: performed on line-replaceable units (LRU's) removed from the operational configuration for repair in a shop at, or near, the using location. (Such shops are assumed to have the necessary test, maintenance, and support equipment and material. Field-level resources may be used to restore equipment to its operational configuration when such restoration exceeds the capabilities of organizational resources.)
- Depot Maintenance: used when special skills, processes, or equipment are not available at the using location.

In the analysis that follows, only organizational maintenance is considered. No attempt has been made to assess field or depot maintenance.

6.2.1 Maintenance Assumptions

The design of the equipment limits most operational maintenance to fault detection, localization, isolation, correction, and verification. These actions are accomplished as follows:

- Detection: primarily by monitoring prime equipment displays and indicators.

- Isolation: by using displays and indicators and rack-mounted or portable test equipment.
- Correction: by adjusting or removing and replacing an LRU.
- Verification: by determining that displays and indicators have been returned to normal operating status.

In assessing corrective maintenance downtime, the following assumptions were made:

- Distribution of estimated repair times is log-normal.
- Required tools, test equipment, and documentation are available.
- Replacement modules and components (LRU's) are readily available.
- Repair time estimates exclude logistics and administration time.
- Organization-level maintenance requires only two men of AFSC "5" skill level per maintenance action.
- Maintenance personnel have attended an equipment-specific training course and are fully qualified to maintain the equipment.

6.2.2 Maintainability Prediction

The prediction technique used in the analysis is a variation of Method IV in MIL-HDBK-472, "Maintainability Prediction," 24 May 1966 (Reference 7). Briefly the steps involved are:

- Identify the equipment and assembly level for which assessments are to be developed (i.e., module or piecepart).
- Determine categories of LRU's within the equipment.
- Identify the failure rates (λ) or service frequencies of these items. (Failure rates were obtained from the reliability analysis detailed in this report.)
- Predict the time required to perform each step in the required sequence of maintenance actions.
- Accumulate per-item maintenance times and compute the MTTR.

The corrective maintenance downtimes (M_{ct}) and failure rates (λ) for the individual SGLS equipments are listed in Table 6-6. The functional MTTR for the total collection of SGLS equipment items is related to the corrective maintenance downtime and failure rate as follows:

$$MTTR = \frac{\sum_{i=1}^N \lambda_i M_{ict}}{\sum_{i=1}^N \lambda_i}$$

where

- N = number of individual equipments
 λ_i = failure rate of the i^{th} equipment in failures per 10^6 hours
 M_{ict} = corrective maintenance repair time of the i^{th} equipment
MTTR = mean-time-to-repair for all equipment items

TABLE 6-6

SGLS EQUIPMENT CORRECTIVE MAINTENANCE DOWNTIME (M_{ct})
AND FAILURE RATES (λ)

Equipment	M_{ct} (Minutes)	Failure Rate (λ) Per 10^6 Hours
Signal Switching Facility	28	165.76
Doppler Frequency Converter	20	13.38
Carrier 2 Demodulator	22	43.13
Diplexer	75	5.00
Terminal Sending & Receiving	15	579.17
Integration & Checkout	26	487.33
Baseband Separation Unit	36	74.57
Baseband Assembly Unit	22	204.99
Transmitter Exciter	25	266.43
Digital Ranging Equipment	23	359.32
Test Transponder	25	197.65
Parametric Preamplifier (Klystron)	45	86.69
Receiver (GRARE)	13	233.86
Selective Filter	90	2.00
Range Rate Extractor	23	152.94
Wideband Transmitter	37	227.38
Uplink Monitor	28	117.74
PCM Ground Station (2 Each)	30	3221.36
PCM Simulator	30	760.46
Tape Recorder (2 Each)	30	1567.39
Radiation Alarm System	45	24.82
CCN's and ECP's (Installed Modifications)	45	103.04

For the SGLS equipment items listed in Table 6-6, the functional MTTR is 27.7 minutes, which compares favorably with the required MTTR of 30.0 minutes.

The MTTR was also computed for each operational function. Subsets of equipment items used and the associated individual MTTR's are listed in Table 6-2 for the high-gain configuration and in Table 6-3 for the low-gain configuration.

Results for the high-gain configuration are shown in Table 6-7. As in the analysis of reliability, the functional MTTR was computed including both SGLS and non-SGls equipment items. These values are listed in Table 6-7 under "Functional Equipment Total." Entries under "Functional Equipment SGls Only" do not include MTTR's for non-SGls equipment items. Asterisks in Table 6-2 identify these non-SGls equipment items.

Table 6-8 shows MTTR's for the low-gain configuration.

As indicated in the tables, the SGls equipment items have an MTTR ranging between 27.1 and 29.3 minutes depending on the operational function. When utilized with non-SGls equipment items, the MTTR ranges between 33.8 and 44.2 minutes.

6.3 POINT AVAILABILITY

For an MTBF of 105 hours and an MTTR of 0.5 hour, the associated overall point availability is

$$\text{Point availability} = \frac{\text{MTBF}}{\text{MTBF} + \text{MTTR}} = 0.9953$$

As noted previously, an approximate 5% degradation is included in the functional MTBF of 105 hours to accommodate future equipment modifications. The analysis indicates that the equipment will satisfy the required MTTR of 30.0 minutes.

TABLE 6-7

MEAN-TIME-TO-REPAIR (MTTR) FOR SGLS FUNCTIONS
(HIGH-GAIN CONFIGURATION)

Operational Function	MTTR (Minutes)	
	Functional Equipment Total	Functional Equipment SGLS Only
Tracking Support	42.1	28.0
Uplink Support	36.1	27.1
Downlink Support	33.8	28.5

TABLE 6-8

MEAN-TIME-TO-REPAIR (MTTR) FOR SGLS FUNCTIONS
(LOW-GAIN CONFIGURATION)

Operational Function	MTTR (Minutes)	
	Functional Equipment Total	Functional Equipment SGLS Only
Tracking Support	44.2	27.7
Uplink Support	37.5	27.2
Downlink Support	35.2	29.3

REFERENCES:

- (1) Reliability and Maintainability Allocations, Assessments, and Analysis Report, Philco-Ford WDL-TR3277, 21 June 1967.
- (2) Satellite Control Facility Design Criteria: Overall Space-Ground Link Subsystem, Aerospace Report TOR-669 (6110-01)-54, 10 May 1966.
- (3) SGLS Integration and Checkout Reliability and Maintainability Quarterly Progress Report, Philco-Ford WDL-TR3369, 16 October 1967.
- (4) SGLS Integration and Checkout Reliability and Maintainability Quarterly Progress Report, Philco-Ford WDL-TR3476, 10 January 1968.
- (5) SGLS Integration and Checkout Reliability and Maintainability Quarterly Progress Report, Philco-Ford WDL-TR3546, 10 April 1968.
- (6) SGLS Integration and Checkout Reliability and Maintainability Quarterly Progress Report, Philco-Ford WDL-TR3628, 1 July 1968.
- (7) Maintainability Program, Philco-Ford WDL-TR3213, March 1967.

SECTION 7

RECOMMENDATIONS

While the current system meets its design objectives, there are several areas where a significant increase in capability can be realized through additional development. The most significant of these is in the automation of the control/display and signal acquisition functions. In these and other areas noted in the following paragraphs, it is recommended that further development be initiated.

7.1 CONTROL AND DISPLAY

In the current SGLS installation at the RTS, controls and the associated displays are located primarily at the equipment racks. SGLS design, however, includes a provision for control from a remote location. The automation of these control functions has been investigated and a design approach developed utilizing a Univac 1230 mTc computer complex. The technique employed and the interface equipment required are discussed in some detail in SGLS Control Equipment, WDL-TR3394, 10 November 1967.

7.2 SIGNAL ACQUISITION

In the SCF environment, further development to automate the signal acquisition function is also highly desirable. The principal objective of this automation should be to minimize the time to acquire.

Detailed analyses of this problem* have resulted in a design approach described in WDL-TR3538, Study Report, Main Beam Acquisition at 2 GHz for 60-Foot TT&C Antennas, 29 March 1968.

* SCF Spatial Acquisition Study, Volumes I, II, III, WDL-TR2904A, 15 July 1966.
Analysis of 60-Foot Antenna S-Band Acquisition Problem, WDL-TR3223, 20 April 1967.

7.3 OTHER RECOMMENDED DEVELOPMENTS

7.3.1 Test Transponder Improvements

The following recommendations related to general performance of the test transponder will improve operation during a quick turnaround and resolve known problems and limitations existing within the transponder:

- Relocate internal subcarrier switches from modules to a panel.
- Evaluate the transponder transmitter RF power metering circuitry and replace it if warranted.
- Replace the flexible coupling on the attenuator with a solid coupling.
Add a movable front panel index.
- Add coax switching and terminations to ensure that all TTT RF outputs are terminated when not in use.
- Modify the 1.7-MHz FM/FM VCO to be compatible with a true simulated FM/FM signal.
- Correct the signal interface between the DYNAIR and the video receiver for simulated PCM.
- Add the capability to insert PRN or similar modulation on Carrier 1 from the transponder front panel. The present system requires the entire uplink.

7.3.2 System Reliability Improvements

The following recommendations will further improve the availability of SGLS:

- Reevaluate the dc power distribution scheme used in SGLS and provide redundant power supplies.
- Add protective fuses to each major PCM drawer, rather than the rack-level fusing now used.
- Add protective insulation or redesign to eliminate potential short circuits in logic cards.

7.3.3 System Alignment/Adjustment Improvements

/ As a result of SGLS testing, the following recommendations are made to improve system alignment and adjustment:

- Modify the 1-kHz adjustment at ATU-A so that the adjustment is less sensitive.
- Add an error-gradient adjustment to the GRARE for conical-scan operation.
- Add a fixed analog output at COMSEC voltage levels to the PCM simulator.
- Modify BSU/ATU-B 1.7-MHz interface for status monitoring.

7.3.4 Test Equipment Upgrading

To effectively align, calibrate, and maintain the tracking station SGIS equipment, additional test equipment capabilities should be provided. The following measures should be taken:

- Add a SGIS-compatible noise figure test set to low-gain sites (similar to that used for high-gain sites).
- Add test equipment such as oscilloscopes, VTVM's and signal generators to data area racks.
- Complete implementation of the RF test-point panel located between the transmitter exciter and driver.
- Provide a boresight tower-mounted range calibration unit.

7.3.5 Tape Playback Improvements

Due to flutter performance of the FR-1600 type recorders, the present system is unable to process 1.024- and 1.7-MHz subcarrier with PCM and composite Carrier 1 baseband during tape playback. This should be corrected to enable utilization of this system feature.

7.3.6 PCM Demodulator Improvements

Limitations of the built-to-print baseband separation unit and Carrier 2 demodulators cause degradations in the expected performance of the system in handling PCM data. Redesign and/or modification of these units would improve this performance by at least 1 to 2 dB.

7.3.7 Automation of the Digital Ranging Equipment

The present ranging process is heavily dependent upon operator actions and decisions. The following changes will optimize the ranging process and eliminate the need for operator intervention:

- Automatic normalization of correlation voltage by adding AGC to the GRARE code clock loop.
- Automatic setting of the DRE integration number as a function of S/N ratio.
- Automatic reset and start of the DRE.

7.3.8 Signal Switching Facility Improvements

More efficient use of the SSF can be realized through the following measures:

- Relocate the recorder fault-isolation equipment to the SGLS/non-SGLS rack, thereby making additional SSF switching capability available for future program requirements.
- Convert SSF indicator panel to a switch/indicator panel.
- Use the card reader to configure non-SSF functions such as the T-7 mode switch, and the Carrier 1 record/playback switch.

7.3.9 Terminal Send/Receive Equipment Improvements

The design of the terminal send/receive equipment should be modified to provide for simple detection of performance degradation. The following improvements are recommended:

- Implement a real-time performance monitoring capability into the video equipment items, such as a pilot tone and detector.
- Add external test points to data terminals A and B.

7.3.10 PCM Ground Station Improvements

The following measures will improve operability and maintainability of the PCM ground station:

- Add a front-panel main-frame synchronization point to the PCM simulator and each decommutator.
- Replace pushbutton switches on PCM equipment with more reliable types, including both the technical control equipment and illuminated types on the bit synchronizer.

7.3.11 Second PCM Bit-Stream Simulate Capability

The present system cannot simulate a full service SGLS downlink signal, since only one PCM bit stream can be simulated at a time. A more realistic checkout can be accomplished by providing a second PCM bit stream as follows:

- Modify the timing terminal unit to accept a second PCM bit stream.
- Augment the data transmission equipment to handle the second bit stream.
- Add a second PCM simulator, or
- Use the existing FR-1600 recorders as a source.

7.3.12 Command Loop Improvements

A number of recommendations associated with SGLS handling of command data have been determined during the test program. These are:

- Modify the data transceiver interface circuitry to be more nearly compatible with the DCBSU and the CCSU for echo check.
- Modify the command echo check loop to eliminate false echo errors at high command rates.
- Provide a command source simulator/echo check comparator to make loop checks without RTS data area equipment.

7.3.13 GRARE Improvements

The operational flexibility and use of the GRARE can be improved by implementing the following measures:

- Modify GRARE phase/amplitude circuitry to allow switching from wideband to phaselock without readjusting phase relationships.
- Evaluate the possibility of expanded use of SGLS wideband capability. As an example, processing of Carrier 1 data via the 3.0-MHz wideband phase detector in the event GRARE phaselock equipment failure provides backup facilities without increasing equipment redundancy.
- Increase sensitivity of the coherent demodulator.

APPENDIX A

COMMAND LINK ANALYSIS

A. 1 INTRODUCTION

A. 1. 1 Purpose

This analysis optimizes the command link performance through selection of an appropriate relative delay between the zero crossings of the synchronizing signal and the leading edge of the command data bits and evaluates the possibility of establishing a fixed value for the nominal delay contributed by the ground station.

To minimize the digital error rate in the presence of disturbances such as noise, the command data pulses should be sampled at a time when the pulse amplitude reaches a maximum value. In the SGLS system, the sampling pulse is derived from a synchronizing signal that is amplitude modulated onto the carrier that contains the data pulses in the form of frequency-shift keyed (FSK) modulation. The phase of the synchronizing signal must be selected such that its zero crossings, which generate the sampling pulses, are coincident with the maximum value of the data pulses. This, in turn, is a function of the response of the filter networks in the vehicle.

A. 1. 2 Scope

The command system may be used in any of several options; at low, medium, or high baud rates. The vehicle equipment design is tailored to support each of these options, but consists of two basic designs: one for the high baud rate and the second for all others. This analysis considers both design techniques and evaluates the performance in terms of the required increase in signal power (to preserve the specified error rate) versus time deviation about the derived optimum delay.

Once the optimum delay has been derived, the relative contributions of both the ground and vehicle equipment are considered from the viewpoint of allocating a fixed value for the ground equipment delay.

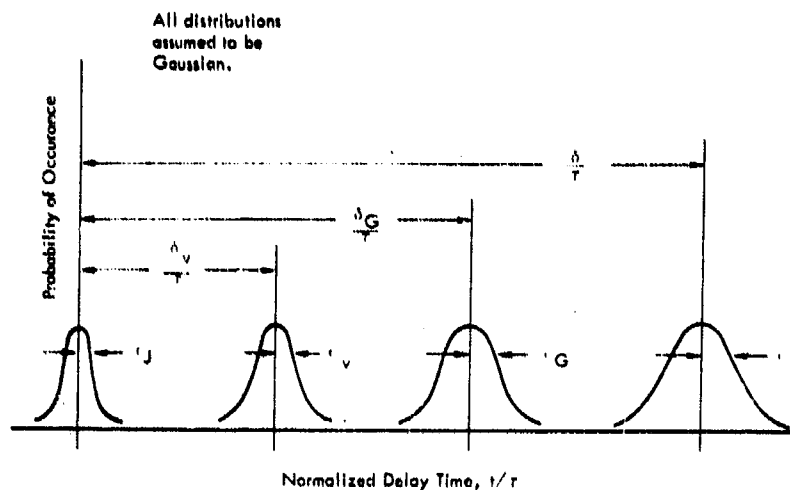
A.2 TECHNICAL SUMMARY AND CONCLUSIONS

A timing model is formulated for the evaluation of overall sync timing uncertainty at 100 kbauds and at the six lower command rates (1, 20, and 100 bauds and 1, 2, and 10 kbauds). Three sources are identified to be the principal contributors to the overall sync uncertainty:

- Ground Equipment Uncertainty, ϵ_G
 $\pm 10\%$ of the bit period at 100 kbauds
 $\pm 3\%$ at the other command rates.
- Sync Jitter Due to Link Noise, ϵ_J
 $\pm 1.7\%$ of the bit period at all rates
- Vehicle Equipment Uncertainty, ϵ_V
Unknown, $\pm 5\%$ of the bit period assumed to be typical.

These parameters are illustrated in Figure A-1. Assuming each of the uncertainties represent the one-sigma level of a Gaussian process, then the equivalent total sync uncertainty may be derived as the square root of the sum of the squares of the components to give $\epsilon_1 = \pm 0.113\tau$ at 100 kbauds and $\epsilon_2 = \pm 0.06\tau$ at the other command rates (τ = bit period).

The optimum overall sync delay was determined to accommodate these uncertainties. The values are $\delta_1 = 0.728\tau$, corresponding to ϵ_1 , and $\delta_2 = 0.94\tau$, corresponding to ϵ_2 . In concept, the signal power must be increased to avoid exceeding the specified error rate in the presence of the timing uncertainty. The required increase is 0.5 dB for the 100-kbaud case and 0.18 dB for the other baud rates.



τ = bit period
 δ_v = mean time delay in vehicle equipment
 δ_G = mean time delay in ground equipment
 $\delta = \delta_v + \delta_G$ = net mean time delay
 ϵ_j = time deviation due to link noise (synch jitter)
 ϵ_v = time deviation in vehicle equipment
 ϵ_G = time deviation in ground equipment
 ϵ = net time deviation
 $\epsilon^2 = \epsilon_j^2 + \epsilon_v^2 + \epsilon_G^2$

Figure A-1 Statistical Model

Since the optimum total sync delay is relatively large for both basic designs considered (δ_1 and δ_2 above), there should be no problem in selecting a fixed value of ground equipment delay for all options and then optimizing the system design by selection of an appropriate delay in the vehicle for the specific command option selected. Also, since the only vehicle design established at the time of this analysis was the 1-kbaud option, it is proposed that the ground delay allocated by that vehicle design be selected as the basis for the fixed value of the ground equipment delay. This results in a delay (δ_G) equal to 0.594τ , with a variation of $\pm 0.1\tau$ at the 100-kbaud rate and $\pm 0.03\tau$ at the other command rates.

A.3 SYSTEM DESCRIPTION

The following subparagraphs describe the important features of the command system (for the ground station and space vehicle) at several levels of detail.

A.3.1 Overall Configuration

The command system is divided between the ground equipment and the vehicle equipment. Figure A-2 illustrates the system. The commands originate in the Integrated Command System (ICS) as four digital channels: three carry command data, and one carries synchronization information. The baseband assembly unit (BAU) receives these four channels, converts them into an amplitude-modulated FSK subcarrier, and phase modulates the main carrier with the composite baseband, of which the command subcarrier is a component (Reference 1). The remaining ground equipment merely upconverts and amplifies the main carrier.

In the space vehicle, the receiver coherently demodulates the main carrier to provide the composite baseband. The command component is routed to the signal conditioner, which demodulates the command subcarrier. A clock and

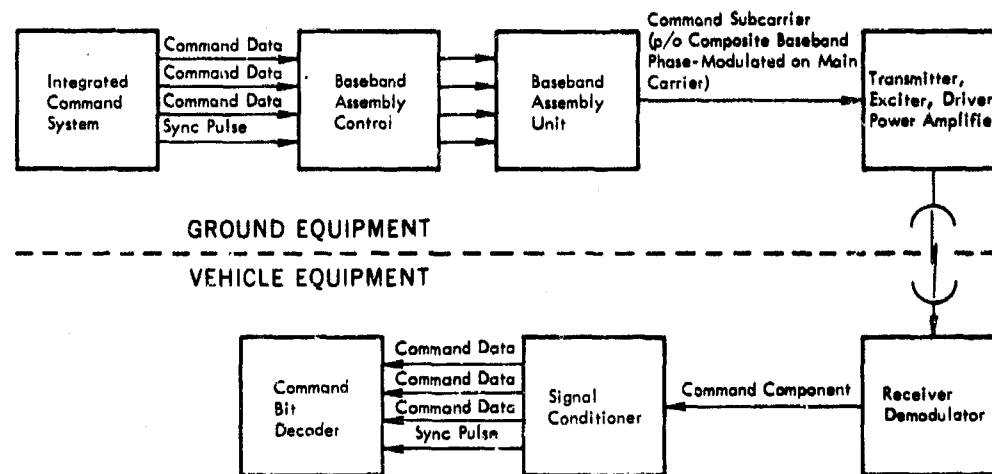


Figure A-2 The Command System

A-4

three command channels are regenerated. These data are sent to the digital command decoder. The decision concerning the state of the regenerated bit is made in the signal conditioner at the 10 and 100 kbaud rates, and in the digital command decoder for the remaining command rates (Reference 2).

A.3.2 Ground Equipment Configuration

For this analysis, the important component in the ground equipment is the baseband assembly unit. The BAU (Figure A-3) accepts each of the three mutually exclusive command channels and converts them to a serial FSK bit stream. The BAU also accepts the sync pulse, which triggers a variable period monostable multivibrator to provide variable sync delay. The trailing edge of this delay pulse triggers a flip-flop that divides the sync pulse rate by two and stretches the sync pulse to a full bit period. This stretched pulse is integrated to generate a triangular wave at a frequency that is half the command bit rate. The triangular waveform is passed through a lowpass filter that has a 100-kHz cutoff frequency. Accordingly, the sync signal for the 100 kbps command rate is passed as a sine wave because of suppression of the harmonics; whereas, at lower command rates, the sync signal has a triangular waveform. The zero crossings of the triangular or sinusoidal sync signal (with respect to the data bit transition) are variable from 0.55τ to 0.70τ with both clock and FSK signals present at the two inputs to the AM modulator. The sync signal amplitude modulates the FSK signal with a modulation index of $m = 0.5$.

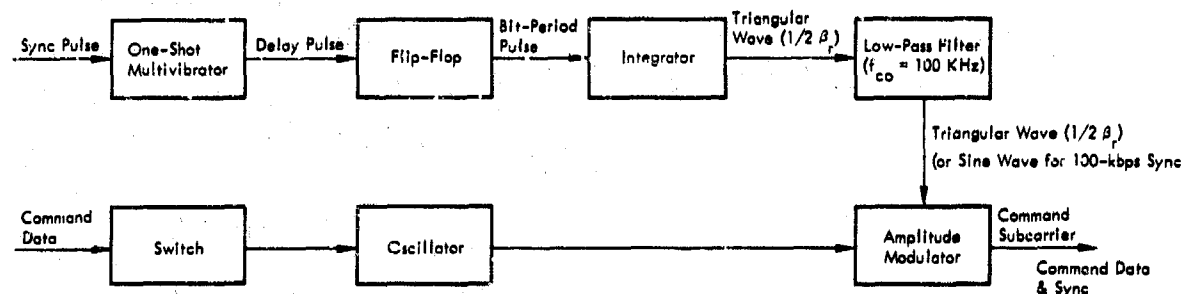


Figure A-3 Major Components of Baseband Assembly Unit (Ground Equipment)

A.3.3 Space Vehicle Equipment Configuration (Reference 2)

The most important component in the space vehicle is the signal conditioner, which demodulates the FSK signal, reconstructs the three digital command channels, and extracts a sync pulse. There are two signal conditioner designs: One basic design applies to the low bit rates (1, 20, 100 bauds) and medium bit rates (1000 and 2000 bauds), while the other basic design applies to the high bit rates (10,000 and 100,000 bauds).

Low and Medium Bit Rate Detection

Figure A-4 is a simplified diagram of the signal conditioner (or demodulator). The three command frequencies are separated by three filters and then envelope detected. After passing through the postdetection lowpass filter, the three channels are compared, one against the others, to determine which channel has the greatest output level. The comparator's outputs are sent to the command bit decoder where the state of comparator output is evaluated (state of command data is clocked into the decoder).

The clock pulse is generated by summing the outputs of the envelope detector and passing them through a narrow bandpass filter, a phase shifter, a zero crossing detector, a differentiator, and a one-shot device.

The characteristics of the significant filters in the receiving system are given below:

- The predetection bandpass filter (B_{pre}) 3-dB bandwidth is four times the bit rate (β_r): $B_{pre} = 4\beta_r$.
- The command signal postdetection lowpass filter (B_{post}) cutoff frequency is one-half the bit rate: $B_{post} = 1/2 \beta_r$.

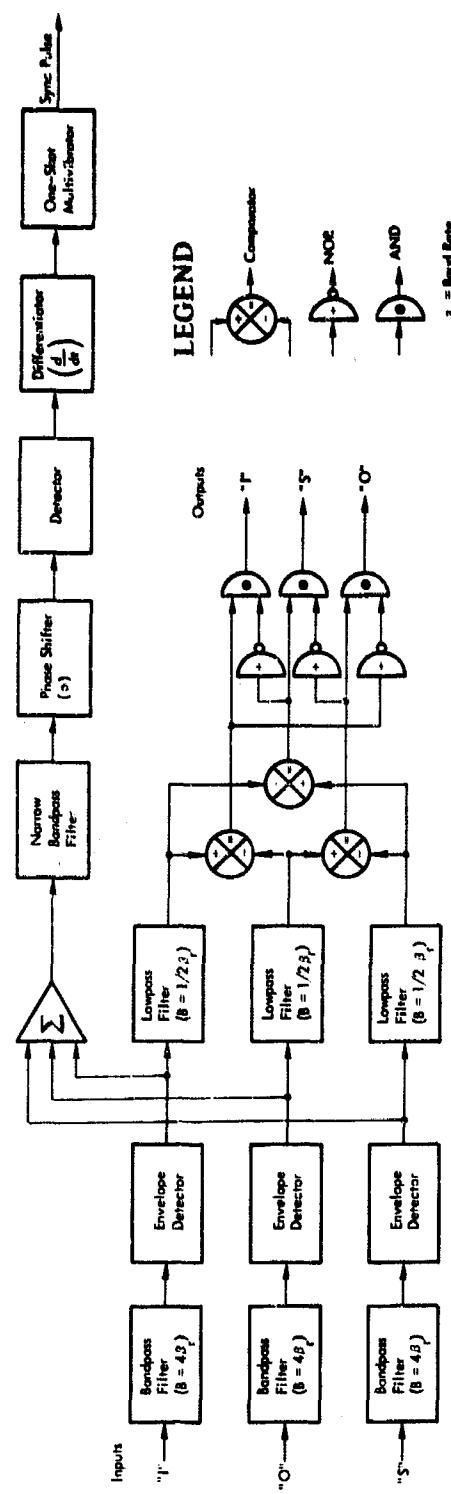


Figure A-4 Typical Signal Conditioner for Low and Medium Bit Rates

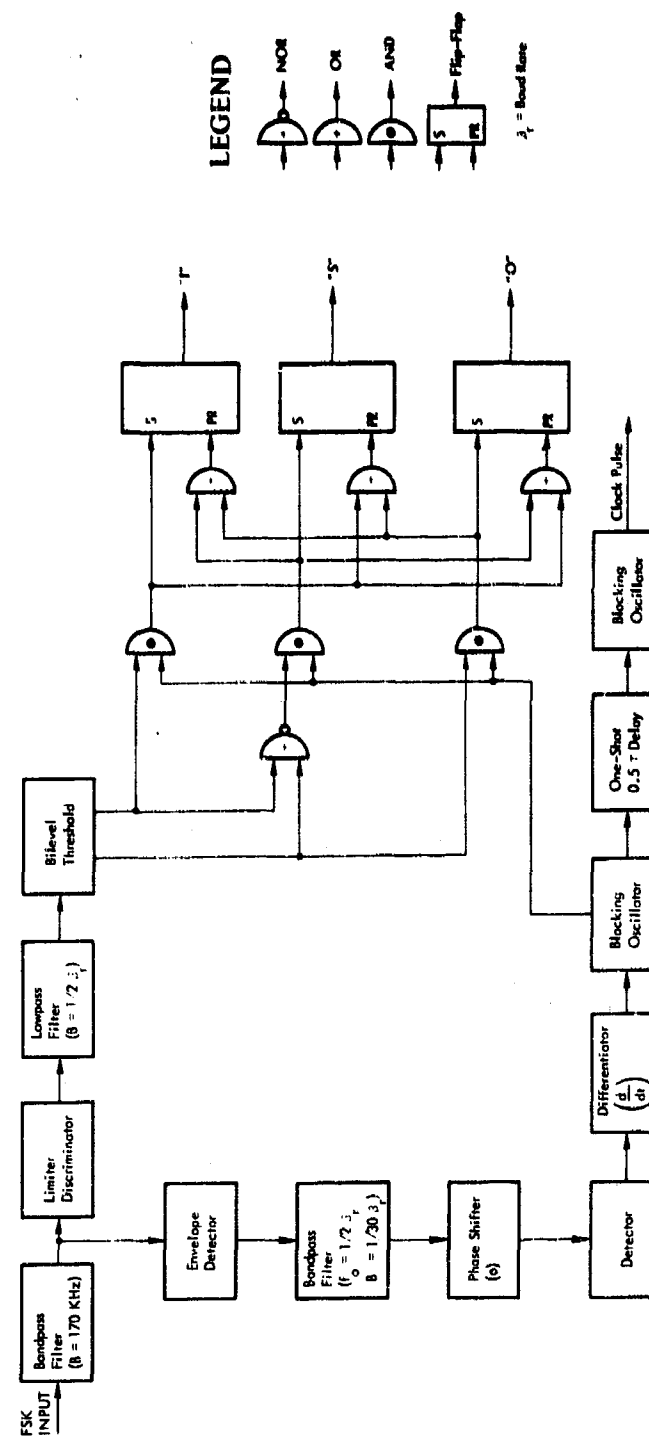


Figure A-5 Typical Signal Conditioner for High Bit Rate

A-7

- The sync signal postdetection bandpass filter (B_s) 3-dB bandwidth is typically one-thirtieth the bit rate: $B_s = 1/30 \beta_r$.
- The center frequency of the sync signal channel (f_o) is one-half the bit rate: $f_o = 1/2 \beta_r$.

High Bit Rate Detection

Figure A-5 is a simplified diagram of the signal conditioner. The filtered FSK input is converted to voltage levels by the limiter discriminator. The voltages are filtered in a postdetection low-pass filter and processed by a two-level threshold device. The output of this threshold device is AND'd with the clock pulse. The bit state is determined by the signal conditioner rather than by the command bit decoder.

The clock circuitry is the same for high bit rates as it is for low and medium bit rates. The expressions for B_{pre} , B_{post} , B_s , and f_o also remain the same. The value for B_{pre} in the high-bit-rate case is 170 kHz.

A.4 ANALYSIS

The following analytical models and supporting analyses were used to determine the system degradation that is caused by sync signal uncertainty. Two basic models for these analyses are described. In this analysis, one model applies to the 100-kbaud system, and the other applies to the remaining baud rates. The model for the low- and medium-rate command options applies to the 10-kbaud option in this case because the significant parameter is the waveform of the detected signal. The 100-kbaud signal is a sinusoidal pulse, the waveform for the other command options is a square wave. Figure A-6 shows the composite timing/command signal waveform.

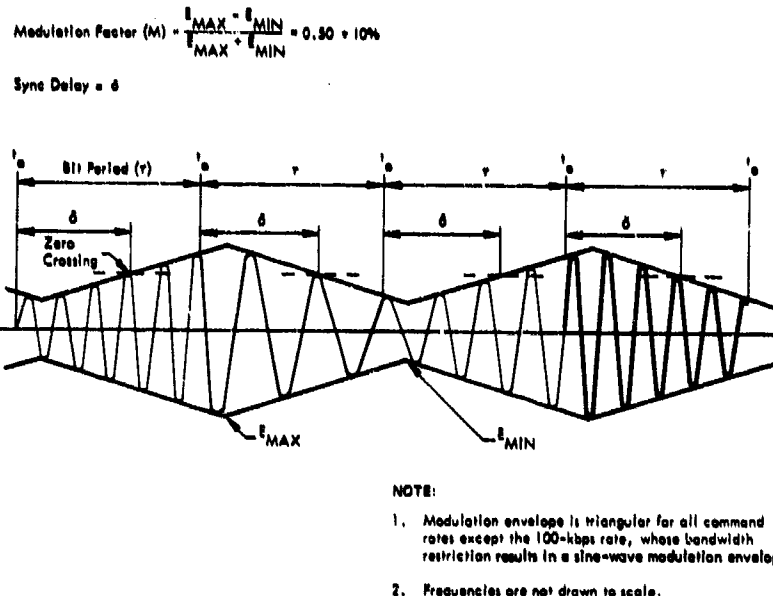


Figure A-6 Typical Command Signal Waveform

A.4.1 Model One (High Bit Rate)

The model for the 100-kbaud rate is shown in Figure A-7. The predetection IF amplifier is very narrow band, removing all but the first set of side bands. The result is narrowband FM that demodulates into a sinusoidal pulse.

The sinusoidal pulse passes through a simple RC lowpass filter with a cutoff frequency at one-half the bit rate. Ideally, after passing through the lowpass filter, the waveform is sampled at its maximum value. Any other sampling point results in a requirement for a greater signal level to guarantee that a bit error rate of one in 10^5 bits is not exceeded.

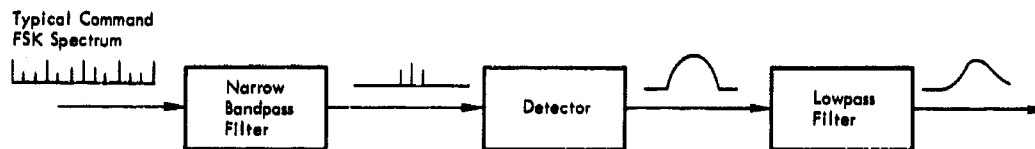


Figure A-7 Model One (for 100-kbaud Bit Rate)

A-9

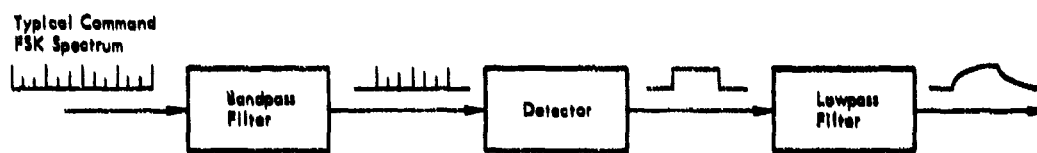


Figure A-8 Model Two (for Bit Rates of 10 kbauds and Less)

A.4.2 Model Two (Low and Medium Bit Rates)

The model for the remaining command rates is shown in Figure A-8. The pre-detection IF amplifier has sufficient bandwidth that enough side bands are passed to permit detection of the waveform as a square wave. This square pulse train is passed through an RC lowpass filter, and is subsequently sampled at (or very near) the filter's peak output. The latter cutoff frequency is one-half the bit rate.

A.4.3 Results of Prior Analysis

The IF SNR required to meet the specified error rate and the sync pulse jitter caused by the presence of gaussian noise is derived in Volume III, Appendix V. Results of that analysis were used to develop the data on sync jitter summarized in Table A-1.

TABLE A-1
IF SIGNAL-TO-NOISE RATIO AND SYNC JITTER

Bit Rate (bauds)	IF SNR (dB)	Jitter (%)
1	14.2	1.6
20	14.2	1.6
100	14.2	1.6
1,000	14.2	1.6
2,000	14.2	1.6
10,000	18.1	1.6
100,000	7.2	1.8

A.4.4 Postdetection Filter Analysis

This section analyzes the jitter output response to two input forcing functions of the postdetection filter. This filter is a simple RC lowpass type whose transfer function is

$$\frac{e_o}{e_{in}}(s) = (sT + 1)^{-1}$$

where

$$T = RC = \omega_o^{-1} = \tau/\pi$$

Input Forcing Functions

The input forcing function is the output of the detector, whether it be an envelope detector or a limiter discriminator.

The forcing function $f(t)$ for the 100-kbaud rate is a sinusoidal pulse

$$f(t) = [\mu(t) - \mu(t-\tau)] \sin(\pi t/\tau)$$

where τ is the bit period.

The forcing function for the remaining bit rates is a square pulse

$$f(t) = \mu(t) - \mu(t-\tau)$$

Output Signal

100 kbauds - Model One. The expression for the portion of the output waveform that includes the maximum is, for $0 \leq t \leq \tau$,

$$e_o(t) = \frac{1}{2} A \mu(t) \left[\exp \left(-\pi \frac{t}{\tau} \right) + \sqrt{2} \sin \left(\pi \frac{t}{\tau} - \frac{\pi}{4} \right) \right]$$

This function is plotted in Figure A-9. By differentiating $e_o(t)$ with respect to time and setting the derivative equal to zero, it is readily determined that e_o is a maximum when $t_m = 0.728\tau$.

If the sampling uncertainty is zero and the sync delay is equal to t_m , then the system is optimum and the signal required to guarantee achievement of the specified error rate is

$$e_o = \frac{1}{2} A_o \left[\exp (-0.728\pi) + \sqrt{2} \sin \left(0.728 - \frac{\pi}{4} \right) \right]$$

A_o is determined by the required SNR.

If the sampling uncertainty is $\pm \epsilon \tau$, then the signal required to achieve the specified bit error rate is, for $0 \leq \epsilon \leq 0.5$,

$$e_o = \frac{1}{2} A \left\{ \exp [-(0.728 \pm \epsilon)\pi] + \sqrt{2} \sin \left[(0.728 \pm \epsilon)\pi - \frac{\pi}{4} \right] \right\}$$

where A , A_o are the filter output signals required to guarantee sampling at the output threshold, e_o .

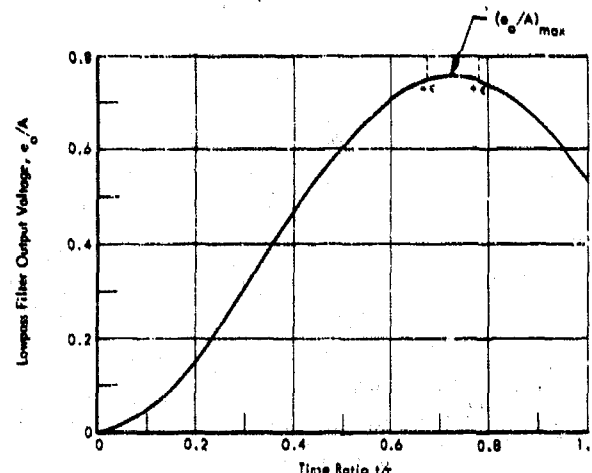


Figure A-9 Waveform at Lowpass Filter Output for Model One

The degradation is thus

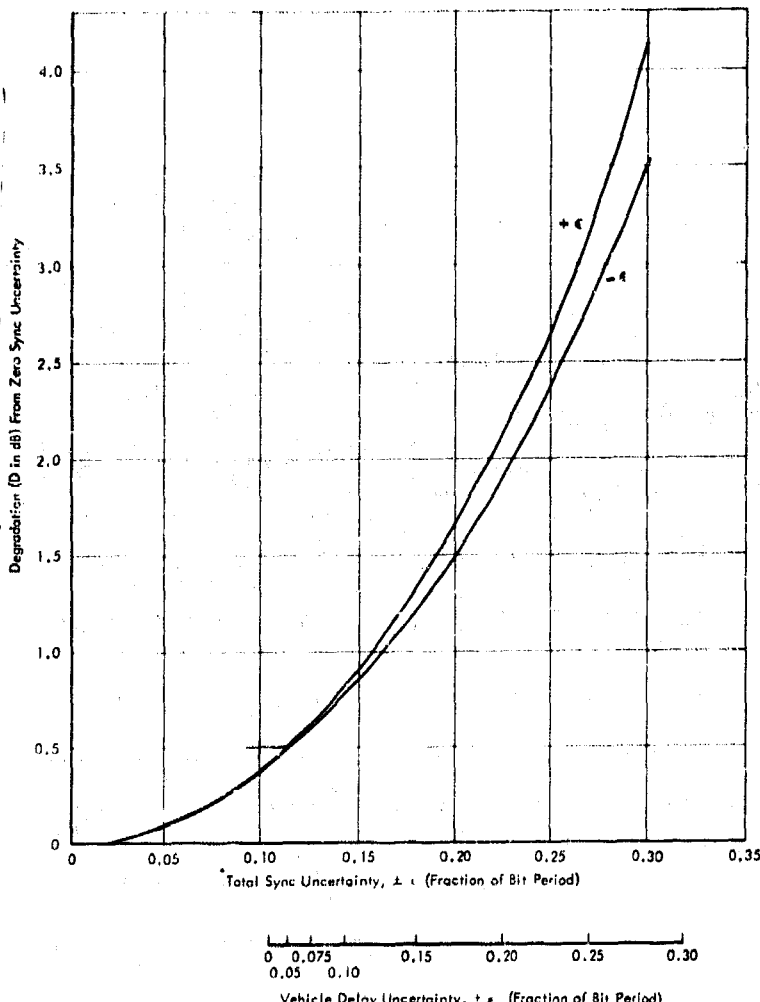
$$D = 20 \log_{10} \left[\exp(-0.728\pi) + \sqrt{2} \sin \left(0.728\pi - \frac{\pi}{4}\right) \right]$$

$$-20 \log_{10} \left\{ \exp [-(0.728 \pm \epsilon)\pi] + \sqrt{2} \sin \left[(0.728 \pm \epsilon)\pi - \frac{\pi}{4}\right] \right\}$$

This function is plotted in Figure A-10. Since the shape of the output waveform is not symmetrical about the peak, both positive and negative sync uncertainty curves are shown in this figure.

The abscissa shows the corresponding values of total (rss) delay uncertainty and of vehicle delay uncertainty (with a ground sync delay uncertainty of $\pm 0.10\tau$ and a sync pulse jitter of $\pm 0.017\tau$). For $\epsilon = \pm 0.113$, corresponding to a vehicle delay uncertainty of $\pm 0.05\tau$, the degradation is 0.52 dB for $+\epsilon$ (worst-case value), and 0.49 dB for $-\epsilon$. Hence, the maximum expected degradation arising from sync delay uncertainties is about 0.5 dB for the assumed vehicle delay uncertainty of $\pm 0.05\tau$.

Although the pulse is asymmetric, the nominal optimum delay (δ) may be taken to be the value corresponding to maximum level (0.728τ) with negligible penalty for all reasonable values of vehicle delay.



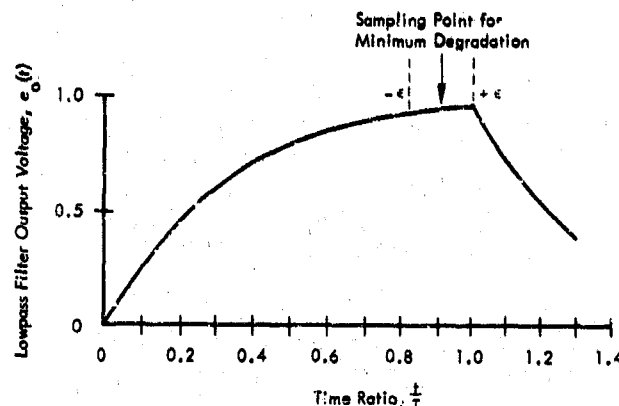
A-10 System Degradation vs Sync Uncertainty for Model One

A-13

10 kbauds and Less - Model Two. The expression for the portion of the output waveform that includes the maximum value is

$$e_o(t) = A \left\{ \mu(t) \left[1 - \exp \left(-\pi \frac{t}{T} \right) \right] - \mu(t-T) \left[1 - \exp \left(-\pi \frac{t-T}{T} \right) \right] \right\}$$

This function is sketched in Figure A-11. The maximum value occurs at the end of the bit period at $t = T$.



A-11 Signal at Output of Lowpass Filter for Model Two

To ensure minimum degradation, the sampling pulse must occur during the bit period as indicated in Figure A-11. The asymmetry of the output waveform must be accounted for.

If the sampling uncertainty is zero, then the system is optimum and the signal required to achieve the specified error rate is

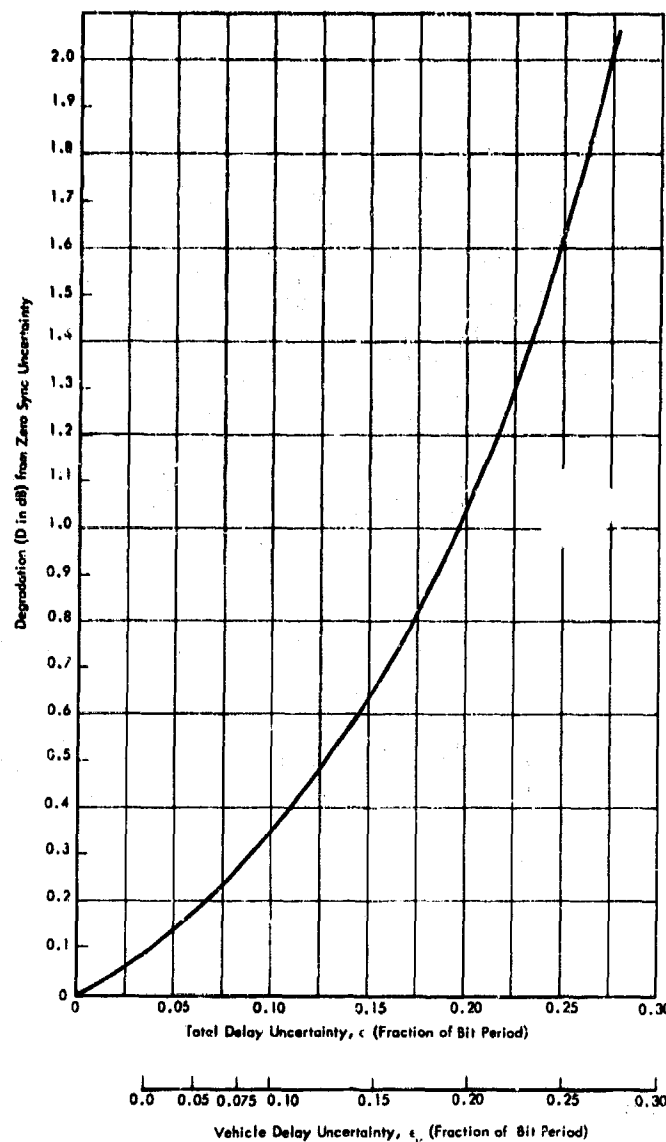
$$e_o = A_o [1 - \exp(-\pi)]$$

If the sampling uncertainty is $\pm \epsilon$, the signal required to achieve the specified bit error rate is, for $0 \leq \epsilon \leq 0.5$,

$$e_o = A \left\{ 1 - \exp [-(1 - 2\epsilon)\pi] \right\}$$

where A and A_o are as for 100 kbauds. The degradation is thus

$$D = 20 \log_{10} [1 - \exp(-\pi)] - 20 \log_{10} \{1 - \exp [-(1 - 2\epsilon)\pi]\}$$



A-12 System Degradation vs Sync Uncertainty for Model Two

This function is plotted in Figure A-12. Because of the gross asymmetry of the filter output waveform, the overall sync delay must be adjusted according to the overall uncertainty of the sync position and, hence, the vehicle uncertainty. The overall time delay is set to $\delta = (1-\epsilon)\tau$.

The abscissa shows the corresponding values of total delay uncertainty and of vehicle delay uncertainty (with a ground sync delay uncertainty of $\pm 0.03\tau$ and a sync pulse jitter of $\pm 0.017\tau$). For $\epsilon = \pm 0.06$, corresponding to a vehicle delay uncertainty of $\pm 0.05\tau$ the degradation is 0.18 dB.

A-15

A. 5 GROUND EQUIPMENT DELAY SETTING

The ground equipment delay must be set to accommodate the existing vehicle design, incorporating a 1-kbaud command system, in accordance with the Lockheed specification (Reference 4). This specification requires that the ground delay be set to a nominal value of $600 \mu\text{sec}$ (0.6τ) with a tolerance of $\pm 15 \mu\text{sec}$ (0.015τ). On the other hand, the SGLS specification for the ground equipment (Reference 5) permits a tolerance of $\pm 0.03\tau$ about the selected delay. This specification anomaly can be simply resolved by reducing the nominal delay in the ground equipment so as to compensate for the SGLS tolerance.

With this particular vehicle, the command system operates in the manner analyzed under Model Two, in the preceding paragraph. That analysis demonstrated that the total nominal delay plus the system variation must equal the bit interval. Referring to Figure A-1, this may be succinctly stated as

$$\delta_G + \epsilon\tau = \tau$$

or, in terms of the component parts of the total delay,

$$\delta_G = (1 - \epsilon)\tau - \alpha_v$$

and

$$\epsilon^2 = \epsilon_J^2 + \epsilon_v^2 + \epsilon_G^2$$

From the above relationships, the compensated ground delay (δ'_G) that corresponds to the increased variation (ϵ') due to the SGLS tolerance (ϵ'_G) is given as

$$\delta'_G = \delta_G - (\epsilon' - \epsilon)\tau$$

and

$$(\epsilon')^2 = \epsilon_J^2 + \epsilon_V^2 + (\epsilon'_G)^2$$

For $\delta_G = 0.6\tau$, $\epsilon_J = 0.017\tau$, $\epsilon_G = 0.015\tau$, $\epsilon'_G = 0.03\tau$, and $\epsilon_V = 0.05\tau$ (assumed), we have $\delta_G = 0.594\tau$.

Since the optimum total sync delay is relatively large for all options of the command system, it is feasible to select a single value for the ground system delay to accommodate these options. It is proposed that the value selected be the one derived above for the only known existing vehicle design. This, of course, will require that appropriate delays be selected for subsequent vehicle designs in accordance with the optimum total system delays derived in the preceding paragraph.

A.6 CONCLUSIONS

(See Paragraph A.2, Technical Summary and Conclusions.)

REFERENCES

1. Baseband Assembly Unit, Technical Manual SCF-TM-3250-3, Philco-Ford WDL, 15 January 1968.
2. Final Design Report, Space Ground Link Subsystem, Vol. I, TRW Systems, February 1967.
3. Functional Test Procedure for Sync Logic Module, Procedure SC-179912, Philco-Ford WDL, 1 November 1967.
4. Development Specification Vehicle-Space Ground Link Subsystem, Lockheed Missiles and Space Company, 5 May 1967.
5. Performance and Design Requirements for the Space-Ground Link System, Philco-Ford WDL-SS-167211, 27 June 1967.

APPENDIX B

DATA DISTORTION DUE TO PHASE NONLINEARITIES AND AMPLITUDE RIPPLE

B. 1 GENERAL

The characteristics of the tandem components in the signal (or sum) channel of the SGLS receiving subsystem have direct bearing upon the quality of the output signal. In particular, the nonlinearity in the phase response and the variations in the amplitude responses of the components could distort the angle-modulated signal to an extent that can render the received information unusable. The effect of the non-ideal, but realistic, component characteristics upon the SGLS performance is an important area of investigation and is thus considered in this distortion analysis.

The alternative techniques available in performing the analysis and the selected approach are discussed below. The selected case for analysis is then identified by carrier designation, signal type, and modulation scheme. Additionally, the combined phase and amplitude characteristics of the tandem components are tabulated. Next, preliminary results are presented in terms of the calculated percent of distortion. Lastly, conclusions based on the specific case analyzed are summarized. For reference purposes, the FM/PM Spectrum Analysis Computer Program is contained in Paragraph B. 6.

B. 2 METHOD OF ANALYSIS

B. 2.1 Selection of Approach

Several alternatives* for analysis are available to assess the effect of phase and amplitude nonlinearities upon the received signal. These alternatives are:

*P. D. Shaft, "Effect of Phase and Amplitude Characteristics on Telemetry Performance," Philco-Ford WDL, Communication Sciences Department Technical Memorandum No. 83, November 1964.

1. Taking the product of the Fourier transform of the signal (signal spectrum) and the transfer function of the component or the network
2. Convolving the signal time function and the impulse time response of the network
3. Making a simplifying assumption such as quasi-stationarity and using alternative 1 or 2
4. Expanding the network characteristics as a polynominal in time or frequency and using one of the above methods
5. Expanding the signal in a Fourier series, modifying the terms by the component or network characteristics, and reconstructing the output waveform by Fourier synthesis

Alternatives 1 and 2, although valid in principle for any case, are mathematically complex except for certain characteristics. Also, these methods require that transfer characteristics are capable of being put in closed mathematical forms. Alternative 3 can lead to erroneous results, as noted by Wang, * except under limited conditions. Alternative 4 is reasonable only when the network characteristics can be expressed with a few terms. Alternative 5 is valid for periodic signals passing through components having any characteristics but has been little used because of the large amount of numerical computation involved. Since a computer program developed at Philco-Ford WDL is available to perform the computations, Alternative 5 was selected.

A comparison of Alternative 2, used by Wang, and Alternative 5 indicates that these two methods are, indeed, similar; the basic difference between them is that Wang combines the harmonic terms before determining the distortion components. An advantage of the WDL method is that curve fitting of the measured phase and gain

*H. S. C. Wang, "Distortion of FM Signals Caused by Channel Phase Nonlinearity and Amplitude Fluctuation," IEEE Transactions on Communication Technology, Vol. CT-14, August 1966.

characteristics is not required since the data are read directly into the computer as discrete points, thereby avoiding errors arising from the "best fit" analytical expressions.

B. 2.2 FM/PM Computer Program

The WDL FM/PM Spectrum Analysis Computer Program simulates frequency or phase modulation of a carrier by use of a periodic waveform. The program calculates the spectrum of the modulated carrier, permits linear filtering of the same, and then demodulates. Linear filtering of the input and the output waveforms is also permitted. The program also analyzes and calculates the spectrum of the output waveform. The computer printout includes plots of the input and output waveforms, if desired, and the amplitude of the input and output spectral components. A more detailed description of the computer program is presented in Paragraph B.6.

B. 2.3 Distortion Criteria

A visual indication of the amount of distortion introduced by the SGLS receiver can be obtained from a comparison of the input and output (time) waveforms. However, a quantitative measure is more desirable, especially when comparing different cases. Two equivalent methods are available to evaluate power distortion: one utilizes the frequency domain and the other the time domain.

In the first method utilizing the frequency domain, the distortion is determined from an analysis of the demodulated output signal by comparing the additional spectral terms arising from the effect of the combined receiver components with the spectral terms in the absence of component distortion. Analytically, the distortion, D, may be written as

$$D \text{ (in percent)} = 100 \times \frac{\sum_{k=0}^M C_k^2}{\sum_{k=0}^M (C_0)_k^2} \quad (\text{B. 2-1})$$

B-3

where the C_k 's are the amplitudes of the additional spectral terms due to distortion, the $(C_0)_k$'s are the amplitudes of the spectral terms in the absence of distortion, and M is the total number of spectral terms considered. When the input signal is a single sinusoid, Equation (B. 2-1) reduces to

$$D \text{ (in percent)} = 100 \times \frac{\sum_{\substack{k=0 \\ k \neq 0}}^M C_k^2}{C_1^2} \quad (\text{B. 2-2})$$

where C_1 is the amplitude of the fundamental.

In the alternate method utilizing time domain, the distortion is determined by comparing the corresponding amplitude samples of the input and output time waveforms (the corresponding amplitudes being paired after accounting for the overall time delay). In this case, the distortion may be written as

$$D \text{ (in percent)} = \frac{100}{2N} \sum_{i=-N}^N (A_i - A'_{i+\tau})^2 \quad (\text{B. 2-3})$$

where A_i and $A'_{i+\tau}$ are the amplitudes of the input and output (time) waveforms at t_i and $t_{i+\tau}$, respectively, and where τ is the time delay, and N is the number of samples per half period.

To obtain a meaningful value of distortion by this procedure, N should be of large enough value that when the time delay is taken into account, the corresponding amplitude samples line up (in time) reasonably well; of course, the better the samples line up, the truer the value of D will be.

B. 3 SGLS CONFIGURATION AND CHARACTERISTICS

B. 3. 1 Configuration for Analysis

Initial analysis is focused upon the most stringent SGLS configuration in terms of signal distortion. Hence, the reception of Carrier 3 is considered in its wideband mode of operation (IF bandwidth of 35 MHz). Since the bandwidth requirements for Carrier 1 and Carrier 2 operation are much less than for Carrier 3, the signals associated with these carriers should be less distorted by the network components than Carrier 3 signals.

The signal and modulation characteristics for Carrier 3 operation are not firmly defined at this time. The following case is believed to be a representative selection for analysis:

A sine wave input having a frequency of 2 MHz with frequency modulation, simulating FM/FM wideband operation.

A modulation index, m , of 5 was used in the analysis; this value fills the IF bandwidth with harmonic terms and also permits a reasonably rapid decrease in the magnitude of the terms beyond the 3-dB IF bandwidth.

B. 3. 2 Phase and Gain Characteristics of Tandem Components

In order to perform a distortion analysis based upon a particular design configuration of the SGLS receiver, it is desirable to have both the phase (β) and amplitude or gain (G) characteristics over the frequency band of interest for each of the tandem components in the sum channel. An alternative form from which the phase characteristic may be determined is the curve of time delay (τ) versus frequency, since by definition $\tau = -d\beta/d\omega$. For our selected approach, measured phase and gain data points versus frequency are preferred as inputs rather than an approximated curve (unless a sufficient number of terms in a power series are used). Thus, the introduction of error at this point in the analysis is avoided.

For wideband operation with Carrier 3, phase and gain data have been obtained for the SGLS solid-state parametric amplifier and the predetection filter assembly with a 35-MHz bandwidth and centered at 129.5 MHz. Data for these components are presented in Table B-1.

The phase and gain characteristics of the other tandem components were omitted at the time the computer runs were made for the wideband cases. In general, these components are wideband devices and are not expected to alter the results appreciably. For example, the 5-pole Chebyshev preselector filter of 120 MHz bandwidth has a calculated linear-phase region of approximately 52 MHz (see Figure B-1), which is much wider than the 35-MHz bandwidth used in the wideband analysis. The validity of this calculated filter characteristic is evident from a comparison of measured and calculated curves for a 3-pole Chebyshev filter having a 2.716-MHz bandwidth (one of the three selectable filters). Figure B-2 indicates good agreement between their linear phase characteristics (linearity being the key property of the phase curve).

B.4 RESULTS OF ANALYSIS

The power distortion was evaluated from the values of C_k^2 and C_1^2 (which are direct computer printouts) and the use of Equation (B.2-2). These values are

$$\sum_{\substack{k=0 \\ k \neq 1}}^{24} C_k^2 \cong 0.0000345 \text{ and } C_1^2 \cong 0.249 \quad (\text{B.4-1})$$

hence,

$$D = \frac{100 \times 0.000345}{0.249} \cong 0.138\% \quad (\text{B.4-2})$$

TABLE B-1
MEASURED PHASE AND LOSS CHARACTERISTICS OF
PREDETECTION FILTER ASSEMBLY
($f_0 = 129.5$ MHz, $BW_{3dB} = 35.0$ MHz)

f MHz	Δf MHz	β deg	L dB	f MHz	Δf MHz	β deg	L dB	f MHz	Δf MHz	β deg	L dB	f MHz	Δf MHz	β deg	L dB
110.0	-19.5	201.06	4.7	120.0	-9.5	90.48	.06	130.0	0.5	-4.55	0	140.0	10.5	-100.85	.20
110.5	-19.0	195.96	4.3	120.5	-9.0	85.33	.01	130.5	1.0	-9.09	0	140.5	11.0	-106.35	.25
111.0	-18.5	190.72	3.9	121.0	-8.5	80.25	0	131.0	1.5	-13.64	0	141.0	11.5	-111.83	.31
111.5	-18.0	185.37	3.5	121.5	-8.0	75.23	0	131.5	2.0	-18.18	0	141.5	12.0	-117.49	.4
112.0	-17.5	179.95	3.0	122.0	-7.5	70.26	0	132.0	2.5	-22.70	0	142.0	12.5	-123.24	.5
112.5	-17.0	174.51	2.7	122.5	-7.0	65.35	0	132.5	3.0	-27.20	0	142.5	13.0	-129.06	.6
113.0	-16.5	168.99	2.3	123.0	-6.5	60.49	0	133.0	3.5	-31.70	0	143.0	13.5	-134.93	.71
113.5	-16.0	163.32	2.1	123.5	-6.0	55.66	0	133.5	4.0	-36.11	0	143.5	14.0	-140.83	.82
114.0	-15.5	157.68	1.7	124.0	-5.5	50.87	0	134.0	4.5	-40.74	0	144.0	14.5	-146.73	1.0
114.5	-15.0	152.01	1.4	124.5	-5.0	46.15	0	134.5	5.0	-45.36	0	144.5	15.0	-152.62	1.2
115.0	-14.5	146.31	1.2	125.0	-4.5	41.49	0	135.0	5.5	-50.06	0	145.0	15.5	-158.49	1.5
115.5	-14.0	140.60	1.0	125.5	-4.0	36.85	0	135.5	6.0	-54.88	0	145.5	16.0	-164.31	1.8
116.0	-13.5	134.88	0.8	126.0	-3.5	32.21	0	136.0	6.5	-59.76	0	146.0	16.5	-170.06	2.2
116.5	-13.0	129.15	0.7	126.5	-3.0	27.58	0	136.5	7.0	-64.67	0	146.5	17.0	-176.70	2.6
117.0	-12.5	123.42	0.58	127.0	-2.5	22.94	0	137.0	7.5	-69.62	0	147.0	17.5	-181.19	3.0
117.5	-12.0	117.72	0.46	127.5	-2.0	18.31	0	137.5	8.0	-74.62	0	147.5	18.0	-186.50	3.5
118.0	-11.5	112.06	.33	128.0	-1.5	13.70	0	138.0	8.5	-79.70	.02	148.0	18.5	-191.63	3.9
118.5	-11.0	106.51	.28	128.5	-1.0	9.11	0	138.5	9.0	-84.85	.05	148.5	19.0	-196.58	4.4
119.0	-10.5	101.07	.20	129.0	-0.5	4.55	0	139.0	9.5	-90.09	.10	149.0	19.5	-201.37	4.9
119.5	-10.0	95.72	.14	129.5	0	0	0	139.5	10.0	-95.42	.14	149.5	20.0	-206.23	5.4
												150.0	20.5	-210.48	5.9

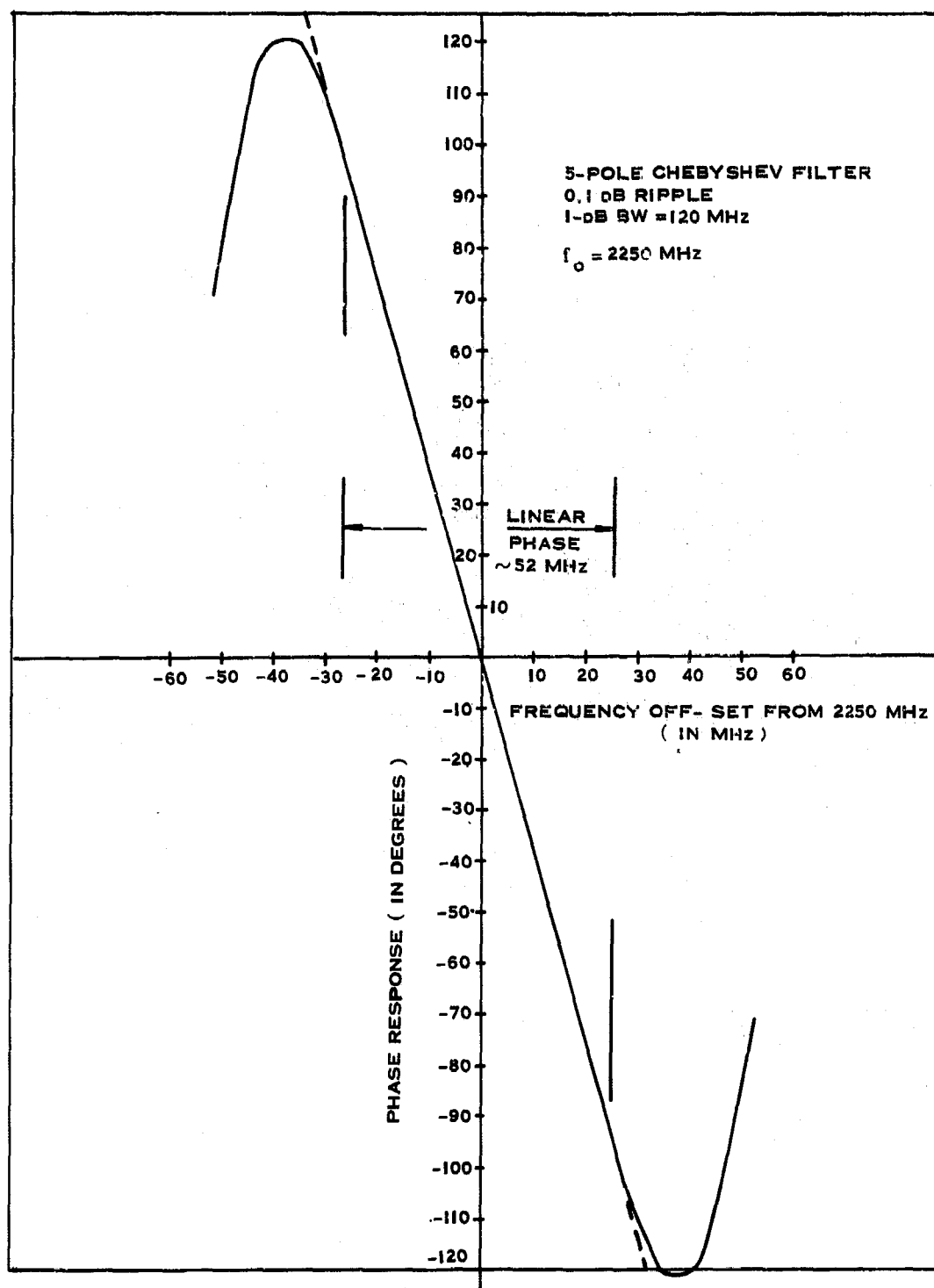


Figure B-1 Calculated Phase Characteristic of 5-Pole Chebyshev Preselector Filter

B-8

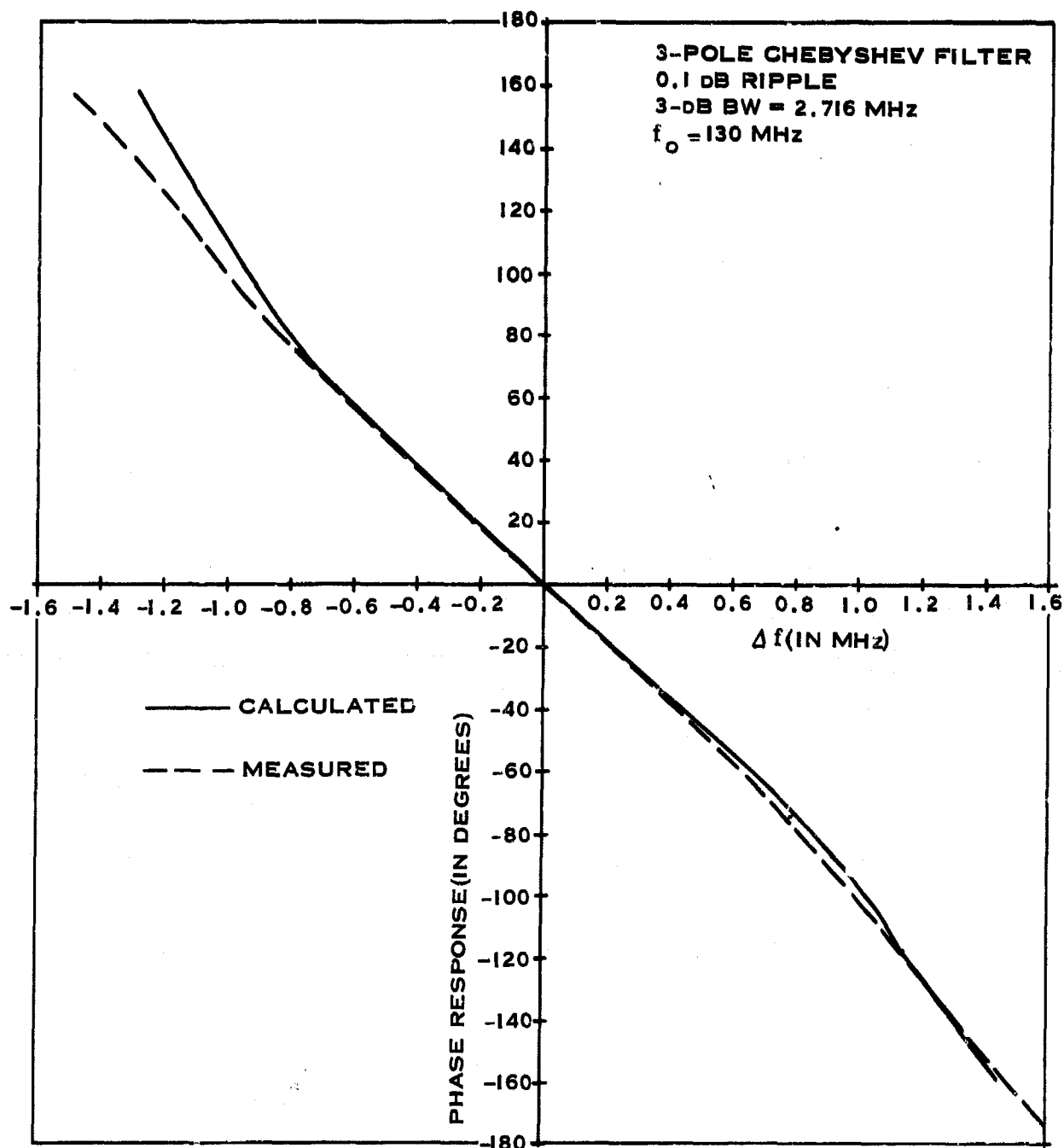


Figure B-2 Measured and Calculated Phase Characteristic of 3-Pole Chebyshev Predetection Filter Assembly
with $B_{3dB} = 2.716$ MHz

B-9

B. 5 CONCLUSIONS

The distortion analysis presented in the preceding sections indicates that the power distortion for Carrier 3 (utilizing the 35-MHz IF bandwidth) is about 0.14% for wideband FM/FM operation with a 2-MHz sine-wave signal when a modulation index, m , of 5 was used. (This value of m was selected since the RF spectrum embraces the IF bandwidth, with a rapid decrease in the amplitude of the terms outside the band.)

The above value of distortion is based upon the combined phase and gain characteristics of the amplifier and the 35-MHz bandwidth predetection filter.

B. 6 THE FM/PM SPECTRUM ANALYSIS COMPUTER PROGRAM

B. 6.1 General

The WDL FM/PM Spectrum Analysis Computer Program essentially performs the simulation of the transmission of a phase- or frequency-modulated signal in four steps as follows:

1. Spectrum-analyzes the modulated signal
2. Modifies the carrier spectrum with the characteristics of the receiving filter-mixer-amplifier chain (hereafter referred to as the filter)
3. Demodulates the carrier
4. Spectrum-analyzes the demodulated signal

The phase-modulation case is described below. For the frequency-modulation case, the signal is first integrated before phase modulating the carrier.

B.6.2 Spectral Analysis of Transmitted Signal

Let $E_s(t)$ be the information signal and be periodic in time with period T . If a carrier of unit amplitude and frequency f_c is phase modulated with $E_s(t)$, the resulting RF signal [$E_1(t)$] can be expanded in a Fourier series as follows:

$$E_1(t) = \cos [2\pi f_c t + E_s(t)] = \sum_{k=-\infty}^{\infty} d_k \cos \left(2\pi f_c t + \frac{2\pi k}{T} t + \beta_k \right) \quad (B.6-1)$$

The PM spectrum of $E_s(t)$ consists of the amplitude d_k and the phase β_k associated with frequency shifts k/T . The complex coefficients of the Fourier series can be found from

$$d_k e^{j\beta_k} = \frac{1}{T} \int_{-\frac{T}{2}}^{\frac{T}{2}} e^{jE_s(t)} e^{-j2\pi \frac{k}{T} t} dt \quad (B.6-2)$$

In real form, this is

$$d_k \cos \beta_k = \frac{1}{T} \int_{-\frac{T}{2}}^{\frac{T}{2}} [\cos E_s(t) \cos \frac{2\pi k}{T} t + \sin E_s(t) \sin \frac{2\pi k}{T} t] dt \quad (B.6-3)$$

$$d_k \sin \beta_k = \frac{1}{T} \int_{-\frac{T}{2}}^{\frac{T}{2}} [-\cos E_s(t) \sin \frac{2\pi k}{T} t + \sin E_s(t) \cos \frac{2\pi k}{T} t] dt \quad (B.6-4)$$

To use these formulas for digital computation, the integrals are replaced by sums. The time scale over a period T is first divided into $2N$ segments of width Δt . The area under the integrant is then replaced by $2N + 1$ rectangles as shown in Figure B-3. The widths of the rectangles are Δt except for the first and last rectangles which have widths of $\Delta t/2$. The integral then becomes the sum of the areas of the rectangles.

$$d_k \cos \beta_k = \frac{1}{T} \sum_{i=-N}^{N'} \left[\cos E_s(t_i) \cos \frac{\pi ik}{N} + \sin E_s(t_i) \sin \frac{\pi ik}{N} \right] \Delta t$$

$$= \frac{1}{2N} \sum_{i=-N}^{N'} \left[\cos E_s(t_i) \cos \frac{\pi ik}{N} + \sin E_s(t_i) \sin \frac{\pi ik}{N} \right] \quad (B.6-5)$$

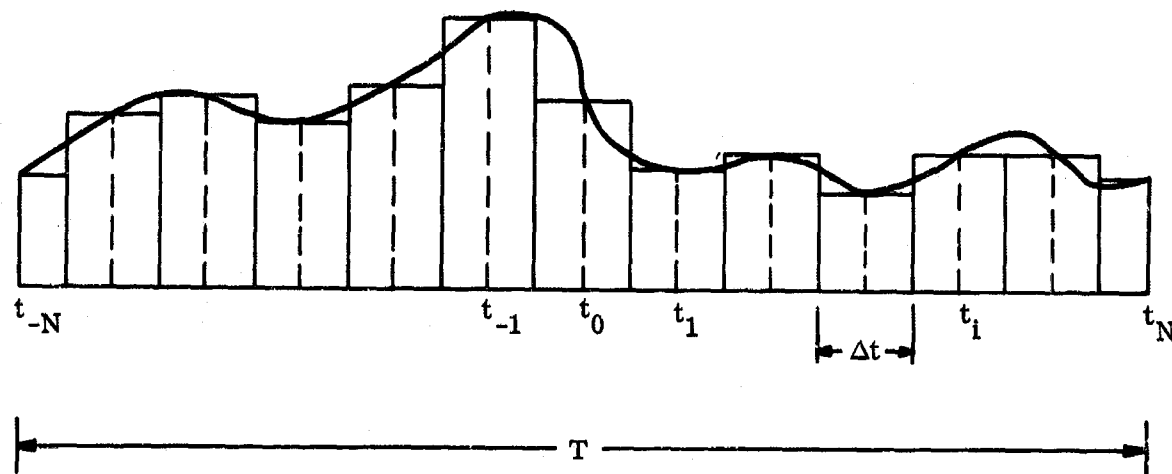


Figure B-3 Partitioning of Integrant Waveform

$$d_k \sin \beta_k = \frac{1}{2N} \sum_{i=-N}^N [-\cos E_s(t_i) \sin \frac{\pi ik}{N} + \sin E_s(t_i) \cos \frac{\pi ik}{N}] \quad (B.6-6)$$

where the prime of Σ' means that the first and last terms have half weights.

Finally, d_k and β_k are computed from

$$d_k = \sqrt{(d_k \cos \beta_k)^2 + (d_k \sin \beta_k)^2} \quad (B.6-7)$$

$$\beta_k = \arctan \left[(d_k \sin \beta_k) / (d_k \cos \beta_k) \right] \quad (B.6-8)$$

The computer computes the d_k and β_k for $-M \leq k \leq M$. Therefore $2M + 1$ spectral lines are computed.

B.6.3 Spectrum Modification

After the RF signal has been spectral analyzed, the computer program then modifies the RF spectrum by the filter (element) characteristics. The filter gain and phase responses are stored in the memory in tabular form as functions of the frequencies. For each spectral component at $f_c + \frac{k}{T}$, the d_k is multiplied by the filter gain, and the phase at $f_c + \frac{k}{T}$ is added to β_k . Linear interpolation is performed when $f_c + \frac{k}{T}$ is not one of the tabulated frequencies.

B. 6.4 Demodulation

The third step is to perform the demodulation. The program assumes perfect phase demodulation is attained; that is, the demodulated output $E_0(t)$ is directly proportional to the phase of the input RF signal. Because of the possible nonlinear behavior of the filter, the modified RF signal (denoted by $E_2(t)$) may not have a constant envelope.

Therefore, the RF signal is assumed to be amplitude as well as phase modulated. This is expressed by

$$E_2(t) = \operatorname{Re} A(t) e^{j(2\pi f_c t + E_0(t))}$$

$$= \operatorname{Re} \sum_{k=-M}^M d'_k e^{j\beta'_k} e^{j(2\pi f_c t + 2\pi \frac{k}{T} t)} \quad (\text{B. 6-9})$$

where the primes on d'_k and β'_k denote the modified d_k and β_k respectively.
At $t = t_i$,

$$A(t_i) e^{jE_0(t_i)} = \sum_{k=-M}^M d'_k e^{j\beta'_k} e^{j\frac{2\pi k}{T} t_i} \quad (\text{B. 6-10})$$

or in real form:

$$A(t_i) \cos E_0(t_i) = d'_0 \cos \beta'_0 + \sum_{k=1}^M \left[(d'_k \cos \beta'_k + d'_{-k} \cos \beta'_{-k}) \right. \\ \left. \cdot \cos \frac{\pi ik}{N} + (-d'_k \sin \beta'_k + d'_{-k} \sin \beta'_{-k}) \cdot \sin \frac{\pi ik}{N} \right] \quad (\text{B. 6-11})$$

$$A(t_i) \sin E_0(t_i) = d'_0 \sin \beta'_0 + \sum_{k=1}^M \left[(d'_k \sin \beta'_k + d'_{-k} \sin \beta'_{-k}) \cos \frac{\pi ik}{N} + (d'_k \cos \beta'_k - d'_{-k} \cos \beta'_{-k}) \sin \frac{\pi ik}{N} \right] \quad (B.6-12)$$

The demodulated signal $E_0(t)$ is computed by

$$E_0(t_i) = \arctan \left[A(t_i) \sin E_0(t_i) / A(t_i) \cos E_0(t_i) \right] \quad (B.6-13)$$

The $E_0(t_i)$'s calculated for $-N \leq i \leq N$ represent the sampled voltage of the demodulated signal waveform over a period T with the sampling interval Δt . The results are plotted to show the demodulated signal visually.

B.6.5 Spectral Analysis of Output Signal

The fourth step is to analyze the output signal into its spectral components. The procedure is similar to step 1. The output of this step also includes the relative power contained in each harmonic, which facilitates the distortion study when the input signal is a sine wave.

APPENDIX C

ANGLE TRACKING ACCURACY

C.1 INTRODUCTION

This appendix presents an analysis of the angle tracking accuracy of the SGLS high-gain and low-gain antenna configurations. Paragraph C.2 describes the sources and types of errors and discusses the methods of combining the errors to determine the overall tracking accuracy.

Paragraph C.3 summarizes the specific sources, types, and magnitudes of errors that are of interest in the two antenna configurations. The results of the analysis are presented in Table C-1.

TABLE C-1
ANGLE TRACKING ACCURACY
(All values in milliradians)

Antenna Axis	High-Gain Antenna		Low-Gain Antenna	
	Bias Error (rms)	Noise Error (rms)	Bias Error (rms)	Noise Error (rms)
Elevation ¹	<0.4	<0.4	<0.3	<0.5
Azimuth ²	<0.9	<0.3	<0.2	<1.1

¹For elevation angles greater than 5° and less than 85°.

²For elevation angles less than 70°.

Lastly, a discussion of each error source is presented in Paragraphs C.4 through C.8 to show the rationale used in deriving individual error contributions.

Special terms used in this appendix are defined as follows:

Tracking accuracy	The accuracy with which the readout devices indicate the true positioning angle to the spacecraft.
Systematic error	An error that is a function of any system parameter susceptible to calibration (or a known function) and capable of removal from the data.
Bias error	An error which is nonvarying over short periods of time but which cannot be compensated. A short period of time will be considered as the duration of the pass.
Noise error	An error that occurs in a random fashion or whose source is of a random nature.

C.2 GENERAL DESCRIPTION

C.2.1 Sources and Types

The sources of angle tracking errors are grouped as follows:

- RF
- Propagation
- Servo
- Mechanical
- Calibration

The error contribution for each source is further identified as a systematic, bias, or noise error. (See Definitions.) Systematic errors are known and are assigned positive or negative values. Bias and noise errors are rms values since they are of a random nature.

In general, errors in both azimuth and elevation will vary with antenna elevation angle; therefore, errors are considered for elevation angles between 0 and 90°.

C.2.2 Combinative Methods

The individual errors must be combined to produce the total noise, bias, and systematic error, as indicated below:

- a. Bias errors. Each bias error is assumed to be a random variable independent of all other bias errors. The total bias error is, therefore, obtained by summing the variance of the random variables. The resultant sum yields the variance of the total bias error. The rms error is then obtained by taking the square root of this quantity.
- b. Noise errors. Noise errors are combined in the same manner as bias errors.

- c. **Systematic errors.** Systematic errors are known and, as such, are combined arithmetically with consideration given to the sense of the error. For example, error sense is chosen as follows:
- Dish sag is negative error.
 - Feed sag is positive error.
 - Servo lag may be either positive or negative.

C.3 SUMMARY OF TRACKING ERRORS

The rms noise and bias tracking errors and the systematic error versus antenna elevation angle are presented in Tables C-2 through C-5. The total error shown at the bottom of each column in the tables is also plotted versus elevation angle in Figures C-1 through C-4. For reference, error tables and graphs are indexed as follows:

<u>Antenna</u>	<u>Axis</u>	<u>Table</u>	<u>Figure</u>
High gain	Azimuth	C-2	C-1
High gain	Elevation	C-3	C-2
Low gain	Azimuth	C-4	C-3
Low gain	Elevation	C-5	C-4

The error tables present the individual error sources under their appropriate headings. Error values are listed under antenna elevation angle and error type, i.e., systematic, bias, or noise.

Examination of the error curves (Figures C-1 through C-4) reveals that the total elevation errors are well below 1 mrad for all elevation angles. Azimuth errors are also below 1 mrad for elevation angles up to about 70° but increase rapidly thereafter. This large increase is due to the secant (elevation angle) correction factor which must be used on most errors in the azimuth axis.

Comparison of the low-gain and high-gain errors shows that noise errors exceed bias errors for the low-gain antenna, whereas the reverse is true for the high-gain antenna. This is due, for the most part, to the large polarization and collimation errors (bias) assigned to the high-gain antenna, plus the phase shift and amplitude unbalance errors which occur for the high-gain antenna and not for the low-gain antenna. On the other hand, the receiver noise error for the low-gain antenna exceeds that for the high-gain.

Since systematic error is correctable, it is not considered as tracking error and is therefore not included on the graphs.

TABLE C-2
HIGH-GAIN ANTENNA AZIMUTH ERRORS

S = Systematic Error B = 1 σ Bias Error N = RMS Noise Error † = Negligible, under 0.01 mrad * = Not Applicable	Azimuth Error (mrad)															
	El. = 5°			El. = 25°			El. = 45°			El. = 65°			El. = 85°			
	S	B	N	S	B	N	S	B	N	S	B	N	S	B	N	
Radio-Frequency Errors																
1. Noise (20-dB SNR in 1-kHz BW)	*	*	0.04	*	*	0.04	*	*	0.06	*	*	0.09	*	*	0.46	
2. Amplitude Unbalance (0.3 dB)	*	0.06	*	*	0.06	*	*	0.08	*	*	0.14	*	*	0.69	*	
3. Phase Shift (Pre: 5°; Post: 10°)	*	0.02	*	*	0.02	*	*	0.03	*	*	0.05	*	*	0.23	*	
Propagation Errors																
4. Radome Refraction	*	*	0.05	*	*	0.06	*	*	0.07	*	*	0.12	*	*	0.57	
5. Atmospheric Propagation	*	*	*	*	*	*	*	*	*	*	*	*	*	*	*	
6. Multipath	*	*	†	*	*	†	*	*	†	*	*	†	*	*	†	
Servo Errors																
7. Lag (Alt. 500 nmi, E _{max} 85°)	†	*	*	†	*	*	†	*	*	†	*	*	±1.05	*	*	
8. Bias	*	0.03	*	*	0.03	*	*	0.04	*	*	0.07	*	*	0.34	*	
Mechanical																
9. Structure and Feed	*	*	*	*	*	*	*	*	*	*	*	*	*	*	*	
10. Acceleration (Alt. 500 nmi, E _{max} 85°)	*	†	*	*	†	*	*	†	*	*	†	*	*	†	†	
Calibration																
11. Orthogonality	*	N	*	*	N	*	*	0.01	*	*	0.02	*	*	0.11	†	
12. Mislevel	*	0.01	*	*	0.06	*	*	0.12	*	*	0.26	*	*	1.34	*	
13. Encoder Error	*	*	0.02	*	*	0.02	*	*	0.02	*	*	0.02	*	*	0.02	
14. Collimation	*	0.11	*	*	0.12	*	*	0.16	*	*	0.26	*	*	1.26	*	
15. Instrumentation (Alt. 500 nmi, E _{max} 85°)	*	†	*	*	†	*	*	†	*	*	†	*	*	0.44	*	
16. Polarization	*	0.20	*	*	0.22	*	*	0.28	*	*	0.47	*	*	2.30	*	
TOTAL ERROR		†	0.24	0.07	†	0.26	0.075	†	0.36	0.094	†	0.65	0.151	±1.05	4.50	0.733

S = Systematic Error
B = 1 σ Bias Error
N = RMS Noise Error
† = Negligible, under 0.01 mrad
* = Not Applicable

Radio-Frequency Errors
1. Noise (20-dB SNR in 1-kHz BW)
2. Amplitude Unbalance (0.3 dB)
3. Phase Shift (Pre: 5°; Post: 10°)

Propagation Errors
4. Radome Refraction
5. Atmospheric Propagation
6. Multipath

Servo Errors
7. Lag (Alt. 500 nmi, E_{max} 85°)
8. Bias

Mechanical
9. Structure and Feed
10. Acceleration (Alt. 500 nmi, E_{max} 85°)

Calibration
11. Orthogonality
12. Mislevel
13. Encoder Error
14. Collimation
15. Instrumentation (Alt. 500 nmi, E_{max} 85°)
16. Polarization

TOTAL

TABLE C-3
HIGH-GAIN ANTENNA ELEVATION ERRORS

S = Systematic Error B = 1 σ Bias Error N = RMS Noise Error † = Negligible, under 0.01 mrad * = Not Applicable	Elevation Error (mrad)															
	El. = 5°			El. = 25°			El. = 45°			El. = 65°			El. = 85°			
	S	B	N	S	B	N	S	B	N	S	B	N	S	B	N	
Radio-Frequency Errors																
1. Noise (20-dB SNR in 1-kHz BW)	*	*	0.04	*	*	0.04	*	*	0.04	*	*	0.04	*	*	0.04	
2. Amplitude Unbalance (0.3 dB)	*	0.06	*	*	0.06	*	*	0.06	*	*	0.06	*	*	0.06	*	
3. Phase Shift (Pre: 5°; Post: 10°)	*	0.02	*	*	0.02	*	*	0.02	*	*	0.02	*	*	0.02	*	
Propagation Errors																
4. Radome Refraction	*	*	0.05	*	*	0.05	*	*	0.05	*	*	0.05	*	*	0.05	
5. Atmospheric Propagation	+3.0	*	0.32	+0.80	*	0.08	+0.4	*	0.02	+0.3	*	0.01	+0.2	*	†	
6. Multipath	*	*	0.05	*	*	†	*	*	†	*	*	†	*	*	†	
Servo Errors																
7. Lag (Alt. 500 nmi, E _{max} 85°)	†	*	*	†	*	*	†	*	*	†	*	*	±0.15	*	*	
8. Bias		0.03			0.03			0.03			0.03			0.03		
Mechanical																
9. Structure and Feed	-0.80	*	*	-0.73	*	*	-0.57	*	*	-0.34	*	*	-0.09	*	*	
10. Acceleration (Alt. 500 nmi, E _{max} 85°)	*	†	*	*	†	*	*	†	*	*	†	*	*	†	*	
Calibration																
11. Orthogonality	*	†	*	*	†	*	*	†	*	*	†	*	*	†	*	
12. Mislevel	*	0.12	*	*	0.12	*	*	0.12	*	*	0.12	*	*	0.12	*	
13. Encoder Error	*	*	0.02	*	*	0.02	*	*	0.02	*	*	0.02	*	*	0.02	
14. Collimation	*	0.11	*	*	0.11	*	*	0.11	*	*	0.11	*	*	0.11	*	
15. Instrumentation (Alt. 500 nmi, E _{max} 85°)	*	†	*	*	†	*	*	†	*	*	†	*	*	0.04	*	
16. Polarization	*	0.30	*	*	0.30	*	*	0.30	*	*	0.30	*	*	0.30	*	
TOTAL ERROR		+2.20	0.35	0.33	+0.07	0.35	0.10	-0.17	0.35	0.07	-0.04	0.35	0.07	+3.35 to -0.04	0.35	0.07

Radio-Frequency Errors
1. Noise (20-dB SNR in 1-kHz BW)
2. Amplitude Unbalance (0.3 dB)
3. Phase Shift (Pre: 5°; Post: 10°)

Propagation Errors
4. Radome Refraction
5. Atmospheric Propagation
6. Multipath

Servo Errors
7. Lag (Alt. 500 nmi, E_{max} 85°)
8. Bias

Mechanical
9. Structure and Feed
10. Acceleration (Alt. 500 nmi, E_{max} 85°)

Calibration
11. Orthogonality
12. Mislevel
13. Encoder Error
14. Collimation
15. Instrumentation (Alt. 500 nmi, E_{max} 85°)
16. Polarization

TOTAL

TABLE C-4
LOW-GAIN ANTENNA AZIMUTH ERRORS

El. = 85°			Azimuth Error (mrad)																	
S	B	N	El. = 5°			El. = 25°			El. = 45°			El. = 65°			El. = 85°					
			S	B	N	S	B	N	S	B	N	S	B	N	S	B	N			
*	*	0.46																		
*	0.69	*																		
*	0.33	*																		
*	*	0.57																		
*	*	*																		
*	*	*																		
±1.05	*	*																		
*	0.34	*																		
*	*	*																		
*	*	*																		
*	0.11	*																		
*	1.34	*																		
*	*	0.02																		
*	1.26	*																		
*	0.44	*																		
*	2.30	*																		
±1.05	4.50	0.733																		
TOTAL ERROR															±0.09	0.07	0.85	±0.14	0.89	4.1

TABLE C-5
LOW-GAIN ANTENNA ELEVATION ERRORS

El. = 85°			Elevation Error (mrad)															
			El. = 5°			El. = 25°			El. = 45°			El. = 65°			El. = 85°			
N	S	B	S	B	N	S	B	N	S	B	N	S	B	N	S	B	N	
0.04	*	*	*	*	0.04													
*	*	*	0.06	*	*													
*	*	*	0.02	*	*													
0.05	*	*	*	*	0.05													
0.01	+0.2	*	*	*	*													
*	*	*	*	*	*													
*	±0.15	*	*	*	*													
*	0.03																	
*	-0.09	*	*	*	*													
*	*	*	*	*	*													
*	0.12	*	*	*	*													
0.02	*	*	*	*	0.02													
*	*	*	0.11	*	*													
*	*	*	0.04	*	*													
*	*	*	0.30	*	*													
0.07	+0.35 to -0.04	0.35	0.07															
+	0.04	0.17	0.82	+0.84	0.17	0.37	+0.43	0.17	0.36	+0.32	0.17	0.36	+0.71 to -0.31	0.18	0.36			

C-5/C-6



At first glance, the azimuth error at high elevation angles seems excessive. However, most passes track at the lower elevation angles where the error is low and, for those passes where elevation angle exceeds 70°, the duration of time that the angle is above 70° is small compared to total pass duration. Thus, only a small part of the azimuth angle data is degraded by error in excess of 1 mrad.

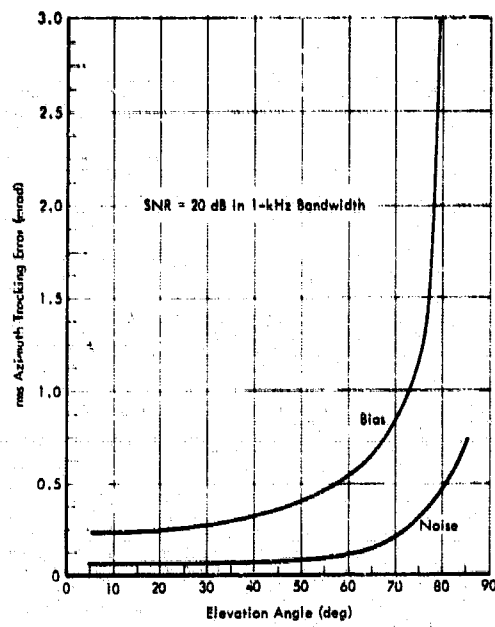


Figure C-1 Azimuth Error vs Elevation Angle (High-Gain Antenna)

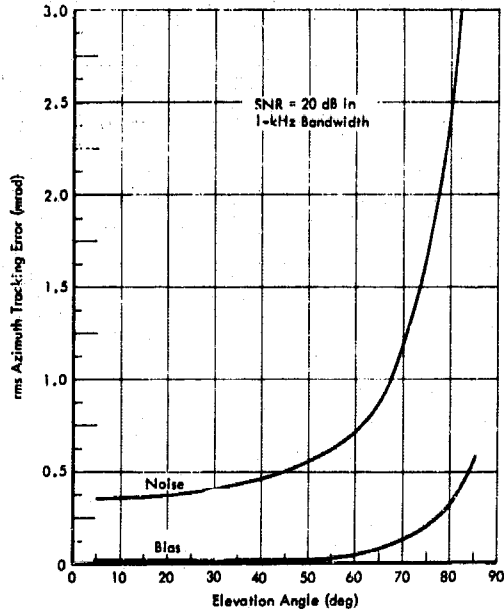


Figure C-3 Azimuth Error vs Elevation Angle (Low-Gain Antenna)

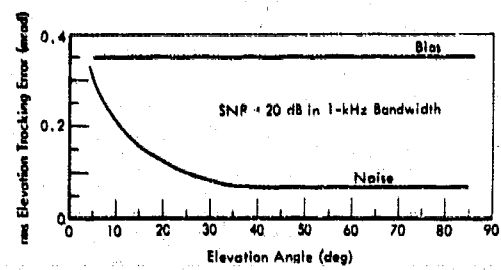


Figure C-2 Elevation Error vs Elevation Angle (High-Gain Antenna)

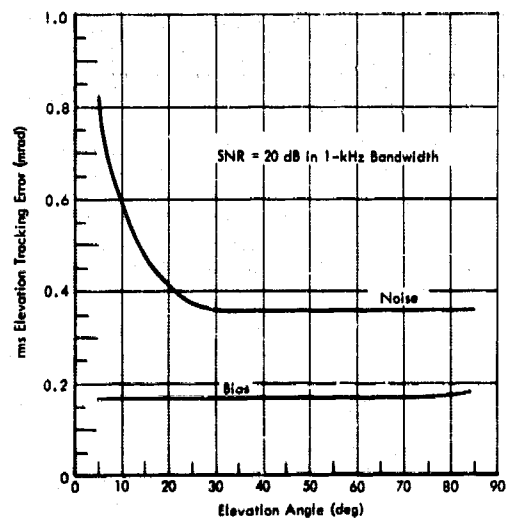


Figure C-4 Elevation Error vs Elevation Angle (Low-Gain Antenna)

C.4 THERMAL ERRORS

This analysis considers the error contribution of receiver thermal noise to angle tracking for both the simultaneous lobing high-gain SGLS configuration and the conical-scan low-gain configuration. In each case both coherent (phase-lock) and correlation detection techniques are analyzed to obtain tracking error due to thermal noise.

To make the mathematics manageable and still obtain valid results for the specific SGLS System application, the analysis and equations utilized assume that:

- Received RF signals are of constant peak amplitude, with information contained in either frequency or phase modulation.
- IF passbands are square (i. e., ignore rolloff).
- Noise is white gaussian throughout the passband.
- Automatic gain control eliminates any variation of servo system gain with signal strength.

Results are plotted on graphs showing rms angle error as a function of signal-to-noise ratio in the tracking bandwidth for phase-lock tracking, and in the IF bandwidth for correlation tracking.

C.4.1 High-Gain Configuration

Angle tracking by the high-gain SGLS configuration utilizes amplitude comparison simultaneous lobing techniques with selectable coherent or correlation detection modes available. Each of these detection modes will be analyzed in the following paragraphs.

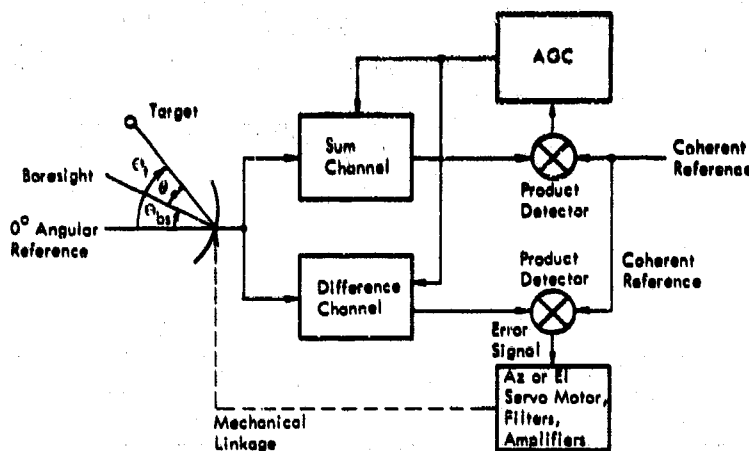


Figure C-5 Tracking Loop for Simultaneous Lobing (Coherent Detection)

Coherent Detection

Figure C-5 is a simplified block diagram of one channel of the tracking loop for the coherent detection mode of operation and will represent the configuration for analysis. The coherent reference is derived from a phase-locked loop tracking the sum channel carrier. The angle tracking error of concern is the angle (θ) between the target angle referred to some arbitrary zero reference (θ_t) and the boresight angle (θ_{bs}) referred to the same zero reference.

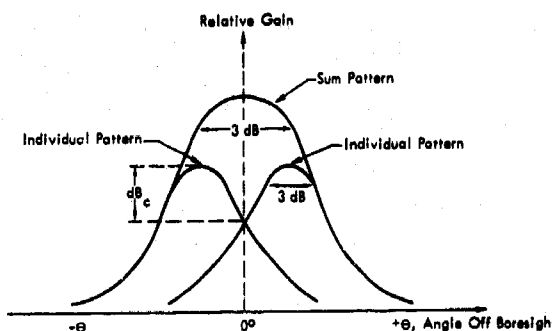


Figure C-6 Typical Amplitudes for Sum and Individual Lobe Patterns

A convenient expression (developed by Develet in Reference 1 but modified slightly to account for unequal noise density in the sum and difference channels) for calculating the mean square of the error can be applied to the SGLS system problem as follows:

C-9

$$\theta_{\text{rms}}^2 = \frac{5\psi^2}{2(\text{dB}_c)\beta^2 (\ln 2) (\ln 10)} \left[\prod_{k=1}^n J_0(\phi_k) \right]^2 \frac{\Phi_d B_n}{S} \text{ rad}^2 \quad (\text{C.1})$$

where

- θ_{rms}^2 = mean-square error in either azimuth or elevation (rad^2)
- ψ = sum antenna beam pattern (rad) at the 3-dB beamwidth
- dB_c = crossover point, expressed in decibels down from the maximum point of the individual lobe pattern (see Figure C-6)
- β = ratio of sum pattern 3-dB beamwidth to individual lobe pattern 3-dB beamwidth
- J_0 = Bessel function, zero order
- ϕ_k = the k^{th} modulation index of the information phase or frequency modulation (rad)
- Φ_d = difference channel noise density = KT_d (watts/Hz)
- B_n = servo noise bandwidth (Hz)
- S = total received signal power on boresight (watts)

Equation (C.1) can be rewritten in terms of carrier power, S_c , from the relation

$$S_c = \left[\prod_{k=1}^n J_0^2(\phi_k) \right] S \quad (\text{C.2})$$

Equation (C.2) indicates the power remaining in the carrier spectral component after multiple subcarrier phase modulation.

Equation (C.1) then reduces to

$$\theta_{\text{rms}}^2 = \frac{5\psi^2}{2(\text{dB}_c)\beta^2 (\ln 2)(\ln 10)} \frac{\Phi_d B_n}{S_c} \quad (\text{C.3})$$

Table C-6 lists the values and reference sources of these parameters for the high-gain configuration.

TABLE C-6
COHERENT DETECTION (HIGH-GAIN CONFIGURATION)

Parameter	Value	Source
ψ	9.6 mrad	Multipurpose feed specifications, WDL-98-151345A - 03 (Ref. 2)
dB_c	2.2 dB	Design Criteria for large multipurpose tracking antennas, WDL-TR1368 (Ref. 3)
β	1.4	Based on gaussian approximation for the individual feed element patterns (Fig. C-6)
B_n	2.5 Hz	Estimated maximum bandwidth for high-gain antenna
Φ_d / Φ_d	0.418	Section 3.3.1 of this report, on system noise temperature

Since it will be convenient to consider angle tracking error in terms of carrier-to-noise ratio (C/N) in the sum channel phase-lock-loop (PLL) tracking bandwidth, the following additional definition is required:

$$\left(\frac{C}{N}\right)_{\text{servo}} = \frac{S_c}{\Phi_d B_n} = \left(\frac{\Phi_s B_t}{\Phi_d B_n}\right) \cdot \left(\frac{C}{N}\right)_{\text{PLL}} \quad (\text{C.4})$$

where B_t is the phase-lock tracking bandwidth and Φ_s is the noise density in the sum channel (which also equals KT_s).

Note that the ratio Φ_s/Φ_d may be replaced in Equation (C.4) by T_s/T_d , since $\Phi_s = KT_s$ and $\Phi_d = KT_d$, where K is Boltzmann's constant (1.38×10^{-23} Joule/ $^{\circ}\text{K}$), T_d is the difference channel noise temperature ($^{\circ}\text{K}$), and T_s is the sum channel noise temperature ($^{\circ}\text{K}$).

Substitution of these values in Equation (C.3) yields

$$\theta_{\text{rms}}^2 = 8.4 \times 10^{-5} \left(\frac{\Phi_d}{\Phi_s B_t}\right) \cdot \left(\frac{N}{S_c}\right) \quad (\text{C.5})$$

where N/S_c is the noise-to-carrier ratio in the sum channel phase-lock-loop bandwidth. Figure C-7 is a graph of Equation (C.5) for a range of signal-to-noise ratios measured in the two available phase-lock-loop bandwidths.

For a multiple-axis antenna system the above result is valid only when the antenna boresight is orthogonal to the axis under consideration. Thus for an az-el antenna it is true only for zero elevation angle. At elevations other than zero, the rms azimuth error must be modified by the secant of the elevation angle as follows:

$$\text{Azimuth rms angle tracking error} = \theta_{\text{rms}} \sec \phi_E \quad (\text{C.6})$$

where

- θ_{rms} = rms angle tracking error at zero degrees elevation
 ϕ_E = elevation angle (deg)

C-11



WDL Division

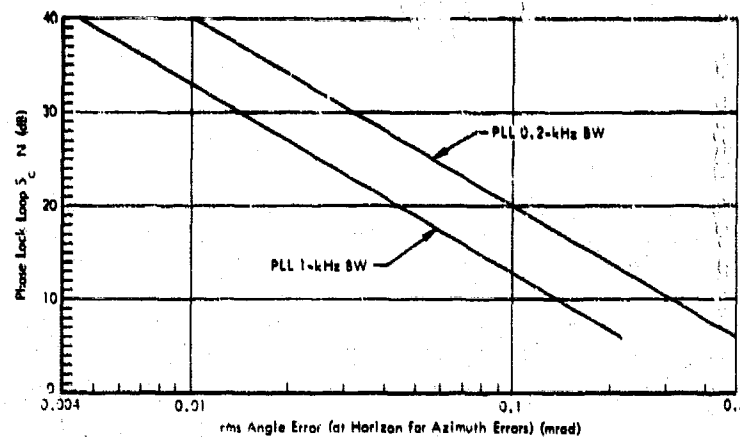


Figure C-7 Carrier-to-Noise Ratio vs Rms Angle Error
(High-Gain Antenna - Coherent Detection)

A curve of rms azimuth error versus antenna elevation angle is given in Figure C-8 for the case where SNR = 20 dB in 1000 Hz tracking bandwidth.

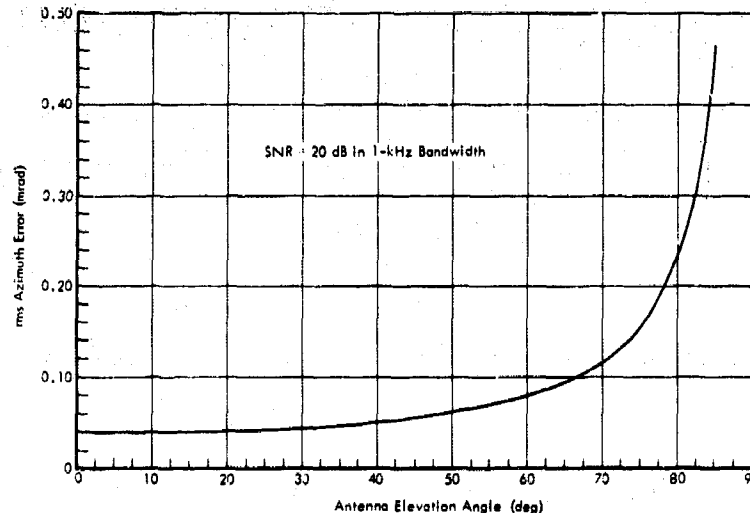


Figure C-8 Receiver rms Noise Error vs Antenna Elevation Angle (High-Gain Antenna)

Crosscorrelation Detection

When tracking is in the crosscorrelation mode using the tracking configuration of Figure C-9, the angle error due to thermal noise can be calculated from the following expression (Reference 1):

$$\theta_{\text{rms}}^2 = \frac{5\psi^2}{2(dB_c) \beta^2 (\ln 2) (\ln 10)} \left(1 + \frac{\Phi_s \text{BW}_{\text{IF}}}{S} \right) \left(\frac{\Phi_d \text{B}_n}{S} \right) \quad (\text{C.7})$$

where BW_{IF} is the intermediate frequency noise bandwidth in hertz.

Note that the expression for angle error in the crosscorrelation mode, Equation (C.7), is similar to the error expression of the coherent mode, Equation (C.1), except that noise in the sum channel as well as the difference channel enters into the equation, total signal power is now of concern, and the signal-to-noise ratio is defined in the IF bandwidth.

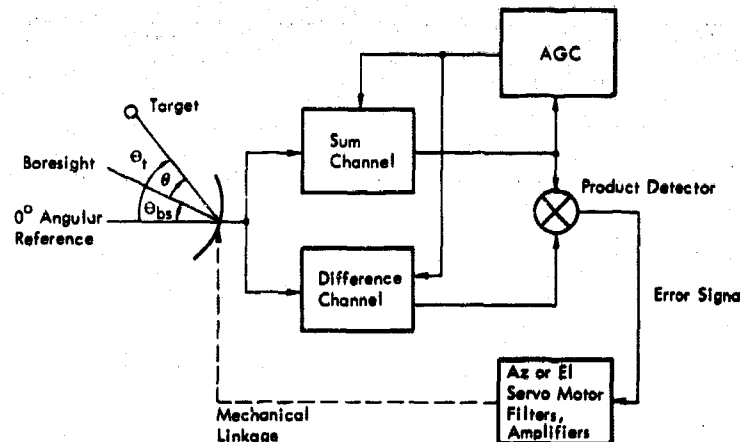


Figure C-9 Tracking Loop for Simultaneous Lobing (Correlation Detection)

TABLE C-7
CROSSCORRELATION DETECTION (HIGH-GAIN CONFIGURATION)

Parameter	Value	Source
ψ	0.0 mrad	WDL-IR-151145A-09 (Ref. 2, page 40)
dB_c	2.2 dB	WDL-TR3228 (Ref. 3, pg. 5-14)
R	1.4	Based on gaussian approximation for the individual feed element patterns (Fig. C-8)
BW_{IF}	500 kHz 3 MHz 35 MHz	GRARE specification, WDL-CP-1080-10A (Ref. 4, page 12)
B_n	2.5 Hz	Estimated maximum bandwidth for high-gain antenna
Φ_s/Φ_d	0.118	Paragraph 3, 3, 1 of this report, on system noise temperature

Table C-7 lists the values and reference sources of the parameters for the high-gain configuration when operating in the crosscorrelation mode. (Note that values for ψ , dB_c , β , ϕ , and B_n are independent of detection mode and are repeated in the table for convenience.)

Substitution of these values into Equation (C.7) yields

$$\theta_{rms}^2 = 8.4 \times 10^{-5} \left(1 + \frac{N}{S}\right) \frac{N}{S} \frac{\Phi_d}{\Phi_s BW_{IF}} \quad (C.8)$$

where N/S is the noise-to-signal ratio in the IF bandwidth BW_{IF} (sum channel).

Figure C-10 is a graph of Equation (C.8) for the three available IF bandwidths of 0.5, 3, and 35 MHz. Modification of Equation (C.8) by the secant of the elevation angle as in Equation (C.6) gives the azimuth angle error in terms of elevation angle.

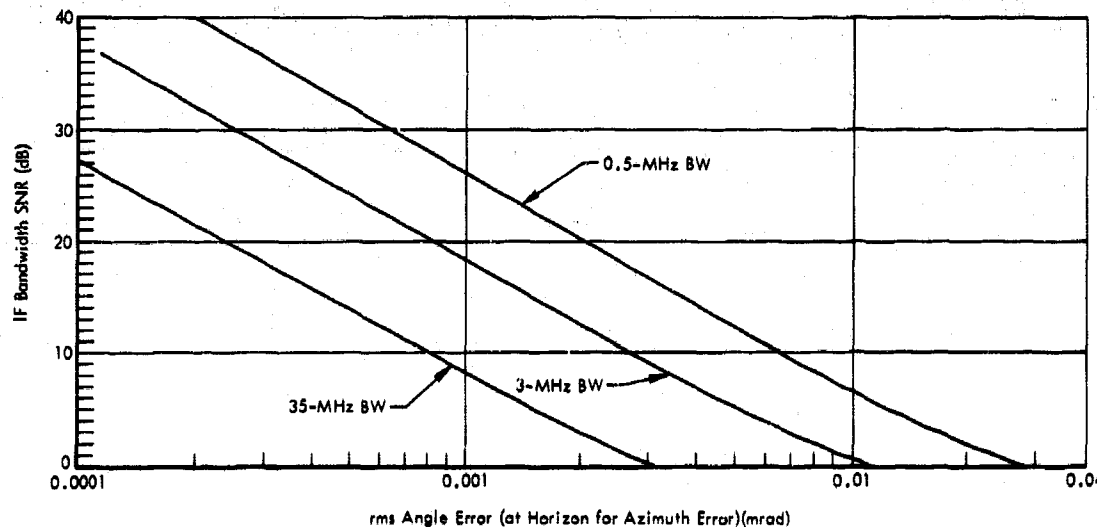


Figure C-10 IF Bandwidth SNR vs Rms Angle Error (High-Gain Antenna - Correlation Detection)

C.4.2 Low-Gain Configuration

The low-gain configuration employs the conical scanning technique and, as in the high-gain configuration, both coherent and crosscorrelation detection modes are available. Figure C-11 is a simplified block diagram of the conical-scan angle tracking system. In the following paragraphs the rms error due to thermal noise is determined for each detection mode.

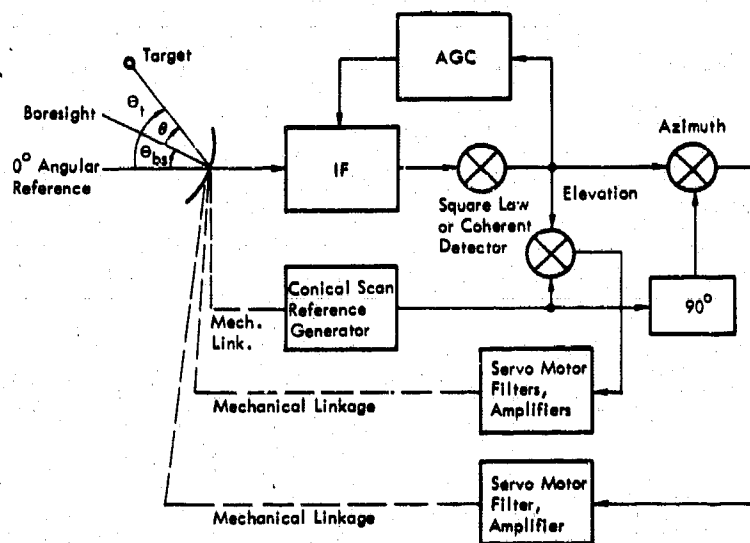


Figure C-11 Tracking Loop for Conical Scan Angle Tracking

Coherent Detection

The mean-square angle error due to noise is calculated from the following expression (Develet, Reference 1):

$$\theta_{\text{rms}}^2 = \frac{5\alpha^2}{(dB_c)(\ln 2)(\ln 10)} \left[\sum_{k=1}^n J_0(\phi_k) \right]^2 \frac{\Phi_n B_n}{S} \text{ rad}^2 \quad (\text{C. 9})$$

C-15

where

- Φ_n = noise density = $K T_s$
 α = 3dB beamwidth of the antenna beam

See Paragraph C.1 for definition of other terms.

Equation (C.9) can be simplified using Equation (C.2) to become

$$\theta_{rms}^2 = \frac{5\alpha^2}{(dB_c)(\ln 2)(\ln 10)} \left(\frac{\Phi_n B_n}{S_c} \right) rad^2 \quad (C.10)$$

Table C-8 lists the values and reference sources for the low-gain configuration parameters.

As in Paragraph C.4.1, under "Coherent Detection," it will be convenient to plot the error versus carrier-to-noise ratio in the phase-lock-loop tracking bandwidth.

TABLE C-8 COHERENT DETECTION (LOW-GAIN CONFIGURATION)		
Parameter	Value	Source
α	0.04 rad	WDL-CP-161761 (Ref. 5)
dB_c	1.3 dB	WDL-CP-161761 (Ref. 5)
B_n	3.2 Hz	Estimated maximum bandwidth

$$\left(\frac{C}{N} \right)_{servo} = \frac{S_c}{\Phi_n B_n} = \left(\frac{B_t}{B_n} \right) \left(\frac{C}{N} \right)_{PLL} \quad (C.11)$$

Equation (C.10) becomes, after substitution,

$$\theta_{rms}^2 = 1.24 \times 10^{-2} \frac{N}{B_t S_c} \quad (C.12)$$

where N/S_c is the noise-to-carrier ratio in the phase-lock tracking bandwidth.

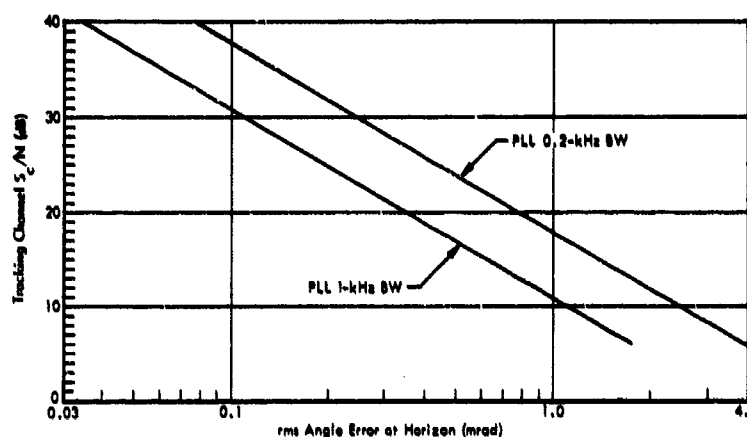


Figure C-12 Carrier-to-Noise Ratio vs Rms Angle Error
(Low-Gain Antenna - Coherent Detection)

Figure C-12 presents a plot of Equation (C.12) for tracking bandwidths of 200 and 1000 Hz. Equation (C.12) is modified by Equation (C.6) for azimuth error at elevation angles above zero degrees elevation. Figure C-13 gives a plot of azimuth error versus antenna elevation angle for a SNR of 20 dB in a 1000-Hz tracking bandwidth.

Square Law Detection

The SGLS wideband tracking mode for conical-scan tracking utilizes square law detection to demodulate the amplitude-modulated error signal. The mean-

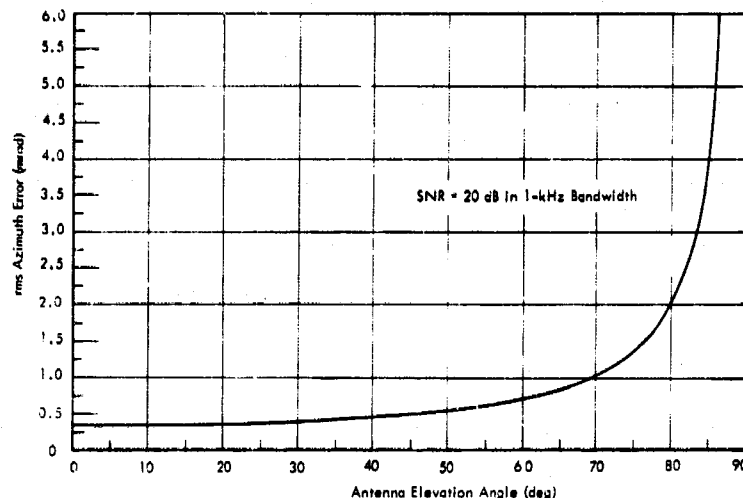


Figure C-13 Receiver rms Noise Error vs Antenna Elevation Angle (Low-Gain Antenna)

square angle error due to noise is calculated from the following expression:

$$\theta_{\text{rms}}^2 = \frac{5\alpha^2}{(\text{dB}_g)(\ln 2)(\ln 10)} \left(1 + \frac{\Phi_n B_{\text{IF}}}{2S}\right) \left(\frac{\Phi_n B_n}{S_c}\right) \text{ rad}^2 \quad (\text{C. 13})$$

To obtain a plot of error versus signal-to-noise ratio in the IF bandwidth requires Equation (C.13) to be modified in the same manner as Equation (C.8). When this is done, the following results:

$$\theta_{\text{rms}}^2 = \frac{5\alpha^2}{(\text{dB}_g)(\ln 2)(\ln 10)} \left(1 + \frac{1}{2} \frac{N}{S}\right) \frac{B_n}{B_{\text{IF}}} \frac{N}{S} \text{ rad}^2 \quad (\text{C. 14})$$

Substituting the values in Table C-8 into Equation (C.14) yields the following:

$$\theta_{\text{rms}}^2 = 1.24 \times 10^{-2} \left(1 + \frac{1}{2} \frac{N}{S}\right) \frac{N}{B_{\text{IF}} S} \text{ rad}^2 \quad (\text{C. 15})$$

where N/S is the noise-to-signal ratio in the IF bandwidth.

Figure C-14 presents a plot of Equation (C.15) for IF bandwidths of 500 kHz, 3 MHz, and 35 MHz. Equation (C.15) is likewise modified by the secant effect for azimuth error at elevation angles above zero degrees.

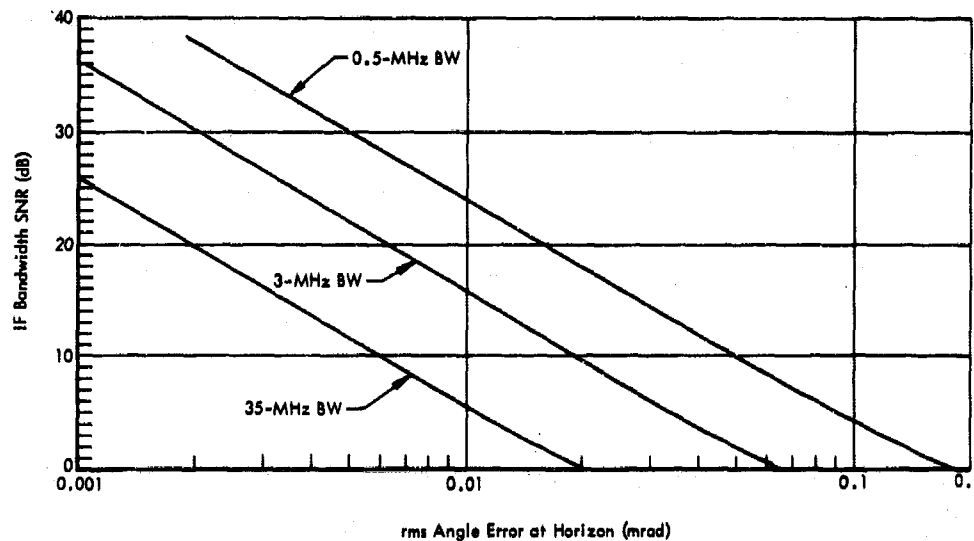


Figure C-14 IF Bandwidth SNR vs Rms Angle Error (Low-Gain Antenna - Square Law Detection)

C.4.3 Angle Tracking Error Due to Phase Shift and Amplitude Unbalance

The effects of phase shift and gain variations on tracking accuracy of the high-gain antenna are treated in Appendix D. The results of this investigation applied to the SGLS are summarized in Table C-9.

TABLE C-9
SUMMARY OF ANGLE TRACKING ERRORS DUE TO PHASE SHIFT
AND AMPLITUDE UNBALANCE (HIGH-GAIN ANTENNA)

Parameter	Parameter Value	Source	Results	
			Angletrack Error (Bore sight Shift) (mrad)	Change in Error Gradient (dB)
Precomparator Phase Shift	+5°	MFP Spec. WDL-98-151335A-03	+0.045 mrad peak	0.1 dB
Postcomparator Phase Shift	+10°	GRARE phase adjust circuitry	+0.02 mrad rms	
Precomparator Amplitude Unbalance	-0.3 dB	Estimate	+0.10 mrad peak	N/A
Postcomparator Amplitude Unbalance	+3.0 dB	GRARE Spec. WDL-CP-108940A	+0.06 mrad rms N/A	+3 dB

Tracking errors due to phase shift and gain variations in the azimuth axis increase with the secant of the elevation angle. Figure C-15 is a plot of these errors versus elevation angle.

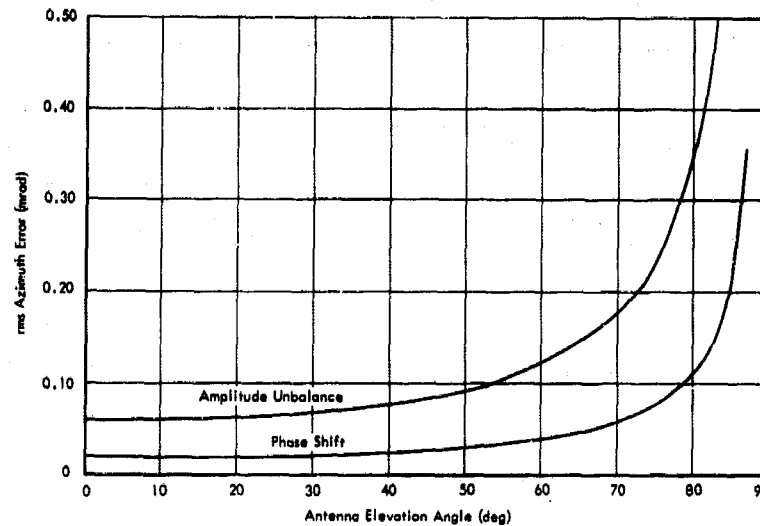


Figure C-15 Phase Shift and Amplitude Unbalance Tracking Errors (Azimuth Axis) vs Elevation Angle (High-Gain Antenna)

C.5 PROPAGATION ERRORS

C.5.1 The Atmosphere and Its Effect on Propagation

In the atmosphere, the regions that influence and affect radio wave propagation are the troposphere and the ionosphere. The major effects produced by the passage of waves through these regions appear as angular refraction, time delays, doppler errors, polarization rotations, attenuation, and reflections.

The ionosphere and the troposphere exhibit both long-term and short-term variations with time (irregularities). Because of these variations, propagation efforts cannot be predicted exactly. In addition, the variations of the atmospheric conditions with altitude are known only approximately, especially in the case of the ionosphere.

The atmosphere is generally considered (at least for purposes of calculation) to be spherically stratified. The assumptions of layer boundaries differ, although the effects of the differences are slight. The density of the atmosphere decreases more or less exponentially with height, so that at a height of 35 nmi (nautical miles) the density is only about 10^{-4} that at the earth's surface. Essentially all of the water vapor and precipitation occurs below 6 nmi. The propagation effects resulting from molecular or larger particles can be considered to occur below 35 nmi. Ionization of the atmosphere occurs above this height, resulting in a sufficiently large density of free electrons to seriously affect radio waves. Consequently, it is convenient to divide the atmosphere into two parts: the troposphere, defined as extending from the ground up to 35 nmi, and the ionosphere, extending on up from there (Reference 6). Millman (Reference 7) makes the assumptions that (1) the troposphere extends to approximately 100,000 ft (16.5 nmi) with refractive index decreasing uniformly with height; (2) the ionosphere lies between 85 to 1000 km (about 45 to 550 nmi) with a minimum refractive index at the level of maximum electron density; and (3) free space or a region of unity refractive index prevails between the tropospheric and ionospheric regions.

The regular troposphere affects the transmission of radio waves chiefly through refraction. In general, the apparent elevation angle of a distant target or source is greater than the true angle, because the average refractive index of the troposphere decreases with increasing height. The average magnitude of the angular correction depends upon the air mass through which the signal passes, the magnitude decreasing with increasing geographic latitude. The refraction at radio frequencies is due mainly to water vapor and is substantially independent of frequency below about 15 GHz.

The x-ray and ultraviolet radiation from the sun is selectively absorbed by molecular constituents of the upper atmosphere to produce ionization and dissociation of the molecules. Because of the selective absorption of the particular constituents, the ionization is concentrated in certain layers. These layers and their average heights are: (1) the D layer at about 46 nmi, (2) the E layer at about 58 nmi, (3) the F₁ layer at about 100 nmi, and (4) the F₂ layer at about 150 nmi. The F₂ layer is more intense than any other, and is responsible for about 90 percent of ionospheric refraction deviation for signal sources above 150 nmi (Reference 6).

The ionosphere can cause total reflection at lower radio frequencies (HF), but it contributes only slightly to the total atmospheric bending at S-band.

Angle Deviations

A typical ray-path trajectory of radio waves traversing the atmosphere in a vertical plane is shown in Figure C-16 (Reference 6). From considerations of path geometry, based on various assumptions, many equations giving angular refraction can be derived. Several such equations have been derived, varying in degree of complexity and accuracy (References 6, 7, 8 and 9).

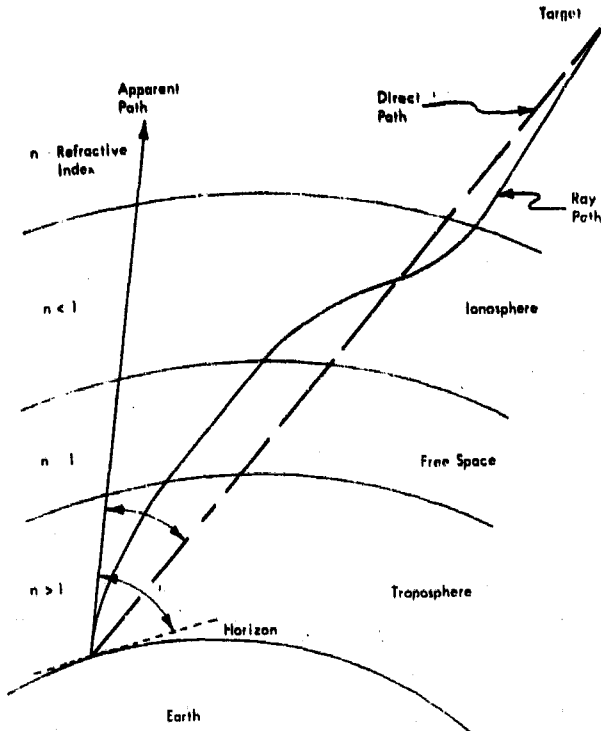


Figure C-16 Typical Ray-Path Trajectory

Smyth Research Associates investigated 3 years of data obtained from at least daily radiosonde ascents, at several northern stations, and found the data distributions to be very nearly normal (Reference 10). This information was then presented statistically by tabulations of median values and standard deviations. Figure C-17 shows the maximum and minimum means for Fairbanks, Alaska, over the 3-year period, based on the arbitrary assumption that the top of the troposphere is at 300,000 ft.

Continual changes in the physical structure of the troposphere cause the instantaneous ray path to deviate about its mean position. Fluctuations about the mean are about 0.2 mrad at 5° elevation, decreasing to about 0.005 mrad at the vertical (Reference 9). The mean period of the fluctuations is of the order of seconds (Reference 11). It should be noted that the refraction errors are the same throughout the VHF and UHF bands, and up to about 30 GHz.

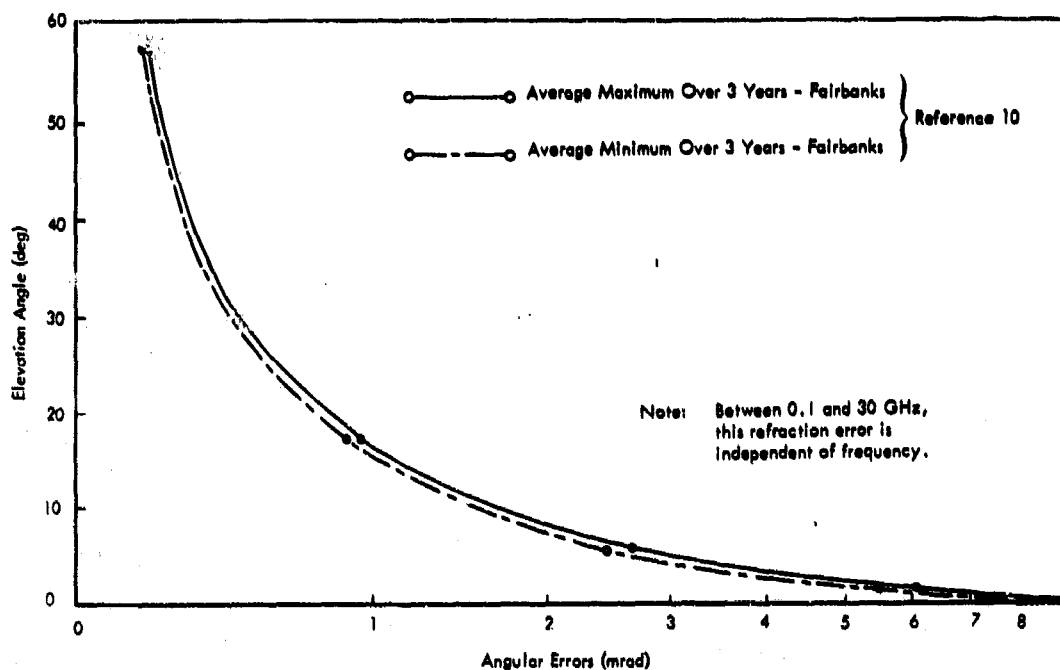


Figure C-17 Tropospheric Refraction Error for A Standard Atmosphere

Results of a study on the use of surface refractivity to predict tropospheric refractive error are shown in Figure C-18.

The ionospheric angular error is inversely proportional to the frequency squared. The angular error is maximum in the vicinity of the maximum ionization. Millman (Reference 7)

has presented several curves of ionospheric refraction errors as a function of target height (to 550 nmi) for typical daytime and nighttime electron density distributions. Figure C-19 shows these errors as a function of elevation angle for a target at a height of 540 nmi.

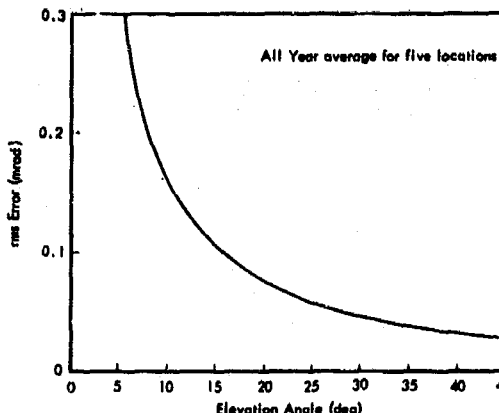


Figure C-18 Total rms Error in the Predicted Fraction at 2-GHz

C-23

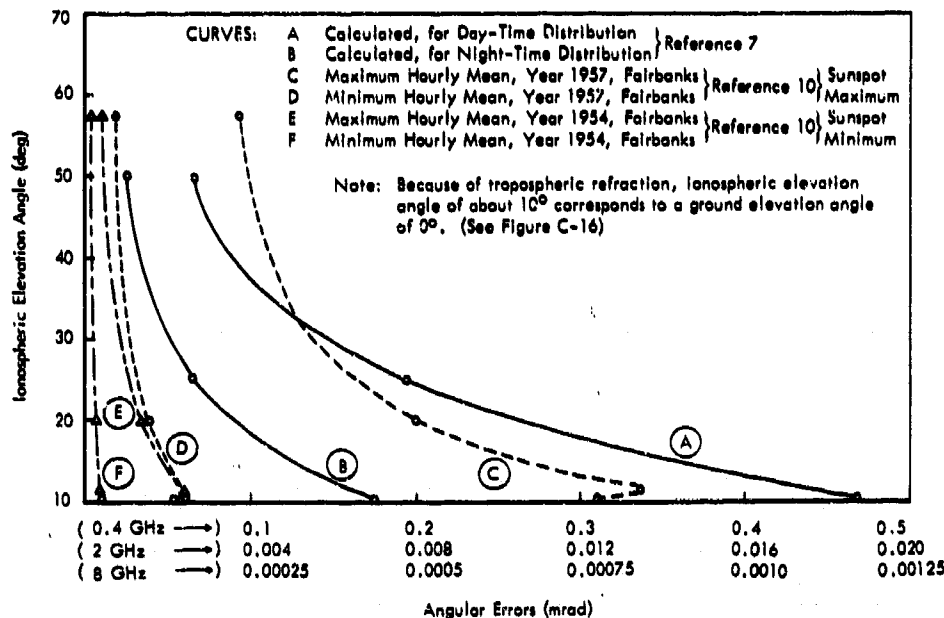


Figure C-19 Ionospheric Refraction Errors

Conclusions

As Figure C-19 indicates, the error due to ionospheric refraction is insignificant at S-band and will therefore be ignored. Tropospheric refractive errors, however, are significant at elevation angles below 20° and must be considered. Since these errors are predictable with an uncertainty of about 10%, they are regarded in this analysis as systematic errors with a noise component. The systematic error is determined from the curve in Figure C-17, and the noise error is determined from Figure C-18.

C.5.2 Angle Tracking Errors Caused by Multipath at 5° Elevation Angle

The angle tracking errors incurred in the SCF antenna tracking systems due to multipath are, in general, complex functions of pointing direction, the surrounding terrain and its moisture content, obstructions, the individual antenna patterns and polarization, signal polarization, etc.

For this report multipath errors are considered to be caused by ground reflections from an assumed "level" earth surrounding the antenna site. Ground reflections cause an amplitude and phase unbalance in the conical-scan beam or monopulse beams, which in turn can result in an angular error between the apparent and true boresight directions.

At an antenna elevation angle of 5°, the energy available as interference is the energy entering the antenna pattern at an angle 10° off boresight. All of this energy, however, does not necessarily cause interference. Some of the energy is lost due to absorption in the ground, generally as a function of moisture content, and a certain amount is effectively lost due to polarization change at the point of reflection. (The SCF systems of concern employ circular polarization.)

The value of ground reflection loss due to absorption is a complex function of the dielectric constant and conductivity of the earth, the frequency, the plane of polarization, and the angle of incidence. The ground constants depend primarily on the type of terrain and its chemical composition, i.e., salinity and moisture content, etc. A conservative value of ground reflection loss of 5 dB is assumed in this analysis.

An estimate of the boresight shift due to multipath can be obtained following the procedure outlined in Reference 12. Boresight error is taken as approximately:

$$\text{Boresight (elevation) error} = 1.85 \left| \frac{E_r}{E_d} \right| \times \frac{\text{half power beamwidth}}{2}$$

where $|E_r|/|E_d|$ is the reflected-wave to direct-wave voltage ratio after modification by the antenna pattern. The reflected wave will be assumed to be

attenuated 5 dB by losses in the earth, and further attenuated by the antenna response to signals 10° off the axis of the main beam.

The 10° response of the high-gain antenna is near -40 dB, and the value of $|E_r|/|E_d|$ will be -45 dB. With 0.55° beamwidth, the elevation error for the high-gain antenna is estimated to be 0.048 mrad.

The 10° response of the low-gain antenna is near -30 dB, so the value to $|E_r|/|E_d|$ will be -35 dB. With 2.3° beamwidth, the elevation error for the low-gain antenna is estimated to be 0.66 mrad.

C.5.3 Radome Refraction

High-Gain Antenna

The high-gain (TT&C) antenna is equipped with an ESSCO Model M110-86 Metal Space Frame Radome. This radome consists of 620 reinforced fibrous glass panels, with radial metal flanges, bolted together and attached to a 75.5-ft-diameter base ring. The completed assembly is a 110-ft truncated sphere rising approximately 95 ft above the base ring. Additional features of interest include windows for boresight and safety hardware such as lightning rods and aircraft warning lights mounted on the apex.

The specified (Reference 13) boresight shift performance is shown in Figure C-20. No experimental data have been collected in the SCF; however, References 14 and 15 state that for this radome, rms errors

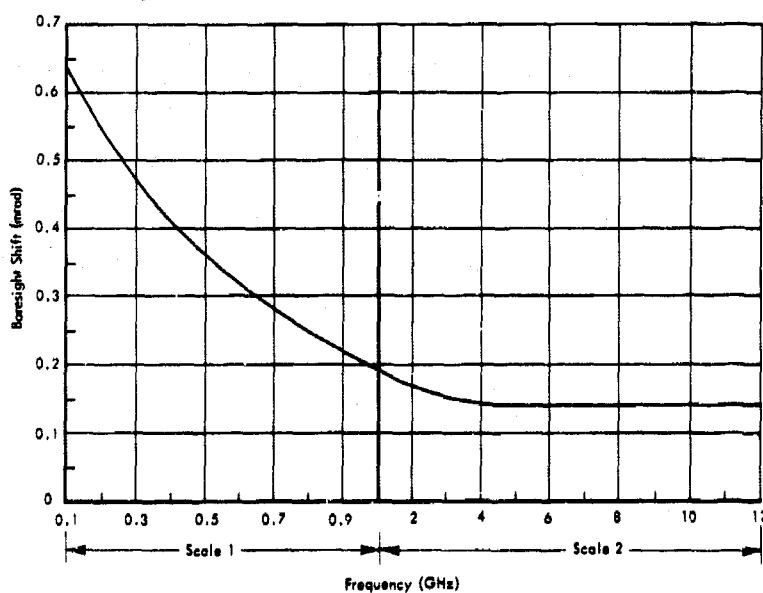


Figure C-20 Allowable Radome Boresight Shift (High-Gain Antenna)

on the order of 0.05 mrad in both azimuth and elevation are normal for the 2-GHz region with maximum errors of 0.1 mrad. The rms error was used in the angle tracking error analysis for the high-gain TT&C antenna.

Since lightning rods and warning lights are attached at the apex of the radome, they will generally be in the tracking "keyhole" and errors attributed to them may be neglected. It can be expected, however, that maximum errors as great as 0.2 mrad may be experienced in areas where boresight windows are attached.

Low-Gain Antenna

The low-gain Prelort antenna is equipped with an Air Force Nomenclature CW-531/GP radome manufactured by Long Sault Woodcraft. The radome is a rigid urethane foam structure mounted on a 22-ft base ring. The complete assembly is a 26.5-ft truncated sphere rising 20.5 ft above the base ring.

The specified (Reference 5) boresight shift in the 2-GHz region is 0.22 mrad. Results of tests on this radome conducted by the National Research Council of Canada indicate an rms error of 0.07 mrad with maximum shift exclusive of attach structures of 0.22 mrad. The rms error was used in the angle tracking error analysis.

Again, the errors attributed to lightning rods and warning lights may be neglected since they are in the tracking keyhole. However, errors as great as 0.53 mrad were reported in the vicinity of radome windows.

C.6 SERVO ERRORS

C.6.1 Servo Lag

Servo lag is the term applied to the angle tracking error incurred due to the characteristics of the servo system when tracking a moving vehicle. The azimuth and elevation servo loops are both type 2 servos which suffer a steady state loop error due to vehicle acceleration but, theoretically, not to a steady vehicle velocity.

Tracking error is calculated from the equation:

$$\text{Servo lag tracking error} = \frac{\text{angular acceleration}}{K_\alpha}$$

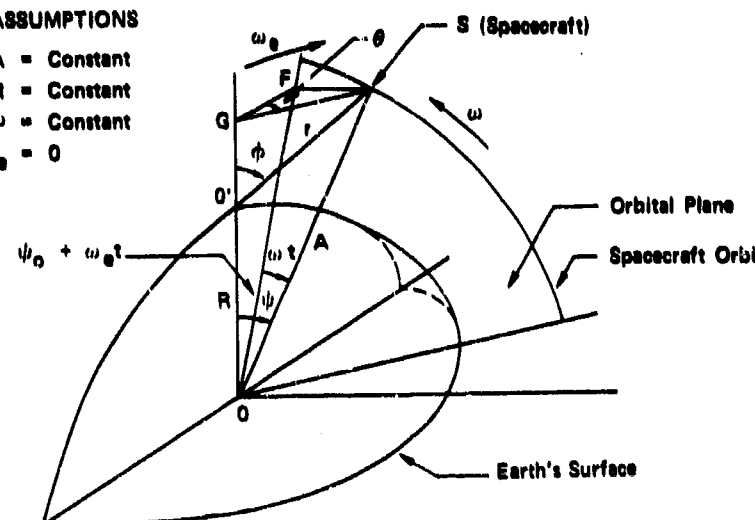
where K_α is the loop acceleration error constant. The required antenna acceleration in each axis is determined by the orbit of the vehicle being tracked. Low-altitude orbits passing close to the zenith place the most stringent tracking requirements on the antenna servo. Calculation of servo lag error requires that the azimuth and elevation accelerations be determined for typical satellite orbits. The required data are now developed in general terms based on the geometry of the vehicle-to-tracking antenna relationship.

Basic Tracking Equations

Equations for the servo requirements of an az-el antenna that is tracking a satellite are quite complex. Some parameters that affect the final relationship are the orbit eccentricity, vehicle height above the earth, rotation of the earth, and the position of the antenna on the earth. For this report, a first order approximation will be used to determine error. The geometry of the problem is illustrated in Figure C-21.

ASSUMPTIONS

A = Constant
R = Constant
 ω = Constant
 $\omega_e = 0$



DEFINITION OF TERMS

- A distance from the earth's center (O) to the spacecraft (S)
- R radius of the earth
- O center of the earth
- O' center of tracking device
- ψ angle subtended by a line (O'O') from the earth's center through the tracking device and a line (OS) from the earth's center through the spacecraft
- ψ_0 minimum value of ψ attained for a given trajectory (for $\omega_e = 0$)
- ϕ angle subtended by a line (O'O') from the earth's center through the tracking device and a line (O'S) from the tracking device through the spacecraft
- θ azimuthal bearing of the spacecraft from the tracking device
- ω angular velocity with which the spacecraft travels about the earth
- t time ($t = 0$ when the spacecraft reaches angle ψ_0)
- r slant range from the tracker to the spacecraft
- ω_e earth's angular velocity
- FGS plane that is perpendicular to the line O'O' and its extension (the local zenith of the tracking device) at point G and that intersects line OS at point S
- F a point on a line that is intersected by the orbital plane and the plane FGS; F also lies on line OS when ψ is a minimum
- G a point on line O'O' and its extension that is intersected by plane FGS

Figure C-21 Geometry of Vehicle-to-Tracking-Antenna Relationship

From the definitions in Figure C-21 and the geometry of the problem the following equations are derived (Reference 3):

$$\theta = \tan^{-1} \left(\frac{\tan \omega t}{\sin \psi_0} \right) \quad (C.16a)$$

$$\dot{\theta} = \frac{\omega \sin \psi_0}{\sin^2 \psi_0 \cos^2 \omega t + \sin^2 \omega t} \quad (C.16b)$$

$$\ddot{\theta} = \frac{-2\omega^2 \sin \psi_0 (1 - \sin^2 \psi_0) (\sin \omega t \cos \omega t)}{(\sin^2 \psi_0 \cos^2 \omega t + \sin^2 \omega t)^2} \quad (C.16c)$$

$$\phi = \sin^{-1} \left[A \left(\frac{1 - \cos^2 \psi_0 \cos^2 \omega t}{R^2 + A^2 - 2RA \cos \psi_0 \cos \omega t} \right)^{1/2} \right] \quad (C.16d)$$

$$\dot{\phi} = \frac{\omega \cos \psi_0 \sin \omega t}{2 \sqrt{1 - \cos^2 \psi_0 \cos^2 \omega t}} \left(1 + \frac{A^2 - R^2}{A^2 + R^2 - 2AR \cos \psi_0 \cos \omega t} \right) \quad (C.16e)$$

$$\ddot{\phi} = \frac{\omega^2 \cos \psi_0}{2 \sqrt{(1 - \cos^2 \psi_0 \cos^2 \omega t)}} \left\{ \left(1 + \frac{A^2 - R^2}{A^2 + R^2 - 2AR \cos \psi_0 \cos \omega t} \right) \right\} \quad (C.16f)$$

$$\begin{aligned} & \cdot \left[\cos \omega t \left(1 - \frac{\sin^2 \omega t \cos^2 \psi_0}{1 - \cos^2 \psi_0 \cos^2 \omega t} \right) \right] \\ & - \left[2AR \cos \psi_0 \sin^2 \omega t \frac{A^2 - R^2}{(A^2 + R^2 - 2AR \cos \psi_0 \cos \omega t)^2} \right] \end{aligned} \quad (C.16f)$$

High-Gain Antenna Performance

The high-gain antenna performance is as follows:

- a. Maximum azimuth tracking velocity is 15 deg/sec
- b. Maximum azimuth tracking acceleration is 5 deg/sec²
- c. Acceleration error constant (K_A) = 5 sec⁻²

Utilizing the equations for acceleration [Eqs. (C.16)] and the acceleration error constant of 5 sec⁻², curves have been prepared showing absolute values of tracking error (servo lag) versus time and, for one case, versus elevation angle, for satellite orbits with given altitude and maximum elevation angle relative to the tracking antenna. (See Figures C-22 through C-29.)

Examination of the azimuth error curves shows that, for a given altitude, the error increases as the maximum elevation angle increases. That is, the overhead passes produce the greatest error. It can be seen that the error is zero at zero time, increasing rapidly to a maximum and then decreasing. This, of course, is due to the acceleration characteristics in the azimuth axis. At $t = 0$ the acceleration passes through zero as it changes to deceleration. The plot of error versus time for positive and negative values of time would produce an odd function about zero. Plots here are for positive time only and for absolute values of error.

All plots are for high maximum elevation angles since the error is greatest for these cases. Further, maximum tolerable azimuth error is taken as 0.27°. This value is selected as maximum allowable tracking error and is based on the antenna beamwidth of 0.55°. Thus, the assumed maximum tracking error defines minimum vehicle altitudes for a given pass. For example, for a maximum elevation angle of about 80° the minimum trackable altitude will be 131 nmi, as indicated by Figure C-22.

Elevation error curves are presented for the same orbits assumed for the azimuth error plots. Elevation error is maximum at zero time and decreases

with time. Note that the magnitude of the elevation error is in general much less than that for the azimuth axis.

Servo lag is not the only limitation on tracking. Tracking velocity must also be considered but only in the sense that the velocity is within the limitations of the tracking antenna.

Maximum angular antenna velocity occurs in both azimuth and elevation as the vehicle passes closest to the zenith, i.e., at the time of maximum elevation. This maximum elevation angle for the orbit considered (31 nmi altitude) is about 83° for the azimuth velocity to reach its limiting level of 15 deg/sec.

Thus in this particular case, a tracking limitation due to angular acceleration-incurred servo lag is of more significance than maximum angular velocity since, as Figure C-22 indicates, a servo lag azimuth error of 0.5° would occur at 83° elevation, possibly causing tracking to cease.

Low-Gain Antenna Performance

The low-gain antenna performance characteristics are:

- Maximum azimuth tracking velocity of 15 deg/sec
- Maximum azimuth tracking acceleration of 5 deg/sec
- Acceleration error constant (K_a) = $40/\text{sec}^2$

Curves of absolute azimuth and elevation error have been prepared in the same manner as that for the high-gain antenna. These are shown in Figures C-30 through C-35. The error is considerably less due to the high acceleration error constant in this case.

The overall tracking capability of the low-gain antenna is superior to the high-gain antenna due to the higher K_a and a larger antenna beamwidth. Although the specified maximum azimuth velocity is the same as for the high gain, it is found that the capability exceeds the specified value to a considerable degree enabling this antenna to track low-altitude vehicles that pass high over head.

ABSOL

F

AZIMUTH ERRORS

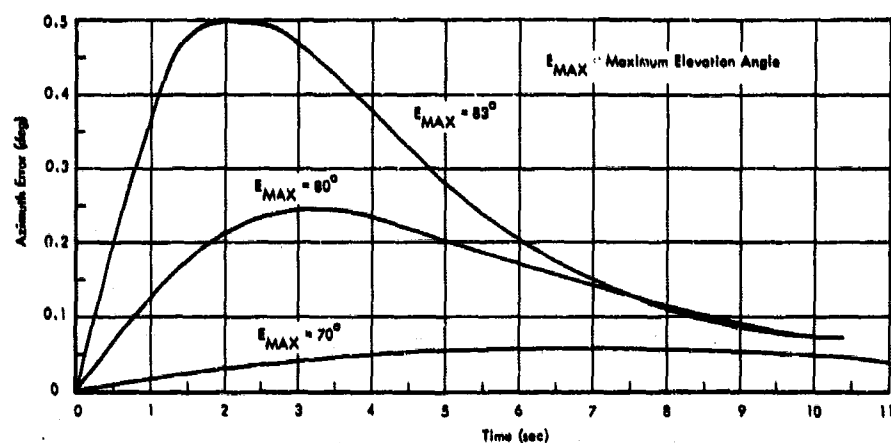


Figure C-22 Error Curves for 131-nmi Orbit (Azimuth Error vs Time)

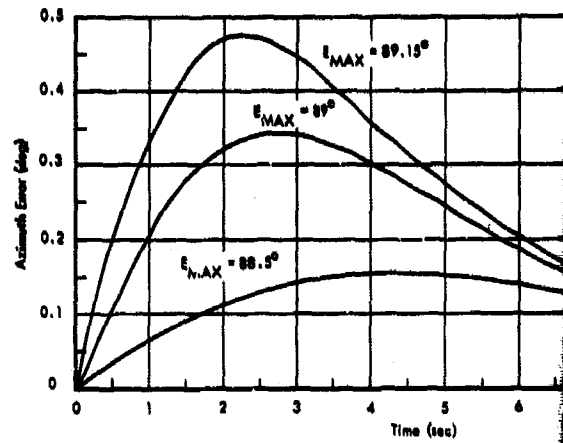


Figure C-24 Error Curves for 1,000-nmi Orbit (Azimuth Error vs Time)

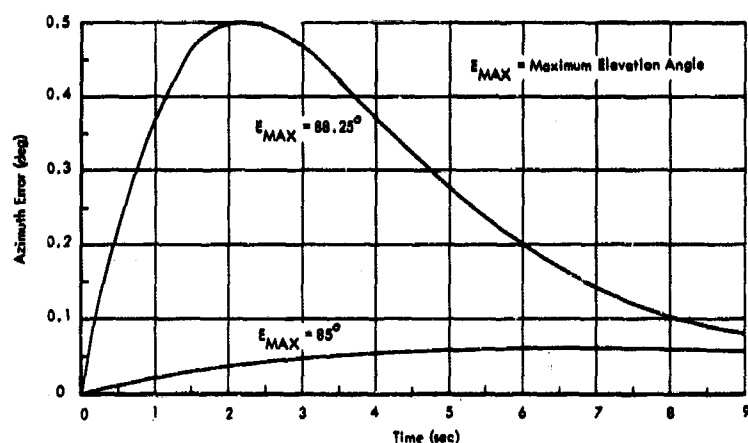


Figure C-23 Error Curves for 500-nmi Orbit (Azimuth Error vs Time)

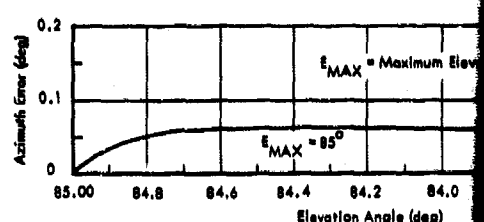


Figure C-25 Error Curve for 500-nmi Orbit (Azimuth Error vs Elevation Angle)

ABSOLUTE VALUES OF TRACKING ERROR (SERVO LAG) FOR THE HIGH-GAIN ANTENNA

ELEVATION ERRORS

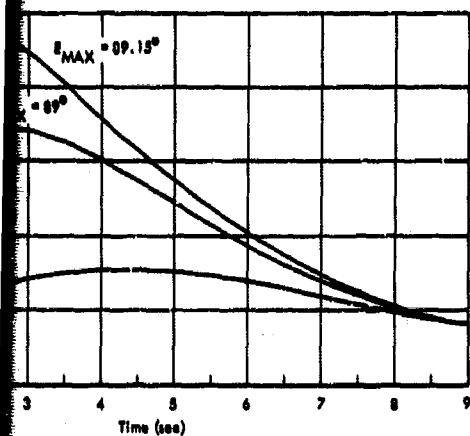


Figure C-25 Error Curves for 1,000-nmi Orbit (Azimuth Error vs Time)

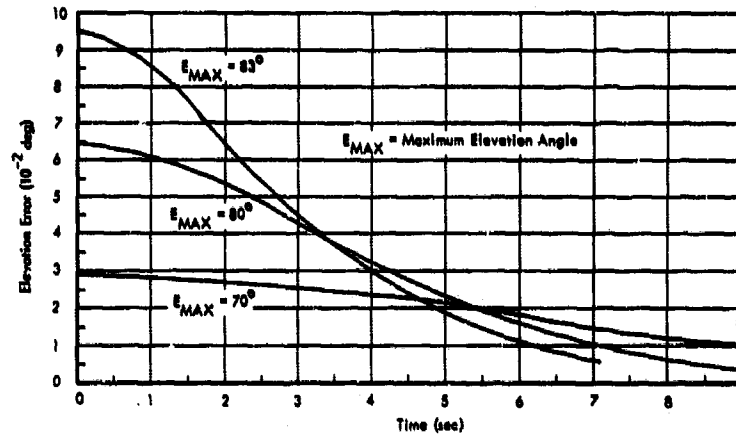


Figure C-26 Error Curves for 131-nmi Orbit (Elevation Error vs Time)

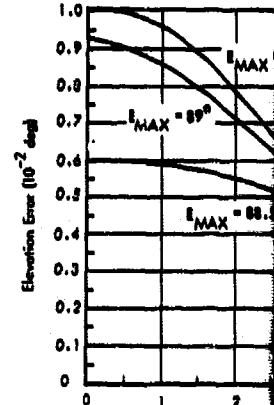


Figure C-28 Error Curves for 131-nmi Orbit (Elevation Error vs Time)

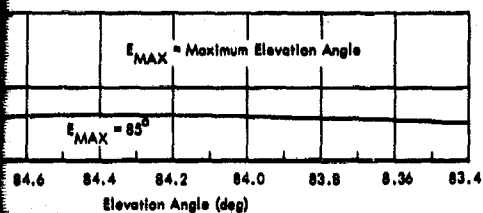


Figure C-25 Error Curve for 500 nmi Orbit (Azimuth Error vs Elevation Angle)

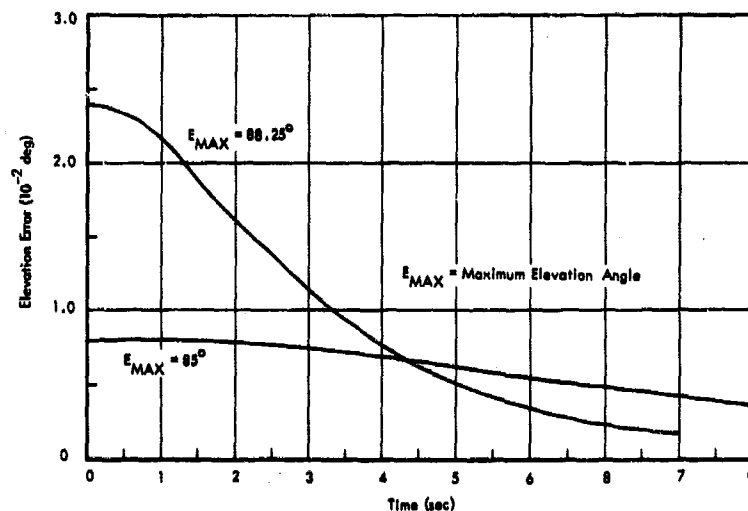


Figure C-27 Error Curves for 500-nmi Orbit (Elevation Error vs Time)

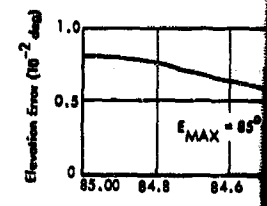


Figure C-28 Error Curves for 500-nmi Orbit (Elevation Error vs Time)



ERROR

ELEVATION ERRORS

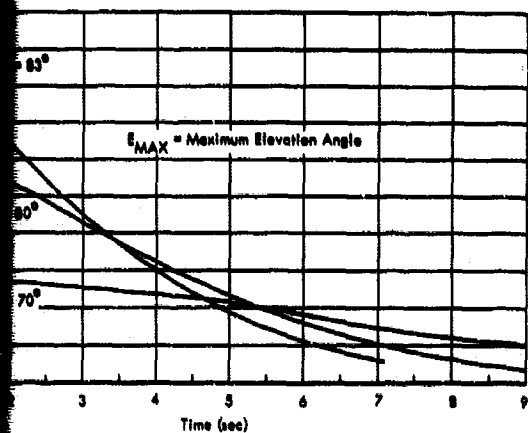


Figure C-27 Error Curves for 131-nmi Orbit (Elevation Error vs Time)

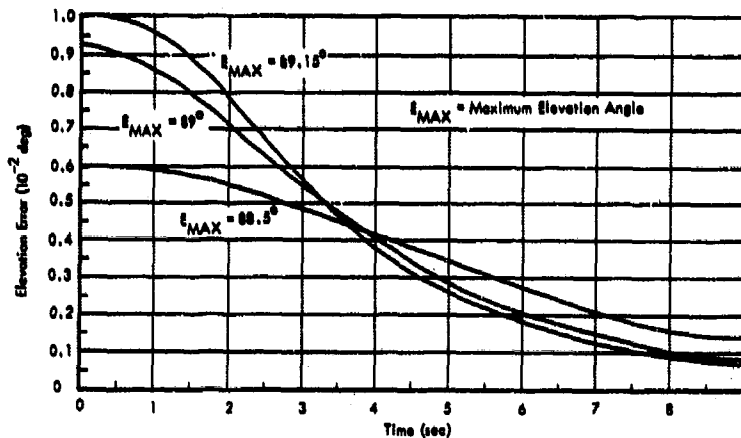


Figure C-28 Error Curves for 1,000-nmi Orbit (Elevation Error vs Time)

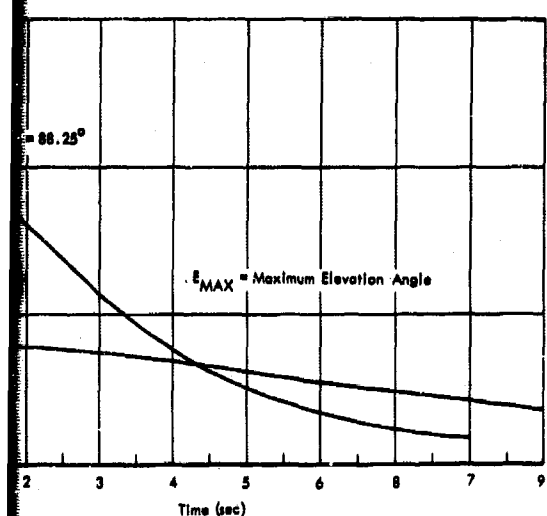


Figure C-29 Error Curve for 500-nmi Orbit (Elevation Error vs Elevation Angle)

AZIMUTH ERRORS

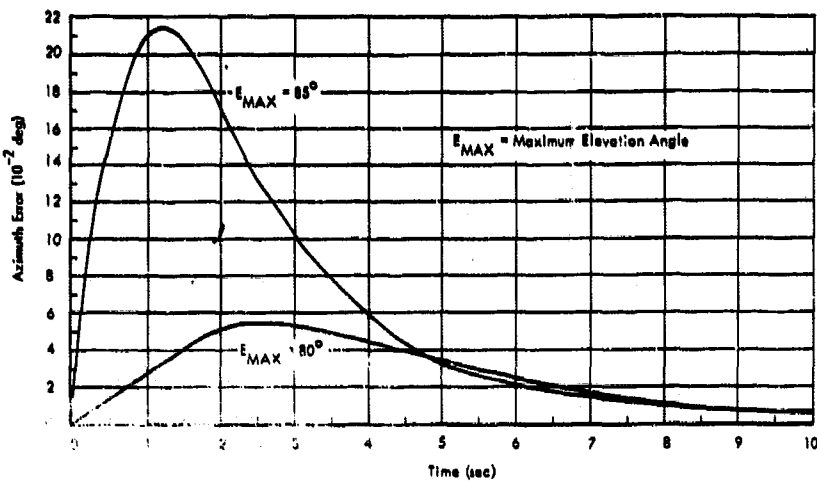


Figure C-30 Error Curves for 100-nmi Orbit (Azimuth Error vs Time)

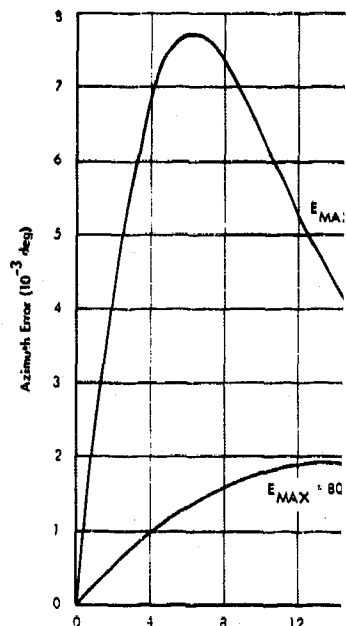


Figure C-31 Error Curve

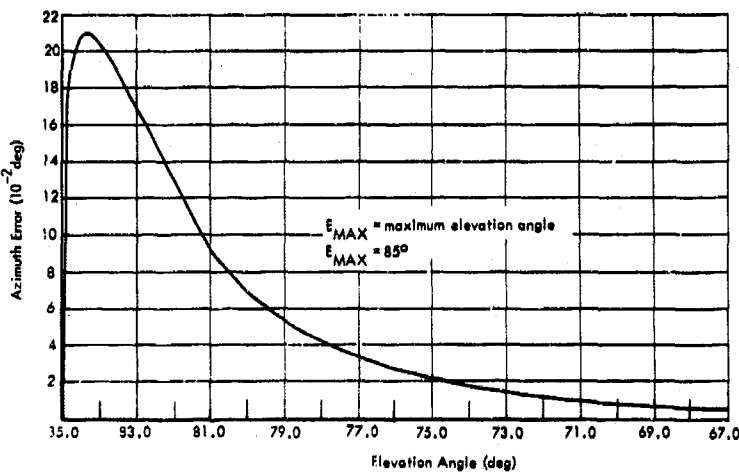


Figure C-32 Error Curve for 100-nmi Orbit (Elevation Error vs Time)



ABSOLUTE VALUES OF TRACKING ERROR (SERVO LAG) FOR THE LOW-GAIN ANTENNA

ERROS

ELEVATION ERROR

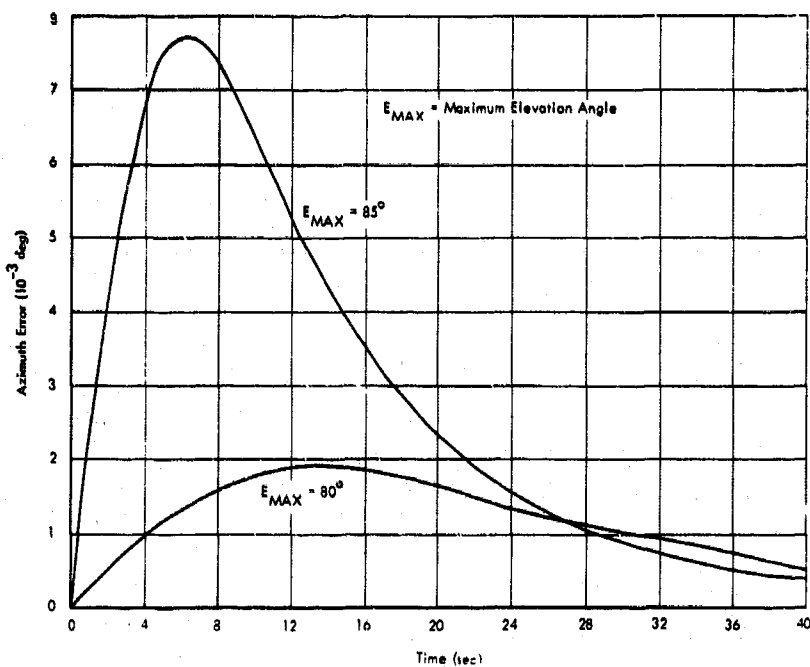


Figure C-31 Error Curves for 500-nmi Orbit (Azimuth Error vs Time)

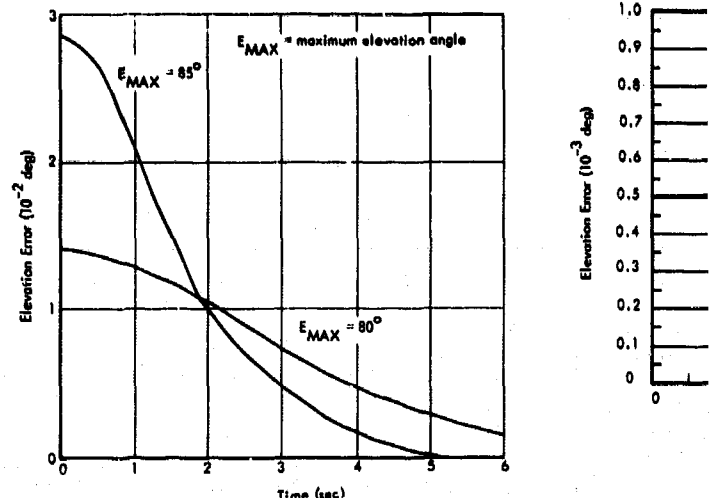


Figure C-33 Error Curves for 100-nmi Orbit
(Elevation Error vs Time)

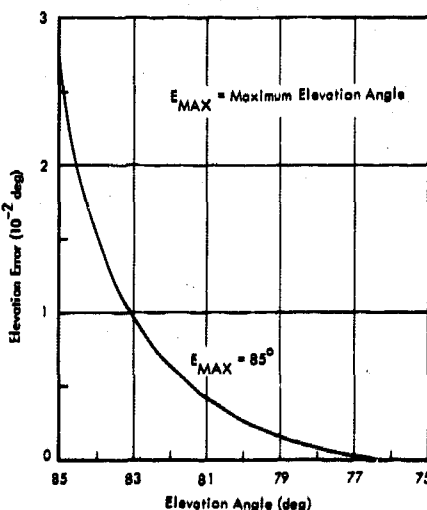


Figure C-35 Error Curve for 100-nmi Orbit
(Elevation Error vs Elevation Angle)

NTENNA

ELEVATION ERRORS

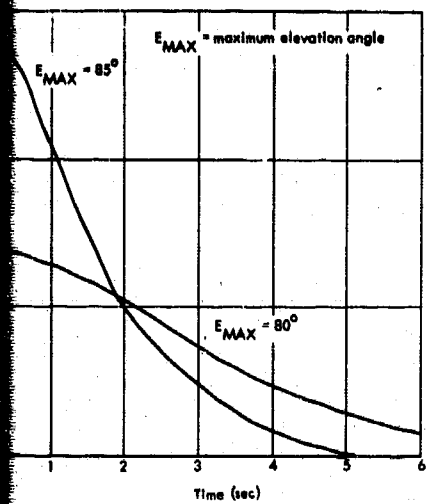


Figure C-33 Error Curves for 100-nmi Orbit (Elevation Error vs Time)

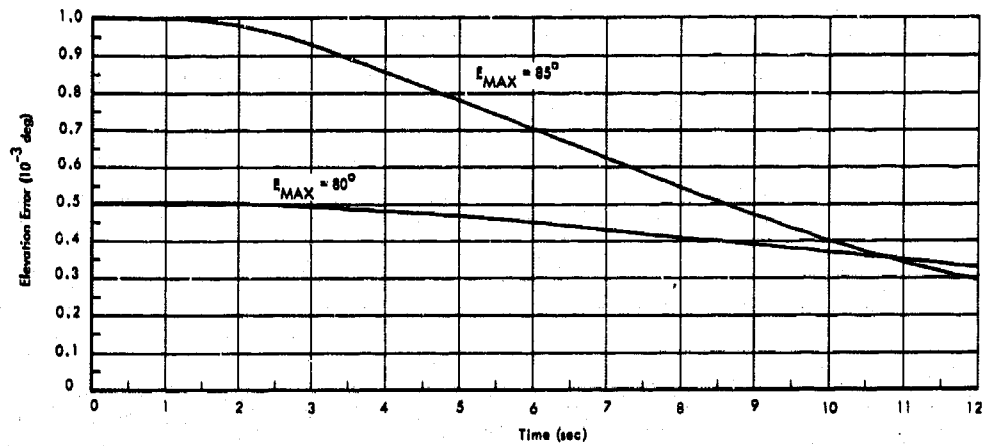
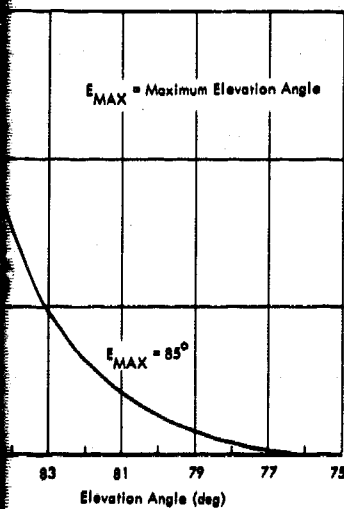


Figure C-34 Error Curves for 500-nmi Orbit (Elevation Error vs Time)



C-35 Error Curve for 100-nmi Orbit (Elevation Error vs Elevation Angle)

C-35/C-36

C. 6.2 Servo Bias Error

The servo systems being considered are classified as type 2 which implies that in order to produce a steady output offset a steady signal must be inserted prior to the first integration following the error detection.

It is possible that a bias error may be introduced between the detection or demodulation stage and the first integrator. It is difficult to estimate this bias, but it would probably follow the usual form of variation attributable to dc operational amplifiers, which exhibit a variation as a function of ambient temperature and a slow drift with time due to aging of components. This bias may be as high as 0.2 mrad per day. This form of drift tends to continue at approximately the same rate. Thus, for a 20-minute pass the variation between pre- and post-pass boresighting would be 0.003 mrad, which is negligible. If the pre- and post-pass boresight errors are either adjusted out or measured and inserted into the data reduction, this error becomes zero along with similar bias errors.

The specification covering the SGLS receiver allows an output offset of ± 60 mV which corresponds to ± 0.1 mrad (WDL-CP-168946, Paragraph 3.1.1.1.2.8). An rms error of 0.03 mrad will be assumed for the high-gain antenna (simultaneous lobing configuration) and negligible error for the low-gain antenna (conical-scan configuration). The receiver error contribution does not apply for the conical-scan configuration since the error signal is in the form of a 30-Hz sine wave.

C.7 MECHANICAL ERRORS

Mechanical errors are those due to deformations of the total antenna structure. They may be caused by:

- Gravitational and acceleration effects
- Climatic effects (wind, ice, temperature, etc)
- Manufacturing tolerances and installation alignment errors

Manufacturing tolerances and installation alignment errors may be controlled by system calibration. Further, climatic effects are controlled by enclosing the antenna system in a radome. Therefore, the only mechanical error sources which must be considered in the analysis are the effects of gravity and acceleration on the antenna structure.

C.7.1 Structural Effects

The analysis of tracking errors due to the antenna structure considers first the effect of a large mass (the dish) supported by a flexible member (the dish support). The error (dish sag) results from the angular deflection between the axis of the antenna and the encoder output. The effect is only evidenced in elevation, being maximum at the horizon and zero at zenith. Since the error introduced by dish sag is systematic in nature, the sense of the error is taken as positive in accordance with the convention established in Paragraph C.2.

The second error under consideration is due to feed sag. The model is a rigid dish which has its feed moved a small amount (δ) from the focus, perpendicular to the axis of the parabola. This model (Figure C-36) is approximate since it employs only simple geometrical optics.

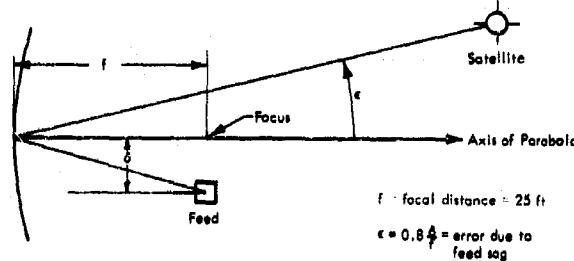


Figure C-36 Tracking Error Due to Feed Sag
(Simplified Model)

High-Gain Antenna

A detailed computer analysis of dish sag effect was performed. The analysis was based upon a well-proved structural deflection program written for a large digital computer. The axis deflection of the parabolic dish was computed assuming a rigid feed structure and using the scale weight of the multipurpose feed. The deflection was found to be 0.3 mrad, with a corresponding RF beam droop of 0.3 mrad.

The feed sag of the multipurpose feed was carefully measured by optical means when it was installed on the Vandenberg Tracking Station (VTS) antenna in April 1966. The repeatable measurement between "normal" and "plunged" positions was found to be 0.8 in. (i.e., 0.4 in. deflection). For small deflections the apparent raising of the beam at horizon is given to a first approximation by (Reference 16).

$$\text{Angle error} = 0.8 \frac{\text{deflection}}{\text{focal length}} = 1.1 \text{ mrad}$$

When combined, the dish sag effect (positive error) and the feed sag effect (negative error) yield an apparent raising of the beam by 0.8 mrad. This error is a function of the elevation angle and is given approximately by

$$\epsilon = \epsilon_0 \cos \phi$$

where ϵ is the angle error at elevation angle ϕ , and ϵ_0 is the angle error at zero elevation angle ($\epsilon_0 = 0.8$ mrad).

Low Gain Antenna

Measurements on the low-gain antenna at Operating Location Five (OL-5) indicate that the apparent elevation boresight angle is $3^\circ 13' 38''$, whereas by optical bore-sighting the angle is found to be $3^\circ 13' 28''$ (Reference 17). Based on these measurements, the angle error due to structural effects is assumed to be 0.04 mrad (10 sec).

C.7.2 Error Due to Antenna Acceleration

Antenna accelerations in azimuth and elevation, while the system is tracking the vehicle, will deflect the antenna structure, causing tracking error. The effect will have the greatest impact at the feed. This is especially true of the high-gain antenna because of the relatively high mass of the multipurpose feed.

To a first approximation the feed deflection can be assumed to be directly proportional to the tangential acceleration, where the tangential acceleration is merely the product of the angular acceleration and the moment arm. The moment arm, in this instance, is the distance from the feed to the axis of rotation measured along the axis of the dish and is approximately 40 ft for the high-gain antenna. Since the acceleration of gravity (1 g) resulted in a feed deflection or sag of 1.1 mrad (as derived in previous section),

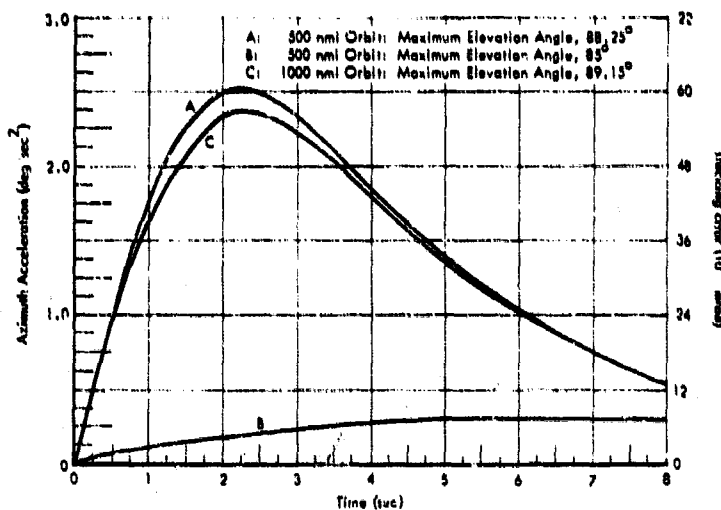


Figure C-37 Tracking Error Due to Azimuth Acceleration (High-Gain Antenna)

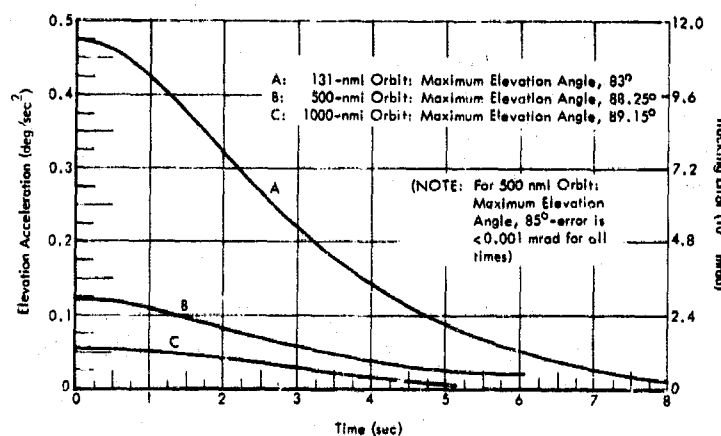


Figure C-38 Tracking Error Due to Elevation Acceleration (High-Gain Antenna)

the deflections associated with the angular accelerations experienced in tracking low altitude vehicles can be estimated. Angular accelerations were computed for various orbits in Paragraph C.6.1, Servo Lag. These and the corresponding feed deflections, are plotted in Figures C-37 and C-38 for the high-gain antenna.

Deflection of the antenna structure for the low-gain antenna will be considerably less because of the lighter feed and shorter moment arm. This is borne out by a comparison of the feed deflections for the two antennas under static conditions; for the high-gain antenna the feed sag was 1.1 mrad; for the low-gain, 0.05 mrad. The ratio 1.1 to 0.05 indicates that feed deflections due to acceleration for the low-gain antenna are a factor of 20 less than those for the high-gain antenna. Referring to Figure C-37, the latter is approximately 0.06 mrad; the corresponding feed deflection of the low-gain antenna is less than 0.003 mrad.

C. 8 CALIBRATION ERROR

C. 8.1 Mislevel and Orthogonality

Errors due to mislevel occur whtn the vertical axis does not coincide with the local vertical. An error in orthogonality is a departure from the desired right angle relationship between the antenna axes. The latter may be corrected with any desired degree of accuracy by shimming and adjusting bearings.

High-Gain Antenna

Orthogonality errors in this analysis are based on measurements at the New Hampshire (NHS) and Indian Ocean (IOS) Tracking Stations. At NHS, the measured orthogonality error was 3 sec; at IOS, less than 2 sec. Based on these measurements, an error of 0.01 mrad at an elevation angle of 45° is assumed. The error will vary as the tangent of the elevation angle.

Leveling errors are also based on previous measurements. At IOS, the leveling error was less than 10 sec (0.05 mrad). At NHS the estimated peak error is 0.2 mrad. In this analysis an rms error of 0.12 mrad at 45° elevation is assumed. Again the error varies as the tangent of the elevation angle.

Low-Gain Antenna

An error in mislevel in the low-gain antenna can be removed by adjustment of the leveling screw jacks provided for this purpose. Field experience indicates that the pedestal can be leveled to within ± 10 sec (0.05 mrad). Therefore, for this analysis, a peak error of 0.05 mrad and an rms error of 0.03 mrad at 45° elevation are assumed. In this analysis, orthogonality error for the low-gain antenna is assumed to be the same as for the high-gain antenna.

C. 8.2 Encoder Linearity

High-Gain Antenna

The encoders used on the high-gain antennas are 17-bit output "DIGISEC" type. (DIGISEC is a Wayne-George Corporation trade name.) The encoder has discrete encoding tracks to 14 bits and uses interpolation to form the remaining bits. The resolution of a 17-bit binary or related code (e.g., Gray code) is 9.89 sec, or 0.04 mrad; however, the accuracy of the interpolation is stated to have a 4-sec standard deviation. The installation of correction cams in the encoder mounting should enable the encoder readout to be adjusted to an accuracy at least as good as the 4-sec standard deviation. (Note that the adjustment of the encoder correction cams is accomplished with a precision clinometer which has an accuracy of 1 sec.) Thus, with correction cams the encoder linearity is assumed to be within 4 sec, i.e., the standard deviation is 0.02 mrad. For tracking, the error is considered a noise error.

Low-Gain Antenna

The low-gain antenna encoders are Wayne-George 17-bit Gray code optical encoders of the Digitsyn Series. These encoders have every bit read from a separate track on a glass code disk.

The basic encoder accuracy has been verified by means of a polygon mirror and an autocollimator. The largest error noted in checking five encoders was stated to be 2/3 quantum, while Wayne-George claimed ± 1 quantum (1 quantum = width of least significant bit = 9.89 sec, 0.04 mrad). The readout of the encoder was again checked when mounted in the pedestal, with the encoder errors referenced to encoder zero. The worst-case bias error for the azimuth encoders (five pedestals checked) was 7 sec and the worst-case rms error was 8.9 sec. The worst cases for the elevation encoders were a bias error of 6 sec and an rms error of 10 sec.

The peak error obtained from the above bias and noise errors is 19 sec, or 0.092 mrad. The 1σ tracking error (noise) of 0.03 mrad will be used for this report.

C. 8.3 RF Beam Collimation

Collimation error is due to the displacement of the RF axes from the mechanical axis caused, for example, by misalignment of the RF feed.

High-Gain Antenna

For the high-gain antenna a measure of the collimation error can be obtained by locking the antenna onto the boresight tower in both the "normal" and the "plunged" positions. The angles obtained in the plunged position are subtracted from 180° . The difference is then subtracted from the angles obtained in the normal position. This result, divided by 2, is defined as the collimation error.

Error data obtained by this technique contain contributions for other sources including RF amplitude imbalance, phase shift, and servo bias. Proper allowance must be made, therefore, in assessing collimation error to insure that these other error sources are not included twice.

Test data from the NHS tracking station at 2.2 GHz (WDL-TR3113, Reference 18) indicate a misalignment of 50 sec (0.24 mrad) in azimuth and 39 sec (0.19 mrad) in elevation. For this report, a 0.24 mrad error peak and a 0.14 mrad 1σ error are assumed. Making allowance for the other error sources included in the measurement (i.e., amplitude unbalance typically 0.06 mrad, phase shift 0.02 mrad, and servo bias 0.05 mrad), the 1σ error becomes 0.11 mrad. Azimuth error will vary with the secant of the elevation angle.

Low-Gain Antenna

Collimation error test data available from three sites (NHS, VTS, and OL-5, see References 17, 18, and 19) are summarized below:

	NHS	VTS	OL-5	Average
Azimuth	0	0	10"	4"
Elevation	9"	1'53"	1'9"	1'7"

Estimates based on these data are 0.02 mrad peak for azimuth, and 0.3 mrad peak for elevation. In this analysis the 1σ error will be 0.01 mrad and 0.17 mrad in azimuth and elevation, respectively. Compensation for error from sources other than collimation is not required since the sources - amplitude unbalance, phase shift, and servo bias - are negligible for the low-gain antenna.

As before, azimuth error will vary with the secant of the elevation angle.

C. 8.4 Site Location Errors

Tracking errors result from the uncertainty in tracking station site location in relation to the geocenter of the earth.

For a first-order survey, which has been used at every site, the maximum angular error is required to be less than 3 sec; however, the uncertainty in position on the earth's surface is believed to be as little as 30 ft for some sites and as much as 1000 ft at others. An uncertainty of 100 ft is assumed for this analysis.

Tracking error in elevation can be obtained from Equation (C.16) (See Paragraph C. 6.1) by incrementing the central angle, ψ_0 , to account for the uncertainty region on the earth's surface and then comparing the resulting elevation angle with previous data.

Elevation angle error was calculated for the 100 and 500 nmi cases (maximum elevation angle of 85°) by varying ψ_0 by 2.8×10^{-4} deg (corresponding to 100 ft at the earth's surface) and calculating elevation angle versus time. When these

results are compared with original data it is found that the maximum elevation error (at elevation angle of 85°) for the 100 nmi orbit is 9.9×10^{-3} deg or 0.17 mrad. At 65° elevation angle the error drops to 0.03 mrad. For the 500 nmi orbit the maximum error is 0.04 mrad.

Maximum azimuth error is calculated at the elevation angle maximum by shifting the tracking station location on the surface of the earth 100 ft parallel to the vehicle trajectory (see Figure C-22). At an altitude of 100 nmi the 100-ft surface displacement becomes 0.017 nmi, and at 500 nmi altitude the displacement is 0.019 nmi. The azimuth angle error is then determined (at maximum elevation angle of 85°) from the displacement and the minimum distance to the vehicle, which is 8.74 nmi (100 nmi altitude) and 43.6 nmi (500 nmi altitude). The errors are:

	<u>Altitude</u>
1.95 mrad	100 nmi
0.44 mrad	500 nmi

These errors decrease rapidly as the vehicle passes the point where antenna elevation angle is maximum.

C.8.5 Polarization Boresight Shift

Changes in polarization of the incident wave produce a boresight shift. The reference polarization for the high-gain antenna is right-hand circular, and for the low-gain antenna it can be right-hand or left-hand circular or linear polarization.

Data available on the VTS high-gain antenna multipurpose feed indicate that linear polarization produced a peak error of 0.7 mrad in azimuth and 1.0 mrad in elevation. To make allowance for cases where the incident wave is not right-hand circularly polarized, rms errors of 0.3 mrad in elevation and 0.2 mrad in azimuth are utilized in this analysis.

Measured data on the polarization boresight shift for the low-gain antenna are not readily available. However, since this antenna can be configured for reception of either left- or right-hand circular or linear polarization, the contribution to tracking errors from this source is not considered significant.

C-47



WDL Division

REFERENCES

1. J. A. Develet Jr., "Thermal Noise Errors in Simultaneous Lobing and Conical Scan Angle Tracking Systems," IEEE Transaction on Space Electronics and Telemetry, pp. 42-51, June 1961.
2. Multipurpose Feed Specifications, WDL-98-151345A-03, 21 April 1962.
3. Design Criteria From a Large Multipurpose Tracking Antenna, WDL-TR1368, 20 January 1961.
4. Ground Receiver and Analog Ranging Equipment Specifications, WDL-CP-168946A, 29 June 1967.
5. Tracking Radar for Satellite Control Facility (SCF) System, WDL-CP-161761B, 13 April 1967.
6. V. A. Counter, Propagation of Radio Waves through the Troposphere and Ionosphere, Lockheed Report LMSD-2066-R1, 14 May 1958.
7. George H. Millman, "Atmospheric Effects on VHF and UHF Propagation," Proceedings of the IRE, Vol. 46, August 1958, pp. 1492-1501.
8. Data Propagation Studies: Correction of Angular Deviation Due to Atmospheric Refraction, Report WDL-TR 1064, 15 July 1958. Secret.
9. Propagation Factors Affecting Long-Range UHF Radars at High Latitudes, Defense Research Telecommunications Establishment, Report No. 41-1-3, August 1958; ASTIA No. AD 210 456.
10. Tropospheric and Ionospheric Refraction Effects, Smyth Research Associates, Report No. SRA-91; ASTIA No. 217 406.
11. Precision of Compensated Tracking Systems, Report AFCRC-TR-59-356, Hermes Electronics Company, 1959; ASTIA No. AD 230 096.
12. A. W. Moeller, "The Effect of Ground Reflections on Antenna Test Range Measurements," Microwave Journal, March 1966.
13. Performance/Design and Product Configuration Requirements (CEI No. 152587F) Tracking, Telemetry and Command Antenna for Satellite Control Facility (SCF) System, WDL-CP-186680A, 9 July 1968.
14. R. C. Hansen, et al, Microwave Scanning Antennas, Vol. 1, Apertures, p. 358, Academic Press, 1964.
15. A. Cohen and A. W. Maltese, Electrical Evaluation of 110-foot Diameter Metal Space-frame Model Radome and CW413 Radomes, Lincoln Laboratory Report No. 76G-0003, 25 April 1961, MIT.

REFERENCES (Continued)

16. S. Silver, "Microwave Antenna Theory and Design," Vol. 12, p. 288, MIT Radiation Laboratory Series, McGraw-Hill, 1949
17. Depot Maintenance - OL-5, On-Site Support, WDL-TR3187, 15 February 1967.
18. Depot Maintenance - NHS, On-Site Support, WDL-TR3113, 15 December 1966.
19. Depot Maintenance - VTS, On-Site Support, WDL-TR3174, 15 January 1967.

C-49



WDL Division

APPENDIX D

EFFECTS OF PHASE SHIFT AND GAIN VARIATIONS ON ANGLE-TRACKING ACCURACY

D. 1 INTRODUCTION

Precomparator and postcomparator differential phase shift and gain variations introduce angle-tracking errors in simultaneous lobing tracking systems. This analysis evaluates the general nature and magnitude of these errors for the SGLS high-gain antenna configuration.

The effects of the following conditions are considered:

- Precomparator phase (differential phase shift introduced between the feed inputs and the comparator)
- Postcomparator phase shift (differential phase shift introduced between the comparator and the product detector)
- Precomparator amplitude unbalance (due to gain differences in the individual feed patterns)
- Postcomparator amplitude unbalance (due to variations in the gain of the reference and difference channel amplifiers)

Equations showing the basic relationships between parameters are developed first. An evaluation of these conditions follows, and graphs that show the effect on angle-tracking accuracy are presented.

Since SGLS includes both phase-lock and crosscorrelation tracking modes, an analysis of each is included. The former is treated in Paragraph D. 2, the latter in Paragraph D. 3.

D-1



WDL Division

D. 2 PHASE-LOCK TRACKING

D. 2. 1 Tracking Model

The effects of differential phase shift and amplitude unbalance can be evaluated by determining the relationship between the voltage output of the product detector and the difference-and-sum-channel input signals in terms of their relative amplitude and phase. Since this analysis is concerned with phase-lock tracking, the received RF signal is assumed to be an unmodulated carrier. Crosscorrelation tracking of a wideband modulated signal is treated in Paragraph D. 3.

A model of the tracking system is shown in Figure D-1. Only one of the two difference (i.e., error) channels is shown. The outputs of two individual feeds connect to the comparator (for tracking on one axis). In the comparator, sum and difference signals are formed and transmitted down separate paths through the channel amplifiers to the product detector. The product detector output is proportional to the relative amplitude and phase of the two input signals.

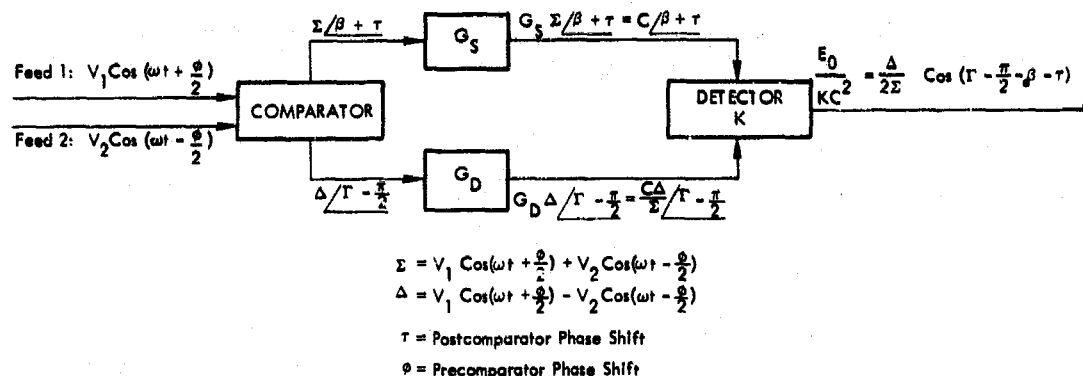


Figure D-1 Model for Phase-Lock Tracking

Since the received signal is assumed to be a pure sinusoid, the signal at the output of feed 1 is

$$V_1 \cos\left(\omega t + \frac{\phi}{2}\right) \quad (1)$$

D-2

and at the output of feed 2, we have

$$V_2 \cos(\omega t - \frac{\phi}{2}) \quad (2)$$

where

$V_{1,2}$ = peak amplitude of the signal from feeds 1 and 2, respectively

ωt = phase angle of the received carrier signal

$\phi = \phi_1 - \phi_2$ = precomparator differential phase shift between channels

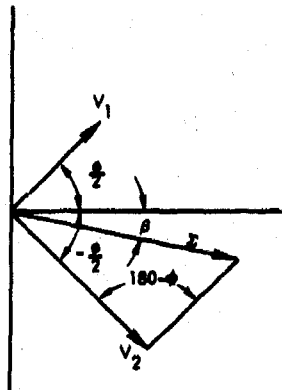
Sum Channel

The signal at the output of the comparator in the sum channel (Σ) is the sum of the two signals at the comparator input, that is,

$$\Sigma = V_1 \cos\left(\omega t + \frac{\phi}{2}\right) + V_2 \cos\left(\omega t - \frac{\phi}{2}\right) \quad (3)$$

From the vector diagram (Figure D-2), the amplitude of the sum signal at the comparator output is given by

$$\Sigma = \left(V_1^2 + V_2^2 + 2V_1 V_2 \cos \phi \right)^{1/2} \quad (4)$$



The associated sum signal phase angle (β) is

$$\beta = \sin^{-1} \frac{(V_1 - V_2) \sin \frac{\phi}{2}}{\left(V_1^2 + V_2^2 + 2V_1 V_2 \cos \phi \right)^{1/2}} \quad (5)$$

Figure D-2 Sum Channel (Σ)
Vector Diagram

If a phase shift is introduced between the comparator output and the amplifier input, the sum signal, written in polar form, becomes $\Sigma / \beta + \tau$, where τ is the postcomparator differential phase shift. Since the gain of the sum channel amplifier is G_s , the signal at the output of the amplifier is $G_s \Sigma / \beta + \tau$. The application of automatic gain control will, however,

maintain a constant amplitude output so that the sum channel input to the product detector can be written

$$G_s \Sigma \angle \beta + \tau = C \angle \beta + \tau \quad (6)$$

where

$$C = G_s \Sigma \quad (7)$$

Difference Channel

In the difference channel, the output of the comparator (Δ) is the vector difference between the two signals from the individual feeds, which is expressed as

$$\Delta = V_1 \cos(\omega t + \frac{\phi}{2}) - V_2 \cos(\omega t - \frac{\phi}{2}) \quad (8)$$

Referring to the vector diagram for the difference channel (Figure D-3), the amplitude of the signal at the output of the comparator in the difference channel is

$$\Delta = \left(V_1^2 + V_2^2 - 2V_1 V_2 \cos \phi \right)^{1/2} \quad (9)$$

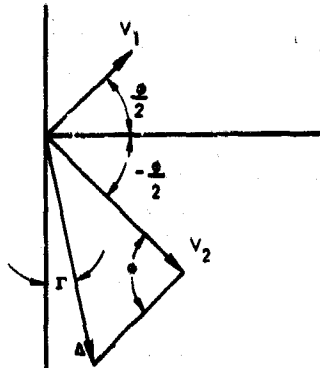


Figure D-3
Difference Channel (Δ)
Vector Diagram

The associated phase angle is $\Gamma - \frac{\pi}{2}$, where Γ is given by

$$\Gamma = \sin^{-1} \frac{(V_2 - V_1) \cos \frac{\phi}{2}}{\left(V_1^2 + V_2^2 - 2V_1 V_2 \cos \phi \right)^{1/2}} \quad (10)$$

Expressed in polar form, the difference channel signal at the comparator output is $\Delta \angle \Gamma - \pi/2$. The input to the product detector, following multiplication by the gain of the difference channel amplifier (G_D), is

$$G_D \Delta \angle \Gamma - \frac{\pi}{2} \quad (11)$$

Assuming the gain in each channel is identical ($G_s = G_D$) and by substitution in Equation (7), we have

$$G_D = \frac{C}{\Sigma} \quad (12)$$

The difference channel input to the detector [Equation (9)] can then be rewritten as

$$\frac{C\Delta}{\Sigma} \sqrt{\Gamma - \frac{\pi}{2}} \quad (13)$$

Product Detection

Figure D-4 represents a typical product detector neglecting the sum frequency term (2ω) which is filtered out. The output voltage (E_0) is given by

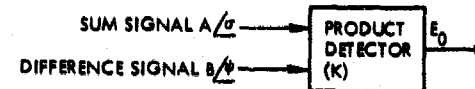


Figure D-4 Typical Product Detector

$$E_0 = \frac{KAB}{2} \cos(\psi - \sigma) \quad (14)$$

where

- E_0 = voltage output of the product detector
- K = detector constant
- A = amplitude of the sum signal input
- B = amplitude of the difference signal input
- ψ = difference signal phase angle
- σ = sum signal phase angle

Substitution of the expressions for the sum signal [Equation (6)] and the difference signal [Equation (13)] into Equation (14) yields

$$E_0 = \frac{KC^2\Delta}{2\Sigma} \cos \left(\Gamma - \frac{\pi}{2} - \beta - \tau \right) \quad (15)$$

The detector output voltage (E_0) in Equation (15) can be expressed in terms of the signal output from the individual feeds (V_1 and V_2) by substitution of the expressions for Σ [Equation (4)] and Δ [Equation (9)] into Equation (15). This yields

$$E_0 = \frac{KC^2}{2} \left[\frac{V_1^2 + V_2^2 - 2V_1 V_2 \cos\phi}{V_1^2 + V_2^2 + 2V_1 V_2 \cos\phi} \right]^{1/2} \cos \left(\Gamma - \frac{\pi}{2} - \beta - \tau \right) \quad (16)$$

where

- E_0 = dc output of the product detector
- K = product detector constant
- V_1, V_2 = peak amplitude of the signals from feeds 1 and 2
[see Equations (1) and (2)]
- C = a constant ($G_s \Sigma$); G_s is gain of the sum channel amplifier
[see Equation (7)]
- ϕ = precomparator differential phase shift ($\phi_1 - \phi_2$)
- τ = postcomparator differential phase shift (arbitrarily introduced
in the sum channel)
- Γ = difference signal phase angle [see Equation (10)]
- β = sum signal phase angle [see Equation (5)]

To relate the detector output voltage (E_0) to the off-boresight angle, the individual feed output voltages (V_1 and V_2) must be expressed in terms of the off-boresight angle. The latter is determined by the feed and antenna design. Assuming gaussian patterns, Figure D-5 shows the individual feed patterns with a normalized gain of 1 for the SGLS high-gain configuration.

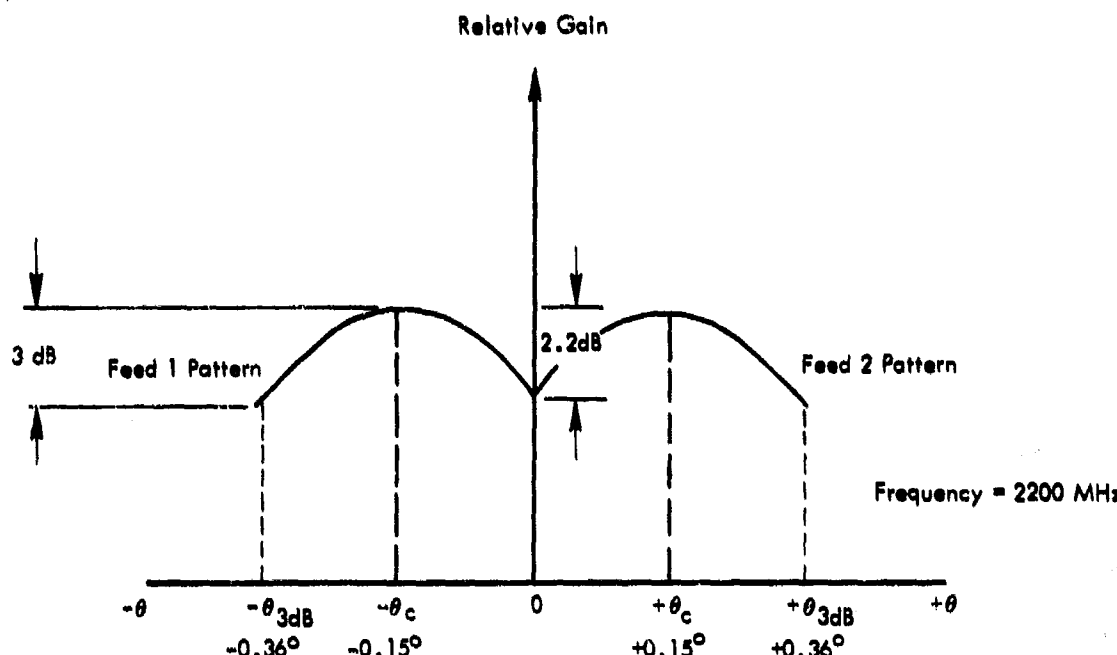


Figure D-5 Individual Feed Patterns

Referring to Figure D-5, the voltage output from the individual feeds is given by*

$$V_1^2 = 2G_1 \exp \left[-2.78 \left(\frac{\theta + \theta_c}{\theta_{3dB}} \right)^2 \right] \quad (17)$$

$$V_2^2 = 2G_2 \exp \left[-2.78 \left(\frac{\theta - \theta_c}{\theta_{3dB}} \right)^2 \right] \quad (18)$$

where

V_1, V_2 = peak output voltage from feeds 1 and 2, respectively

G_1, G_2 = power gain of the individual feeds

θ = off-boresight angle

θ_c = off-boresight angle for maximum feed gain

θ_{3dB} = off-boresight angle where feed gain is 3 dB down from maximum

*WDL-98-151345A-03, Feed-Multipurpose, for 60-Foot Paraboloid Antenna;
Detail Performance Specification.

For the high-gain antenna, $\theta_c = \pm 0.15^\circ$ and $\theta_{3\text{dB}} = \pm 0.36^\circ$. Substitution of these values in Equations (17) and (18) yields the feed output in terms of the individual feed gain (G_1, G_2) and off-boresight angle (θ), i.e.,

$$V_1^2 = 2G_1 \exp \left[-2.78 \left(\frac{\theta + 0.15}{0.36} \right)^2 \right] \quad (19)$$

$$V_2^2 = 2G_2 \exp \left[-2.78 \left(\frac{\theta - 0.15}{0.36} \right)^2 \right] \quad (20)$$

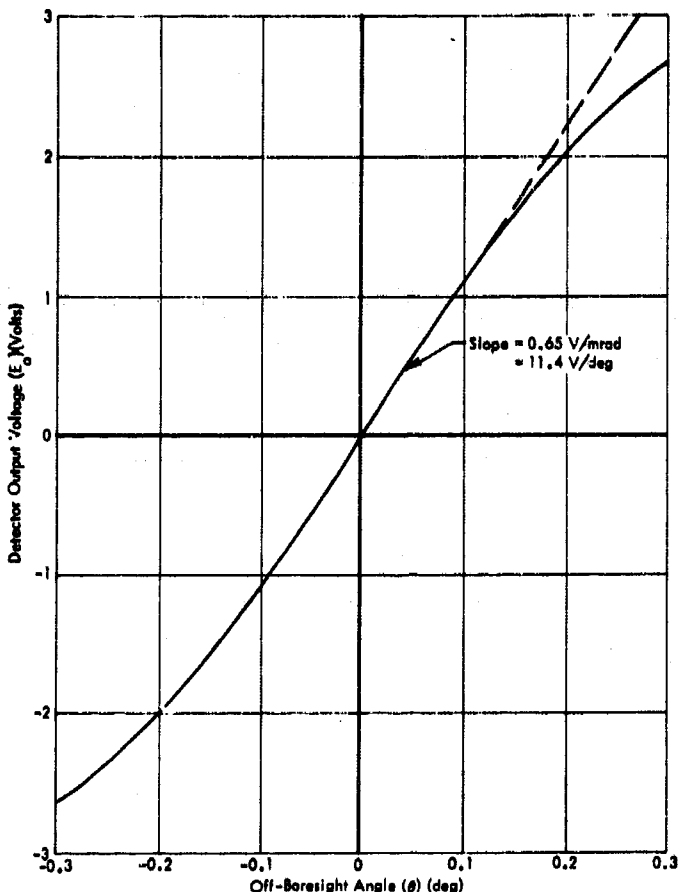


Figure D-6 Detector Output Voltage vs Off-Boresight Angle

Equation (16) is plotted in Figure D-6 for the high-gain antenna showing detector voltage output (E_0) versus the off-boresight angle (θ) for zero precomparator and postcomparator phase shift ($\phi = 0^\circ$, $\tau = 0^\circ$). Note that the gradient at boresight ($\theta = 0^\circ$) is 0.65 V/mrad; the curve is linear to approximately 0.1° .

The effects of introducing differential phase shift and amplitude unbalance are evaluated in Paragraphs D.2.2 and D.2.3.

D.2.2 Effects of Differential Phase Shift

An examination of Equation (16) indicates that a precomparator or postcomparator differential phase shift causes a boresight shift. This is illustrated in Figure D-7, which shows boresight shift (θ) as a function of postcomparator phase shift (τ) for various values of precomparator phase shift (ϕ). Note that if either τ or ϕ is zero, the boresight shift is also zero. For $\tau \neq 0$ and $\phi \neq 0$, the resulting boresight shift increases as either τ or ϕ is increased. Note also that postcomparator phase shift changes the slope of the detector output voltage. Although servo loop gain is affected to some extent, the effect is secondary. Boresight is not affected.

Provisions have been made in the SGLS receiver to control postcomparator phase shift through phase-adjust circuitry in the reference channel. This adjustment permits reduction of differential phase shifts between the sum and difference channels to approximately $\pm 10^\circ$.

The specified* null depth for the high-gain antenna is 30 dB in the 2200- to 2300-MHz frequency range; the related precomparator phase shift is 5° . From Equation (16) and under these conditions ($\tau = \pm 10^\circ$, $\phi = \pm 5^\circ$), the resultant boresight shift is $\pm 0.0026^\circ$ or ± 0.045 mrad.

*WDL-98-151345A-03, Feed-Multipurpose, for 60-Foot Paraboloid Antenna;
Detail Performance Specification.

D-9

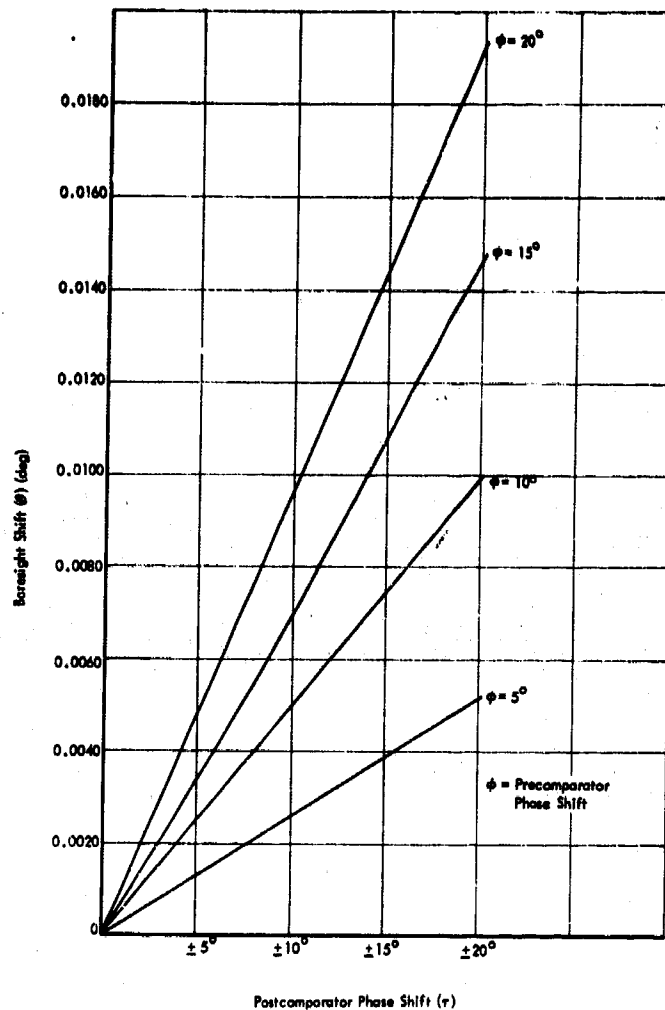


Figure D-7 Angle-Tracking Error Due to Phase Shift

D. 2.3 Effects of Amplitude Unbalance

Precomparator Amplitude Unbalance

Precomparator differential amplitude variations also result in a shift in the boresight angle. These variations are generally caused by unequal gains in the individual feeds. The resultant boresight shift is determined from Equations (19) and (20) by setting $V_1 = V_2$ and solving for the ratio of individual feed gains (G_1/G_2). This yields

$$\frac{G_1}{G_2} = e^{12.8\theta} \quad (21)$$

The variation in boresight (θ) is plotted in Figure D-8 for various values of the above ratio [Equation (21)].

For the SGLS high-gain antenna configuration, a feed amplitude unbalance of 0.3 dB can be expected with a corresponding angle-tracking error (boresight shift) of 0.006°.

Postcomparator Amplitude Unbalance

Figure D-8 Boresight Angle Variation Due to Feed Amplitude Unbalance

The effect of postcomparator amplitude unbalance is evident from inspection of Equation (15). This equation was derived on the basis that the gain in the sum and difference channels was identical; i.e., $G_s = G_D$. If the gain of the channels differ such that $G_s = AG_D$ then the detector output will be modified by the constant A as follows:

$$E_0 = \frac{AKC^2\Delta}{2\Sigma} \cos \left(\Gamma - \frac{\pi}{2} - \beta - \tau \right) \quad (22)$$

D-10

Note that postcomparator amplitude unbalance does not introduce a boresight shift but will change the slope of the product detector output. This change in slope will affect the servo, either increasing or decreasing loop gain. In the SGLS receiver, gain variations of ± 3 dB* can be expected over the input signal dynamic range. These variations in receiver gradient affect the servo acceleration error constant, which, in turn, can introduce tracking errors due to servo lag. The latter errors are minimized, however, by adjustments to the error gradient available in the receiver.

D.3 CROSSCORRELATION TRACKING

In Paragraph D.2, the effects of differential phase shift and amplitude unbalance were analyzed in tracking an unmodulated carrier in the phase-lock mode. This section is concerned with tracking a modulated carrier in the crosscorrelation (wideband) mode.

D.3.1 Tracking Model

The analyses for the phase-lock and crosscorrelation tracking modes are quite similar; therefore, the model for crosscorrelation tracking (Figure D-9) is a simplified version of Figure D-1.

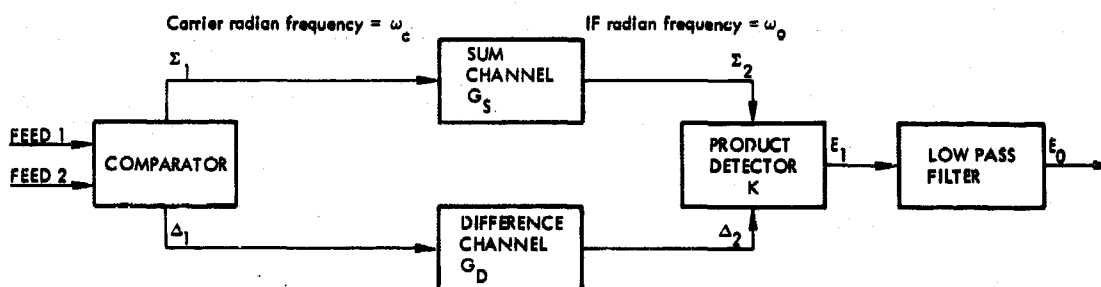


Figure D-9 Crosscorrelation Tracking Model

*WDL-CP-168946A, Receiver and Analog Ranging Equipment, Ground, CEI Detail Specification.

Since the input signal to the antenna system is a modulated carrier, the signals at the outputs of the feeds are

$$\text{Feed 1 output} = V_1 \cos \left[\omega_c \left(t + \frac{\phi}{2} \right) + \alpha \cos \omega_m \left(t + \frac{\phi}{2} \right) \right] \quad (23)$$

$$\text{Feed 2 output} = V_2 \cos \left[\omega_c \left(t - \frac{\phi}{2} \right) + \alpha \cos \omega_m \left(t - \frac{\phi}{2} \right) \right] \quad (24)$$

where

ω_c = carrier radian frequency

ϕ = precomparator differential time delay*

ω_m = sinusoidal modulation radian frequency

α = modulation index

V_1, V_2 = peak output voltages from feeds 1 and 2 [see Equation (17)]

The signal at the output of the comparator in the sum channel (Σ_1) is the vector sum of the signals from feeds 1 and 2, and is given by

$$\begin{aligned} \Sigma_1 = & V_1 \cos \left[\omega_c \left(t + \frac{\phi}{2} \right) + \alpha \cos \omega_m \left(t + \frac{\phi}{2} \right) \right] \\ & + V_2 \cos \left[\omega_c \left(t - \frac{\phi}{2} \right) + \alpha \cos \omega_m \left(t - \frac{\phi}{2} \right) \right] \end{aligned} \quad (25)$$

After amplification by the sum channel gain (G_s), the signal is down-converted to an intermediate frequency. At this point, a postcomparator differential time delay (τ) is introduced, as well as an arbitrary phase shift to the carrier (β). (The latter is of interest in determining the effect of phase-adjust circuitry in the receiver.) The input signal to the product detector (Σ_2) is then:

* In Paragraph D.2, " ϕ " was defined as precomparator differential phase shift.

$$\begin{aligned}\Sigma_2 &= G_s V_1 \cos \left[\omega_0 \left(t + \frac{\tau}{2} \right) + \omega_c \frac{\phi}{2} + \frac{\beta}{2} + \alpha \cos \omega_m \left(t + \frac{\phi}{2} + \frac{\tau}{2} \right) \right] \\ &\quad + G_s V_2 \cos \left[\omega_0 \left(t + \frac{\tau}{2} \right) - \omega_c \frac{\phi}{2} + \frac{\beta}{2} + \alpha \cos \omega_m \left(t - \frac{\phi}{2} + \frac{\tau}{2} \right) \right]\end{aligned}\quad (26)$$

where

- G_s = gain of the sum channel amplifier
- τ = postcomparator differential time delay
- ω_0 = intermediate radian frequency = $2\pi \times 130$ MHz
- β = arbitrary phase shift to carrier to represent phase adjust circuitry in the receiver
- ω_c = carrier radian frequency = $2\pi \times 2200$ MHz

In the difference channel, the output of the comparator (Δ_1) is the vector difference of the signals from feeds 1 and 2, which is given by

$$\begin{aligned}\Delta_1 &= V_1 \cos \left[\omega_c \left(t + \frac{\phi}{2} \right) + \alpha \cos \omega_m \left(t + \frac{\phi}{2} \right) \right] \\ &\quad - V_2 \cos \left[\omega_c \left(t - \frac{\phi}{2} \right) + \alpha \cos \omega_m \left(t - \frac{\phi}{2} \right) \right]\end{aligned}\quad (27)$$

After amplification, frequency down conversion, and introduction of postcomparator time delay and phase shift, the signal at the input to the product detector is

$$\begin{aligned}\Delta_2 &= G_D V_1 \cos \left[\omega_0 \left(t - \frac{\tau}{2} \right) + \omega_c \frac{\phi}{2} - \frac{\beta}{2} + \alpha \cos \omega_m \left(t + \frac{\phi}{2} - \frac{\tau}{2} \right) \right] \\ &\quad - G_D V_2 \cos \left[\omega_0 \left(t - \frac{\tau}{2} \right) - \omega_c \frac{\phi}{2} - \frac{\beta}{2} + \alpha \cos \omega_m \left(t - \frac{\phi}{2} - \frac{\tau}{2} \right) \right]\end{aligned}\quad (28)$$

where G_D is the gain in the difference channel.



Figure D-10 Product Detector

The output of the detector (E_1), as shown in Figure D-10, is given by

$$E_1 = \Sigma_2 \Delta_2 K$$

Substituting Σ_2 from Equation (26) and Δ_2 from Equation (28) yields

$$\begin{aligned}
 \frac{E_1}{K} = & G_s G_D V_1^2 \cos \left[\omega_0 \left(t + \frac{\tau}{2} \right) + \omega_c \frac{\phi}{2} + \frac{\beta}{2} + \alpha \cos \omega_m \left(t + \frac{\phi}{2} + \frac{\tau}{2} \right) \right] \\
 & \cdot \cos \left[\omega_0 \left(t - \frac{\tau}{2} \right) + \omega_c \frac{\phi}{2} - \frac{\beta}{2} + \alpha \cos \omega_m \left(t + \frac{\phi}{2} - \frac{\tau}{2} \right) \right] \\
 & - G_s G_D V_1 V_2 \cos \left[\omega_0 \left(t + \frac{\tau}{2} \right) + \omega_c \frac{\phi}{2} + \frac{\beta}{2} + \alpha \cos \omega_m \left(t + \frac{\phi}{2} + \frac{\tau}{2} \right) \right] \\
 & \cdot \cos \left[\omega_0 \left(t - \frac{\tau}{2} \right) - \omega_c \frac{\phi}{2} - \frac{\beta}{2} + \alpha \cos \omega_m \left(t - \frac{\phi}{2} - \frac{\tau}{2} \right) \right] \\
 & + G_s G_D V_1 V_2 \cos \left[\omega_0 \left(t + \frac{\tau}{2} \right) - \omega_c \frac{\phi}{2} + \frac{\beta}{2} + \alpha \cos \omega_m \left(t - \frac{\phi}{2} + \frac{\tau}{2} \right) \right] \\
 & \cdot \cos \left[\omega_0 \left(t - \frac{\tau}{2} \right) + \omega_c \frac{\phi}{2} - \frac{\beta}{2} + \alpha \cos \omega_m \left(t + \frac{\phi}{2} - \frac{\tau}{2} \right) \right] \\
 & - G_s G_D V_2^2 \cos \left[\omega_0 \left(t + \frac{\tau}{2} \right) - \omega_c \frac{\phi}{2} + \frac{\beta}{2} + \alpha \cos \omega_m \left(t - \frac{\phi}{2} + \frac{\tau}{2} \right) \right] \\
 & \cdot \cos \left[\omega_0 \left(t - \frac{\tau}{2} \right) - \omega_c \frac{\phi}{2} - \frac{\beta}{2} + \alpha \cos \omega_m \left(t - \frac{\phi}{2} - \frac{\tau}{2} \right) \right]
 \end{aligned} \tag{29}$$

Equation (29) may be simplified by using the following identities:

$$\cos x \cos y = 1/2[\cos(x+y) + \cos(x-y)] \tag{30}$$

$$\cos \alpha - \cos \beta = -2 \sin 1/2(\alpha + \beta) \cdot \sin 1/2(\alpha - \beta) \tag{31}$$

$$\cos(\alpha - \beta) = \cos \alpha \cos \beta + \sin \alpha \sin \beta \tag{32}$$

$$\cos(x \sin y) = J_0(x) + 2 \sum_{k=1}^{\infty} J_{2k}(x) \cos 2ky \tag{33}$$

$$\sin(x \sin y) = 2 \sum_{k=1}^{\infty} J_{2k-1}(x) \sin(2k-1)y \quad (34)$$

After substitution, collection of terms, and passage through the lowpass filter, the voltage output (E_0) becomes

$$\begin{aligned} \frac{E_0}{KG_s G_D} &= \left(\frac{V_1^2}{2} + \frac{V_2^2}{2} \right) \cos(\omega_0 \tau + \beta) J_0 \left[2\alpha \sin \omega_m \frac{\tau}{2} \right] \\ &\quad - \frac{V_1 V_2}{2} \cos(\omega_0 \tau + \omega_c \phi + \beta) J_0 \left[2\alpha \sin \omega_m \left(\frac{\phi}{2} + \frac{\tau}{2} \right) \right] \\ &\quad + \frac{V_1 V_2}{2} \cos(\omega_0 \tau - \omega_c \phi + \beta) J_0 \left[2\alpha \sin \omega_m \left(\frac{\tau}{2} - \frac{\phi}{2} \right) \right] \end{aligned} \quad (35)$$

D. 3.2 Effect of Differential Time Delay

The plot of Equation (35) (Figure D-11) shows the output voltage $E_0/KG_s G_D$ versus the off-boresight angle (θ) for various values of postcomparator differential time delay (τ). The values of modulation index ($\alpha = 2.4$) and modulation frequency $\omega_m = (2\pi)(6.5 \text{ MHz})$ represent the maximum specified modulation requirements.* In addition, the value of precomparator differential time delay ($\phi = 6.3 \times 10^{-12} \text{ sec}$) is the time delay associated with a 5° phase shift to the carrier at 2200 MHz. In Figure D-11, for $\tau = 0$, the boresight shift is zero; for the time delay associated with a 10° phase shift to the IF carrier ($\tau = 2.1 \times 10^{-10} \text{ sec}$), the boresight shift is 0.0026°. As might be expected, the latter is identical to the result obtained when tracking an unmodulated carrier in the phase-lock mode (Paragraph 2.2). In general, as the differential time delay increases, the boresight shift increases and the gradient or slope of the output voltage decreases.

*WDL-CP-168946A, Receiver and Analog Ranging Equipment, Ground, CEI Detail Specification, Paragraph 3.1.1.1.2.8.

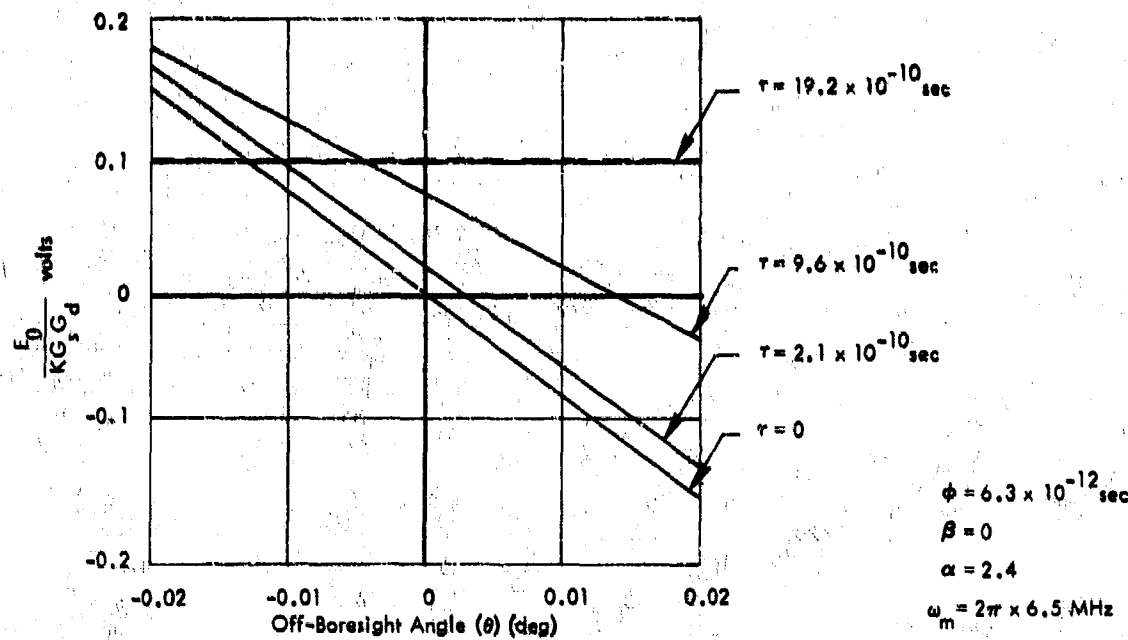


Figure D-11 Error Voltage vs Off-Boresight Angle (Crosscorrelation Tracking)

As noted earlier, the postcomparator differential phase shift can be maintained at 10° or less by phase adjustments available in the receiver. The boresight shift and slope degradation are therefore bounded, precluding, for example, the curves for $\tau = 9.6 \times 10^{-10}$ sec and $\tau = 19.2 \times 10^{-10}$ sec shown in Figure D-11.

At this point, the analysis indicates that postcomparator differential time delays cause an identical boresight shift when tracking either a modulated or an unmodulated carrier. When tracking a modulated carrier, however, an additional degradation (over that which occurs when tracking an unmodulated carrier) is caused by the modulation envelope delay when it degrades the slope of the receiver output voltage.

Consider the case [Equation (35)] in which the phase adjustment in the receiver (β) is such that $\omega_o \tau = -\beta$ and $\omega_c \phi$ is small. That is, the phase adjustment in the receiver is set to compensate for the postcomparator-carrier differential phase shift, and the precomparator-carrier differential phase shift ($\omega_c \phi$) is less than or equal to 5°. Since $\phi \ll \tau$, Equation (35) reduces to:

$$\frac{E_0}{KG_s G_D} = \left[\frac{V_1^2}{2} - \frac{V_2^2}{2} \right] J_0 \left(2\alpha \sin \omega_m \frac{\tau}{2} \right) \quad (36)$$

For $V_1 = V_2$, the output of the receiver is zero, as expected. However for $V_1 \neq V_2$, the output is proportional to the factor $J_0(2\alpha \sin \omega_m \frac{\tau}{2})$. This factor is a function of the modulation index and the modulation frequency. When $\alpha = 0$ (no modulation), $J_0(0) = 1$, and the result depends only on V_1, V_2 , the detector constant, and the channel gain, as was the case in Paragraph 2.2.

The plot of $J_0(2\alpha \sin \omega_m \frac{\tau}{2})$ versus τ , for a modulation index of $\alpha = 2.4$ and a modulating frequency of $\omega_m = (2\pi)(6.5 \text{ MHz})$, in Figure D-12 shows the effect on the output voltage; namely, a degradation of the voltage gradient. A degradation in

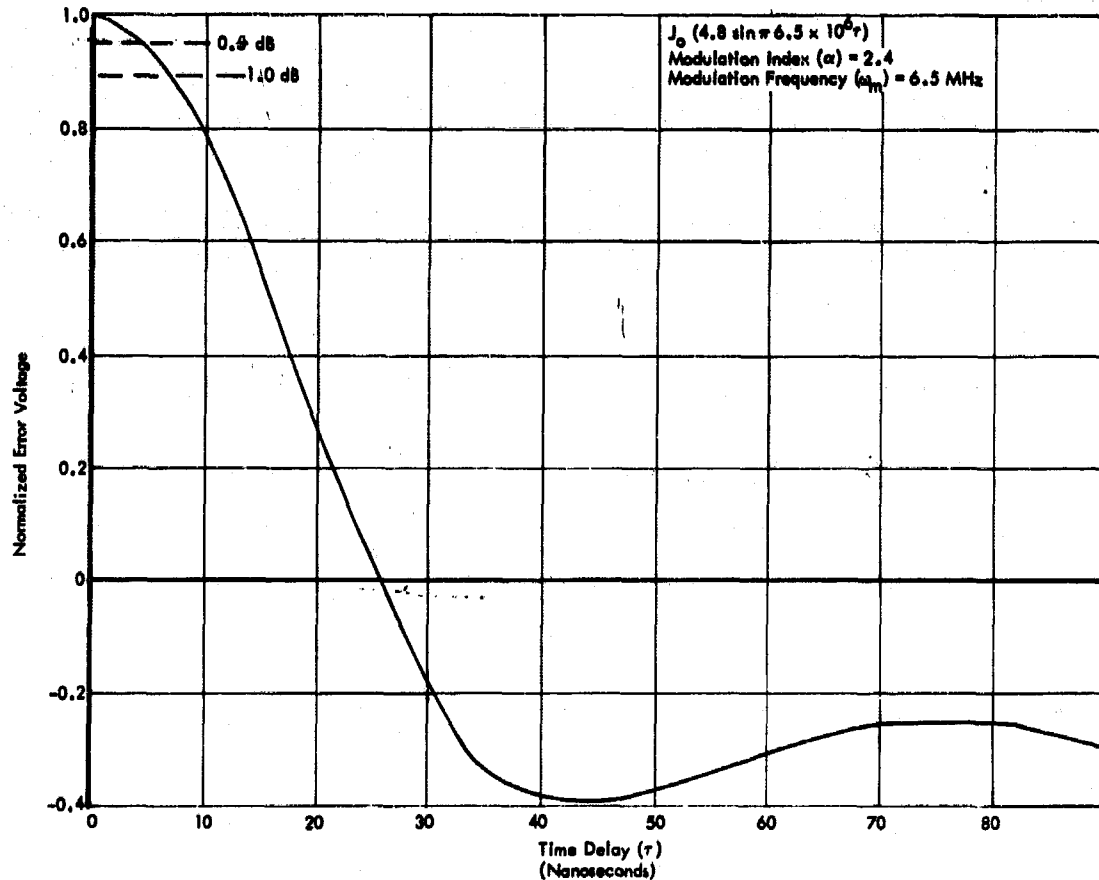


Figure D-12 Angle-Error Voltage vs Differential Time Delay (Crosscorrelation Tracking)

the output voltage gradient of 1 dB is considered acceptable. This in turn corresponds to a postcomparator differential time delay of 7 ns, as indicated in Figure D-12. This time-delay differential can be realized through appropriate installation design involving equipment location and the selection, routing, and length of transmission lines.

D.3.3 Summary of Tracking Errors

Table D-1 summarizes the effects of differential phase shift and gain variations on angle-tracking accuracy in both the phase-lock and crosscorrelation tracking modes. As indicated in the table, boresight shifts result from precomparator differential amplitude unbalance and precomparator and postcomparator differential phase shift. The magnitude of boresight shift is the same for either tracking mode.

A change in the slope of the detector output voltage results from postcomparator differential amplitude imbalance and postcomparator phase differential phase shift. In the crosscorrelation tracking mode, the detector output voltage is, however, subject to greater degradation due to the envelope delay which cannot be compensated for in the receiver.

TABLE D-1
SUMMARY OF ANGLE-TRACKING ERRORS DUE TO DIFFERENTIAL PHASE SHIFT AND AMPLITUDE UNBALANCE

Condition	Parameter Value	Source*	Effect in Phase-Lock Tracking		Effect in Crosscorrelation Tracking	
			Boresight Shift	Detector Output Slope	Boresight Shift	Detector Output Slope
Precomparator differential phase shift	$\pm 5^\circ$	A	$\pm 0.045 \text{ mrad (peak)}$ $\pm 0.03 \text{ mrad (rms)}$	No effect	$\pm 0.045 \text{ mrad (peak)}$ $\pm 0.03 \text{ mrad (rms)}$	No effect
Postcomparator differential phase shift	$\pm 10^\circ$	B		0.1 dB		1.1 dB**
Precomparator differential amplitude unbalance	0.3 dB	C	$\pm 0.10 \text{ mrad (peak)}$ $\pm 0.06 \text{ mrad (rms)}$	No effect	$\pm 0.10 \text{ mrad (peak)}$ $\pm 0.06 \text{ mrad (rms)}$	No effect
Postcomparator differential amplitude unbalance	$\pm 3 \text{ dB}$	B	No effect	$\pm 3 \text{ dB}$	No effect	$\pm 3 \text{ dB}$

*A: WDL-98-151345A-03, Feed, Multipurpose, for 60-Foot Paraboloid Antenna, Detail Performance Specification.

B: WDL-CP-168946A, Receiver and Analog Ranging Equipment, Ground, CEI Detail Specification.

C: Estimated.

**1 dB due to 7 ns envelope delay for: modulation index $\alpha = 2.4$; modulation frequency $\omega_m = (2\pi)(6.5 \text{ MHz})$.

UNCLASSIFIED

Security Classification

DOCUMENT CONTROL DATA - R & D

(Security classification of title, body of abstract and indexing annotation must be entered when the overall report is classified)

1. ORIGINATING ACTIVITY (Corporate author) Philco-Ford Corporation, WDL Division 3939 Fabian Way Palo Alto, California 94303		2d. REPORT SECURITY CLASSIFICATION Unclassified
		2d. GROUP (N/A)
3. REPORT TITLE Q SPACE-GROUND LINK SUBSYSTEM GROUND STATION SYSTEM ANALYSIS SUMMARY REPORT. Volume I, System Design Analysis,		
4. DESCRIPTIVE NOTES (Type of report and inclusive dates) Summary Report		
5. AUTHOR(S) (First name, middle initial, last name) P. Marshall Fitzgerald Jackson Witherspoon		
6. REPORT DATE 15 November 1968	7a. TOTAL NO. OF PAGES 891	7b. NO. OF REFS 83
8. CONTRACT OR GRANT NO. F04695-67-C-0115	9. ORIGINATOR'S REPORT NUMBER/REF ID SAMSO/TR 69-189-Vol-1	
10. PROJECT NO.	11. OTHER REPORT NO(S) (Any other numbers that may be assigned to this report) WDL-TR3227-1-Vol-1	
12. DISTRIBUTION STATEMENT STATEMENT NO. 4 (UNCLASSIFIED document) - Each transmittal of this document outside the Department of Defense must have prior approval of Equipment Development Branch (SMOND-2), HQ AFSCF, AF Unit Post Office, Los Angeles, Ca. 90045		
13. SUPPLEMENTARY NOTES PHILCO-FORD WDL-TR3227-1 SPACE-GROUND LINK SUBSYSTEM GROUND STATION SYSTEM ANALYSIS SUMMARY REPORT 15 November 1968		12. SPONSORING MILITARY ACTIVITY HQ AFSCF, Equipment Dev. Br. (SMOND-2) AF Unit Post Office Los Angeles, California 90045
14. ABSTRACT This report provides a technical description of the ground station of the Space-Ground Link Subsystem (SGLS) and integrates the analyses performed by contractors who contributed to its development. The report is in three volumes: Volume I, System Design Analysis contains the ground station description and related analyses. Volume II, Receiver Design Analysis contains a detailed analysis of the SGLS receiver. Volume III, Supplementary Analyses is a reprint of analyses originally presented in the SGLS final design report.		

DD FORM 1 NOV 65 1473

UNCLASSIFIED

Security Classification

462 711

14

UNCLASSIFIED

Security Classification

KEY WORDS	LINK A		LINK B		LINK C	
	ROLE	WT	ROLE	WT	ROLE	WT
Pulse Code Modulation (PCM)						
Space-Ground Link Subsystem (SGLS)						
Ranging						
Telemetry						
Commanding						

UNCLASSIFIED

Security Classification